JACOBS
UNIVERSITY

ELONGATOR DEPENDENT ANTICODON MODIFICATIONS IN DICTYOSTELIUM DISCOIDEUM

and the effect on glutamine codon translation

by

MANFRED ANDREAS SCHÄCK

A thesis submitted in partial fulfillment
of the requirements for the degree of

Doctor of Philosophy

in Biochemistry

Approved Dissertation Committee:

Prof. Dr. Christian Hammann
Biochemistry, Jacobs University Bremen

Prof. Dr. Matthias Ullrich
Microbiology, Jacobs University Bremen

Prof. Dr. Raffael Schaffrath
Microbiology, Universität Kassel

Date of Defense 12.10.2017

Life Science & Chemistry

Manfred Andreas Schäck: *Elongator Dependent Anticodon Modifications in Dictyostelium discoideum* and the effect on glutamine codon translation. A thesis submitted in partial fulfillment of the requirements for the degree of **Doctor of Philosophy in Biochemistry**, © Date of Defense 12.10.2017

JACOBS
UNIVERSITY

STATUTORY DECLARATION

Manfred Andreas Schäck
Matr.-No.: 20330785
PhD-Thesis

Declaration of Authorship
I hereby declare that the thesis submitted was created and written solely by myself without any external support. Any sources, direct or indirect, are marked as such. I am aware of the fact that the contents of the thesis in digital form may be revised with regard to usage of unauthorized aid as well as whether the whole or parts of it may be identified as plagiarism. I do agree my work to be entered into a database for it to be compared with existing sources, where it will remain in order to enable further comparisons with future theses. This does not grant any rights of reproduction and usage, however.
This document was neither presented to any other examination board nor has it been published.

Erklärung der Autorenschaft
Ich erkläre hiermit, dass die vorliegende Arbeit ohne fremde Hilfe ausschließlich von mir erstellt und geschrieben worden ist. Jedwede verwendeten Quellen, direkter oder indirekter Art, sind als solche kenntlich gemacht worden. Mir ist die Tatsache bewusst, dass der Inhalt der Thesis in digitaler Form geprüft werden kann im Hinblick darauf, ob es sich ganz oder in Teilen um ein Plagiat handelt. Ich bin damit einverstanden, dass meine Arbeit in einer Datenbank eingegeben werden kann, um mit bereits bestehenden Quellen verglichen zu werden und dort auch verbleibt, um mit zukünftigen Arbeiten verglichen werden zu können. Dies berechtigt jedoch nicht zur Verwendung oder Vervielfältigung.
Diese Arbeit wurde noch keiner anderen Prüfungsbehörde vorgelegt noch wurde sie bisher veröffentlicht.

Bremen, Date of Defense 12.10.2017

Manfred Andreas Schäck

ABSTRACT

Transfer RNAs (tRNA) are among the most posttranscriptionally modified RNA molecules in nature. The RNA modifications contribute to the stability of the secondary and tertiary structure of the tRNA. Anticodon modifications at *wobble* position U_{34} are particularly important, since they help to modulate the codon - anticodon interaction and *wobble* recognition in the process of translation.

The eukaryotic Elongator complex catalyzes the first step in the Elongator dependent U_{34} modification pathway. The complex consists of 6 proteins (Elp1-Elp6) that can be divided into two subcomplexes (Elp123 and Elp456). Both, Elp123 and Elp456 form heterodimers. One Elp1 protein binds the Elp456 subcomplex, resulting in in an overall stoichiometry of the holocomplex with two proteins of every subunit. Elongator dysfuncion has severe effects on different cellular processes and Elongator mutants in yeast and *Arabidopsis thaliana* display specific stress phenotypes. Elongator dysfunction is lethal in most higher metazoa. Brain tissue specific splicing defects in Elongator genes are associated with formation of neuropathies including amyotrophic lateral sclerosis, familial dysautonomia and rolandic epilepsy in humans.

This thesis presents the first investigation on Elongator dependent anticodon U_{34} modification in the evolutionary supergroup of Amoebozoa. The first part of the thesis focused on the identity of the complex. Pulldown studies with ectopically overexpressed Elongator subunits revealed that the *Dictyostelium discoideum* Elongator complex also consists of 6 proteins and the two subcomplexes are mainly found independently. Blue native PAGE and gel filtration experiments on the Elp456 subcomplex and recombinant Elp456 suggest that the subcomplex could be larger than the Elp456 subcomplex of other organisms. Furthermore, it was shown, using the viral 2A peptide sequence, that the Elp3 protein is unstable. The peptide sequence allowed discrimination between translational efficiency and protein stability for different proteins.

The second part of the thesis focused on the Elongator dependent modifications. A series of mutant strains was generated that interrupted the Elongator dependent modification pathway at all major steps. Different analytic techniques were applied to investigate the modifications. It could be shown that the Elongator dependent modifications 5-carbamyl-methyl uridine (ncm^5U), 5-methoxy-carbonyl-methyl uridine (mcm^5U) and 5-methoxy-carbonyl-methyl-2-thiouridine (mcm^5s^2U) are conserved in *D. discoideum*.

The effect of loss of the mcm^{5}s^{2}U modifications was tested on the decoding capability of tQ^{UUG} towards glutamine codon translation with artificial gene constructs. Polyglutamine leaders with different CAA/CAG codon ratios fused to GFP were expressed in the background of different mutant strains and the Ax2 wild type. The expression differences were measured via flow cytometry and Western blot. Polyglutamine stretches are known to form amyloid structures which are toxic for most eukaryotes. This is not the case for *D. discoideum*, which possesses the prion-richest proteome known. A significant portion of proteins feature long polyglutamine stretches within their amino acid sequences. The corresponding genes use almost exclusively one codon, which leads to an overall glutamine codon usage of 96% CAA to 4% CAG. Within this thesis, the first unconditional tQ^{CUG} null mutant in an eukaryotic model organism was generated. This fact and data generated with the polyglutamine leaders provide evidence that *wobbling* of tQ^{UUG} over CAG codon can occur in *D. discoideum*.

CONTENTS

1 INTRODUCTION 1
1.1 Transfer RNA . . . 1
1.1.1 Elongator dependent anticodon modification . 2
1.2 Translational elongation . . . 5
1.3 The Elongator complex . . . 6
1.3.1 Elongator mutant phenotypes . . . 9
1.3.2 γ-toxin, an Elongator modification dependent ribonuclease of tE^{UUC} . . . 9
1.4 *Dictyostelium discoideum* . . . 10
1.5 Aim of this thesis . . . 11
2 MATERIALS AND METHODS 13
2.1 Materials . . . 13
2.1.1 Equipment and Apparatus . . . 13
2.1.2 Consumables . . . 14
2.1.3 Chemicals . . . 15
2.1.4 Buffers and Solutions . . . 17
2.1.5 Antibiotics . . . 20
2.1.6 Nutrition media . . . 20
2.1.7 Nucleotides . . . 22
2.1.8 Antibodies . . . 22
2.1.9 Kits . . . 22
2.1.10 Size markers . . . 22
2.1.11 Enzymes and Enzyme buffers . . . 23
2.1.12 Oligonucleotides . . . 23
2.1.13 Software . . . 23
2.1.14 Sequences . . . 24
2.1.15 Plasmids . . . 24
2.1.16 Organisms . . . 25
2.2 Methods . . . 26
2.2.1 Data analysis . . . 26
2.2.2 Cell biological Methods . . . 26
2.2.3 Molecular biological Methods . . . 30
3 RESULTS 45
3.1 Investigations on the identity of the Elongator complex 45
3.1.1 Intracellular localization of Elongator proteins . 46
3.1.2 Protein co-immunoprecipitation and affinity chromatography of *D. discoideum* Elongator proteins 47
3.1.3 Recombinant *D. discoideum* Elp456 subcomplex in *E. coli* . . . 51
3.1.4 The 2A peptide sequence - a tool to investigate the reduced Elp3 level upon "overexpression" . 56

3.2 Investigations on the Elongator dependent anticodon U_{34} modifications in *D. discoideum* 60
3.2.1 Genes involved in the modification pathway . . 60
3.2.2 Generation of null mutant strains in *D. discoideum* 60
3.2.3 The Elongator dependent anticodon U_{34} modification in different null mutant strains 67
3.2.4 Elongator dependent codon usage is favored in *D. discoideum* 70
3.2.5 The generation of an unconditional tQ^{CUG} null mutant and tRNA overexpressors in *D. discoideum* 73
3.2.6 The effect of the loss of anticodon U_{34} modification on glutamine codon translation 76
3.3 γ-toxin, a tool to investigate defects in Elongator dependent tRNA modification 81
4 DISCUSSION 85
4.1 The identity of the Elongator complex 85
4.1.1 Complex formation in *D. discoideum* 85
4.1.2 Cross complementation 86
4.1.3 Recombinant Elp456 in *E. coli* 87
4.1.4 The stability of Elp3 88
4.2 Elongator dependent U_{34} modifications 89
4.2.1 Gene deletion strain generation 89
4.2.2 Elongator dependent modifications 90
4.2.3 Codon usage and tRNA genes 91
4.2.4 The effect of loss of modification on glutamine codon translation 92
4.2.5 Global translation in modification deficient mutants 93
4.2.6 Elongator mutants and +1 translational frameshifting 94
4.2.7 Elongator mutants growth phenotypes 95
4.2.8 Translational regulation by tRNA modification 95
4.3 γ-toxin 96

BIBLIOGRAPHY 98

A APPENDIX 112
A.1 Additional experiments on Elongator localization and Complex identity 112
A.1.1 Fluorescence microscopy 112
A.1.2 Additonal data on Elongator proteins 114
A.1.3 Cross complementation with yeast Elongator proteins in *D. discoideum* 121
A.1.4 Recombinant Elps in *E. coli* 121
A.1.5 Elp gene fusions with the 2A sequence 123
A.2 Additional data and experimental data on Elongator dependent tRNA modification 125

A.2.1 tRNA modification analysis by Stefanie Kellner 125
A.2.2 APM Northern blots to determine if ectopically overexpressed Elongator proteins can rescue the s^2U modification 130
A.2.3 Codon usage and tRNA gene 132
A.2.4 PolyQ-GFP expression in mutant strains 133
A.2.5 Growth and Development 136
A.3 γ-toxin 138
A.4 supplementary Materials 139
A.4.1 Plasmids 139
A.4.2 Oligo nucleotides 154
A.4.3 Strains generated in this thesis 159

LIST OF FIGURES

Figure 1 The secondary structure of an eukaryotic tRNA with RNA modification sites 3
Figure 2 The genetic code and decoding abilities of individual tRNA species 4
Figure 3 The tRNA species that carry Elongator dependent modifications 5
Figure 4 The proteins of the Elongator complex 6
Figure 5 Model of the Elongator complex 8
Figure 6 *D. discoideum* life cycle 11
Figure 7 Principle of the Ligase independent cloning (LIC) Systems. 32
Figure 8 LSM fluorescence imaging of Elp5 and Elp6 . 47
Figure 9 GFP-trap pulldown of ectopically overexpressed Elongator proteins 3, 4, 5, and 6 48
Figure 10 GFP-trap pulldown of *in vivo* crosslinked Elp3 and Elp4 49
Figure 11 Strep affinity chromatographic pulldown of Elp3 and Elp4 51
Figure 12 Blue native PAGE and Western blot of the Elongator subcomplexes 52
Figure 13 Sketch of the expression and purification of the recombinant *D.discoideum* Elp456 subcomplex in *E. coli* 53
Figure 14 SDS-PAGE recElp456 purified from *E. coli* . . . 54
Figure 15 The size of the recHAP purified from *E. coli* . . 55
Figure 16 ATP releases nucleic acids from the recElp456 subcomplex 56
Figure 17 RFP-2A-GFP 58
Figure 18 Elp3 2A sequence experiment in *D. discoideum* 59
Figure 19 *Elp3* gene deletion 63
Figure 20 *Elp4* gene deletion 64
Figure 21 *Trm9* gene deletion 65
Figure 22 *Ctu1* gene deletion in Ax2 and *elp3*$^{-}$ 66
Figure 23 Analysis of the different Elongator dependent anticodon modifications and their appearance in different mutant backgrounds 68
Figure 24 Thiolation level of specific tRNAs in different mutant strains 69
Figure 25 APM Northern blots on strains expressing different Elp3 variants 71

Figure 26 Pie chart comparison of Elongator dependent modified tRNA copy number to the global tRNA gene copy number in *S. cerevisae* and *D. discoideum* 73
Figure 27 Histogram of the relative codon usage for lysine AAA/AAG and glutamate GAA/GAG . 73
Figure 28 Bar chart of the relative codon usage for lysine AAA/AAG and glutamate GAA/GAG in different functional pathways 74
Figure 29 Deletion of the single copy tRNA tQ^{CUG} 75
Figure 30 Northern blot confirmation of tQ^{CUG} null mutant and tQ^{CUG} overexpressor strains. 76
Figure 31 Relative CAA codon usage and PolyQ-stretches in *D. discoideum* 76
Figure 32 Sketch of different polyglutamine leader constructs fused to GFP, used to determine the translation efficiency of the different mutant strains 77
Figure 33 Q103-GFP expression in mutant strains compared to Ax2 wild type 79
Figure 34 Q52-GFP expression in mutant strains compared to Ax2 wild type 80
Figure 35 Q15-GFP expression in mutant strains compared to Ax2 wild type 81
Figure 36 γ-toxin expression and *in vivo* effect on *E. coli* tRNA level 83
Figure 37 Northern blot images of cleavage assays with γ-toxin 84
Figure 38 Expression of ectopically expressed, GFP-tagged Elp3 and Elp4 proteins. 112
Figure 39 Expression of ectopically expressed, GFP-tagged Elp3 variants 113
Figure 40 LSM 3D images of cells expressing mRFP-Elp5 GFP-Elp6 113
Figure 41 Additional Western blots on strains expressing Elongator proteins 114
Figure 42 Expression of mRFP-Elp5 and GFP-Elp6 from a single pDM Vector 115
Figure 43 GFP trap pulldown without protease inhibitor 116
Figure 44 Different Elution fractions of recElp456 after SEC 117
Figure 45 Gel picture of the GFP-trap pulldown of Elp3-Elp6 118
Figure 46 Gel picture of the crosslinked GFP-trap pulldown of Elp3 and Elp4 (N- and C-terminal) . . 119
Figure 47 Gel picture of the Elp3 and Elp4 Strep pulldown 120

Figure 48 Expression of GFP-yElp1 and GFP-yElp3 in *D. discoideum* 121
Figure 49 MBP-Elp3 expression and purification from *E. coli* 122
Figure 50 MBP-Elp4, MBP-Elp5 and MBP-Elp6 expression and purification from *E. coli* 122
Figure 51 Elongator 2A fusion construct expression . . . 124
Figure 52 tRNA modifications 1.1 126
Figure 53 tRNA modifications 1.2 127
Figure 54 tRNA modifications 2.1 128
Figure 55 tRNA modifications 2.2 129
Figure 56 APM Northern blot against tRNAs from Ax2, *elp4*⁻ and *elp2*⁻ strain 130
Figure 57 APM Northern blot against tE^{UUC} from Ax2, *elp4*⁻ and *elp1*⁻ strain 131
Figure 58 Codon usage and tRNA genes of *S. cerevisiae* and *D. discoideum* 132
Figure 59 Flow cytometric detected expression profile of GFP and Q103-GFP in different strains. 133
Figure 60 The Umber stop codon experiment 135
Figure 61 Doubling time of Elongator mutants compared to Ax2 136
Figure 62 Spore heads from Ax2, *elp1*⁻, *elp3*⁻ and *elp4*⁻ after 48h of development. 137
Figure 63 Purification of recombinant γ-toxin produced in *E. coli* 138
Figure 64 Elp3 expression plasmids for *D. discoideum* . . 140
Figure 65 Elp4 expression plasmids for *D. discoideum* . . 141
Figure 66 Expression plasmids with BS(r) for *D. discoideum* 142
Figure 67 Elp5 expression plasmids for *D. discoideum* . . 143
Figure 68 Elp6 expression plasmids for *D. discoideum* . . 144
Figure 69 pDM-fusion plasmids for expression of several proteins in *D. discoideum* 145
Figure 70 Yeast Elongator proteins on expression plasmids for *D. discoideum* 146
Figure 71 pKOSG vectors for knockout generation in *D. discoideum* 1 147
Figure 72 pKOSG vectors for knockout generation in *D. discoideum* 2 148
Figure 73 pDM2A plasmids for *D. discoideum* 1 149
Figure 74 pDM2A plasmids for *D. discoideum* 2 150
Figure 75 Glutamine leader expression plasmids for *D. discoideum* 151
Figure 76 Umber stop codon experiment expression plasmids for *D. discoideum* 152
Figure 77 Expression plasmids for *E. coli* 153

LIST OF TABLES

Table 1 Overview of DNA sequences used in this thesis 24
Table 2 Analytic restriction digestion mix 30
Table 3 Preparative restriction digestion mix 30
Table 4 Ligation mix 31
Table 5 PCR recipe LIC 33
Table 6 PCR program LIC 33
Table 7 Generation of the 5′-overhang of the vector . . 33
Table 8 Generation of the 5′-overhang of the PCR product 34
Table 9 PCR mix 35
Table 10 PCR program 36
Table 11 PCR mix colony PCR 36
Table 12 PCR program colony PCR 37
Table 13 Reaction mix for radioactive endlabelling . . . 39
Table 14 Elongator proteins in *D. discoideum* 46
Table 15 *D. discoideum* genes involved in the Elongator dependent modification pathway 61
Table 16 Codon usage and tRNA gene copy number of *S. pombe*, *S. cerevisiae* and *D. discoideum* 72
Table 17 MALDI mass spectrometric analysis of GFP-trap pulldowns from Elp3 116
Table 18 MALDI mass spectrometric analysis of recElp456 purified from *E. coli* 117
Table 19 MALDI mass spectrometric analysis of GFP-trap pulldowns from Elp3-Elp6 118
Table 20 MALDI mass spectrometric analysis crosslinked GFP-trap 119
Table 21 MALDI mass spectrometric analysis strep pull-down 120
Table 22 Primer and Oligo DNA list 1 155
Table 23 Primer and Oligo DNA list 2 156
Table 24 Primer and Oligo DNA list 3 157
Table 25 Primer and Oligo DNA list 4 158
Table 26 Overview of bacterial strains generated in this thesis 159
Table 27 Overview of *D. discoideum* strains created in this thesis 1 161
Table 28 Overview of *D. discoideum* strains created in this thesis 2 162
Table 29 Overview of *D. discoideum* strains created in this thesis 3 163

Table 30 Overview of *D. discoideum* strains created in this thesis 4 164
Table 31 Overview of *D. discoideum* strains created in this thesis 5 165
Table 32 Overview of *D. discoideum* strains created in this thesis 6 166

LIST OF ABBREVIATIONS

′	Prime
aa	Amino acid
Amp	Ampicillin
AP	Alkaline phosphatase
APM	[p-(N-acrylamino)-phenyl] mercuric chloride
APS	Ammonium persulfate
ATP	Adenosine triphosphate
BCIP	5-Brom-4-chlor-3-indolylphosphate
bp	Base pairs
BSA	Bovine serum albumin
BS(r)	Blasticidin resistance
CBB	Coomassie brillant blue
Cdn	Codon
CDS	Coding sequence
CTP	Cytidine triphosphate
DMF	N,N-Dimethylformamide
DNA	Desoxyribonucleic acid
ds	Double stranded
dNTP	Desoxyribonucleoside triphosphate
EDTA	Ethylenediaminetetraacetic acid
flox	knockout strain with BS(r) resistance cassette
G418	Geneticin
GFP	Green fluorescent protein
GTC	Guanidinium thiocyanate
GTP	Guanosine triphosphate
h	Hours
HEPES	2-(4-/2-Hydroxyethyl)-1-piperazineethanesulfonic acid
HSP	Heat shock protein
hp	Hairpin
IPTG	Isopropyl-β-D-thiogalactopyranoside
Kan	Kanamycin
kDa	Kilodalton
L	Liter

LB	Lysogeny broth
LSM	Laser scanning microscopy
MALDI	Matrix-Assisted Laser Desorption/Ionization
M	Molar
mA	Milliampere
mg	Milligramm
min	Minute
mL	Milliliter
mM	Millimolar
mRRFP	Red fluorecent protein (monomeric)
mRNA	Messenger RNA
MWCO	Molecular weight cut off
n.a.	not applicable
n.d.	not determined
ng	Nanogramm
nm	Nanometer
nM	Nanomolar
NP40	Nonident®P40
nt	Nucleotide
NTP	Nucleoside triphosphate
OD	Optic density
ORF	Open reading frame
Pol	Polymerase
polyQ	Polyglutamine tract
PAA	Polyacrylamide
PAGE	Polyacrylamide gelelectrophoresis
PBS	Phosphate buffered saline
PCR	Polymerase chain reaction
rcf	Relative centrifugal force
RFP	Red fluorescent protein
RNA	Ribonucleic acid
rRNA	Ribosomal RNA
rte	Retro transoposable elements
rNTP	Ribonucleotide
rox	knockout strain without BS(r) cassette
rpm	Rounds per minute
s	Second
SDS	Sodium dodecylsulfate
sec	Second
TBE	Tris-Borate-EDTA
TE	Tris-EDTA
TEMED	Tetramethylethylendiamine
Tris	Tris(hydroxymethyl)aminomethane
tRNA	Transfer RNA
u	Unit (Enzyme unit)
UTP	Uridine triphosphate

UV	Ultraviolett
V	Volt
v/v	Volume per volume
wt	Wilde type
w/v	Weight per volume
µg	Microgramm
µL	Microliter
°C	Degree celsius

Amino acids

A	Alanine (Ala)
C	Cysteine (Cys)
D	Aspartate (Asp)
E	Glutamate (Glu)
F	Phenylalanine (Phe)
G	Glycine (Gly)
H	Histidine (His)
I	Isoleucine (Ile)
K	Lysine (Lys)
L	Leucine (Leu)
M	Methionine (Met)
N	Asparagine (Asn)
P	Proline (Pro)
Q	Glutamine (Gln)
R	Arginine (Arg)
S	Serine (Ser)
T	Threonine (Thr)
V	Valine (Val)
W	Tryptophane (Trp)
Y	Tyrosin (Tyr)

Nucleotides

A	Adenine
C	Cytocine
G	Guanine
U	Uridine

tRNA genes

tX^{XXX}	tRNA-aa-Anticodon nucelotide sequence
(example: tQ^{CUG}	= tRNA-Gln-CUG)
tQ^{CUG-}	knockout of the tRNA-Gln-CUG-1 gene
+ tQ^{CUG}	tRNA-Gln-CUG-1 gene +/− 250 bp
+ tQ^{UUG}	tRNA-Gln-UUG-13 gene +/− 250 bp

1 INTRODUCTION

Protein synthesis is a fundamental process of gene expression in all living organisms. Ribosomes, composed of large RNA molecules, are the factories in which the translation from the messenger RNA (mRNA) sequence into amino acid sequence takes place. The mRNA serves as a blueprint in which the information of the protein sequence is to be build upon. On the mRNA, the specification for each amino acid is given by codons, which are defined as three consecutive bases in the genetic code. The nearly universal genetic code itself features 64 codons of which 61 code for 20 amino acids. The physical link between messenger RNA and amino acid sequence of proteins are small adapter molecules, called transfer RNAs (tRNA). mRNA, rRNA and tRNA harbor many posttranscriptional modifications (RNA modifications). Over 100 different RNA modifications are known today [1]. The largest group of these modifications are posttranscriptional methylations which make up over two thirds of the total number [2]. These RNA methylations, as most modifications, contribute to stability and structure of the RNA molecule and are also known to be quality control steps in the RNA maturation[3, 4].

1.1 TRANSFER RNA

Tranfer RNAs deliver the cognate amino acid to the designated codon of the mRNA in the process of translation. tRNA are transcribed by RNA polymerase III followed by a series of maturation events. These events include removal of the 5´leader and trimming of the 3´end, addition of CCA nucleotides by the CCA-adding enzyme and covalent modification of RNA nucleotides [5]. Only correctly processed tRNAs leave the nucleus via a nuclear receptor-mediated export process [6].

There are over 100 different modifications known in the mature tRNA, which makes it one if not the most modified RNA molecules known [7]. In average 17 percent of tRNA residues are modified [8]. Figure 1 A gives an overview of the particular sites, type of modifications and the enzymes responsible for the modification in *Saccharomyces cerevisiae*. Most of these post transcriptional modifications ensure the proper folding and stabilize the tertiary L-shaped structure of the molecule. For example, 2´ O-methylated pyrimidine ribonucleotides favor the C_3 endo conformation thereby increasing the melting temperature of the tRNA [9]. Other modifications at the anticodon stem loop, particularly nucleotide 37 and 34, contribute to anticodon stability and help to modulate the codon-anticodon inter-

action at the A-Site and support the transition to the P-site inside the ribosome [7, 8, 10, 11]. For example, modifications at position 37 prevent a fourth base pairing between mRNA and tRNA [8].

Modifications at the anticodon position 34 are of particular nature: In the *wobble* hypothesis proposed by Francis Crick, nucleotides 35 and 36 of the tRNA anticodon and the the first two nucleotide of the codon would form canonical pairing of purine with pyrimidine or vice versa (U-A and A-U, C-G and G-C). Nucleotide 34 of the tRNA and the third base of the codon, however, do not necessarily need to be canonical, extending the recognition capability of tRNAs [12]. The non-canonical base pairs possible in this hypothesis were thought to be G-U and to a lesser extent U-G pairs. Another non-canonical base pair involved inosine, that was found in the alanine tRNA tA^{IGC} [12, 13]. A variety of post transcriptional modifications not known to Crick, allows tRNAs to extend the non-canonical base pairing even further, with up to 4-fold degenerate codon recognition by one single tRNA (reviewed [14–16]). In fact, up to 40% of all codon recognitions are realized by tRNA *wobbling* [14]. This is also reflected by the fact, that only approximately 40 unique tRNA genes exist that decode the 61 codons [16]. Figure 2 gives an overview over the genetic code and the decoding capabilities of the unique tRNA genes in *S. cerevisiae*.

1.1.1 *Elongator dependent anticodon modification*

The *wobble* uridines at position 34 (U_{34}) are almost always modified in any organism [10]. Uridines are structurally flexible and form only weak stacking interactions with neighboring nucleosides [18]. All tRNAs – except two – with a Uracil at position 34 feature an Elongator dependent modification. The two exceptions are tL^{UAG}, which does not feature any U_{34} modification and tI^{UAU}, which features a pseudo-uridine at the very position [19]. The modifications are shown to stabilize the anticodon and extend the decoding capability of the tRNAs.

The eukaryotic Elongator complex catalyzes the first step in the modification pathway [20–22] (structural basis reviewed in [23]). Acetate is covalently attached to the C5 of the pyrimidine ring via a radical based reaction.[1] The resulting 5-carbonyl-methyl uridine (cm^5U) is further processed to 5-carbamyl-methyl uridine (ncm^5U) by an unknown enzyme [21]. 5-carbamyl-methyl (ncm^5) uridine, as the final modification of U_{34}, is present in 6 tRNAs, as shown in Figure 3. All tRNA have in common that they feature a purin base at position 35. The leucine tRNA tL^{UAA} is particular in this group, since it features

1 There is little doubt about the reaction carried out by the Elongator complex and particular by its catalytic protein Elp3, but no study could observe the reaction in eukaryotes. Only one study on Elp3 of the *archaeon Methanocaldococcus infernus*, could show an *in vitro* reconstitution of this modification reaction [24].

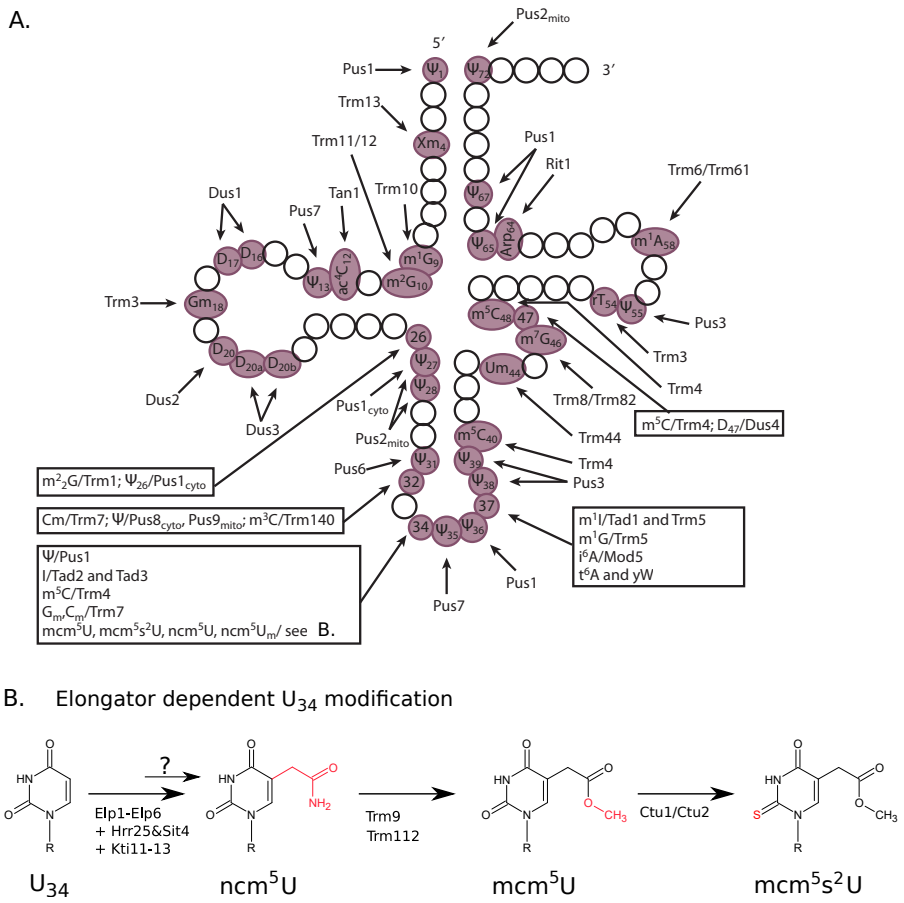

Figure 1: The secondary structure of a eukaryotic tRNA with RNA modification sites.

A. Schematic representation of the secondary structure of a eukaryotic tRNA from *S. cerevisiae*. Indicated in red are the specific modification sites with the different modification types. The particular enzymes responsible for the modification are given as well. Picture taken and modified from [7]. **B.** Elongator dependent modification pathway of the anticodon uridine at position 34. The initial cm^5 modification is carried out by the Elongator complex, while the following ncm^5 modification is carried out by an unknown enzyme (indicated by a question mark). The ncm^5U modification can be found in 6 different tRNAs. Trm9/Trm112 are thought to be responsible for the conversion into mcm^5 found in 2 tRNAs. Ctu1/Ctu2 are thiolating the C2 of the pyrimidine ring resulting in mcm^5s^2U, which is found in 3 tRNA.

an additional methylation at the 2'OH of the ribose [25].

The ncm^5U can be further modified to 5-methoxy-carbonyl-methyl (mcm^5) uridine, which is found in the 2 tRNAs tG^{UCC} and tR^{UCU} (Figure 3). Both feature a cytosine at position 35. The mcm^5 formation can be disrupted by Trm9 and Trm112 inhibition [21].

tK^{UUU}, tE^{UUC} and tQ^{UUG} feature a double modification with mcm^5 and an additional thiolation at the C2 of the pyrimidine ring (5-

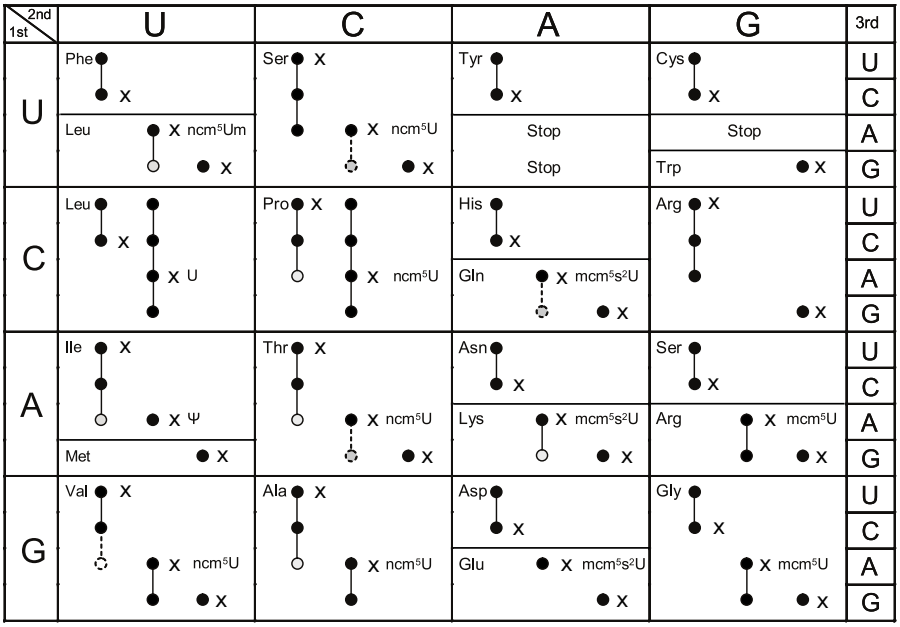

Figure 2: The genetic code and decoding abilities of individual tRNA species.

Shown are the first (left column), second (top row) and third (right column) nucleotide of the anticodon, with the corresponding amino acid. X indicates tRNA genes existing with anticodons complementary to the codons of the very position. (All U_{34} modifications are indicated.) Codons read by a tRNA are indicated by circles and connecting lines. Grey dots indicate a lower decoding capability of the tRNA to the particular codon. Dashed lines indicate that the tRNA can only read over the particular codon when overexpressed. The table refers to data generated in *S. cerevisiae*. Picture taken and modified from [17].

methoxy-carbonyl-methyl-2-thiouracil, short mcm^5s^2U). All 3 mcm^5s^2U containing tRNAs feature a uridine at position 35. The thiourydilation is catalyzed by the Ctu1/Ctu2 protein complex, which is regulated via an urmylation by Urm1 [26–28].

The modifications ncm^5 and mcm^5 are modulating the electron distribution of the pyrimidine ring shifting the keto enol equilibrium towards the enol. This enables hydrogen bonding between U_{34} and a guanosine base. The s^2U modification, on the other hand, leads to an adaptation of a C3 endo, gauche plus [C4-C5] anti conformation, which is more hydrophobic and more restricted. This appears to be best suited for anticodon base stacking, thereby stabilizing the anticodon stem loop (ASL) and favoring the interaction with A in the codon [29, 30]. The modifications were shown to increase A-site binding during codon recognition [11]. While loss of Elongator dependent modifications have minor effects on A-site binding on most of the tRNAs, the A-site binding of tK^{UUU}, tE^{UUC} and tQ^{UUG} is highly reduced [11, 31]. In fact, most of the growth phenotypes of Elongator

mutants in yeast can be associated to loss of modification of the lysine tRNA tK^{UUU} [32, 33].

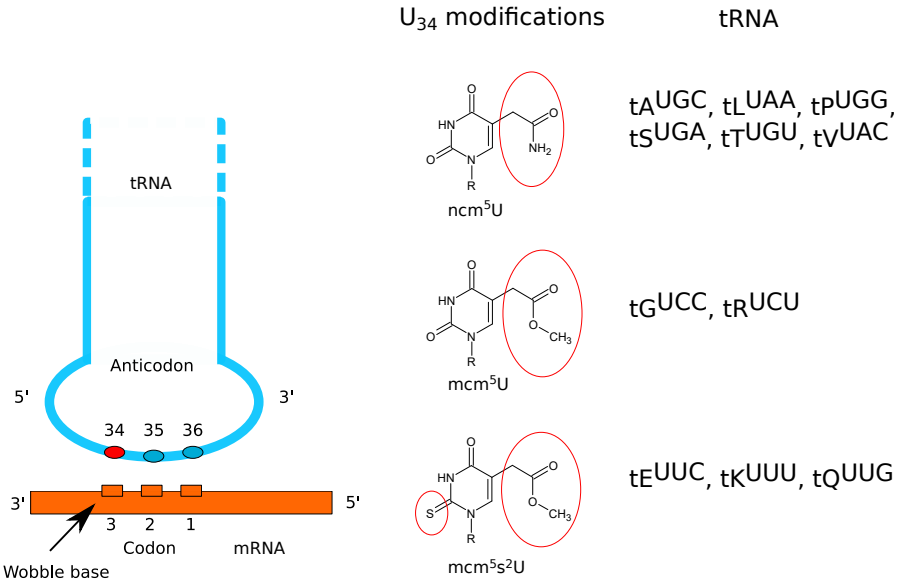

Figure 3: The tRNA species that carry Elongator dependent modifications. **left:** tRNA anticodon positioned above an mRNA codon. Indicated in red is the anticodon position 34, which basepairs with the *wobble* position of the codon. **right:** the different Elongator dependent U_{34} modifications ncm^5, mcm^5 and $mcm^5s^2$and the tRNAs that display these specific U34 modifications.

1.2 TRANSLATIONAL ELONGATION

Translation takes place in ribosomes and is a fundamental partial process of gene expression in all living organisms. The ribosome is composed of 2 subunits. The large subunit, refereed to as 60S subunit, consists of the 28S rRNA the 5.8S rRNA, the 5S rRNA and 46 ribosomal proteins that bind to the surface of the rRNA. The small subunit, called 40S subunit, is composed of the 18S rRNA and 33 proteins. The ribosome has 3 tRNA binding sites named A-(aminoacyl-), P-(peptidyl-) und E-(exit-)Site. At the A-site codon recognition takes place and at the E-site the empty tRNA leaves the ribosome. The P-site is the only site that is permanently occupied during translational elongation. Translational initiation as well as translational termination are highly complex processes which are comprehensively reviewed in [34, 35]. Translational elongation can be divided in 4 major steps. The first, and rate limiting step of translational elongation is the codon recognition, in which the eukaryotic eF-Tu counterpart eEF1-GTP-tRNA complex binds to the ribosomal A-site [36]. Followed by GTP hydrolysis, eEF1-GDP leaves the ribosome. If the tRNA does not recognize its designated codon, the tRNA is rejected and leaves the A-site. The process of codon recognition starts from the beginning. If

the codon-anticodon recognition is correct, the accommodation process takes place where the amino acid of the A-site tRNA is brought in spacial vicinity of the amino acid chain of the tRNA in the P-site. This is followed by the peptide bond formation, where the amino acid chain of the P-site tRNA is covalently bound to the A-site tRNA. Afterwards, translocation occurs in which the eEF2-GTP complex binds to the ribosome and pushes it (under GTP hydrolysis) one codon further and the tRNAs are moving from their initial ribosomal site to the next. The structural basis of the translational elongation cycle is reviewed in [37].

1.3 THE ELONGATOR COMPLEX

The Elongator complex was first discovered in 1999 as part of the RNA polymerase II holoenzyme [38]. The complex consists of 6 proteins (Elp1 - Elp6) and can be divided in 2 subcomplexes; The Elp123 subcomplex, also referred to as the core complex and the Elp456 subcomplex, referred to as the HAP (Histone acetyl transferase Associated Protein) complex [39]. Figure 4 shows the 6 different proteins with their different domains.

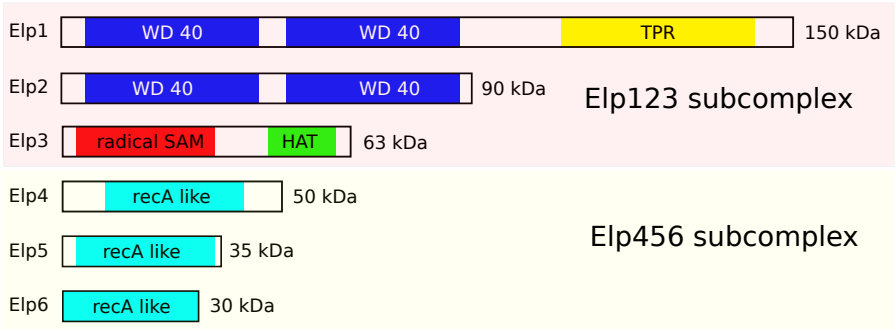

Figure 4: The proteins of the Elongator complex.

A schematic overview of the 6 Elongator subunits. Different protein domains indicated. The WD40 repeat beta propeller domains of Elp1 and Elp2 indicated in blue. The TPR (tetratricopeptide repeat) domain of Elp1 is marked yellow. The radical SAM domain indicated in red and the HAT (histone acetyltransferase) domain indicated in green. The recA like domains of Elp4, Elp5 and Elp6 are indicated in turquoise. Picture taken and modified from [23].

Elp1 is the largest of the Elongator proteins. It has a size of about 150 kDa and consists of 2 WD 40 repeat domains that form beta propeller structures and a TPR (tetratricopeptide repeat) domain. It serves as the major scaffold protein of the complex and binds Elp2, Elp3 as well as to itself [40] (Figure 5 A). One side of the Elp123 dimer then binds Elp4 of the Elp456 subcomplex [41, 42] (Figure 5 C). Elongator activity is modulated by a complex phosphorylation pattern at

the TPR domain of Elp1 [43, 44]. Additonally, it was shown that a conserved and essential basic region at the C-terminus of Elp1 mediates tRNA binding to the Elp1 subunit [45].
Elp2 consists of two WD 40 repeat domains that form beta propeller [46]. It was shown in yeast that Elp2 is the only protein of the complex that is not required for complex formation but it is indispensable (like all other Elongator proteins) for the activity of the complex [47, 48].
Elp3 is the catalytic subunit of the complex. It is the only subunit that can also be found in some prokaryotes and even some viruses. It consists of a radical S-adenosylmethionine (SAM) domain and a histone acetyltransferase (HAT) domain. Both domains are required for the 5-carboxyl modification of Uracil 34 in the anticodon of certain tRNA. Several studies associate the HAT domain with a variety of processes other than tRNA modification. The findings of those studies are based on loss of function and *in vitro* experiments [49, 50]. Glatt and colleagues showed with a crystal structure of Elp3 from *Dehalococcoides mccartyi*, that the peptide binding site of the HAT domain is fully blocked by the radical SAM domain [51]. Therefore it is unlikely that Elp3 shows any HAT activity towards proteins.
The Elp456 subcomplex features recA-like protein folding and adopts heterocyclic conformation with two copies of every subunit in the ring (Figure 5 B). Two independent crystal structures are available [52, 53]. It was shown that the ring binds to tRNA and releases it on ATP hydrolysis [53].

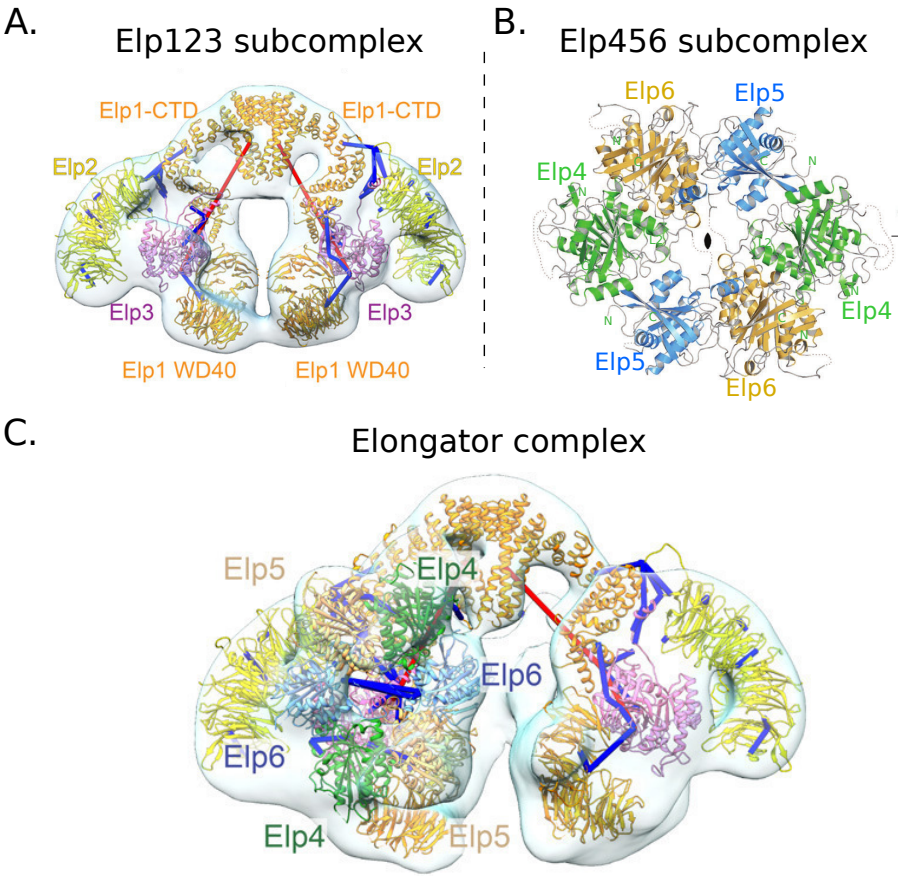

Figure 5: Model of the Elongator complex and its subcomplexes.
A. The Elp123 subcomplex. Elp1 is the major scaffold protein that binds Elp2 and Elp3. Elp1 forms also a dimer at the C-terminal end of the TPR domain, resulting in a stoichiometry of two Elp1, two Elp2 and two Elp3 proteins in the subcomplex. **B.** The Elp456 subcomplex. The subcomplex forms a heterocyclic recA like ring structure with two copies of every subunit. **C.** Model of the holo-Elongator. Interaction of the two subcomplexes is mediated via the beta propeller structure of Elp1 with the Elp4 subunit of the Elp456 subcomplex. Panel A and C taken and modified from [41]. Panel B taken and modified from [53].

1.3.1 *Elongator mutant phenotypes*

Since the discovery of the complex, many different functions in different organisms were associated with the Elongator complex ranging from enhancing transcriptional elongation [38], histone acetylation [50], DNA demethylation [54], tubulin acetylation [55], polarized exocytosis [56] to tRNA modification [20]. Most of the associated functions are based on phenotypes of Elongator-deficient cells. In yeast, at least the phenotypes of transcriptional elongation and polarized exocytosis can be rescued by elevated levels of unmodificed tRNA tK^{UUU} and tQ^{UUG} [32]. Investigations on tRNA copy number and codon usage of genes grouped in functional pathways brought some striking observations in *Schizosaccharomyces pombe* [57] and it is equally true for *S. cerivisiae*. Unlike one would expect by looking at the overall codon usage of the lysine (60% AAA and 40% AAG), highly expressed genes prefer AAG (70%) over AAA (30%). Genes of functional pathways associated with Elongator mutant phenotypes have a codon usage that prefers the lysine AAA codon over AAG [57]. In Elongator mutants, expression levels of the corresponding gene products are reduced, giving rise to the specific phenotypes. Bauer and colleagues showed that the Cdr2 expression level, which is reduced in Elongator mutants, can be increased to wild type level by either overexpression of tK^{UUU} or changing the AAA codon to the synonymous AAG codon [57]. Their data supports a transcript specific expression phenotype by codon bias.

Nedialkova and Leidel found in their study, by performing ribosome profiling of yeast cells, that translation efficiency of codons, which rely on Elongator dependent modified tRNA, is reduced in Elongator deficient cells [31]. As a consequence, they found that the whole translational machinery can become aggregated if the translation efficiency is reduced. Surprisingly, when further analyzing the protein aggregates that formed in the yeast mutants, they found no enrichment of proteins with an AAA codon bias. Instead "error prone" proteins, that rely on high abundance of chaperones, were the predominant proteins in the aggregates. They concluded from these observations, that Elongator mutants do not show specific phenotypes due to loss of function of gene products with a certain codon bias, but that the growth phenotypes of the mutants are due to proteolytic stress and different signaling pathways [31].

Both models are not mutually exclusive since there is clear experimental evidence for both of them as reviewed in [30].

1.3.2 *γ-toxin, an Elongator modification dependent ribonuclease of* tE^{UUC}

Γ-toxin is the γ-subunit of the trimeric *K. lactis* killer-toxin zymocin [58]. Zymocin is secreted to the surrounding environment to inhibit

the growth of other yeast [59]. The α- and β-subunit of the secreted toxin are virulence factors that facilitate the transfer of the γ-subunit into cell [60].

The discovery of the function and intracellular target of γ-toxin is directly connected to the discovery of the function of the Elongator complex. Screenings of yeast mutant libraries on γ-toxin sensitivity/insensitivity found 14 different genes named killer toxin insensitive (kti 1-14) and toxin target (tot 1-7). Under those kti and tot genes *elp1* to *elp6* were found [61–63]. The Elongator complex was associated with many different cellular functions and distinct stress phenotypes (see 1.3.1). In fact all kti and tot genes were found to be directly involved in or modulators of the U_{34} modification. Two studies discovered that γ-toxin is an anticodon endonuclease targeting tE^{UUC} at the fully modified mcm^5s^2U34 nucleotide [20, 64]. Intracellular γ-toxin leads to tE^{UUC} translation impairment, resulting in growth inhibition and eventually to cell death [64]. Mutants missing parts of or full Elongator dependent U_{34} modification are resistant to the presence of γ-toxin since the toxin does not cleave unmodified tE^{UUC} (*in vivo*) [47, 64, 65].

The study on γ-toxin not only provided the first indications of the function of the Elongator complex, it also provided the tools that allowed to investigate on the complex and gene network involved in the Elongator dependent U_{34} modification. So called killer assays, plug growth assays of different *S. cerevisiae* strains together with the zymocin secreting killer yeast *K. lactis*, were one of the fundamental experiments that formed our understanding of the genes involved in the Elongator dependent U_{34} modifications [43, 47, 61, 63, 65–68]. Today, these assays remain a fast and inexpensive molecular diagnostic tool to assign function to different proteins and protein motifs that are involved in the the U_{34} modification [69].

1.4 DICTYOSTELIUM DISCOIDEUM

Dictyostelium discoideum is a eukaryotic model organism that belongs to the evolutionary supergroup of Amoebozoa. The organism features a haploid genome of 34 Mb on 6 chromosomes with 12,500 genes [70]. Like all Amoebozoa species, the rDNA has no chromosomal location and is instead located on extrachromosomal elements. The overall GC content of 23% (27% in gene coding sequences) of the genome is one of the lowest found among eukaryotes [70]. The proteome of the organism shows a high abundance of low complexity stretches with extended polyglutamine and polyasparagine stretches that are known to form amyloid structures, making it the prion-richest proteome known to date [71].

Also the life cycle of the organism is nothing less than astonishing. *Dictyostelium discoideum* is a soil living protist that feeds on bacteria.

Upon starvation the cells secrete cyclicAMP (cAMP) as a quorum sensing signal. The cells then migrate towards the peak concentration of the cAMP. In the process 100,000 to 1,000,000 cells come together and form a multicellular organism that can react to chemical and light stimuli. The so called slug looks for a suitable position for culmination. The end of the process results in the emergence of a fruiting body that releases spores to the surrounding. [72]. Figure 6 illustrates the life cycle of *D. discoideum*.

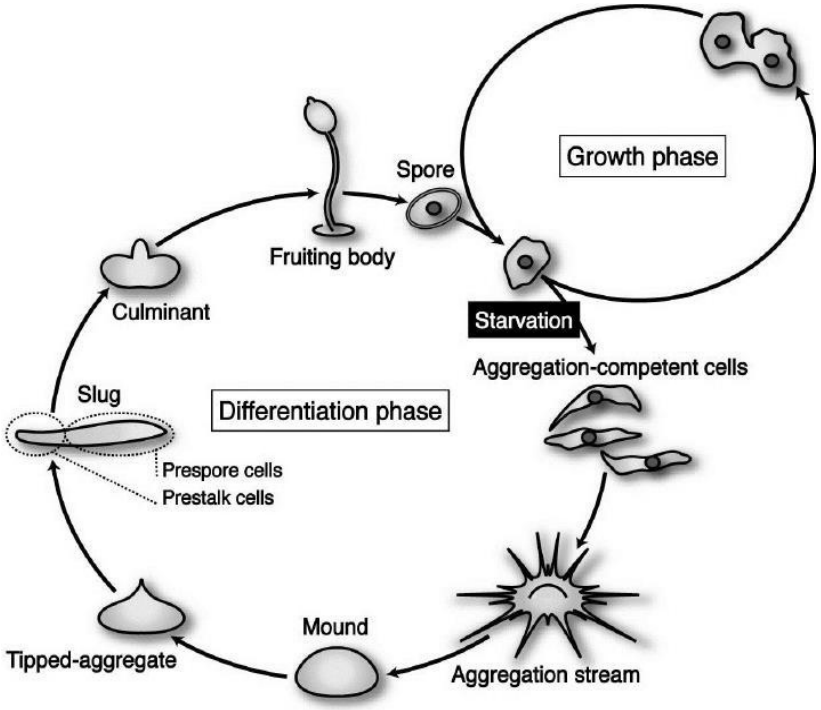

7

Figure 6: *D. discoideum* life cycle.

The image shows the different developmental phases of *D. discoideum*. *D. discoideum* is a soil living protist that feeds on bacteria. Upon starvation 100,000 to 1,000,000 cells aggregate and undergo differentiation. The end of the process results in the emergence of a fruiting body that releases spores to the surrounding. Picture taken from [73].

1.5 AIM OF THIS THESIS

The study and comparison of fundamental cellular processes in different phyla provides an inside into evolutionary processes. Sometimes the findings even give rise to new technologies, like CRISPR/Cas9 - the most famous example nowadays [74, 75].

Ciliata, for example, feature 4 instead of 2 codons for glutamine [76, 77]. The tRNA decoding the codons do not feature any Elongator dependent modification [78]. So far no functional studies of Elongator

dependent tRNA modification have been reported in the evolutionary supergroup of Amoebozoa. The aim of the thesis is to elucidate the presence and effects of the Elongator dependent U_{34} modification in *Dictyostelium discoideum* as well as the identity of the complex itself.

In particular, the following questions were addressed:

- How many proteins does the Elongator consist of in *D. discoideum*?
- What is the stoichiometry of the Elongator complex in *D. discoideum*?
- Are the Elongator dependent tRNA modifications conserved in *D. discoideum*?
- Can effects on translation of glutamine codons be observed?

2 MATERIALS AND METHODS

2.1 MATERIALS

2.1.1 *Equipment and Apparatus*

Äkta FPLC	GE Healthcare, Pharmacia
Autoclave (3870 ELVC)	Tuttnauer, Wesel
Binocular	Zeiss, Jena
Blotting equipment	
PAA gels (Trans-Blot Cell 170-3949)	Biorad, München
Semidry blot (Fastplot)	Biometra, Göttingen
Tank blot (XCell II^{TM} Blot Module)	Invitrogen, Karlsruhe
Incubator	Memmert, Schwabach
Coulter Counter model ZM	Coulter Electronics, Krefeld
Casy Cell Counter and Analyzer	Roche, Basel
Electrophoresis chambers	
Agarose gels	Metallwerkstatt, Universität Kassel
Agarose gels (Mupid One)	Advance Co., LTD Japan
PAA Gels	Metallwerkstatt, Universität Kassel
Protein gels (SE 250)	Hoefer Pharmacia, SF, USA
Protein gels (Xcell-SureLock^{TM}-Mini-Cell)	Invitrogen, Karlsruhe
Electroporator (GenePulser Xcell^{TM})	Invitrogen, Karlsruhe
Precision balance (1413 MP8)	Sartorius, Göttingen
Gel documentation	Intas, Göttingen
Geiger counter (Mini-Monitor)	Mini-Instruments, GB
Heating blocks	
Accu Block Digital Dry Bath	LabNet International, Edison, USA
Block thermostat BT100	Kleinfeld Labortechnik, Gehrden
Magnet stirrer	IKA Labortechnik, Staufen
MALDI mass spectrometer AutoflexII TOF/TOF	Bruker Daltonics, Bremen
Microliter pipetts Discovery Comfort	Abimed, Langenfeld
Microscopes	
Axioplan 2	Zeiss, Jena
Axio Zoom	Zeiss, Jena
LSM 510 ConfoCor 2	Zeiss, Jena
Microwave (Lunik 250)	Aldi, Essen
Neubauer counting chamber	Brand, Wertheim/Main

PCR machines	
FlexCycler	Analytik Jena, Jena
Mastercycler personal	Eppendorf, Hamburg
Mastercycler ep realplex	Eppendorf, Hamburg
Primus 25 advanced®	PEQLAB, Erlangen
pH-Meter (HI 221)	Hanna Instruments, Kehl am Rhein
Photometer	
BioPhotometer plus	Eppendorf, Hamburg
NanoDrop 2000 Spectrophotometer	Fisher Scientific, Schwerte
Phospho imager (FLA-5000)	Fujifilm, Düsseldorf
Rolling incubator	Schütt, Göttingen
Shaking incubators	
Cell culture shaker	Infors AG, Bottmingen
Cell culture shaker (Laboshake RO 500)	Gerhardt, Königswinter
Thermo shaker (TS-100)	ProfiLab24, Berlin
Power supply	
Consort EV 232	Consort, Turnhout, Belgien
Enduro^{TM} 300V	LabNet International, Edison, USA
EPS 200, EPS 600, EPS 3500	Pharmacia Biotech, Freiburg
Superose 6 Increase (3.2 x 300 mm) FPLC column	GE Healthcare, Pharmacia
Sterile bench (*E. coli*)	Galaire, Italien
Sterile bench (*D. discoideum*)	Nunc, Wiesbaden
UV table	Biostep, Jahnsdorf
UV crosslinker (Biolink DNA Crosslinker)	Biometra, Göttingen
Vacuum centrifuge	Bachofer, Reutlingen
Vortex (Genie 2)	Scientific Industries, Boehemia, USA
Water bath (Multitemp III)	Pharmacia Biotech, Freiburg
Centrifuges	
Centrifuge 5415R	Eppendorf, Hamburg
Centrifuge 5417C	Eppendorf, Hamburg
Centrifuge 5424	Eppendorf, Hamburg
Multifuge 1 S-R	Heraeus, Hanau
Rotina 380 R	Hettich, Tuttlingen
Sprout® Mini-Centrifuge	Heathrow Scientific, Northgate, UK
Universal 32	Hettich, Tut

2.1.2 *Consumables*

Beakers	Schott, Mainz
Costar plates	Sarstedt, Nürnbrecht
Dialysis tube (ZelluTrans V-Serie MWCO 25000) — Roth, Karlsruhe	

Gloves (Hansa Medical)	Kirchhoff Group, Hamburg
Scalpel	Bayha, Tuttlingen
Cuvettes (1 mL)	Sarstedt, Nümbrecht
Syringes (Omni-Fix 1 mL)	B. Braun, Melsungen
Tissue	Kimberly-Clark, Forchheim
EP Cuvettes (VWR Collection 4 mm)	VWR, Darmstadt
Erlenmeyer flask	Roth, Karlsruhe
Falcon tube (15 mL, 50 mL)	Sarstedt, Nürnbrecht
Filter paper (3 mm Chr)	Whatman, Dassel
Fritten für PP-Säule	Roth, Karlsruhe
Glass bottles	Schott, Mainz
Glass pipettes	Hirschmann, Eberstadt
Ni-NTA Agarose	Qiagen, Hilden
Nitro cellulose filter (Typ HAWP 04700)	Millipore, Eschborn
Porablot™ NCP (Protein)	Macherey-Nagel, Düren
Mounts	Menzel-Gläser, Braunschweig
Parafilm	Schütt, Göttingen

PCR reaction tubes

PCR reaction tubes	Sarstedt, Nürnbrecht
0.2 mL LP Strips Tubes, 8-Strips	Biozym, Oldendorf
Optical Flat Cap Strips	Biozym, Hess. Oldendorf
Petri dish	Sarstedt, Nürnbrecht
Pipette tips	Sarstedt, Nürnbrecht
Test tubes	Roth, Karlsruhe
Reaction vessel (1.5 mL; 2 mL)	Sarstedt, Nürnbrecht
Reaction vessel with Screw cap (1.5 mL; 2 mL)	— Sarstedt, Nürnbrecht
SPE-Column 6 mL	Roth, Karlsruhe
Sterile filter	Sarstedt, Nürnbrecht
Streptactin column	Iba, Göttingen

2.1.3 *Chemicals*

Acetic acid (99%)	Roth, Karlsruhe
Acetonitrile	Merck, Darmstadt
Acrylamide/Bisacrylamide (30%, 40%)	Roth, Karlsruhe
Agarose	Biozym, Hess. Oldendorf
Agar-Agar	AppliChem, Darmstadt
Aluminium bicarbonate	Sigma, Taufkirchen
Aluminium sulfate	Roth, Karlsruhe
APM	AG Leidel, MPI Münster
APS	Roth, Karlsruhe
Bacto-Trypton	Roth, Karlsruhe
Biotin	Iba, Göttingen
BCIP-T	Thermo Scientific, Waltham, MA

Boric acid	Roth, Karlsruhe
Bromophenol blue	Fluka, Deisenhofen
BSA	Roth, Karlsruhe
Calcium chloride	Roth, Karlsruhe
Chloroform	Sigma, Taufkirchen
Coomassie Brillant Blue G-250	Serva, Heidelberg
Desthiobiotin	Iba, Göttingen
Disodium hydrogen phosphate	Roth, Karlsruhe
Dipotassium hydrogen phosphate	Roth, Karlsruhe
DMF	Merck, Darmstadt
DMSO	Sigma, Taufkirchen
DTBP	Thermo Scientific, Waltham, MA
DTT	Roth, Karlsruhe
EDTA	Roth, Karlsruhe
Ethanol (>99.8%)	Roth, Karlsruhe
Ethidium bromide	Roth, Karlsruhe
Formamide	Roth, Karlsruhe
Glucose	Roth, Karlsruhe
Glycerol (86%)	Roth, Karlsruhe
Glycine	Roth, Karlsruhe
Urea	Roth, Karlsruhe
Yeast extract	Roth, Karlsruhe
HEPES	Roth, Karlsruhe
HL5 medium	ForMedium, Norfolk GB
Imidazole	Roth, Karlsruhe
IPTG	Roth, Karlsruhe
Isopropanol (99%)	Roth, Karlsruhe
Lithium chloride	Roth, Karlsruhe
Potassium chloride	Roth, Karlsruhe
Potassium dihydrogen phosphate	Roth, Karlsruhe
Milk powder (skim)	Roth, Karlsruhe
Magnesium chloride	Roth, Karlsruhe
Magnesium sulfate	Merck, Darmstadt
β-Mercaptoethanol	Fluka, Deisenhofen
Methanol (99%)	Roth, Karlsruhe
MOPS	Roth, Karlsruhe
Nonident®P40 (NP40)	Fluka, Deisenhofen
Peptone from Casein	Roth, Karlsruhe
Phenol/Chloroform/Isoamylalkohol	Roth, Karlsruhe
Phosphoric acid	Fluka, Deisenhofen
Roti®-Quant (Bradford reagent)	Roth, Karlsruhe
Saccharose	Roth, Karlsruhe
hydrochloric acid (37%)	Merck, Darmstadt
SDS	Roth, Karlsruhe
Sephadex G-50 (Fine)	GE Healthcare, München
Sodium acetat	Roth, Karlsruhe

Sodium chloride	Roth, Karlsruhe
Sodium citrate	Roth, Karlsruhe
Sodium dihydrogen phosphate	Roth, Karlsruhe
Sodium hydrogen phosphate	Roth, Karlsruhe
Sodium hydroxide	Roth, Karlsruhe
Trichloroacetic acid	Roth, Karlsruhe
TEMED	Roth, Karlsruhe
Tris	Roth, Karlsruhe
Tri sodium citrate	Merck, Darmstadt
Tris acetate	Roth, Karlsruhe
TritonX-100	Roth, Karlsruhe
Tween® 20	Roth, Karlsruhe
Xylencyanol	Fluka, Deisenhofen

2.1.4 *Buffers and Solutions*

Alkaline Phosphatase (AP) buffer	100 mM Tris/HCl, pH 9.5 100 mM NaCl 5 mM $MgCl_2$
BCIP solution	50 mg/mL BCIP-T in DMF
Blocking solution	2% w/v skim milk powder in 1× NCP
Coomassie solution (colloidal)	0.02% w/v Coomassie BrillantBlue G-250 5% w/v Aluminum sulfate 2% v/v ortho-Phosphoric acid 10% Ethanol
Coomassie destaining solution	10% Ethanol 2% v/v ortho-Phosphoric acid
Transcription buffer (10×)	400 mM Tris/HCl, pH 8.0 200 mM $MgCl_2$ 20 mM Spermidin 0.1% w/v TritonX-100
DNA loading dye (6×)	20 mM Tris/HCl, pH 8.0 120 mM EDTA 50% w/v Glycerin 0.03% w/v Bromphenol blue 0.03% w/v Xylene cyanol
Electroporation (EP) buffer	10 mM Na_2HPO_4 50 mM Saccharose adjust with H_3PO_4 pH 6.1 , sterile filtrated
Ethidium bromide solution	1 mg/mL Ethidiumbromide in dH_2O
γ-toxin RNA cleavage buffer	50 mM KCl 30 mM $KHPO_4$, pH 7 16.7% v / v Glycerin 0.1 mM EDTA 1 mM DTT

Lämmli buffer (2×)	125 mM Tris/HCl, pH 6.8
	4% w/v SDS
	20% v/v Glycerin
	5% β-Mercaptoethanol
	0.02% w/v Bromphenol blue
Solution I	25 mM Tris/HCl, pH 7.4
	10 mM EDTA
	15% w/v Saccharose
Solution II	200 mM NaOH
	1% w/v SDS
Solution III	3 M Sodium acetate pH 4.7
MOPS buffer for PAA gels	20 mM MOPS, pH 7.0
NCP buffer (10×)	100 mM Tris/HCl, pH 8.0
	1.5 M NaCl
	0.5% w/v Tween® 20
Neutralization solution	1.5 M NaCl
	500 mM Tris/HCl, pH 7.0
Novex®Tris-Glycin transfer buffer (1×)	15 mM Tris
	120 mM Glycin
	10% v/v Methanol
NP40 solution (20%)	20% w/v Nonident® P40 in dH2O
Protease Inhibitor Cocktail (50 x)	50 mM Pefabloc SC
	1.25 mg/mL Leupeptin
	0.5 mg/mL Tosyl-arginine-methylester
	0.5 mg/mL Soybean Trypsin Inhibitor
	0.05 mg/mL Aprotinine
	0.05 mg/mL Pepstatin
	100 mM Benzamidine
adjusted to pH 7.0, store at -80°C	
Protein gel running buffer (5×)	125 mM Tris
	959 mM Glycine
	5% w/v SDS
Protein stacking gel buffer	500 mM Tris/HCl, pH 6.8
	14 mM SDS
Protein seperation gel buffer	1.5 M Tris/HCl, pH 8.8
	14 mM SDS
RNA loading dye	95% v/v Formamide
	17 mM EDTA pH 8.0
	0.025% w/v Bromphenol blue
	0.025% w/v Xylencyanol
γ-toxin cleavage buffer	50 mM NaCl
	30 mM $NaHPO_4$, pH 7
	16.7% v/v Glycerin
	0.1 mM EDTA
	1 mM DTT
SDS running buffer	0.7% w/v SDS in 1× TE-Puffer

Semi dry transfer buffer (1×)	50 mM Tris 40 mM Glycine 1.3 mM SDS 20% v/v Ethanol
Sephadex G-50 Solution	5 g Sephadex G50 100 mL 1× TE Puffer
Soerensen phosphate buffer (1×)	2 mM Na_2HPO_4 15 mM KH_2PO_4 with H_3PO_4 pH 6.0
SSC (20×)	3 M NaCl 300 mM Natriumcitrat pH 7.0
Tankblot buffer (20 x)	300 mM Tris-Base 2.4 M Glycine
TBE buffer (5×)	445 mM Tris pH 8.2 445 mM Boric acid 10 mM EDTA
TE buffer (1×)	10 mM Tris/HCl, pH 7.5 or 8.0 1 mM EDTA
Quick and Dirty DNA extr. buffer	50 mM KCl 10 mM TRIS pH 8.3 2.5 mM MgCl2 0.45% NP40 0.45% Tween 20 + Proteinase K*

*1 µL of Proteinase K [20 mg/mL] was added freshly to every sample

Buffers for protein purification:

buffer composition for protein purification (otherwise stated)
D. discoideum:
GFP trap:

Lysis buffer	100 mM NaH_2PO_4 25 mM Tris HCl, pH 7 0.1 mM DTT 1 mM $MgCl_2$ *1% NP40

* only added when detergent lysis was performed

Wash buffer:	100 mM NaH_2PO_4 25 mM Tris Cl Tris, pH 7 0.1 mM DTT 1 mM $MgCl_2$

Strep purification:

Lysis buffer	100 mM NaH_2PO_4 25 mM Tris Cl Tris, pH 7.5 0.1 mM DTT 1 mM $MgCl_2$
Wash buffer	100 mM NaH_2PO_4 25 mM Tris Cl Tris, pH 7.5

	0.1 mM DTT
	1 mM $MgCl_2$
Elution buffer Lysis buffer	100 mM NaH_2PO_4
	25 mM Tris Cl Tris, pH 7.5
	0.1 mM DTT
	1 mM $MgCl_2$
	2.5 mM Desthiobiotin
E. coli:	
MBP-purification:	
Lysis buffer	125 mM NaH_2PO_4
	50 mM Tris Cl Tris, pH 7
	0.1 mM DTT
	1 mM $MgCl_2$
	*Lysozym
* 1 mg per mL cell suspension desolved in lysis buffer	
Wash buffer	125 mM NaH_2PO_4
	50 mM Tris Cl Tris, pH 7
	0.1 mM DTT
	1 mM $MgCl_2$
Elution buffer:	125 mM NaH_2PO_4
	50 mM Tris Cl Tris, pH 7
	0.1 mM DTT
	1 mM $MgCl_2$
	10 mM Maltose

Fresh protease inhibitor mix was added to all lysis buffers before cell lysis was performed

2.1.5 *Antibiotics*

Amphotericin (0.25 mg/mL)	PAA, Cölbe
Ampicillin (50 mg/mL)	Roth, Karlsruhe
Blasticidin (5 mg/mL)	Sigma, Taufkirchen
Geniticin G418 (100 mg/mL)	PAA, Cölbe
Penicillin (10000 u/mL)/Streptomycin (10 mg/mL) —	PAA, Cölbe
Kanamycin (50 mg/mL)	Roth, Karlsruhe
Chloramphenicol (35 mg/mL)	Roth, Karlsruhe
Hygromycin B (20 - 100 mg/mL)	Applichem-Panreac, Darmstadt

2.1.6 *Nutrition media*

2.1.6.1 *Media for E. coli cultivation*

LB medium, pH 7.0	10 g Bacto-Trypton
	5 g yeast extract

	5 g H_2O NaCl ad 1 L dH_2O
LB Amp medium	LB-Medium + 50 µg/mL Ampicillin
LB Amp/CAM medium	LB-Medium 35 µg/mL Chloramphenicol + 50 µg/mL Ampicillin
LB Kan medium	LB-Medium + 50 µg/mL Kanamycin
LB Kan/CAM medium	LB-Medium 35 µg/mL Chloramphenicol + 50 µg/mL Kanamycin
LB Agar	LB-Medium + 13 g/L Agar-Agar
LB Amp Agar	LB-Agar + 50 µg/mL Ampicillin
LB Kan Agar	LB-Agar + 50 µg/mL Kanamycin

2.1.6.2 *Media for D. discoideum*

BS10 Medium	G0 Medium + 10 µg/mL Blasticidin
BS10/G10 Medium	G0-Medium + 10 µg/mL Blasticidin + 10 µg/mL Geniticin (G418)
G0 Medium	HL5 Medium + 50 µg/mL Ampicillin + 0.25 µg/mL Amphotericin + 100 Einheiten/mL Penicillin + 100 µg/mL Streptomycin
G10 Medium	G0 Medium + 10 µg/mL Geniticin (G418)
HL5 Medium pH 6,7 (ForMedium)	14 g Pepton 7 g Yeast extract 13.5 g Glucose 0.5 g KH_2PO_4 0.5 g Na_2HPO_4 ad 1 L d H_2O
Phosphate agar	Soerensen Phosphate buffer 13 g/L Agar-Agar
SM-Agar pH 6.5	13 g Agar-Agar 10 g Peptone from Casein 10 g Glucose 1 g yeast extract 1 g $MgSO4 \cdot 5\ H_2O$

2.2 g KH_2PO_4
1.43 g $Na_2HPO_4 \cdot 3\ H_2O$
ad 1 L d H_2O

2.1.7 *Nucleotides*

Desoxyribonucleotides	Thermo Scientific, Waltham, MA
Ribonucleotides	Thermo Scientific, Waltham, MA
^{32}P-UTP (3000 Ci/mmol, 10 µCi/µl)	Hartmann Analytic, Braunschweig
^{32}P-UTP (110 TBq/mmol)	Hartmann Analytic, Braunschweig

2.1.8 *Antibodies*

Mouse anti GFP (264–449–2)	Universität Kassel, Kassel
Mouse anti Coronin	AG Markus Maniak, Universität Kassel
Mouse anti Discoidin	AG Markus Maniak, Universität Kassel
Rabbit anti GFP	Dianova, Hamburg
Mouse anti Biotin (B7653)	Sigma, Taufkirchen
Rabbit anti RFP Antibody (R10367)	Invitrogen, Darmstadt
AP coupled goat anti rabbit (115-055-003)	Dianova, Hamburg
AP coupled goat anti mouse (111-055-003)	Dianova, Hamburg
Mouse anti FLAG	Sigma, Taufkirchen
Mouse anti Strep-Tag II	Novagen, Darmstadt

2.1.9 *Kits*

GeneJET™ Gel Extraction Kit	Thermo Scientific, Waltham, MA
Gene Elute HP Plasmid Miniprep Kit	Sigma, Taufkirchen
CloneJET™ PCR cloning Kit (pJET1.2)	Thermo Scientific, Waltham, MA
StarGate® cloning kit	IBA, Göttingen

2.1.10 *Size markers*

GeneRuler Ultra Low Range DNA Ladder (#SM1213)	Thermo Scientific, Waltham, MA
GeneRuler 100bp DNA Ladder Plus (#SM0321)	Thermo Scientific, Waltham, MA
GeneRuler 1kb DNA Ladder (#SM0311)	Thermo Scientific, Waltham, MA
pUC 19 DNA/Msp I Marker (#SM0221)	Thermo Scientific, Waltham, MA
Prestaind Protein Molecular Weight Marker (#SM0441)	Thermo Scientific, Waltham, MA
PageRuler™ Plus Prestained Protein Ladder (#SM1811)	Thermo Scientific, Waltham, MA

2.1.11 *Enzymes and Enzyme buffers*

DNaseI (RNase free) (1 u/µL)	Thermo Scientific, Waltham, MA
FastAP™ thermos. Alkaline Phosphatase (1 u/µL)	Thermo Scientific, Waltham, MA
HRV 3C Protease	Novagen, Darmstadt
10 × HRV 3C Protease buffer	Novagen, Darmstadt
conventional Restriction enzymes (10 u/µL)	Thermo Scientific, Waltham, MA
Pfu DNA polymerase (recombinant)	Universität Kassel, Kassel
Pfu DNA polymerase (recombinant) (2.5 u/µL)	Thermo Scientific, Waltham, MA
ProteinaseK	Roth, Karlsruhe
RiboLock™ RNase Inhibitor (40 u/µL)	Thermo Scientific, Waltham, MA
RNaseA (1 mg/mL)	Merck Biosciences, Bad Soden
S1 Nuclease (100 u/µL)	Thermo Scientific, Waltham, MA
Taq DNA Polymerase (recombinant)	Universität Kassel, Kassel
Taq DNA Polymerase (recombinant) (1 u/µL)	Thermo Scientific, Waltham, MA
T4 DNA Ligase (5 u/µL)	Thermo Scientific, Waltham, MA
T4 DNA Polymerase (5 u/µL)	Thermo Scientific, Waltham, MA
T4 Polynucleotid Kinase (T4 PNK) (10 u/µL)	Thermo Scientific, Waltham, MA
T7 RNA-Polymerase (20 u/µL)	Thermo Scientific, Waltham, MA
10× FastAP™ buffer	Thermo Scientific, Waltham, MA
10× Taq buffer (+KCl, +$MgCl_2$)	Thermo Scientific, Waltham, MA
10× T4 Ligase buffer (+DTT)	Thermo Scientific, Waltham, MA
10× T4 PNK Reaction buffer A	Thermo Scientific, Waltham, MA

Unless otherwise indicated all other enzymes were purchased from Thermo Scientific, Waltham, MA

2.1.12 *Oligonucleotides*

All the oligonucleotides used were obtained from Sigma (Taufkirchen) and are listed in Section A.4.2

2.1.13 *Software*

AIDA Imager Analyzer	Raytest, Straubenhardt
AxioVision	Zeiss, Jena
Benchling	Benchling inc, San Francisco, USA
BioEdit Sequence Alignment Editor	Ibis Biosciences, Carlsbad
GIMP 2 (GNU Image Manipulation Program)	The GIMP Team
Inkscape	Vector Graphic Program
Latex	
LSM Image Browser	Zeiss, Jena
Vector NTI AdvanceTM 9	Invitrogen, Karlsruhe
ZEN	Zeiss, Jena
python	Python Software Foundation
Unicorn	GE Healthcare, Pharmacia
Excel	Microsoft, USA
FlowJo	FlowJo, LLC
MSConvert	http://proteowizard.sourceforge.net/
mMass	http://www.mmass.org
MultiGauge 3.2	Fujifilm, Deutschland

2.1.14 *Sequences*

Table 1: Overview of DNA sequences used in this thesis

GENE	ORGANISM	DATABASE ENTRY
ctu1	*D. discoideum*	DDB_G0282921
elp1	*D. discoideum*	DDB_G0284075
elp2	*D. discoideum*	DDB_G0275651
elp3	*D. discoideum*	DDB_G0290103
elp4	*D. discoideum*	DDB_G0278783
elp5	*D. discoideum*	DDB_G0276569
elp6	*D. discoideum*	DDB_G0268624
erkA	*D. discoideum*	DDB_G0286353
ppp6c	*D. discoideum*	DDB_G0272118
urm1	*D. discoideum*	DDB_G0283737
trm9	*D. discoideum*	DDB_G0292448
trm112	*D. discoideum*	DDB_G0285489
tRNA-Gln-UUG-13	*D. discoideum*	DDB_G0295309
tRNA-Gln-CUG-1	*D. discoideum*	DDB_G0294975
tRNA-Glu-UUC-5	*D. discoideum*	DDB_G0294789
tRNA-Gly-GCC-5	*D. discoideum*	DDB_G0295037
tRNA-Lys-UUU-23	*D. discoideum*	DDB_G0284075
malE	*E. coli*	948538[a]
tRNA-Glu-UUC	*E. coli*	2658478[a]
extended human huntingin exon 1	*H. sapiens*	3064[a]
γ-toxin	*K. lactis*	P09807[a]
IKI3 (*elp1*)	*S. cerevisiae*	851100[a]
elp3	*S. cerevisiae*	856019[a]
tRNA-Lys-UUU	*S. cerevisiae*	852671[a]
tRNA-Glu-UUC	*S. cerevisiae*	852784[a]
Q15	synthetic	-

[a] NCBI database (www.ncbi.nlm.nih.gov/gene/)

2.1.15 *Plasmids*

The here presented plasmids were generated by others or purchased from commercial producers. These plasmids were either used directly in experiments or served as a basis for own plasmid generation.

pDEX RH NLS-Cre	[79]
pDM304	[80]
pDM304 TwinStrep-Flag(N)	[81]
pDM304 TwinStrep-Flag(C)	[81]
pDM317 GFP	[80]
pDM318 mRFP	[80]
pDM323 GFP	[80]
pDM324 mRFP	[80]
pDM326	[80]
pDM353	[80]
pDM359 TwinStrep-Flag(N)	[82]
pDM359	[83]
pDneo2a GFP	[84]
pDM353 Q103	[71]
pET-2E	https://www.addgene.org/29665/
pET-LIC (2A-T)	https://www.addgene.org/29775/
pJET1.2/blunt Cloning Vector	Thermo Scientific, Waltham, MA
pET-2E Elp456	[85]
pDneo2a Elp1 Strep	[86]
pDneo2a Elp3-GFP	[87]
pABY1633	[64]
pABY1650	[64]
pKOSG	Iba, Göttingen

2.1.16 *Organisms*

The here presented strains were generated by others or purchased from commercial producers. These strains were either used in experiments or served as a basis for own strain generation.

bacterial strains

E. coli DH5α	Invitrogen, Karlsruhe
E. coli BL21 (DE3) pLysS	Invitrogen, Karlsruhe
E. coli BL21 (Codon plus (R)) RIL	Invitrogen, Karlsruhe
Enterobacter aerogenes (Klebsiella aerogenes)	DictyStock Center, Universität Chicago, USA

eukaryotic Strains

D. discoideum Ax2 wilde type	[88]
D. discoideum elp1^{rox}	[86]
D. discoideum elp2^{flox}	[87]
D. discoideum Ax2 pDneo2a DrnA-GFP	[82]

2.1.16.1 *Overview of D. discoideum and E. coli strains*

An overview of all *D. discoideum* and *E. coli* strains generated in this thesis can be found in the Appendix Section A.4.3.

2.2 METHODS

Parts of the Methods section (particular the Molecular Methods) were taken and modified from the PhD thesis of Janis Melanie Kruse [82] and Marek Malicki [81]. 2.2.3.3 was taken and modified from "Genetik-Praktikumskript 2011 der AG Hammann TU-Darmstadt".

2.2.1 *Data analysis*

- *D. discoideum* codon usage analysis was performed on *D. discoideum* primary CDS (downloaded from www.dictybase.org/). The analysis was performed with biopython (CAI module: https://goo.gl/dgTkdE) and modified to the needs of the analysis. Data visualization was done with matplotlib and excel.
- All Flow cytometer data analysis was performed with the FlowJo software. Comparison of the relative fluorescence intensity of different strains was performed by comparing the geometric means of the peak area of the living *D. discoideum* populations.
- Data from MALDI mass spectrometry was analysed with mMass and the build in MASCOT blast search tool.

2.2.2 *Cell biological Methods*

2.2.2.1 *Cultivation of E. coli*

The cultivation of *E. coli* was performed at 37°C; either on LB agar petri dishes or in LB medium under constant shaking (185 rpm). Antibiotics were added appropriate to the selectable markers carried by the cells. For long term storage, 1 mL of an exponentially growing cell culture (OD_{600} between 0.4 and 1) were mixed with 200 µL sterile glycerol and frozen at -80°C.

2.2.2.2 *Preparation of chemically competent E. coli cells via $RbCl_2$*

10 mL of LB medium was inoculated with a desired *E. coli* cell line and incubated overnight at 37°C and 185 rpm. On the next day, 100 mL of LB medium was inoculated with 2 mL of the preculture and grown to an OD_{600} (optical density at 600 nm) of 0.8. The culture was cooled 15 minutes in an ice bath and then centrifuged at 4000 rpm for 10 minutes. The cell pellet was then resuspended in 40 ml of ice-cold TfbI buffer and again placed on ice for 10 minutes. The cell suspension was again centrifuged at 4000 rpm for 10 minutes and resuspended in 4 mL of ice-cold TfbII buffer. After 20 minutes of incubation on ice, the cell suspension was frozen in 100 µL aliquots (in liquid nitrogen) and stored at -80°C.

2.2.2.3 *Transformation of chemically competent E. coli cells*

Cell aliquots were taken from the -80°C freezer and put on ice for 10 minutes. 10 ng Plasmid (or 50 to 100 ng from a ligation reaction) were added to the cells and incubated for an additional 10 minutes on ice. A Heatshock at 42°C for 90 seconds was performed, followed by a 2 minute incubation on ice. Afterwards 900 µL LB media (without antibiotics) was added to the cells and then incubated at 37°C for 30 minutes to 1 hour (depending on the selectable markers on the Plasmids). After that time, the cells were centrifuged at 4000 rpm for 10 minutes, resuspended in 100 µL fresh LB medium and spread out on LB agar petri dishes containing the respective antibiotic. [89].

2.2.2.4 *Cultivation of E. coli for recombinant protein expression*

The *E. coli* cell line BL 21 Codon$^+$ RIL was generally used for recombinant protein expression. 50 mL of LB medium was inoculated with a desired *E. coli* strain and incubated overnight at 37°C and 185 rpm. On the next day, 1 Volume preculture was mixed with 50 Volumes LB medium and grown to an OD_{600} (optical density at 600 nm) between 0.5 and 0.8. The culture was put on ice for 30 minutes, then inoculated with 0.5 mM IPTG and incubated for 16h to 24h at 16°C 185 rpm.

Cells were harvested by centrifugation at 4000 rpm for 10 minutes and resupended in lysis buffer containing 1 mg Lysozym per 1 mL buffer. Afer 30 minutes incubation on ice the protease inhibitor was added and the cells were lysed via ultrasonication with 20 pulses 5s on 10s off at an amplitude of 85%.

2.2.2.5 *Cultivation of D. discoideum*

The cultivation of *D. discoideum* was carried out at 22°C with constant light. Cells were kept in axenic medium containing various antibiotics to ensure constant selection pressure and reduce a contamination risk. Strains were either kept in petri dishes or in shaking cultures at 150 rpm. Medium exchange was performed every second day.

2.2.2.6 *Transformation of Dictyostelium discoideum cells via electroporation*

2×10^7 cells of a exponential growing cell culture (1×10^6 to 4×10^6 per mL) were spun down at 390 g for 3 minutes. The cell pellets were twice washed with 20 mL Soerensen phosphate buffer and once with 10 mL electroporation buffer. The cells were resuspended in <800 µL electroporation buffer and 10 to 30 µg plasmid DNA was added. The cell suspension was transferred to electroporation cuvettes (4 mm gap) and incubated on ice for 10 minutes. The electroporation had the following parameters: 25 µF, 1 kV (2.5 kV/cm) and 200 Ω. The cuvettes were again incubated for 10 minutes on ice. The cells were then

transferred to petri dishes containing 6 µL 100 mM CaCl and 6 µL 100 mM MgCl and incubated for an additional 15 minutes at room temperature. After that, the cells were covered with 10 mL Go-medium and left over night. The next day the medium was exchanged with HL5 medium containing the proper selection markers. [90];[91].

2.2.2.7 *Subcloning of Dictyostelium discoideum*

For some applications it is necessary to subclone *D. discoideum* cells since after transformation a heterogeneous cell culture is obtained. In order to obtain a homogeneous cultures, subclones from single colonies are cultivated. Therefore the media was removed from petri dishes containing axenic grown *D. discoideum* and the cells were resuspended in 5 mL new medium. 100 µL of this cell suspension were added to 900 µL Soerensen buffer. The cells of 2 *Klebsiella aerogenes* (*K.a.*) covered SM agar plates were resuspended in 5 mL Soerensen buffer. 500 µL of the *Klebsiella aerogenes* suspension were inoculated with 2 to 4 µL of the (1/10) *D. discoideum* cell suspension and plated out on SM Agar plates. The plates were placed on a shelf and incubated at 22°C till feeding halos corresponding to *D. discoideum* colonies were emerging (generally after 3 days incubation). The colonies were picked with a tooth pick and transferred to 24 well plates containing Go medium. On the next day, the Go medium was exchanged with the designated selection medium.

2.2.2.8 *Cultivation of Klebsiella aerogenes (K.a.)*

The taxonomic right name of this organism is *Enterobacter aerogenes* or *Klebsiella mobilis* (homotypisches Synonym). This prokaryot serves as food for *D. discoideum* that are cultivated on agar plates. 100 µL of a *K.a.* stock were defrozen and plated out on SM agar plates. The plates were then incubated at 30°C for 12 h to 24 h and afterwards one additional day at room temperature till the surface was covered with a thick cell layer. The plates could then be stored at 4°C.

2.2.2.9 *Generation of D. discoideum spores*

The permanent storage of *D. discoideum* is done in form of spores. To generate spores, 2×10^8 to 4×10^8 cells were pelleted down with 390 g for 3 minutes and twice washed with 20 mL Soerensen phosphate buffer. The cell pellets were then resuspended in 0.6 to 1 mL Soerensen phosphate buffer and plated on phosphate agar plates. The plates were incubated upside down for 2 to 3 days at room temperature, till the spore heads were formed. The spores were harvested by knocking the plates on a surface. The spore heads thereby lost contact to the agar surface and could be resuspended in an appropriate amount of phosphate buffer (500 µL to 1 mL) and stored at -80°C.

2.2.2.10 *Paraformaldehyde cell fixation of D. discoideum*

D. discoideum cells were usually fixed prior to fluorescent microscopy and confocal laser scanning microscopy (LSM). 20 - 60 µL of the a cell suspension from a petri dish were added on top of a cover slip. After an incubation time of > 30 minutes to allow the cells to attach the media was removed and the cells were covered with 2% paraformaldehyde (PFA) and incubated at 4°C > 2 h or over night. After that fixation was neutralized with 0.2% glycine sultion, followed by 2 times TE buffer wash. DAPI staining was performed for 10 minutes at RT with DAPI solution (4',6-Diamidin-2-phenylindol in TE [0.2 µg/ml]). The cover slip was washed 3 times with TE buffer and once with ddH_2O. Afterwards 20 to 40 µL Mowiol 88 + DABCO were put on the cover slip before it was transferred onto a glass slide.

2.2.2.11 *Fluorescence microscopy*

Strains with GFP and mRFP tagged fusion proteins were subject of localization studies with fluorescence microscopy. Excitation of GFP is at around 395 nm and the characteristic emission is at 509 nm. mRFP exitation is at 584 nm and the emission wave length is at 607 nm. The documentation and generation of the pictures was done either with the software AxioVision or ZEN from Zeiss.

2.2.2.12 *Flow cytometry*

Different *D. discoideum* strains were grown in sterile filtrated HL5 medium on Petri dishes. The use of sterile filtrated medium is crucial to reduce auto fluorescence coming from the media. At a cell density of 80% confluent cover of the Petri dish, cells were harvested by washing them off the plate. 200 to 400 µL of the cell suspension was mixed with 1600 µL Soerensen buffer and injected into the flow cytometer. The injection speed was set to 1 µL per second. The measurement was completed when 30000 events (corresponding to *D. discoideum* cells) were detected. A strain which does not express any fluorescent protein served as a negative control. Fluorescence intensity detection was performed with a logarithmic scale. The Data analysis was performed with the FlowJo software.

2.2.2.13 *Development*

1×10^8 cells were collected from petri dishes (equal to cells from 4 to 5 petri dishes, non-shaking), pelleted down with 390 g for 3 minutes and twice washed with 20 mL Soerensen phosphate buffer. Cell pellets were resuspended in 1 mL Soerensen phosphate buffer and put on one half of a 2 compartment petri dish (mutant strain vs Ax2). The cells were evenly distributed by gentle shaking on an even surface. The cells were allowed to settle for 10 minutes. Excess liquid

was removed from the petri dish. The cultures were then moved to the binocular and pictures were taken every 30 minutes for > 28 h.

2.2.3 *Molecular biological Methods*

2.2.3.1 *Restriction digestion of nucleic acids*

Restriction digestion particular of plasmid DNA was applied to open the plasimds at specific sites for directed cloning or for analytical reasons to verify correct size of the plasmid or correct insertion of an DNA fragment into a plasimd. For this reason (type II) restriction enzymes were used that cleave the phosphodiester bond within a defined recognitions site (usually within a 6 nt long and palindromic). Depending on the chosen enzyme the restriction occurs blunt (without overhangs) or sticky with overhangs on the 5‘ end of the respective stand. Table 2 shows a typical restriction mix of an analytic digestion and Table 3 shows the restriction mix of an preparative restriction digestion. All restriction buffers as well as enzymes are purchased from thermo scientific or NEB.

Table 2: Analytic restriction digestion mix

COMPONENT	VOLUME / AMMOUNT
10× Reaction buffer	5 µL
Restriction enzyme	1 µL
DNA	1–4 µg
dH_2O	ad 50 µL

Table 3: Preparative restriction digestion mix

COMPONENT	VOLUME / AMMOUNT
10× Reaction buffer	5 µL
Restriction enzyme	2 µL
DNA	2–20 µg
dH_2O	ad 50 µL

2.2.3.2 *Ligation of restriction fragments*

DNA ligases catalyze a phosphodiester bond between two compatible DNA fragments. The T_4 DNA ligase was used to ligate the restriction fragments of any used plasmids in this thesis. Before ligation, the linearized plasmid was incubated with the thermosensitive alkalic

Table 4: Ligation mix

COMPONENT	VOLUME / AMMOUNT
10× ligation buffer	2 µL
Backbone	100 ng
Insert	x ng[a]
dH_2O	ad 20 µL

[a]dependent on the length of the insert

phosphatase (FastAP) to remove any free phosphate on the the single ends and thereby preventing selfligation in the ligation process. With this step it can be ensured that the ligation reaction only occurs between the Insert, which features a terminal phosphate and the plasmid backbone. To ensure a good ligation efficiency, the molar masses of the vector and the insert were calculated and a molar ratio of 3 to 1 insert to backbone was used in the ligation reaction. The following formula was used to calculate the amount to be used in the ligation reaction.

$$\frac{\text{Mass Vector [ng]} \times \text{Size Insert [kB]}}{\text{Size Vector [kB]}} \times \text{molar ratio } \frac{\text{Insert}}{\text{Vector}} = \text{Mass Insert [ng]} \tag{1}$$

The ligation reaction itself was usually incubated for 1 hour at room temperature. Table 4 shows the pipetting sheme of the ligation mix.

2.2.3.3 *Ligase independent cloning (LIC)*

Contrary to the classical, directed cloning via restriction nucleases and DNA ligases, it is also possible to to clone PCR fragments into plasmids via simple base pairing. The ligation of the fragment and plasmid will only occur inside the transformed cell. Ligase independent cloning (LIC) is based on sequence specific 5′ overhangs at the vector and the PCR product which are generated via the 3′ – 5′ exonuclease activity of the T4 DNA polymerase [92]. Stable basepairing requires at least 12 nt large overhangs. These overhangs are characterized by the absence of a specific base (marked red in Figure 7). Is the particular base present as a nucleotide triphosphate at the process of the exonucleolytic reduction then the reaction stops at this base and a equilibrium forms between hydrolysis and polymerization. Table 5 shows the pipetting scheme of PCR mixtures to amplify specific genes and gene fragments for LIC cloning. The vector used for the LIC cloning was pET24a-HM3C. It was linearized with *Sma*I prior to the LIC reaction. The reaction mixtures for generation of the 5′ overhangs are given in Table 7 and Table 8. The reactions were incubated

for 40 minutes at room temperature before heat inactivation of the T4 DNA polymerase. 2 µL of the insert mix and 3 µL of the vector mix were combined and incubated for 10 minutes at room temperature. After that 1.3 µL 25 mM EDTA were added and the mix was transformed into *E. coli* Dh5α cells. Please note that the here documented procedure only applied for the cloning into the pET24a-HM3C vector. Cloning of genes into the pET LIC (2A-T) vector had a slightly different protocol. All necessary information and the protocol can be found at addgene (https://www.addgene.org/29665/).

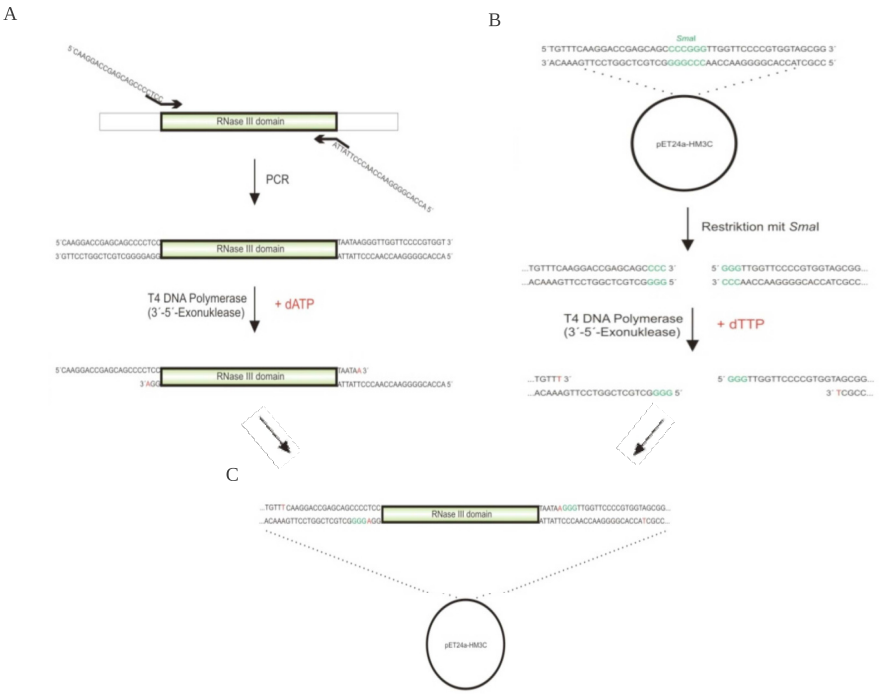

Figure 7: Principle of the ligase independent cloning.
A. In the first step, specific sequences are added to the insert via PCR. The clean PCR product was used in the 3'-5' exonucleolytic cleavage reaction by the T4 DNA polymerase to generate the 5' overhangs. The length of the overhang is determined by the addition of dATP. **B.** The vector was linearized with *Sma*I and the clean restriction product was used for the exonuclease reaction. The length of the overhang was determined by addition of dTTP. After that, vector and insert and formed complementary base pairs. Picture taken from Genetik Praktikum 2011 of the TU-Darmstadt.

2.2.3.4 *Generation of knockout vectors (pKOSG - StarGate (IBA GmbH))*

For the generation of the null mutants in this thesis, the pKOSG vector (purchased from IBA lifescience) was used [93]. The vector features a blasticidin resistance cassette (BS(r)) that can be flanked by, so called, left arm (LA) and right arm (RA), which are DNA fragments homologous to regions of the gene of interest. The arms were generated by PCR amplification of designated regions flanking the

Table 5: PCR recipe LIC

COMPONENT	VOLUME/AMMOUNT
Taq polymerase buffer	5 µL
$MgCl_2$ (25 mM)	4 µL
dNTPs (je 5 mM)	3 µL
forward Primer (5 µM)	5 µL
reverse Primer (5 µM)	5 µL
DNA template	50 ng
Pfu Taq polymerase mix (1:4)	1 µL
dH_2O	ad 50 µL

Table 6: PCR program LIC

STEPS	DURATION	TEMP	CYCLES
denaturation	30 s	95 °C	1
denaturation	10 s	95 °C	⎤
annealing	30 s	52 °C	× 30
elongation	60 s	72 °C	⎦
final elongation	60 s	72 °C	1

Table 7: Generation of the 5′-overhang of the vector

COMPONENT	VOLUME/AMMOUNT
linearized vector	150 ng
5× T4 DNA polymerase buffer	4 µL
dTTP (25 mM)	2 µL
DTT (100 mM)	1 µL
T4 DNA polymerase	1 µL
dH_2O	ad 20 µL

GOI. The PCR amplicons feature specific recognition sites that had been added to the arms during PCR amplification. The commercial available pKOSG vector permits simultaneous cloning of two PCR-products in one vector based on recombination. Additional *Spe*I restriction sites were included to permit excision of the knockout cassette from the vector prior transformation.

Table 8: Generation of the 5'-overhang of the PCR product

COMPONENT	VOLUME / AMMOUNT
PCR product	50 ng
5× T4 DNA polymerase buffer	4 µL
dATP (25 mM)	4 µL
DTT (100 mM)	1 µL
T4 DNA polymerase	1 µL
dH_2O	ad 20 µL

2.2.3.5 *Ethanol precipitation of nucleic acids*

Small amounts of DNA or RNA can be isolated from a watery solution via ethanol precipitation. Nucleic acids precipitate as salt after addition of alcohol in presence of monovalent metal ions like Na^+ or Li^+. The salt can be separated from the solution via centrifugation at 12000 x g. For the purpose of DNA and RNA precipitation 0.1 Vol. 3 M sodium acetate pH 4.7 and 3 Vol. pure ethanol were added to and incubated for at least 30 minutes at -20°C. Additional salt was washed out with washing steps with 70% ethanol. The DNA or RNA was air dried and dissolved in pure dH_2O.

2.2.3.6 *Plasmid minipreparation*

The plasmid mini preparation was done with the "Gene Elute HP Plasmid Miniprep Kit" from Sigma. The *E. coli* cells were lysed under alkaline conditions. The DNA was bound on a silica membrane and purified. The DNA was eluted in elution buffer or alternatively in dH_2O.

2.2.3.7 *Plasmid maxi preparation via alkalic lysis*

100 mL Erlenmeyer flasks were filled with selective LB medium and inoculated with the *E. coli* culture carrying the plasmid of interest. The culture was incubated over night at 37 °C under constant shaking (185 rpm). The cells were harvested by centrifugation at 4000 x g for 20 min. The supernatant was discarded and cells were resuspended in 4 mL Solution I. 8 mL Solution II were added, mixed and incubated for 5 minutes at room temperature. The sodium hydroxide and SDS inside Solution II lyse the cells. Afterwards 6 mL solution III is added and incubated on ice for 5 minutes to neutralize the suspension. The suspension is than centrifuged for 30 minutes 10000 x g at 4 °C. The supernatant is filtrated and 0.6 volumes isopropanol are added. After a additional centrifugation step with 10000 x g for 5 minutes the supernatant is discarded and the pellet is solved in 200

µL pure dH_2O. 1 volume 8 M LiCl is added and incubated for 30 minutes at -20°C before being centrifuged for 10 minutes at 10000 x g. the supernatant is transferred to a new Eppendorf tube and 1 volume pure ethanol is added. After an incubation of 30 minutes at room temperature the DNA is pelleted down at 20000 x g for 10 minutes followed by 2 washing steps with 70% ethanol. Finally the DNA pellet is air dried and resolved in 100 µL dH_2O. The DNA solution was stored at -20°C.

2.2.3.8 *Polymerase chain reaction*

This method is used for *in vitro* amplification of DNA fagments [94, 95]. Short and specific single stranded DNA oligonucleotides (Primers) bind complementary regions of heat denatured DNA molecules and are elongated via the heat stable DNA polymerase. There are many different DNA polymerases commercially available. In this thesis, for analytic PCR amplifications the Taq DNA polymerase was used while for gene amplification the Pfu DNA polymerase was used. The Taq polymerase was initially isolated from the thermophilic bacterium *Thermus aquaticus*. The optimal activity temperature of the polymerase is 74 °C. Under this condition the synthesis rate is around 2800 bp per minute. The polymerase features no 3′– 5′ exonuclease activity and is therefor missing proof reading capability. The error rate of DNA synthesis of the Tag polymerase is around 10^{-5}.

The Pfu DNA polymerase from the archeae *Pyrococcus furiosus* features a 3′– 5′ exonuclease activity and the error rate of the polymerase is at 10^{-6}. The synthesis rate is with around 500 bp per minute significantly lower than the synthesis rate of the Tag polymerase. Table 9 shows an exemplary PCR approach.

Table 9: PCR mix

COMPONENT	VOLUME / AMMOUNT
10× Taq Puffer	5 µL
$MgCl_2$ (25 mM)	4 µL
Primer 1 (5 µM)	3 µL
Primer 2 (5 µM)	3 µL
dNTPs (je 5 mM)	2 µL
DNA-Template	$<$ 50 ng
Pfu/Taq polymerase (1:4)	1 µL
dH_2O	ad 50 µL

The typical PCR process consists of of 20 to 35 cycles. Every cycle consists of 3 steps; the denaturation step, the hybridization step, and the elongation step. The cycles lead to exponential duplication

of a desired DNA. A typical PCR program is shown in Table 10. The annealing temperature of the hybridization step depends on the GC content of the individual Primers and the elongation time depends on the length of the DNA fragment that is desired for amplification.

Table 10: PCR program

STEPS	DURATION	TEMP	CYCLES
Denaturation	60 s	95 °C	1
Denaturation	30 s	95 °C	⎤
Annealing	30 s	[b]	× 30
Elongation[a]	x s	72 °C*	⎦
end	∞	12 °C	1

*PCRs on *D. discoideum* DNA were performed at 62°C elongation temperature. [a] dependent on the size of the fragment. [b] melting temperature (T_M) of the primer pair +/− 2 °C.

COLONY PCR Colony PCRs were performed for fast analysis and verification of plasmid DNA in single clones of transformed *E. coli* cells or knockout screenings in *D. discoideum*. *E. coli* colonies grown on LB agar plates were scraped off with a pipette tip and individually transferred into 50 µL PCR reaction vessel. Table 11 and Table 12 shows an exemplary PCR mix and PCR programm. In the first step the cells were heat lysed by incubation for 10 min at 95 °C.

D. discoideum colony PCRs were performed by lysing the cell pellet of 1 mL *D. discoideum* suspension in 50 to 100 µL Quick and Dirty lysis buffer and incubating it for 10 min at 95°C. 1 to 2 µL are added to PCR mix shown in Table 11. [96]

Table 11: PCR mix colony PCR

COMPONENT	VOLUME/AMMOUNT
10× Taq Puffer	5 µL
$MgCl_2$ (25 mM)	4 µL
Primer 1 (5 µM)	3 µL
Primer 2 (5 µM)	3 µL
dNTPs (je 5 mM)	2 µL
Taq polymerase	1 µL
dH_2O	32 µL

Table 12: PCR program colony PCR

STEPS	DURATION	TEMP	CYCLES
Lysis and Denaturation	10 min	95 °C	1
Denaturation	60 s	95 °C	⎤
Primer annealing	30 s	[b]	× 30
Elongation[a]	x s	72 °C*	⎦
End	∞	12 °C	1

*PCRs on *D. discoideum* DNA were performed at 62°C elongation temperature. [a] dependent on the size of the fragment. [b] melting temperature (T_M) of the primer pair +/– 2 °C.

2.2.3.9 *Isolation of genomic DNA from D. discoideum*

2 x 10^8 cells were collected via centrifugation at 390 x g for 5 min at 4°C and once washed with 40 mL Soerensen phosphate buffer. After a second centrifugation step, the cells were resuspended in 40 mL cell lysis buffer. Lysis of cell membranes was accomplished by adding 10% NP-40 until the lysate became transparent (maximum 4 mL). The nuclei of the lysed cells suspension were collected by centrifugation at 5000 x g for 30 min at 4°C. The supernatant was discarded and the nuclei were resuspended in 5 mL SDS-lysis buffer, where 100 µL of proteinase K [25 mg/ml] and 4 µL RNaseA (Merck) were freshly added. The suspension was incubated at 60°C for at least 3 h. The genomic DNA was purified via phenol/chloroform extraction and concentrated by ethanol precipitation (with 0.1/2 (v/v) 8M LiCl and 100% EtOH). After an incubation at -20°C over night and a centrifugation step at 12000 x g (4°C) for 30 min, the precipitated and pelleted DNA was washed with 75% ethanol and dried at 60°C. Dried DNA was usually dissolved in 100 to 200 µL preheated dH_2O. If needed, an additional RNA digestion step with 1 µL RNaseA was performed (10 min 37°C). The DNA was stored at -20°C.

2.2.3.10 *Phenol/chloroform extraction of nucleic acids*

Separation of nucleic acids from proteins was performed by phenol chloroform extraction. A given sample or suspension was 1:1 (v/v) diluted with phenol:chloroform:isoamyl alcohol (25:24:1, v/v) and gently mixed by repetitive inverting (for the isolation of gDNA from *D. discoideum* the inverting step was performed for at least 10 min). The organic phase (proteins) was seperated from the aqueous phase (nucleic acids) by centrifugation at 12000 x g (4°C) for 30 min. The upper, aqueous phase was transferred to the fresh tube and mixed 1:1 (v/v) with chloroform. After mixing, the suspension was again

centrifuged at 12000 x g (4°C) for 15 to 30 min and the upper phase was again transferred to a fresh tube, followed by ethanol precipitation. The precipitated and pelleted nucleic acids were washed with 75% ethanol and dried at room temperature. Dried RNA was usually dissolved in 100 µl dH_2O.

2.2.3.11 *Isolation of total RNA from D. discoideum*

For the extraction of total RNA from *D. discoideum* the Trizol® reagent was used as described in [97]. 5 x 10^7 cells were collected via centrifugation and lysed with 1 ml Trizol® by passing the cells through a pipette several times. An incubation for 5 min at room temperature established complete dissociation of nucleoprotein complexes and was followed by removal of cell debris by centrifugation at 12000 x g at 4 °C. Addition of 0.2 ml chloroform and centrifugation at 12000 x g for 30 min separated the solution in an RNA containing aqueous phase and a protein/DNA containing inter- and organic phase. The upper aqueous phase was transferred into a fresh tube and mixed with 0.5 mL 2-propanol. The precipitated and pelleted RNA was washed with 75% ethanol and dried at room temperature. Dried RNA was usually dissolved in 100 µl dH_2O.

2.2.3.12 *Isolation of total RNA from S. cerevisiae and E. coli*

For the extraction of total RNA from *S. cerevisiae* and *E. coli* 1 mL of the respective cell culture was spun down and resuspended in 1 mL Trizol® reagent. After resuspension with Trizol the sample was heated at 85°C for 10 minutes (similar to hot phenol extraction protocols). The rest of the protocol is similar to 2.2.3.11.

2.2.3.13 *Radioactive endlabeling of oligo nucleotides*

Synthetic oligonucleotides lack phosphate groups at their 5´-termini and were radio-labeled by the T4 polynucleotide kinase that transfers γ-^{32}P from [γ-^{32}P] ATP to the nucleic acid. Table 13 displays the detailed reaction setup. Commercial available DNA and RNA ladders (GeneRulerTM Ultra Low Range DNA Ladder (SM1211) und RiboRulerTM Low Range RNA Ladder (SM1831)) and RNA samples were labeled after dephosphorylation of their 5´-termini according to the Table below.

The reaction mixes were incubated for 30 min at 37°C. Prior hybridization of the blot, the removal of non-incorporated radioactive nucleotides was achieved by gel filtration via sephadex G-50 columns. For this purpose a 1 ml syringe was plugged by adding a small amount of glass wool and filled with sephadex G-50, dissolved in 1 x TE. The syringe was placed into a 15 ml Falcon tube. The reaction mix was put through the sephadex column by centrifugation at 1,000 x g for 5 min. The single nucleotides retained in the column

Table 13: Reaction mix for radioactive endlabelling

COMPONENT	VOLUME / AMOUNT
DNA oligo (100 µM)	0.5 µL
PNK buffer A (10 x)	5 µL
γ-^{32}P ATP (5000 Ci/mmol; 10 µCi/µl)	5 µL
T4 PNK (10 u/µL)	1 µL
H_2O	11.5 µL

whereas longer oligonucleotides were allowed to pass through. The flowthrough was transferred into an 1.5 mL reaction vessel and denatured by boiling at 85°C for 5 min.

2.2.3.14 *Removal of radioactive endlabeled probes of membranes (Stripping)*

Radioactive probes were stripped from the membrane by washing the membrane for 3 times 10 minutes at 85°C with stripping solution (0.1 x SSCS, 0.1% SDS).

2.2.3.15 *Northern blot*

Dependent on the experiment 5[1] to 10 µg total RNA was loaded on a 8 to 11% PAA gel (7 M Urea in 1x TBE) and run at 25 mA (per gel) constant til the bromophenol blue dye reached the lower end of the gel. (APM PAA gel setups and the electrophoresis runs were performed as described in [98]. The gel run was performed at 50 to 65 mA for 3h). After the run, the gel was incubated for 30 minutes in 0.5 x TBE containing Ethidium bromid. The stained gel was put on an UV table inside a documentation system and a picture was taken to document the quality and quantity of the loaded RNA as well as the electrophoretic separation. The gel was trimmed and semidry electroblotting was performed. Therefore, the gel was covered with a sheet of uncharged nylon membrane of appropriate size (Amersham Hybond TM-NX) and placed between 2 thick filter papers (soaked in 0.5 x TBE). Transfer was carried out at 20 V for 30 min at room temperature. Fixation of the RNA to nylon membranes were accomplished by UV crosslinking for 116 second (0.5 joule per centimeter). Afterwards, the membrane was covered with Church buffer and transferred to a rolling incubator at 45°C. After 30 minutes incubation the Church buffer was exchanged with Church buffer containing radioactive labeled DNA oligonucleotides complementary to the RNA of interest and incubated over night. On the next day the church buffer was removed and the membrane was washed 10 minutes in wash

1 only applied for the tQ^{CUG} Northern blot Figure 30.

buffer I (2 x SSC; 0.1% SDS) followed by 2 times wash with wash buffer II (0.5 x SSC; 0.1% SDS). The membrane was sealed in a plastic bag and put into a lightproof cassette containing a phospho-imaging plate and incubated for 1 hour to 2 days. The phospho-imaging plate was read out by the Phospho imager (FLA-5000) from Fuji. Image manipulation was done with Multigauge.

2.2.3.16 *Co-Immunoprecipitation of GFP tagged proteins*

Co-Immunoprecipitation (Co-IP) of GFP tagged proteins was accomplished using the GFP-Nanotrap® (Chromotek) [99]. 200 to 400 mL of exponentially growing (2–4 x 10^6 cells/mL) *D. discoideum* strains were harvested by centrifugation at 390 x g. Cells were resuspended in 15 to 20 ml cold lysis buffer (50 mM Tris-HCl pH 7.5; 100 mM NaCl; 1 mM $MgCl_2$, 1 x Protease inhibitor) and lysed by sonication with 20 cycles of 5 seconds pulse and 10 seconds break with 50% amplitude. The cell debris was removed by centrifugation at 20000 x g for 30 minutes at 4 °C. The cleared lysate was incubated for 1 hour at 4°C on a rolling incubator. (This incubation led to polymerization of cytoskeleton proteins in the cell extract that would otherwise cover the agarose beads in downstream purification process). The lysate was centrifuged at 20000 x g for 30 minutes at 4 °C. The supernatent was transferred to a new Falcon tube and diluted to 40 to 50 mL. 20 to 40 µL GFP-trap beads slurry were added to the diluted lysate and incubated for 1h hour (maximum 2 hours) on a rolling incubator at 4°C. After the incubation the beads were spun down by centrifugation at 1,000 x g for 5 min with slow deceleration to avoid dispersion of the beads. The beads were transferred to 1.5 mL Eppendorf tubes and then washed three to five times with lysis buffer. After the last wash step, all liquid was removed and 1 volume 2 x Laemmli buffer added. The sample was heated at 85°C for 5 minutes to denature the proteins. The samples were stored at -20°C until analysis by SDS PAGE.

2.2.3.17 *Strep tactin affinity chromatography*

400 mL of exponentially growing (2–4 x 10^6 cells/mL) *D. discoideum* strains were harvested by centrifugation at 390 x g. Cells were resuspended in 15 to 20 ml cold Strep-lysis buffer (50 mM Tris-HCl pH 7.5; 100 mM NaCl; 1 mM $MgCl_2$, 1 x Protease inhibitor) and lysed by sonication with 20 cycles of 5 seconds pulse and 10 seconds break with 50% amplitude. The cell debris was removed by centrifugation at 20,000 x g for 30 minutes at 4°C. The cleared supernatant was transferred to a new Falcon tube and 40 µL Avidin solution was added prior to an 1 hour incubation at 4°C on a rolling incubator. (This incubation step is necessary to block any biotin containing proteins in the cell extract to reduce unspecific binding inside the Strep tactin column. The incubation also reduced the amount of cytoskeleton pro-

teins in the solution. Within that hour, a fraction of these cytoskeleton proteins polymerized and were found as fluffy whitish aggregates at the bottom of the tube.) The suspension was centrifuged for another 30 minutes at 20000 x g. The supernatant was again transferred to a new Falcon tube and diluted to 50 mL. The diluted cell extract was added into a gravity flow column filled with 1 ml Strep-Tactin coupled Sepharose (Gravity flow Strep-Tactin Superflow column, IBA GmbH). The chromatography was carried out in the cold room at 4°C. After flow through of the cell extract, unbound proteins were washed off by with 100 mL Strep-lysis buffer. Elution of bound proteins has been attained afterwards by adding 3 x 1 ml Strep-elution buffer containing 5 mM desthiobiotin that competes for Strep-Tactin binding with the Strep-tag. The desthiobiotin can be removed from the matrix by adding 3 ml regeneration buffer containing 1 mM HABA (hydroxyazophenyl-benzoic acid) followed by rinsing with 9 ml 50 mM Tris-HCl, pH 8.0; 150 mM NaCl; 1 mM EDTA. The elution fractions were combined and differential centrifugation with amicons (MWCO 30 kDa or 100 kDa) was applied to concentrate the proteins and enhance the purity of the elution.

2.2.3.18 *MBP affinity chromatography*

The cultivation procedure of BL21 strains expressing the protein of interest can be found under 2.2.2.4. Cells were harvested by centrifugation at 4000 rpm for 10 minutes and resupended in lysis buffer (50 mM Tris-HCl pH 7.5; 150 mM NaCl; 1 mM $MgCl_2$) containing 1 mg Lysozym per 1 mL buffer. Afer 30 minutes incubation on ice the protease inhibitor was added and the cells were lysed via ultrasonication with 20 pulses 5s on 10s off at an amplitude of 85%. The resulting suspension was centrifuged with 20000 x g for 30 minutes. The supernatant was sterile filtrated and diluted 1:5 to 1:6 with lysis buffer. 600 µL amylose beads were put in a gravity flow column and equilibrated with 20-40 mL lysis buffer. The flow rate was adjusted to 0.5 mL (max 1 mL) per minute. The diluted supernatant was put over the gravity flow column (a low flow rate is crucial for a clean purification; higher flow rates led to more unspecific binding). Washing was performed with 4 times the volume (lysis buffer) of the diluted supernatant. Elution was performed with 10 mL lysis-/wash buffer containing 10 mM maltose. The elution fraction was concentrated with Amicons MWCO 100 kDa (MBP-Elp456 complex) or MWCO 30 kDa (MBP-γ-toxin).

2.2.3.19 *HRV3c protease cleavage*

His-MBP removal from the POI was performed by incubating a 200 to 400 µL concentrated elution (0.5-3 mg/mL) with 2 µL HRV3c protease from NEB for 20 to 24h at 4°C. The protease was removed from the sample by differential centrifugation with Amicons.

2.2.3.20 *γ-toxin RNA cleavage assay*

10 µg total RNA was incubated with different concentrations of MBP-γ-toxin in 20 µL buffer containing 25 mM Tris-HCl pH 7.5 and 50 mM NaCl for 30 minutes at room temperature or 30°C. After the incubation 20 µL 2 x RNA loading dye were added and the sample was heated for 3 minutes at 85°C. The sample was then loaded on a denaturating PAA gel (8% in TBE). Following the electrophoretic separation, a northern blot was performed. Procedural details are found in 2.2.3.15.

2.2.3.21 *Size exclusion chromatography via FPLC*

Proteins purified in 2.2.3.18 were subject to size exclusion chromatography on an Äkta FPLC. The column used was the Superose 6 Increase (3.2 x 300 mm) the liquid phase buffer used contained 50 mM Tris-HCl pH 7.5, 150 mM NaCl and 1 mM $MgCl_2$. 20 to 60 µL protein concentrate were injected into the column. The flow rate was set to 20 µL per minute. Detection of proteins was done with UV_{280nm}. Elution fraction of 100 µL were collected for downstream analysis.

2.2.3.22 *TCA precipitation of proteins in watery solution*

Proteins were precipitated from watery solution by addition of 0.25 vol of 100% trichloroacetic acid (TCA). After the solution was mixed and incubated on ice for at least 10 min, it was centrifuged for 5 min at 16000 x g (4°C). Subsequently, the supernatant was removed and the fluffy pellet was washed with 200 µL of ice-cold acetone followed by a centrifugation step at 16000 x g (4°C). The washing process with acetone was repeated two times. Afterwards, the precipitated protein pellet was air dried at 80°C and resuspended in 2x Laemmli Loading Dye.

2.2.3.23 *SDS-PAGE*

Protein separation was performed via denaturing SDS polyacrylamide electrophoresis (SDS-PAGE) according to [100]. Protein or cell samples were mixed with equal amounts of 2 x Laemmli sample buffer and denatured at 85°C for 5 minutes. Generally, 10 µL (1×10^7 *E. coli* cells or 1×10^6 *D. discoideum* cells) of samples the sample were loaded in a pocket of the gel. Standard PAA concentration for the separating gel was 12.5% when the gel was produced homemade. Commercially bought gradient gels had a PAA concentration range of 4-12%. Gel electrophoresis for homemade gels was carried out at 25 mA currency and maximum 200 V. NuPAGE gels were run on 200 V constant.

2.2.3.24 *Colloidal Coomassie staining*

Detection of protein quantity and quality in a SDS-PAGE was done by colloidal Coomassie staining. Therefore, after electrophoretic separation, the gel was washed 3 x 10 minutes with dH_2O to remove SDS from the gel. Staining was carried out by covering the gel with colloidal Coomassie solution and incubating it over night at room temperature while gentle shaking. Destaining was carried out by incubating the stained gel with destaining solution for 30 minutes followed by 4 x 30 minutes incubation with dH_2O. Gels were photographed and when required stored in dH_2O at 4°C.

2.2.3.25 *Blue Native PAGE*

Detection of the Elongator subcomplexes and a size estimation was done by Blue Native PAGE followed by Western blot detection of the tagged protein of interest. Approximately 2 µg to 4 µg of protein concentrate (estimated from colloidal Coomassie stained SDS-PAGE experiments) received from Co-IP purification were mixed with 2 x Sample buffer (0.1% Coomassie G250 and 0.025% Triton X-100) and loaded on a 4-12% gradient gels (ServaGel™ Native Gel kit, Serva GmbH). Gel electrophoresis was carried out discontinuously by use of cathode- and anode buffer, whereas the cathode buffer was supplemented with 0.02% Coomassie to attend migration of proteins to the anode. After 120 min run at constant 200 V the gel was removed from the cassette and destained in dH_2O. After destaining a picture for documentation was taken. Prior to the transfer on PVDF membrane, the gel was incubated for 10 min in 0.02% SDS and the membrane was activated by a methanol bath (30s). The transfer buffer was composed of 5% methanol and 0.02% SDS in 1 x Xcell blot buffer. Transfer was carried out for 1h at 30 V constant. After the transfer the proteins were crosslinked to the membrane by incubation with 10% acetic acid and air drying (minimum 30 minutes). Immunological detection was carried out following 2.2.3.26.

2.2.3.26 *Western blot*

For identification and detection of specific proteins from SDS-PAGE runs, the proteins were transferred to nitrocellulose membranes by electroblotting. Transfer was carried out in a tank blot (Xcell SureLock® blot module, Life Technologies), filled with Novex®Tris-Glycine transfer buffer, at 30 V constantly for 1 hour at 4°C. The membrane was incubated for 30 minutes in blocking solution (2% skim milk in 1x NCP). Afterwards the blotted membrane was subjected to bind the primary antibody (antibody was added to fresh blocking solution) over night at 4°C by gentle shaking. After removal of the primary antibody by washing the membrane 3 times with 1 x NCP, the appropriate secondary antibody conjugated to alkaline phosphatase

was added at a dilution of 1:10,000 and allowed to bind for 1 hour at room temperature. After washing again 3 times with 1 x NCP the membrane was incubated in 20 ml AP buffer and 50 µl BCIP until blue stain of protein bands was apparent. At this time the reaction was stopped by draining the BCIP-solution and rinsing the membrane with dH_2O.

2.2.3.27 *In-gel protein digestion for mass spectrometric analysis*

The procedure followed the detailed description in here [101].

Selected protein bands were excised with a scalpel and sliced into small cubes < 1 x 1 mm and transferred to a 0.5 mL reaction tube. Destaining of the gel pieces was done with 100 µL 1:1 (v/v) 100 mM ammonium bicarbonate/acetonitrile (ACN) for 30 min with occasional vortexing. the liquid was exchanged with 500 µL ACN and incubated for another 15 min. After complete gel dehydration, the liquid was removed and the samples were air dried >10 minutes. Finally, the cubes were covered with 15 to 20 µL of freshly prepared Trypsin Digestion Mixture (10 mM ammonium bicarbonate, 10% ACN, 13 ng/µL). After an incubation of 30 min on ice 5 to 15 µL of the Trypsin Digestion Mixture was added, depending on the volume of the gel. The samples were incubated at 37°C over night

2.2.3.28 *Mass spectrometry sample preparation*

The dried-droplet method on ground steel plate was employed. 1 µL of MALDI (Matrix-assisted laser desorption/ionization) Matrix Solution was directly mixed with 1 µL of in-gel digested sample. The mixed sample was deposited on a ground steal target plate (MTP 384 target ground steel, Bruker Daltonics GmbH) and left for drying. Subsequently, 20 µL MALDI matrix solution was mixed with 1 L of Peptide Calibration Standard II. 0.5 L of the standard mix was spotted in a sectors neighboring the spotted samples. After the liquid evaporated, the samples were loaded into the mass spectrometer.

2.2.3.29 *Spectra acquisition*

For the MALDI mass spectrometric analysis the instrument Autoflex II TOF/TOF (Bruker Daltonics GmbH) was used. The spectra were acquired in the linear, positive reflection mode. Voltages applied from the source ion I and II were 19 and 16.9 kV, respectively. The laser intensity was adjusted as needed (depending on sample quality in the range between 30% and 60%). An average of 2000 laser shots were collected. Bruker specific data formats .xmL were converted to the mzXML data format. Data analysis was performed with mMass and the MASCOT server.

3 RESULTS

Prior to the work presented in this thesis, former group members generated an *elp1* deficient strain [86], an *elp2* deficient strain [87] and performed Elp1-GFP trap pulldown experiments on the Elongator complex of *D. discoideum* [86]. They identified the core subcomplex Elp123, but found no evidence for the Elp456 subcomplex. Growth phenotype determination revealed a slightly prolonged cell cycle in the Elongator mutant strains compared to the wild type strain [87].

Maps of all plasmids generated in this work are shown in Section A.4.1.

3.1 INVESTIGATIONS ON THE IDENTITY OF THE ELONGATOR COMPLEX

The dictybase.org database features four out of the six different Elongator genes. No entries are given for the *elp5* and *elp6* genes. Ncbi protein blast searches revealed 2 protein candidates as the potential Elp5 and Elp6. Both proteins show sequence identities below 20% to the *S. cerevisiae* proteins (Table 14). The sequence identity values are largest for cucumber *elp5* and tomato *elp6* (data not shown). Individual cDNA of *elp3*, *elp5* and *elp6* candidates were obtained via reverse transcription with gene specific primers from total RNA (data not shown). The cDNAs and the gene of *elp4* were PCR amplified and cloned into the pJet1.2 shuttling vector. After verification of the individual sequences, they were cloned from the shuttling vector into the pDM plasmid series. This vector series features different fluorescence tags and affinity tags either 5´ or 3´ of the gene sequence. The expression cassette is under the control of an actin 15 promotor, enabling constant overexpression of a gene of interest (GOI) under axenic growth conditions [80].

The plasmids were transformed in different *D. discoideum* strains based on the Ax2 wild type. Strains with ectopically expressed, tagged Elongator proteins were used for localization and immunoprecipitation studies to investigate the identity of the Elongator complex in *D. discoideum*. The generation and characterization of the used Elongator mutant strains is described in Section 3.2.

Table 14: Elongator proteins in D. discoideum

NAME	GENE ID	ORF SIZE	PROT SIZE	SEQU IDENTITY *
Elp1	DDB_G0284075	4286 bp	160 kDa	28%
Elp2	DDB_G0275651	2706 bp	100 kDa	27%
Elp3	DDB_G0290103	1680 bp	63 kDa	70%
Elp4	DDB_G0278783	1320 bp	48 kDa	20%
Elp5	DDB_G0276569	1270 bp	45 kDa	<20%
Elp6	DDB_G0268624	1130 bp	38 kDa	<20%

[*]Protein sequence identity to *S. cerevisae* homologue

3.1.1 *Intracellular localization of Elongator proteins*

Strains with GFP and mRFP tagged Elongator proteins Elp3, Elp4, Elp5 and Elp6 were subjected to fluorescence microscopy and laser scanning microscopy studies. Fluorescence microscopy of cells expressing GFP-Elp3 or GFP-Elp4 revealed GFP signals throughout the cytoplasm of cells (Appendix Figure 38 A). The images provided no indication for a specific localization of these proteins.

The Elongator complex was initially found associated to RNA polymerase II holoenzyme and the literature suggests a cytoplasmic and nuclear localization [38]. In recent years, however, a nuclear localization of complex was doubted and more evidence emerged that the Elongator complex is exclusively cytoplasmic (personal communication with Raffael Schaffrath and Sebastian Glatt). To investigate whether a nuclear localization of different Elongator subunits exists in *D. discoideum*, laser scanning microscopy was carried out. Figure 8 shows fluorescence images taken from different sections of cells expressing mRFP-Elp5 and GFP-Elp6. The GFP signal was found predominantly cytoplasmic. The nuclei and other organelles appear black in the image (Figure 8 B). The RFP signal seems to be predominantly cytoplasmic as well, but in the upper left cell in z7 (Figure 8 C) two distinct red spots can be observed. Only a small percentage of the cells displayed such fluorescence enriched spots. The spots localized in organelles with otherwise low fluorescence background. They may represent protein aggregates, that are occasionally observed as artifacts due to high overexpression. The results of the fluorescence imaging indicate that the Elongator complex *D. discoideum* is (predominantly) cytoplasmic, without any specific localization. The observation made here are in line with the observations for Elp1 and Elp2 [86], [87]. A 3D LSM microscopy image is shown in the Appendix (Figure 40).

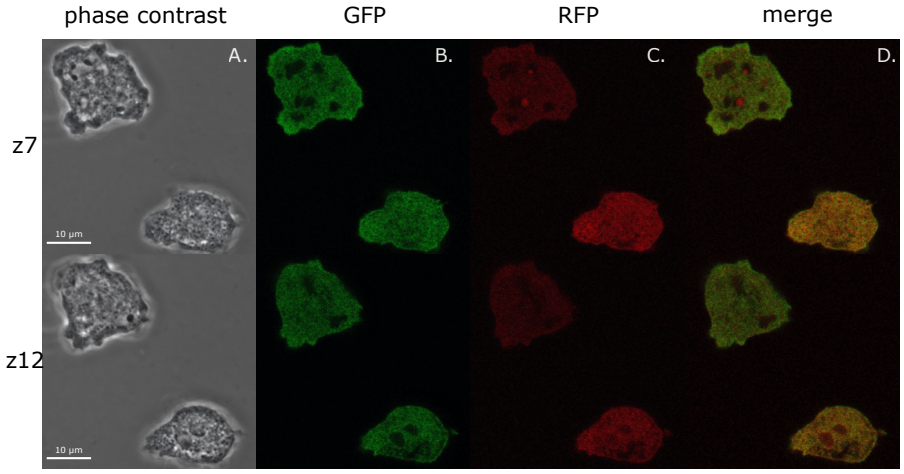

Figure 8: LSM fluorescence image of *D. discoideum* cells expressing mRFP-Elp5 and GFP-Elp6
Laser scanning confocal microscopy images of mRFP-Elp5 and GFP-Elp6 in Ax2 wild type background (pDM318 mRFP-Elp5 GFP-Elp6). Z7 indicates z-stack image 7 of 26 and z12 indicates z-stack image 12 of 26. **A.** phase contrast image of z-stack image 7 and 12. **B.** Fluorescence signal of GFP. The signal appears to be cytoplasmic. **C.** Fluorescence signal of RFP. The signal appears to be cytoplasmic. **D.** Overlay of the GFP and RFP signal. The white bar indicates length of 10 µm.

3.1.2 *Protein co-immunoprecipitation and affinity chromatography of D. discoideum Elongator proteins*

To investigate the identity of the Elongator complex in *D. discoideum*, ectopically overexpressed fusion proteins were generated and transformed into Ax2 wild type cells and different Elongator mutant backgrounds.

3.1.2.1 *Anti-GFP co-immunoprecipitation Elp 3 and Elp4*

The GFP-Nanotrap® ([99]; purchased as GFP-Trap A, Chromotek) was applied to purify protein complexes from the same strains used in the localization studies (Section A.1.1 and Section 3.1.1). It was known from previous studies in *S. cerevisiae* that the holo-Elongator dissociates at a salt concentration above 125 mM sodium chloride [39]. Therefore, the salt concentration in the co-IP was adjusted to 100 mM sodium chloride to prevent potential dissociation of the holocomplex into the two subcomplexes. All GFP co-IPs were carried out in batch mode. A *D. discoideum* strain expressing only GFP served as control in these experiments. This control enables the discrimination between interactions of proteins with the protein of interest and other interactions that occur between the GFP antibody and *D. discoideum* proteins, as well as GFP and *D. discoideum* proteins. In the process of these experiments, it became evident that the majority of unspecific

interactions were due to the interaction of *D. discoideum* proteins with the agarose beads. Cell lysis was carried out by addition of 1% NP-40. Figure 9 shows the results of co-IP experiments carried out on different strains.

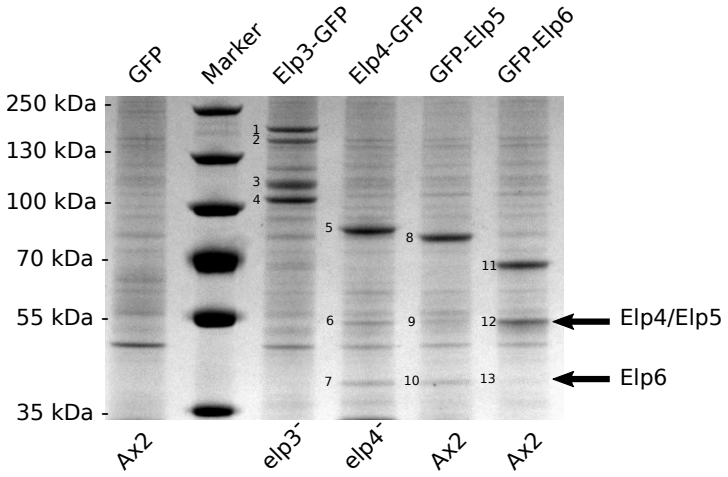

Figure 9: GFP-trap pulldown of ectopically overexpressed Elongator proteins 3, 4, 5, and 6 in the indicated genetic background.
Image of a colloidal Coomassie stained gradient (4-12%) SDS-PAGE. The individual sample lanes were loaded with 10 µL of the different GFP-trap pulldown co-immunoprecipitations. The black arrows at the right hand side indicate the individual endogenous subunits; the upper arrow represents Elp4 and Elp5, the lower arrow Elp6. Detailed description of the single lanes are found in the text below. Marker = PageRuler Plus Prestained Protein Ladder.

The Elp3-GFP co-IP was carried out in the background of an *elp3*$^{-}$ strain. Above 70 kDa, 4 strong bands were visible. By mass spectrometric analysis (Table 19), band number 1 and 2 could be identified as Elp1 and a truncated form of Elp1[1]. Band number 3 could be identified as Elp2 and Band number 4 as the GFP tagged Elp3. Analysis of the bands below GFP-Elp3 revealed no evidence for the presence of the Elp456 subcomplex.

The Elp4 co-IP was performed in an *elp4*$^{-}$— strain while the co-IPs for Elp5 and Elp6 were done in the Ax2 wild type background. In the lane corresponding to the Elp4-GFP co-IP, mass spectrometric analysis could identify band 5 as bait, band 6 as the Elp5 subunit and band 7 as Elp6. In the GFP-Elp5 co-IP, the analysis identified band 8 as bait and band 9 as a mixture of Elp4 and the endogenous Elp5. The protein in band 10 was identified as Elp6. In the GFP-Elp6 co-IP, mass

1 The truncated Elp1 is likely to be the result of a protease cleavage reaction, due to insufficient protease inhibition in the purification procedure. This observation is in line with the observations by Xu et al.[102], that found the Prb1p protease responsible for the specific cleavage product of Elp1. Appendix Figure 43 showes a co-IP where the use of protease inhibitor cocktail was omitted.

spectrometric analysis identified the bait in band 11, a mixture of Elp4 and Elp5 in band 12 and the faint band 13 could not be determined.

Taken together, the results shown in Figure 9 indicate that the Elp123 and Elp456 subcomplexes do exist in *D. discoideum*. The fact that a mixture of endogenous and ectopically expressed, tagged proteins of the same subunit could be identified in these co-IP of Elp5 and Elp6, points towards a stoichiometry of the Elp456 subcomplex with more than one protein of each subunit.

The co-IP experiments failed to bring down the holo-Elongator. However, it cannot be excluded that the purification procedures led to a dissociation of the complex. To address this possibility, *in vivo* crosslinking with DTBP (Di-tert-butyl peroxide) was performed prior to the purification procedure. The results of the subsequent co-IP are shown in Figure 10.

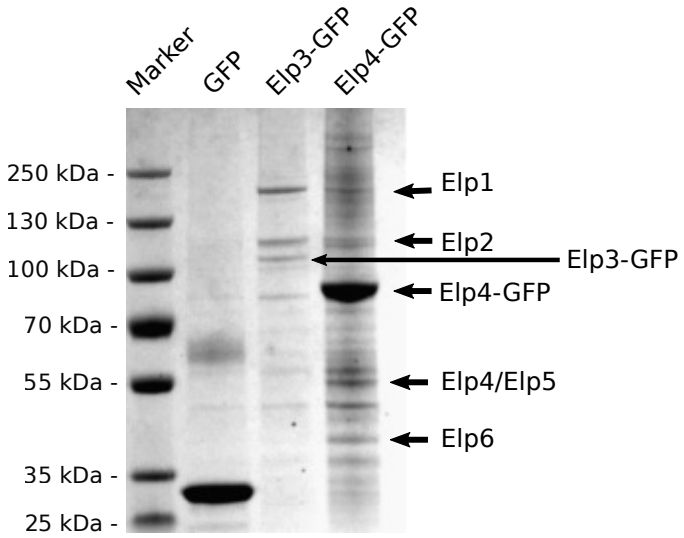

Figure 10: Results of *in vivo* crosslinked GFP-trap pulldown of Elp3 and Elp4 in the Ax2 background.
Image of a colloidal Coomassie stained gradient SDS-PAGE. Running fronts of the individual Elongator proteins identified in MALDI mass spectrometry are indicated by the black arrows (Table 20). Detailed description of the single lanes are found in the text below. Marker = PageRuler Plus Prestained Protein Ladder.

After crosslinking, additional bands in the range of 200 kDa to 100 kDa appeared in the lane representing the Elp4-GFP pulldown. MALDI mass spectrometry could identify Elp1 and Elp2 in that lane (Table 20). The individual proteins are marked with arrows next to the gel picture. Unfortunately, the overall poor quality of the pulldown did not allow for complete identification of the holo-Elongator. No peptides corresponding to Elp3 could be detected in gel slices of this lane. The band intensities of Elp1 and Elp2 were significantly weaker than the ones of Elp5 and Elp6, respectively. The lane of the crosslinked Elp3-GFP pulldown showed no evidence for an associ-

ated Elp456 subcomplex. The only strong band, other than Elp1 and Elp2, that always appeared, just above the 70 kDa Marker band in all Elp3 pulldowns, was Hsp70.

While it thus was possible to identify Elp1 and Elp2 associated to the Elp456 subcomplex, none of the Elp456 subunits associated to the Elp123 subcomplex were found when the co-IP was performed with the Elp3 protein. Large protein tags, like GFP, may interfere with complex formation or influence protein folding in an unpredictable manner. This could result in an inoperative ectopic fusion protein, which may not be loaded into the protein holocomplex. These and other questions were addressed in Section 3.2.3.1 and A.2.1. The Results of those experiments (Figure 25) provided evidence for a fully functional Elp3-GFP fusion proteins independent of the GFP location. Elp4-GFP – unlike GFP-Elp4 – could not rescue the wild type situation although it binds to the other Elongator proteins (Section A.2.2 and A.2.5 and Figure 46).

3.1.2.2 *Strep-Tactin affinity chromatography of FLAG-Strep-tagged Elongator proteins 3 and 4*

Contrary to GFP-Nanotrap used in 3.1.2.1, affinity chromatography with the Strep-Tactin system allows for elution of the protein of interest without shifting to a non-physiological pH. Further, the reduction of unspecific protein interactions through different washing steps, combined with differential centrifugation, is expected to make complex identification easier with Strep-Tactin columns, compared to the batch mode of the GFP-trap. The results of such an approach which omitted any detergent for cell lysis is shown in Figure 11. The elution fraction was subject to differential centrifugation with a MWCO of 100 kDa. This lead to a reduction of unspecific protein bands compared to the GFP-Trap. It also allowed to investigate whether the Elp456 subcomplex is still intact or dissociates during purification.

The MALDI mass spectrometric analysis of the FLAG-Strep-Elp4 lane could identify Elp1 associated with the Elp456 subcomplex. But again, there was no evidence of the Elp456 subcomplex being associated to Elp3 or the entire Elp123 subcomplex (Table 21).

Another advantage of this method is, that it allows to investigate subcomplex stoichiometry. The elution fractions shown in Figure 11 were used to determine the subcomplex sizes via a blue native PAGE experiment combined with a Western blot. The resulting images are shown in Figure 12 A and B. In the lane corresponding to the FLAG-Strep-Elp4 pulldown, the FLAG antibody gave rise to a signal at the height of the 480 kDa marker band. The expected mass of the *D. discoideum* Elp456 complex is around 260 kDa, when a heterocyclic dimer is assumed. In the lane of the FLAG-Strep-Elp3 pulldown, the

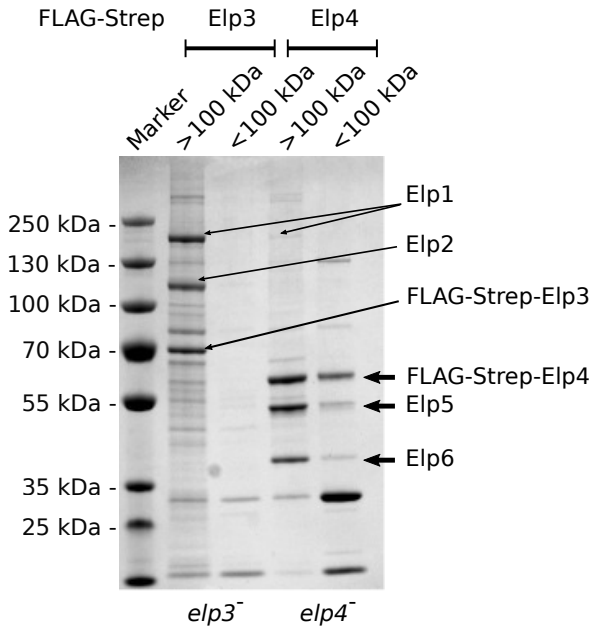

Figure 11: Strep affinity chromatographic pulldown of Elp3 and Elp4.
Image of an colloidal Coomassie stained gradient SDS-PAGE with samples from the elutions fractions of the strep tactin affinity chromatography pulldowns of FLAG-Strep-Elp3 and FLAG-Strep-Elp4. Indicated with > 100 kDa is the protein fraction of the retentate after differential centrifugation with a MWCO of 100 ka. Indicated with < 100 kDa is the protein fraction of the flow through of differential centrifugation. Marker = PageRuler Plus Prestained Protein Ladder.

FLAG antibody gave two signals; one below 480 kDa and one at 480 kDa. An Elp123 monomer has an estimated size of around 325 kDa.

3.1.3 *Recombinant D. discoideum Elp456 subcomplex in E. coli*

Studies of proteins produced in *D. discoideum* have their limitations, particularly with respect to the overall protein amounts that can be produced in a reasonable price range, due to the cost of media and consumables cost. *E. coli*, on the other hand, is a fast growing, easy to cultivate prokaryote that is widely used for heterologous protein production. There is a large collection of genetically engineered strains and other protein biochemical engineered tools available, including vectors, protein tags and purification kits, that allow for purification of different proteins under a large variety of conditions.

Initially, the *D. discoideum* Elp4, Elp5 and Elp6 subunits were separately cloned into the pET24a-HM3C Vector and purified from *E. coli* (Appendix Figure 50). The purified protein fractions were then combined in an assembly buffer and ran on a blue native PAGE (data not shown). The resulting Western blot image showed no evidence for an interaction of the protein subunits (data not shown). It was concluded

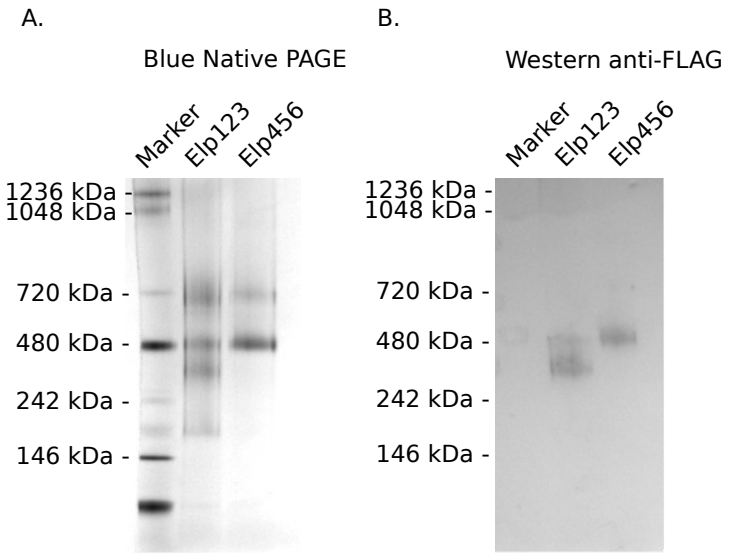

Figure 12: Blue native PAGE and Western blot of the Elongator subcomplexes.
A. Image of gradient (4-12%) blue native PAGE after electrophoretic separation of the elutions fractions from the strep tactin affinity chromatography pulldowns shown in Figure 11. **B.** Western blot image anti-FLAG of the gel shown in A.
Marker = PageRuler Plus Prestained Protein Ladder.

from those experiments that the majority of the different subunits are soluble when expressed in *E. coli*. The bacterial expression approach was then changed to a vector that allowed polycistronic gene expression under one T7 promotor. The polycistronic expression has the advantage that multiple gene products can be simultaneously expressed in similar ratios. The complex was expected to assemble within the cell, allowing for easy purification for downstream experiments (Figure 13).

The following results are based on the previous work of Alina Stein. Alina Stein constructed the final pET2E-Elp456, narrowed down the purification conditions and performed the first blue native PAGE and Western blot analysis of the heterologous recombinant Elp456 complex produced in bacteria [85].

3.1.3.1 *Narrowing down the size of the Elp456 subcomplex*

The Elp456 subcomplex was purified from *E. coli* according to the protocol provided by Alina Stein. The resulting elution fractions were combined and differential centrifugation with 100 kDa MWCO was applied (Figure 14). The MBP-tag was removed from the complex by incubation with HRV3C protease, which recognizes a peptide sequence in between His-MBP and Elp4 (Figure 14).

The protein retentates were subjected to size exclusion chromatography (SEC). The elution fractions (0.1 mL) were collected and used

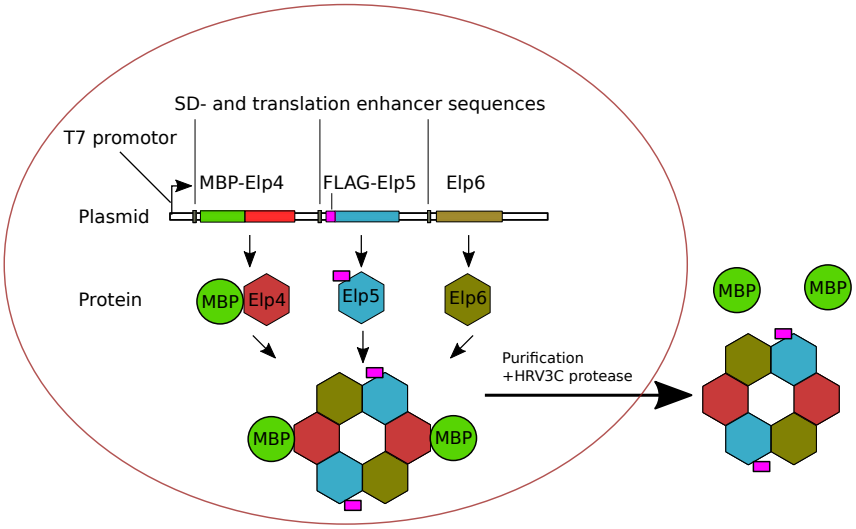

Figure 13: Sketch of the expression and purification of the recombinant *D.discoideum* Elp456 subcomplex in *E. coli*.

The complex is expressed from the polycistronic pET-2E expression Plasmid. Purification is performed via the MBP affinity tag on amylose beads. The MBP tag can be cleaved off Elp4 with HRV3C protease.

for further analysis of protein identity and RNA content. Figure 15 A shows an overlay of the resulting UV_{280nm} curves obtained from 3 different runs. The black curve represents the protein standard with UV_{280nm} peaks corresponding to protein sizes from 670 kDa to 1.35 kDa. The blue curve represents the result of the MBP-Elp456 run. The major peak just below 670 kDa corresponds to the recombinant complex. The two smaller peaks correspond to MBP-Elp4 (1.75 mL) and MBP (1.9 mL). This was concluded from an SDS-PAGE analysis of the single elution fractions (Figure 15 B). Mass spectrometric analysis of the elution fraction 1.4 – 1.5 mL found additional to the recombinant Elongator subunits and MBP also the *E. coli* chaperone DnaK and the chaperonin GroEL in the elution fraction (Table 18). The red curve (Figure 15 A) represents the UV_{280nm} curve obtained from the run with recombinant Elp456 where the MBP was cleaved off. 2 strong UV_{280nm} peaks are visible; the first peak at around 1.5 to 1.6 mL elution corresponds to the recombinant complex while the second, larger peak at 1.8 – 1.9 mL corresponds to the MBP tag that was cleaved off, the endogenous MBP and Elp4, as judged from the SDS-PAGE (Figure 15 C) and confirmed by mass spectrometry (Table 18).

The size of the recombinant Elp456 complex was estimated by plotting the elution peak on a regression curve obtained from the elution peaks of the standard with known protein sizes. From this, the size of MBP-Elp456 was estimated to be around 612 kDa and the size of Elp456 (– MBP) around 452 kDa. The expected sizes for an as-

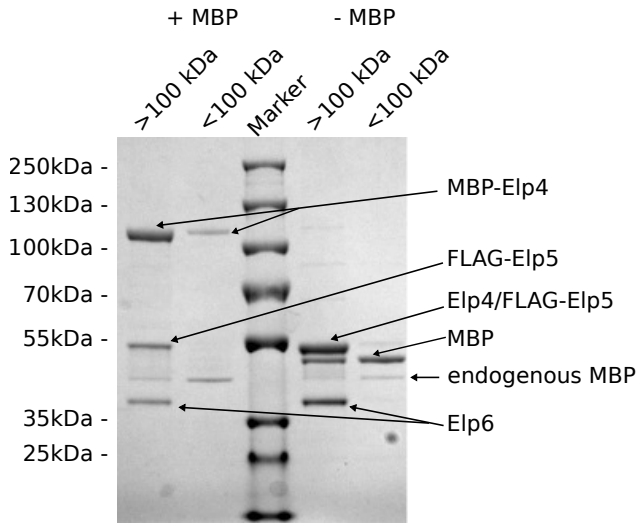

Figure 14: SDS-PAGE recElp456 purified from *E. coli*.

Image of an colloidal Coomassie stained gradient SDS-PAGE. **+MBP**: Shows the result of the purification of the recMBP-Elp456 subcomplex. Elution fractions were combined and concentrated via differential centrifugation using amicons with 100 kDa MWCO. The retanate is indicated as > 100 kDa. The flow through of the 100 kDa amicon was concentrated with an amicon with 10 kDa MWCO. **-MBP**: recElp456 after treatment with HVR3C protease followed by differential centrifugation with amicons. The retanate is indicated as > 100 kDa. The flow through is indicated with < 100 kDa. Elp4 now shows up in the same band as FLAG-Elp5. Marker = PageRuler Plus Prestained Protein Ladder.

sumed heterodimer were 348 kDa for MBP-Elp456 and 266 kDa for the complex without the MBP-tag. Next, the functionality of the recombinant Elp456 complex was addressed. The *S. cerevisiae* subcomplex is known to bind tRNA and to release it upon ATP hydrolysis [53]. To determine if the recombinant Elp456 holds RNA and releases it in an ATP dependent manner, the MBP-Elp456 complex was incubated with 10 mM ATP for half an hour on ice before injection into the SEC column. The analysis of the gel filtration in Figure 16 shows a dramatic increase of a peak around 25 kDa (orange curve compared to blue curve). The fraction could be radioactively end labeled using T4 PNK, which indicated that this peak contained nucleic acids (data not shown). The findings from this Section are discussed in Section 4.1.3.

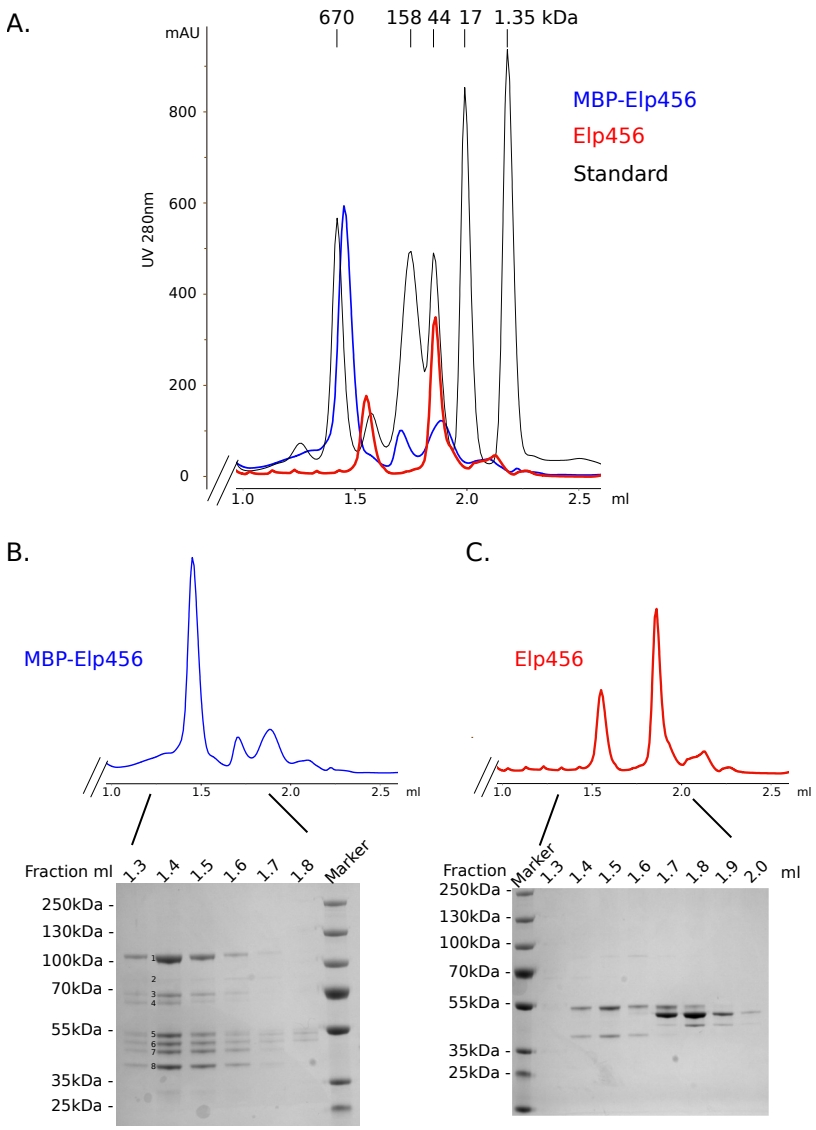

Figure 15: The size of the recHAP purified from *E. coli*

A. Overlay of UV_{280nm} curves from 3 different SEC runs. The Biorad Gel Filtration Standard 151-1901 (black) shows 6 protein peaks of known mass which are indicated above the graph. The blue curve (MBP-Elp456) shows one large peak just below 670 kDa and two small peaks below 158 kDa. The red curve corresponding to Elp456 without MBP tag. **B.** UV_{280nm} curve of SEC run of MBP-Elp456 (top) with colloidal Coomassie stained gradient SDS-PAGE of different elution fractions. The strong peak above 1.5 mL corresponds to the MBP-Elp456 subcomplex while the lower peaks correspond to MBP-Elp4 and endogenous MBP. Lane 1.4 mL was subject of MALDI mass spectrometric analysis (Table 18). **C.** UV_{280nm} curve of SEC run of Elp456 (top) with colloidal Coomassie stained gradient SDS-PAGE of different elution fractions. Also here the Elp456 are only found in the first peak just below 1.5 mL. The second peak at 1.9 mL corresponds to Elp4, the MBP-tag and endogenous MBP. Marker = PageRuler Plus Prestained Protein Ladder.

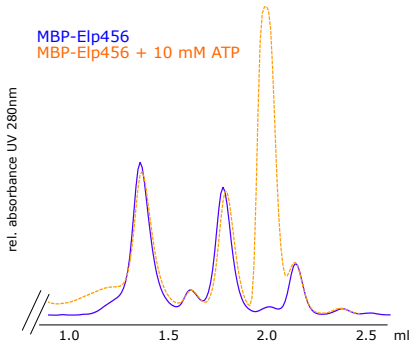

Figure 16: ATP releases nucleic acids from the recElp456 subcomplex.
UV_{280nm} curves of two SEC runs of MBP-Elp456 (blue) and the same MBP-Elp456 sample prior incubated with 10 mM ATP for half an hour (yellow). The peak at 1.4 mL corresponds to the MBP-Elp456 complex. The second peak at around 1.8 mL corresponds to MBP-Elp4 and endogenous MBP. The strong peak that shows up at 2 mL in the yellow sample corresponds to nucleic acids that are thought to be ATP-dependently released from the Elp456 complex.

3.1.4 *The 2A peptide sequence - a tool to investigate the reduced Elp3 level upon "overexpression"*

The idea for the experimental setup in the following subsection came from Felix Uecker, who also generated also the majority of cloning intermediates.

All co-IPs and affinity chromatographic purification of Elp3 shown in Sections 3.1.2.1 and 3.1.2.2 featured a nearly identical band intensity of Elp3 and its interaction partners Elp2 and Elp1, respectively. This observation is contrary to the findings for the other Elongator proteins, where the ectopically expressed protein is much more abundant than its respective interaction partners. Furthermore, the heterologous expression of MBP-Elp3 alone led to formation of inclusion bodies in *E. coli*, as it was predominantly found in the pellet (Appendix, Figure 49). These observations point towards the possibility that Elp3 is instable without interaction partners. However, there are other possibilities that could explain the lack of larger protein amounts upon overexpression, including a tight posttranscriptional regulation mechanism. This might prevent the expression of Elp3 above the level of its interaction partners. To address this question, different fusion genes connected by the 2A sequence were generated.

The 2A peptide sequence consists of 19 amino acids and was found in the Foot-and-Mouth Disease Virus (FMDV) [103]. It impairs normal peptide bond formation through a ribosomal skipping mechanism [104]. The sequence (LLNFDLLKLAGDVESNPG↓P-) prevents the ribosome from elongating the polypeptide chain after the second

glycine and a new polypeptide chain is started with proline as the N-terminal amino acid. A 2A sequence between two genes will result in two individual proteins in an equimolar ratio [105, 106]. To test whether the ribosomal skipping will occur in *D. discoideum*, a fusion construct was designed, consisting of mRFP, 2A and GFP. The results of the flow cytometric analysis with a control Western blot are shown in Figure 17. The Western blot image shows two signal bands for GFP. The lower band is the expected GFP signal and the upper band corresponds to the fusion protein product where ribosomal skipping did not occur. It can be concluded that the ribosomal skipping does also occur in *D. discoideum*, although the efficiency of this mechanism is incomplete for the mRFP-2A-GFP fusion construct. The 2D scatter plot confirms a clear correlation of GFP and RFP expression in an equimolar ratio (Figure 17).

Since the 2A induced ribosomal skipping could be verified in *D. discoideum*, it was used to determine if stability of the protein itself or regulation influence the expression level of Elp3. Elp3 was either fused between the mRFP and the 2A sequence or the 2A sequence and GFP (Figure 18). A posttranscriptional regulation mechanism would result in the 2 gene products in equimolar ratio independent of the position of the *elp3* gene in the construct. An instable Elp3 protein, on the other hand, would lead to 2 gene products in an unequal ratio with a lower amount of the Elp3-fusion protein. Figure 18 B shows the results of the flow cytometric analysis. The 2D scatter plot displays a considerable lower amount of the Elp3-fusion protein, independent of an N-or C-terminal localization of the 2A sequence. The connected Western blot images are shown in Figure 18 C. Further experiments with Elp-fusion constructs of different Elongator subunits can be found in the Appendix Figure 51. The *elp3* gene seems to have a direct negative effect on protein level of its fused gene (= the gene seperated from *elp3* by the 2A sequence) when placed 5´ of the 2A sequence, while this is not the case when *elp3* is placed 3´ of the 2A sequence. In conclusion, these experiments suggest an instability of the Elp3 protein. The protein stability might be increased by complex formation.

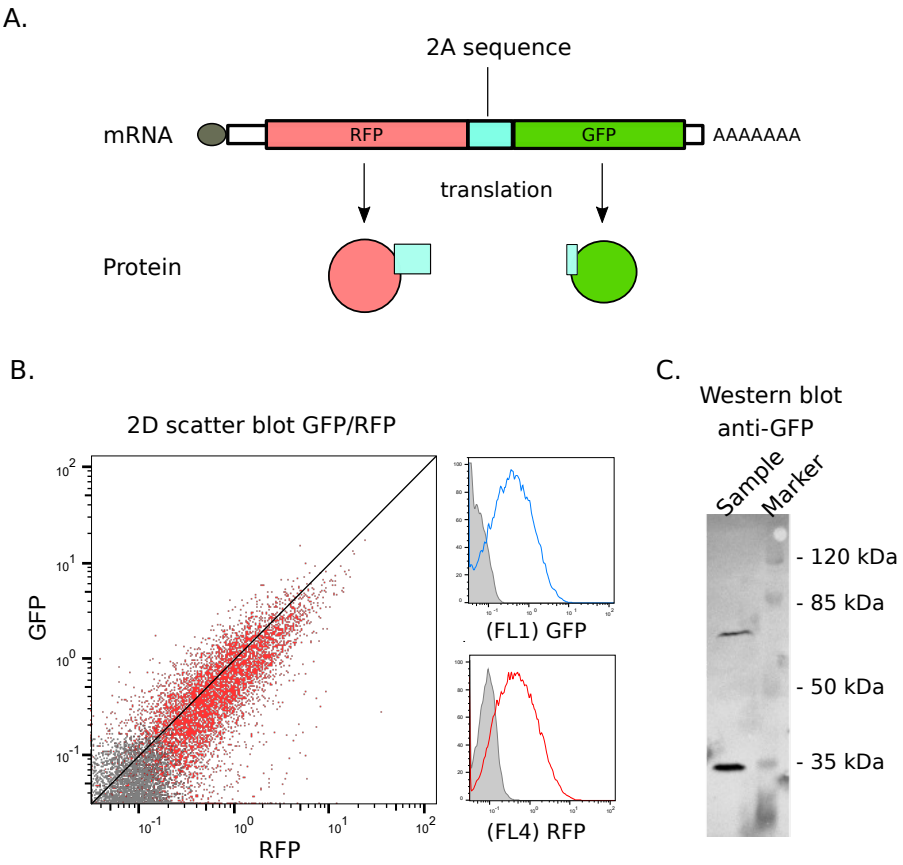

Figure 17: Testing the 2A peptide sequence in *D. discoideum*.

A. Sketch of the gene fusion with mRFP-2A-GFP. In the process of translation 2 proteins are produced; mRFP and GFP. The 2A sequence (LLNFDLLKLAGDVESNPG↓P-) prevents the ribosome from elongating the amino acid chain after the second glycine and a new amino acid chain is started with proline. **B. left:** 2D scatter plot of the relative fluorescence signals from the GFP and RFP channel (flow cytometry). Gray = negative control (7622 counts). Red = mRFP-2A-GFP sample (30000 counts). The majority of the cells a direct correlation of GFP signal to RFP signal is given. **right:** the GFP and RFP channels individual. **C.** Western blot anti-GFP. 2 bands are visable; the lower band correspondes to GFP and indicates that ribosomal skipping occurred, the higher band corresponds to the mRFP-2A-GFP fusion protein product where ribosomal skipping did not occur. Protein Marker = Prestained Molecular Weight Marker.

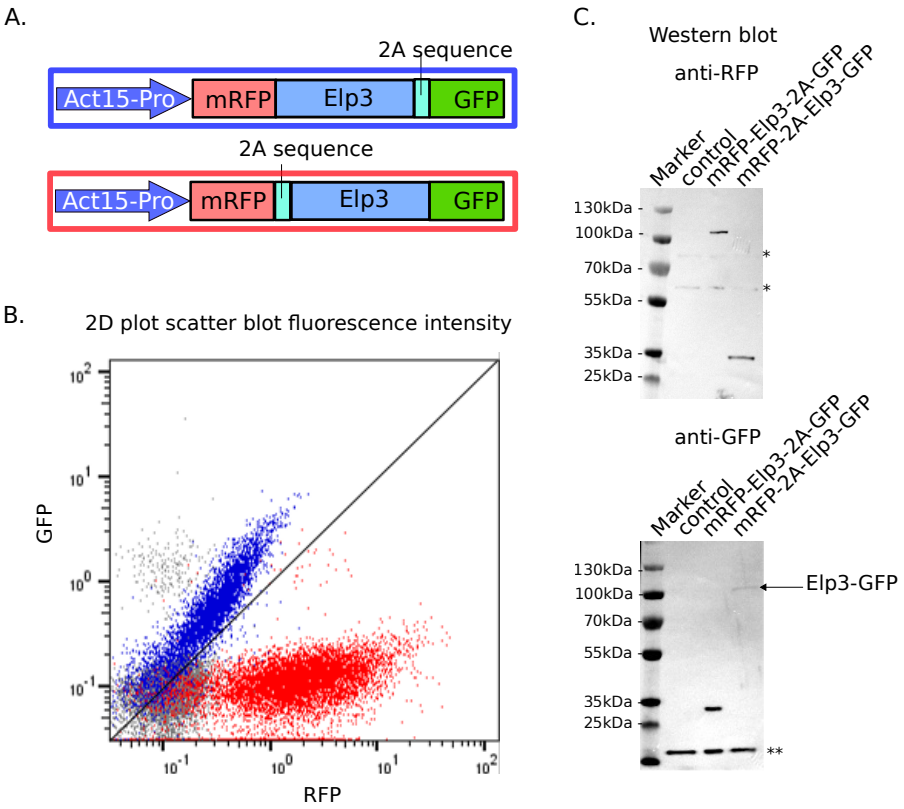

Figure 18: Elp3 2A sequence experiment in *D. discoideum*

A. Sketch of two constructs used in to determine Elp3 stability. Blue frame = mRFP-Elp3-2A-GFP. Red frame = mRFP-2A-Elp3-GFP. The plasmid used is based on the pDM318 plasmid, that features an actin 15 promotor in front of the expression cassette. **B.** 2D scatter plot relative fluorescence signal of GFP and RFP (flow cytometry). Cells expressing mRFP-Elp3-2A-GFP (blue) show a higher expression profile of GFP compared to mRFP-Elp3. In cells expressing mRFP-2A-Elp3-GFP a strong red fluorescence signal can be detected while there is little green fluorescence signal to be found. **C.** Western blots anti-RFP and anti-GFP. They serve as a quality control for complete ribosomal skipping. upper: Western blot anti-RFP. * Unspecific antibody reaction from the secondary goat-anti-rabbit antibody. Lower, Western blot anti-GFP. ** Unspecific antibody reaction of the secondary goat-anti-mouse antibody. The signal is used as a loading control. Marker = PageRuler Plus Prestained Protein Ladder.

3.2 INVESTIGATIONS ON THE ELONGATOR DEPENDENT ANTICODON U_{34} MODIFICATION IN D. DISCOIDEUM

As described in the introduction, ncm^5, mcm^5 and mcm^5s^2 modifications at *wobble* uridines of the anticodons can be found in almost all eukaryotes. Figure 3 shows which tRNAs carry the different modifications. The modifications are thought to stabilize the codon anticodon interaction in the ribosomal A- and P-Site. Loss of the mcm^5s^2U modification in yeast was shown to have a direct negative effect on translation efficiency of codons that are decoded by these tRNA species [11].

Most of the research on the Elongator dependent modification was done in yeast, *C. elegans*, mammalian cell lines and *A. thaliana*. So far, there was no information on these modification in Amoebozoa. This part of the thesis aims to answer the question if the Elongator dependent modification pathway is fully conserved in *D. discoideum*. If so, is the s^2U_{34} modification completely absent in Elongator mutants, like in *S. pombe* [57] and mammals, or is it to some extent independent of the Elongator complex akin to *S. cerevisiae* [47, 107]?

3.2.1 *Genes involved in the modification pathway*

The homologous *D. discoideum* genes involved in the Elongator dependent modification pathway are found in the dictybase.org database. Table 15 gives an overview of these genes and in which step of the pathway they are involved. Loss of function of any of these gene products leads to absence of the particular modification step (or greatly influences the levels of modification) [47]. The table also indicates gene deletion attempts in *D. discoideum* and their success within the AG Hammann. A detailed description of the successful gene deletion attempts within this thesis is included in the following Section 3.2.2.

3.2.2 *Generation of null mutant strains in D. discoideum*

D. discoideum possesses a haploid genome and gene deletion via homologous recombination is an established method for loss of function studies [109]. For the generation of the null mutants in this thesis, the pKOSG vector (purchased from IBA lifescience) was used [93]. The vector features a blasticidin resistance cassette (BS(r)) that can be flanked by, so called, left arm (LA) and right arm (RA), which are DNA fragments homologous to regions of the gene of interest. Gene deletion is accomplished by introduction of these constructs into the cell via electroporation. Upon homologous recombination, blasticidin resistant cells can be selected. The blasticidin cassette is additionally flanked by 2 loxP sites that allow for removal of the resistance cas-

Table 15: *D. discoideum* genes involved in the Elongator dependent modification pathway

GENE NAME	ID	MODIFICATION	MUTANT
elp1	DDB_G0284075	ncm^5	√ [a]
elp2	DDB_G0275651	ncm^5	√ [b]
elp3	DDB_G0290103	ncm^5	√
elp4	DDB_G0278783	ncm^5	√
elp5	DDB_G0276569	ncm^5	√ [c]
elp6	DDB_G0268624	ncm^5	×
kti11 (*dph3*)	DDB_G0277061	ncm^5	-
kti12	DDB_G0275667	ncm^5	× [b]
kti13	unknown	ncm^5	-
ppp6c	DDB_G0272118	ncm^5	×
cak1	DDB_G0273059	ncm^5	-
trm9	DDB_G0292448	mcm^5	√
trm112	DDB_G0285489	mcm^5	×
ctu1	DDB_G0282921	s^2	√
ctu2	DDB_G0268714	s^2	-
urm1	DDB_G0283737	s^2	×

[a][86]; [b][87]; [c][108]
√ = successful mutant strain generation; × = mutant strain generation failed; - = not subject to any gene deletion experiment

sette after gene deletion by transient expression of Cre recombinase [79].

3.2.2.1 *Gene deletion of elp3*

The catalytic subunit of the Elongator complex has a genomic DNA sequence of 1852 base pairs with 2 introns. Figure 19 A shows a sketch of the elp3 gene sequence with part of its genomic surrounding. Colony PCR screenings for correct pKOSG integration were performed on genomic DNA isolated from different subclones. Left arm and right arm integration were screened for with a combination of loxP specific primers and outer wild type primers. Figure 19 B shows a ethidium bromide stained agarose gel after electrophoretic separation. The PCR samples from clone 15 show signals at the expected sizes for both, left arm loxP and right arm loxP. All other clones, as well as the controls without DNA and the Ax2 wild type, show no amplicon. Figure 19 C shows the result of a PCR using the outer wild type primers. The wild type control shows a signal at around 2100 bp, while knockouts with blasticidin resistance cassette show a signal

at 2500 bp (clone 1 and 2 oligo method[2] and clone 1). As mentioned before, the resistance cassette can be removed from the genome. Figure 19 D shows the result of a PCR with the outer wild type primer on genomic DNA from *elp3*$^-$ clones after transient Cre recombinase expression. Removal of the cassette reduced the size of the PCR amplicon from approx. 2500 bp to approx. 1100 bp (Figure 19 D clone 5).

3.2.2.2 *Gene deletion of elp4*

Figure 20 A shows the sketch of the *elp4* genomic DNA sequence and a part of its genomic surrounding, as well as the blasticidin resistance cassette of the pKOSG vector with homologous regions to the the *elp4* gene. Figure 20 B shows the result of the PCR screening for left and right arm integration. Clone 1, 13 and 16 gave amplification signals of the expected size. Clone 2 showed only a signal for integration of the right arm, an indication for incomplete homologous recombination. Figure 20 C shows the result of the PCR screening with the outer wild type primer over the whole genomic surrounding. The size of the amplicon in the wild type situation is approx. 2100 bp while pKOSG integration results in an amplification size of approx. 2600 bp. Figure 20 D shows the comparison of the sizes from the Ax2 wild type, the *elp4*$^-$ strain and the *elp4*$^-$ after removal of the blasticidin resistance cassette, which reduces the amplification size to approx. 1200 bp.

3.2.2.3 *Gene deletion of trm9*

Trm9 gene deletion is shown to prevent the mcm^{5}U formation in yeast. A sketch of the *D. discoideum trm9* gene homologue is shown in Figure 21. The gel picture in Figure 21 B shows no left wild type signal for the two selected clones number 2 and 8, but a signal at around 800 bp, indicative of BS(r) cassette integration. Figure 21 C shows a similar result as in B, with no right arm wild type signal for the 2 selected clones but a loxP signal at 530 bp indicate proper BS(r) integration. A PCR amplification over the whole genomic region with the outer wild type primers was not successful, as well as an attempt to remove the resistance cassette via Cre recombination.

3.2.2.4 *Generation of ctu1*$^-$ *and elp3*$^-$*/ctu1*$^-$ *strains*

In yeast, the gene products of *ctu1* and *ctu2* form a protein dimer that functions as a thiourydilase responsible for the thiolation of the C2 of the pyrimidine ring at U_{34} of the anticodon as part of the mcm^{5}s^2 modification found in 3 tRNAs [26]. Disruption of any of the 2 genes leads to a loss of the s^2 modification. In order to obtain a thiolation

2 *elp3*$^-$ clones labeled oligo method are clones from a separate knockout generation experiment. The method involves addition of 100 µM oligos complementary to the end of the LA and RA to the electroporation [110]

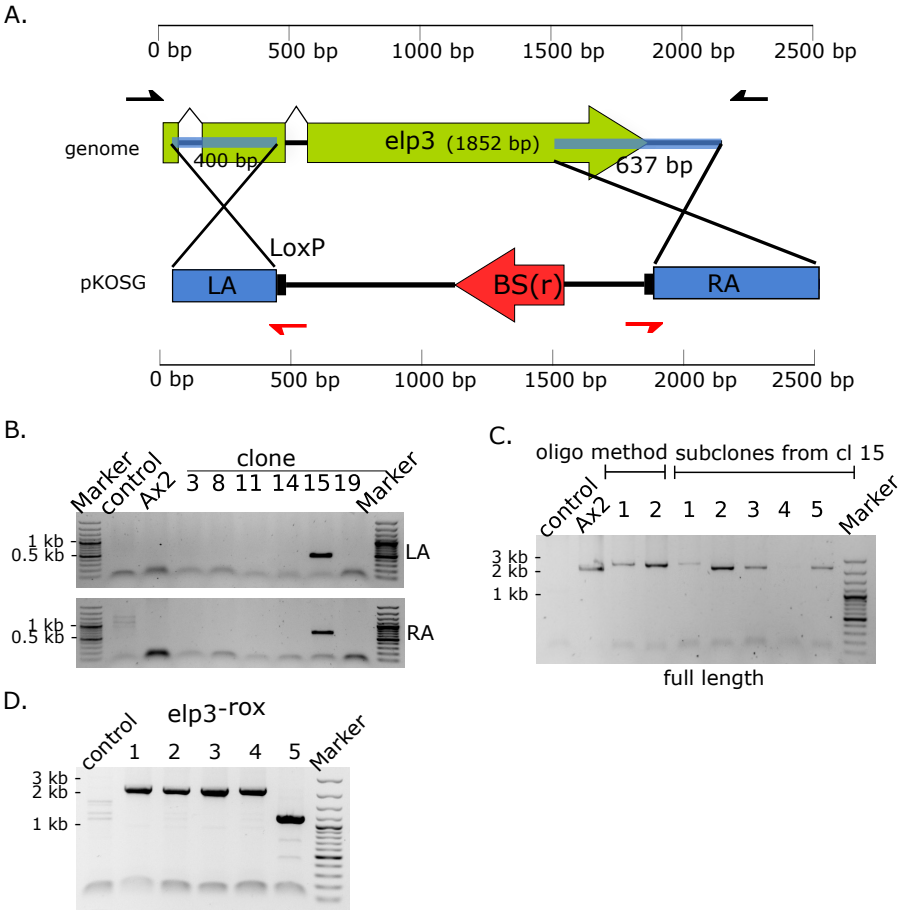

Figure 19: *Elp3* gene deletion.

A. Sketch of the elp3 gene (large olive arrow) and genomic surrounding. Left and right arm are indicated blue and have a size of 400 bp and 637 bp, respectively. The gene region that will be replaced by the BS(r) cassette lies in between the two arms. The small black (outer wild type primer) and red arrows (loxP primer) represent specific primer binding sites. The primer binding sites are not represented according to their size. **B.** PCR screening for LA and RA integration. Image of an EtBr stained 1% agarose gel electrophoresis with colony PCRs screening for pKOSG integration. Primers specific for genomic locus and loxP-sites in the construct. The signal is only expected when integration occurred at the right genomic locus. **C.** Screening over the whole genomic area. Image of an EtBr stained 0.8% agarose gel with a PCR screening with outer wild type primers (black arrows). After pKOSG integration, the amplicon is 374 bp larger compared to the Ax2 wild type. **D.** 0.8% Agarose gel image of a PCR screening for removal of the BS(r) cassette. When recombination occurred, the amplicon was 1500 bp smaller (clone 5). Control = PCR sample without DNA template. Marker = GeneRuler 100bp DNA Ladder Plus.

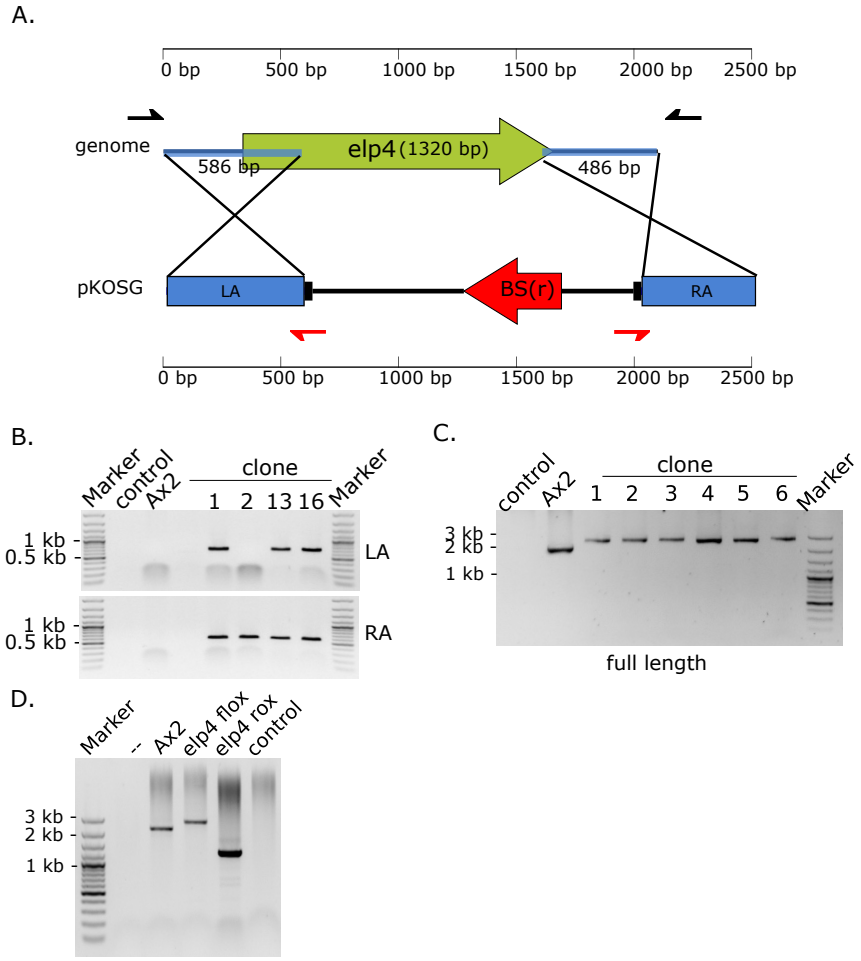

Figure 20: *Elp4* gene deletion.

A. Sketch of the elp4 gene (green arrow). Left an right arm (blue) have sizes of 586 bp and 486 bp, respectively. The gene region that will be replaced by the BS(r) cassette lies in between the two arms. The small black (outer wild type primer) and red arrows (loxP primer) represent specific primer binding sites used for the PCR screenings. **B.** Image of an EtBr stained 1% agarose gel with a PCR screening for pKOSG integration with specific primers for genomic locus (black arrows) and loxP-sites (red arrows). Clone 1, 13 and 16 show correct pKOSG integration. **C.** Agarose gel (0.8%) image with amplicons from a PCR screening over the whole genomic locus (primers used = black arrows). After pKOSG integrated the amplicon is around 500 bp larger. All 6 tested clones show an amplification size of correct pKOSG integration **D.** Agarose gel picture of a PCR screening for removal of the BS(r) cassette. The sizes of the amplicons are: Ax2 wild type (2100 bp), cassette integration = $elp4^{flox}$ (2600 bp) and after removal of the BS(r) cassette $elp4^{rox}$ (1200 bp). Control = PCR sample without DNA template. Marker = GeneRuler 100bp DNA Ladder Plus.

deficient strain in *D. discoideum* the *ctu1* gene was chosen for gene dis-

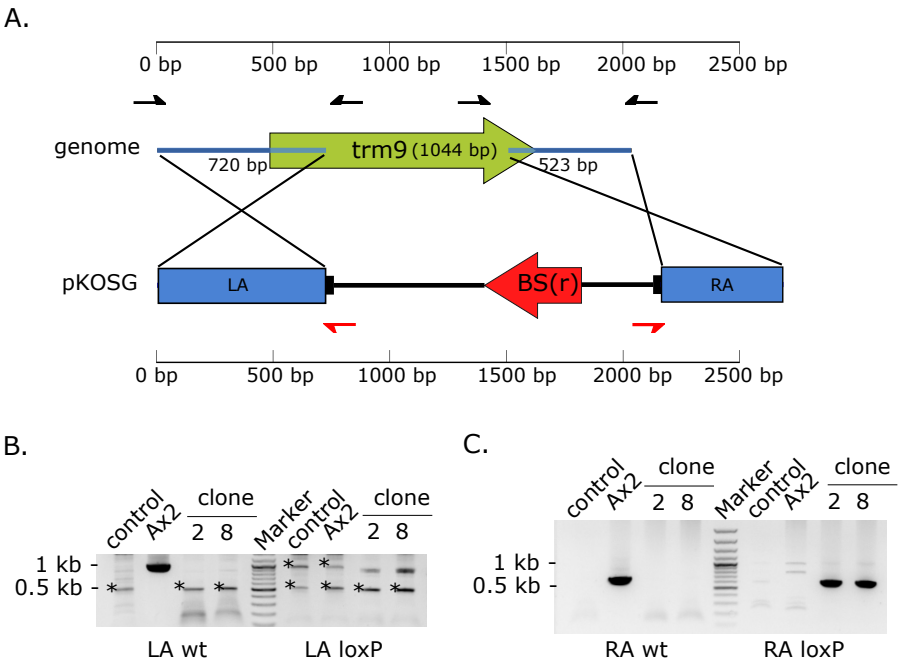

Figure 21: *Trm9* gene deletion.

A. Sketch of the trm9 gene (green arrow) and pKOSG fragment. Left and right arm are indicated in blue and have a size of 720 bp and 523 bp, respectively. The gene region that will be replaced by the BS(r) cassette lies in between the two arms. The black arrows indicate the inner and outer wild type primer binding sites used for the PCR screening in Figure 21 B and C (left arm and right arm wild type). The small red arrows indicate primer binding sites for the loxP sites. **B.** Image of an EtBr stained 1% agarose gel with amplicons of different PCR screenings. On the left side the screening for the left wild type signal is shown ((inner (left) and outer (left) wild type primer combination). A PCR amplification is only possible if the wild type situation is given. On the right side the PCR screening for pKOSG integration. Primers specific for left part of the genomic locus (outer wild type primer) and loxP-sites in the construct (red). Signal is only received when integration occurred at the right genomic locus. * = indicates unspecific PCR products produced by the primers, also seen in the control without template DNA **C.** Image of a EtBr stained 1% agarose gel with amplicons for the right arm (pKOSG) integration. Clone 2 and 8 could be identified as trm9 deficient. Control = PCR sample without DNA template. Marker = GeneRuler 100bp DNA Ladder Plus.

ruption. Figure 22 A shows scheme of the *ctu1* gene and the pKOSG fragment used for knockout generation. Figure 22 B shows the results of the PCR screening for BS(r) cassette integration with loxP specific primer and outer wild type primer. Clone 61 shows proper integration of the cassette with signals for the left and the right part of the cassette. Figure 22 C shows the result of a PCR screening with the

outer wild type primer. The wild type amplicon has a size of 2380 bp and the mutant amplicon has a size of 2680 bp. Figure 22 D shows the screening for ctu1 left arm loxP and right arm loxP integration in the *elp3*$^-$ background. Clone 20, 26 and 33 could be identified as *elp3*$^-$*ctu1*$^-$ double mutant.

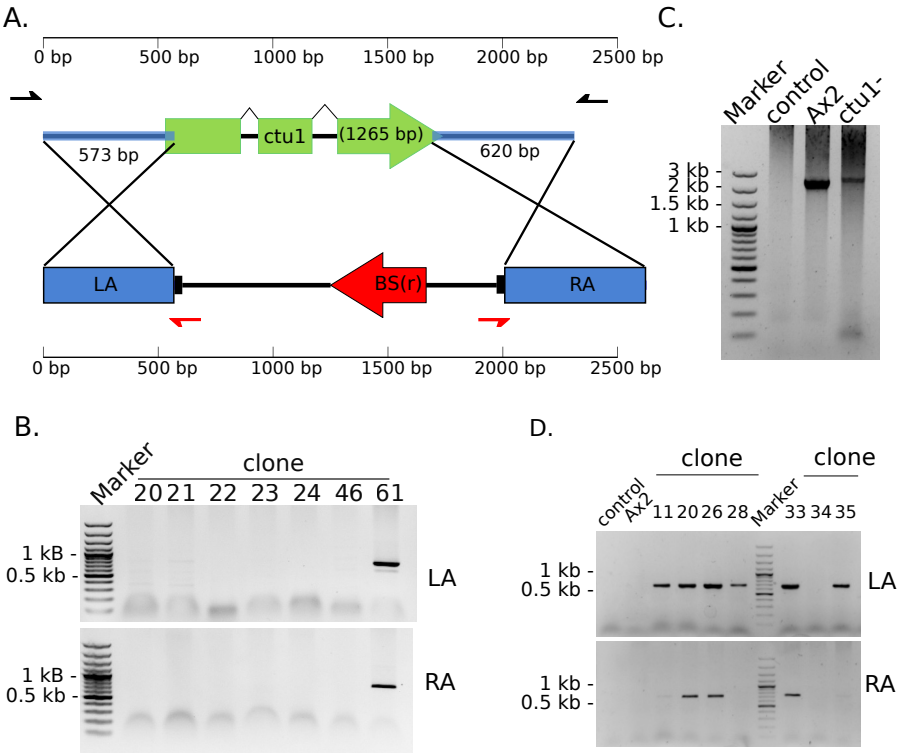

Figure 22: *Ctu1* gene deletion in Ax2 and *elp3*$^-$.

A. Sketch of the ctu1 gene (green arrow) and pKOSG fragment. Indicated in blue are the left arm (573 bp) and right arm (620 bp). The gene region that will be replaced by the BS(r) cassette lies in between the two arms. The small black (outer wild type primer) and red arrows (loxP primer) represent specific primer binding sites used for the PCR screenings. **B.** 1% Agarose gel picture of the PCR screening for pKOSG integration. Primers specific for the genomic locus and loxP-sites were used. A signal is only received when integration occurred at the right genomic locus. **C.** Agarose gel picture of the PCR screening over the whole genomic locus. If pKOSG integrated, the amplicon is 300 bp larger. **D.** Agarose gel picture of the PCR screening for pKOSG integration in the elp3^{flox} background. Clone 20, 26 and 33 could be identified as successful double knockouts. Control = PCR sample without DNA template. Marker = GeneRuler 100bp DNA Ladder Plus.

In the process of this thesis also other genes were targeted for loss of function via gene deletion. Gene disruption of *elp6*, *trm112* and *urm1* failed (data not shown).

3.2.3 *The Elongator dependent anticodon U_{34} modification in different null mutant strains*

The investigation of the Elongator dependent modifications themselves is not that trivial. Ncm^5, mcm^5 and mcm^{5}s^2 are small and only add 88, 103 or 119 Dalton in mass to an, in average, approximately 25 kDa molecule. There are also no antibodies available against these modifications. But these modifications are, in fact, very specific and only occur at the anticodon uridine position 34 [1]. To investigate the presence of these modifications in *D. discoideum*, total RNA from different strains was sent to the research group of Stefanie Kellner at the LMU Munich. There, the total RNA was separated on an HPLC to obtain the total tRNA fraction. This tRNA fraction was then digested to nucleosides, which were then separated and analyzed with a high performance liquid chromatography coupled to triple quadrupole mass spectrometry (HPLC-QqQ-MS-MS).

The results of the analysis performed by Stefanie Kellner are shown in Figure 23. The modified uridines cm^{5}U, ncm^{5}U, mcm^{5}U and mcm^{5}s^{2}U are present in the Ax2 wild type strain. Strains missing one of the Elongator subunits exhibit loss of cm^{5}U and consequently the ncm^{5}U, mcm^{5}U and mcm5^5s^{2}U modifications. In the *trm9*$^-$ strain, the cm^{5}U and ncm^{5}U modifications are detectable, while mcm^5 is absent. The levels of the cm^{5}U and ncm^{5}U modifications, however, do not increase in the mutant (discussed in Section 4.2.2). Deletion of *ctu1* leads to a loss of the mcm^{5}s^{2}U modification, which results in a drastic accumulation of the mcm^{5}U modification. The increase of the mcm^{5}U level corresponds to the decrease of mcm^{5}s^{2}U modification in this mutant.

Two modifications appear in different mutants, which are not found in the Ax2 wild type. In *elp3* deficient strains, the s^{2}U modification is found (Figure 23 E) and in the *trm9* deficient strain the ncm^{5}s^{2}U can be observed (Figure 23 F). However, the s^{2}U level is 20 fold below, and ncm^{5}s^{2}U is at least 3 fold below the mcm^{5}s^2 U level observed in the wild type.

Next, APM Northern blot analysis was performed to address the specificity of the thiolation to the tRNAs tK^{UUU}, tE^{UUC} and tQ^{UUG}. Acryloylaminophenylmercuric chloride (APM) is an organic mercury compound that can be embedded into a polyacrylamid matrix of normal poly acrylamide gels (PAA) [98, 111]. Molecules carrying sulfur atoms will be held back in the gel matrix, resulting in a shift that does not correspond to the migration distance of their molecular size. In combination with Northern blot analyses, thiolation levels of specific RNA molecules thus can be determined by use of APM [26]. Figure 24 shows Northern blots of tQ^{UUG} (**A**) and tK^{UUU} (**B**) with and without APM. The diffuse signal in the upper third (indicated by s^{2}U) of the lane corresponded to the thiolated fraction of the tRNA while the

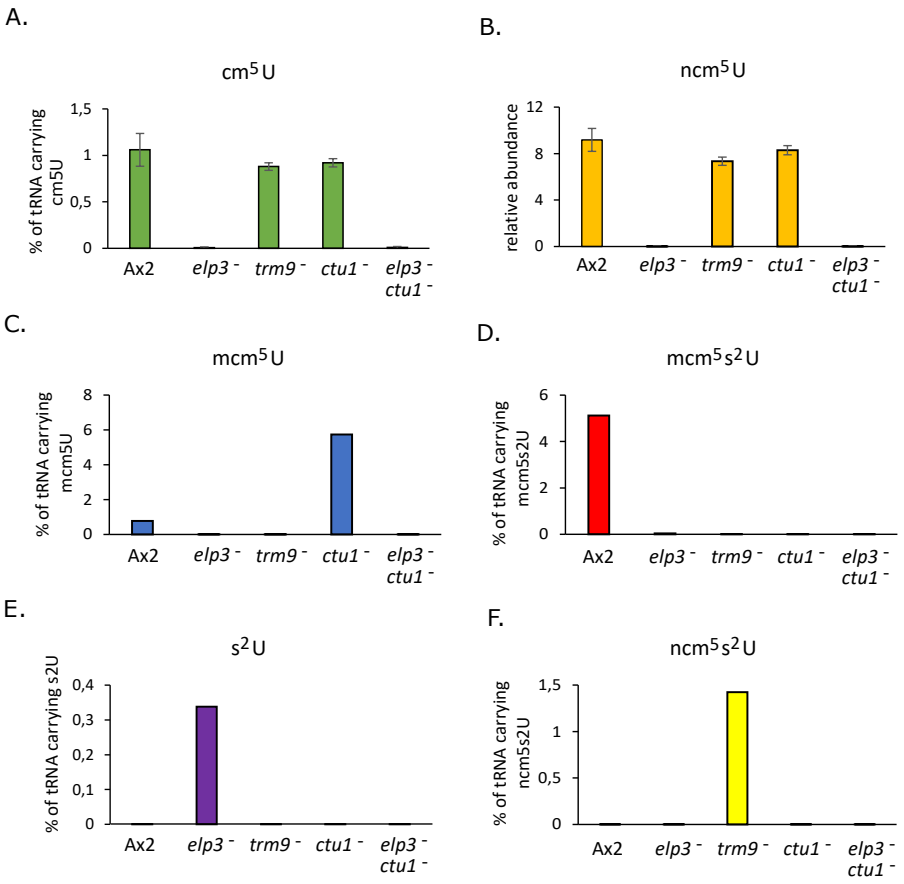

Figure 23: Analysis of the different Elongator dependent anticodon modifications and their appearance in different knockout backgrounds. **A.** % of tRNA carrying the cm^5U modification. **B.** relative abundance of the ncm^5U modification. Only the relative peak areas of the different samples could be compared, since no synthetic standard ncm^5U was used in the analysis. **C.** % of tRNA carrying the mcm^5U modification. **D.** % of tRNA carrying the mcm^5s^2U. **E.** % of tRNA carrying the s^2U modification. **F.**% of tRNA carrying the ncm^5s^2U modification. Error bars shown in A. and B. represent standard deviation of the repetition of the analysis. The repetition was not necessary for C. to F.

unthiolated fraction is found at the bottom. This analysis indicates that a significant fraction of both, tQ^{UUG} and tK^{UUU} is thiolated in the Ax2 wild type. Only a faint upper signal can be observed for tQ^{UUG} in the *elp3*$^-$ strain. tK^{UUU} and tQ^{UUG} of the *trm9*$^-$ strain show a slightly stronger thiolation signal compared to the *elp3*$^-$ strain. The *ctu1*$^-$ strain and the *elp3*$^-$*ctu1*$^-$ strain show no signals that would correspond to a thiolated fraction of these tRNAs. Taken together, the results shown in Figure 23 and Figure 24 indicate that the thiolation of the U_{34} is conditionally dependent on the initial Elongator modification ncm^5 but only the full conversion to mcm^5 leads to a high thi-

olation level. The complete analysis of Stefanie Kellner can be found in the Appendix Section A.2.1 (Figure 52 to Figure 55).

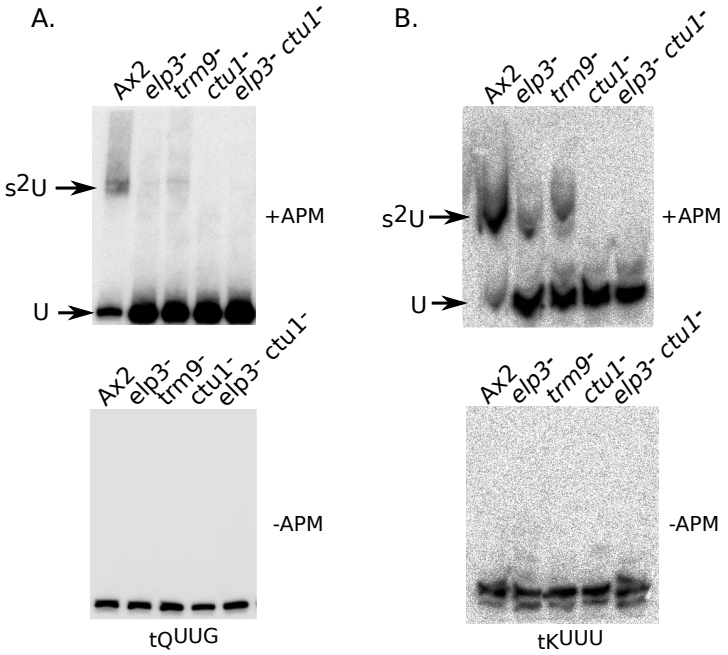

Figure 24: Thiolation level of specific tRNAs in different mutant strains. **A.** Image of a Northern blot against tQ^{UUG} with RNA from the Ax2 wild type compared to the modification deficient mutant strains. Top: APM was included in the PAA matrix. Thiolated RNA molecules interact with the mercury embedded in the gel matrix, resulting in a electrophoretic shift that does not correspond to their size (indicated with s^2U). Bottom: Control northern without APM. **B.** Top: APM Northern blot images against tK^{UUU}. The different thiolation level between Ax2 wild type, *elp3*$^-$ and *trm9*$^-$ are clearly visible. The *ctu* deficient strains do not show any thiolation signal. Bottom: Control Northern blot without APM.

3.2.3.1 *The radical SAM and HAT domains of Elp3 are both required for tRNA modification*

A significant part of the literature connects the protein domains of Elp3 to different cellular functions of the Elongator complex. The HAT domain is connected to histone and tubulin acetylation [49, 50, 55], taking part in epigenetic gene regulation and directed transport [56], while the radicalSAM domain is connected to tRNA modification [20] and DNA demethylation [54]. In yeast, it was shown that both catalytic domains are indispensable for the tRNA modification at U_{34}.

Two point mutated GFP-Elp3 constructs were generated to address whether Elp3 is the catalytic subunit of the Elongator complex in *D. discoideum* and if both catalytic domains are needed also in the amoeba for the modification of the U_{34} in tRNAs. The introduced

point mutations are similar to the mutations used in the study of Okada [54]. In the radicalSAM domain, two cysteines of the cysteine tetrade in the catalytic core were changed to serines. In the HAT domain, two glycines in the catalytic core were replaced by phenylalanines. Whether these point mutants can rescue the Elongator dependent U_{34} modification was investigated by APM Northern blotting, using RNA from *elp3*$^-$ strains carrying pDM317 GFP-mutSAM-Elp3 or GFP-mutHAT-Elp3. This was compared to RNA extracted from the Ax2 wild type and the *elp3*$^-$ strains. The result of the experiment is shown in Figure 25. The upper signal corresponds to the thiolated fraction of the tRNAs tK^{UUU}, tE^{UUC} and tQ^{UUG} and the lower to the unthiolated fraction. A strong thiolation signal is detectable in the Ax2 strain, while the *elp3*$^-$ strain displays only a faint signal. The tRNAs from the point mutants display a similar low thiolation signal as the *elp3*$^-$ strain, indicating that both mutations result in proteins that cannot rescue the phenotype to the wild type situation. The ectopically overexpressed N- and C-terminal GFP Elp3 fusion proteins, however, are capable to rescue the phenotype, resulting in the wild type situation. This indicates that these fusion proteins are functional. Together with data shown in Section A.2.1, both domains of Elp3 thus appear to be indispensable for the Elongator dependent U_{34} modifications.

3.2.4 *Elongator dependent codon usage is favored in D. discoideum*

In their study on Elongator mutants in *S. pombe*, Bauer and colleagues suggest a direct connection between codon usage of genes in specific functional pathways and expression level of the corresponding proteins in Elongator deficient mutants [112]. The phenotypes of the mutants could be rescued by elevated levels of unmodified tK^{UUU} and tE^{UUC} or changing the lysine AAA codon of the gene to the Elongator independent codon AAG [112].

The observations made in yeast might be helpful for predicting stress phenotypes in *D. discoideum*. For this purpose, genome statistics available on dictybase.org and yeastgenome.org were compared. The first striking observation was the low copy number of tK^{UUU} genes in the yeast genomes (Table 16 A and B; Figure 26). This is especially interesting, since for the overall lysine codon usage the A ending codon is favored (Table 16 A and B). Bauer and colleagues showed that strongly expressed genes, like ribosomal proteins, prefer AAG over AAA in a 2:1 ratio [112]. This is contrary to the global codon usage for lysine in *S. pombe* with 60% AAA and 40% AAG and the same holds true for *S. cerevisiae*. The lysine codon usage ratio in highly expressed genes of the translational pathway seems to be similar to the ratio of tRNA genes decoding for the two different lysine codons. The two yeast species feature twice more gene copies for tK^{CUU} than

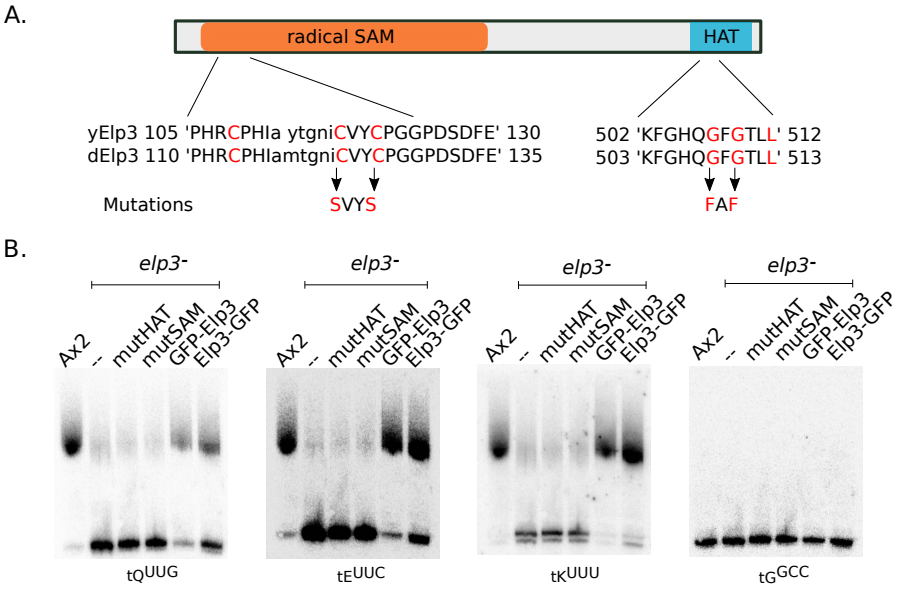

Figure 25: APM Northern blots on strains expressing different Elp3 variants. **A.** Schematic representation of the Elongator protein 3 and its catalytic domains. yElp3 = Elp3 from *S. cerevisiae*. dElp3 = Elp3 from *D. discoideum*. Capital letters indicate strict conservation between Elp3 proteins. Lower case letters indicate less conserved amino acids. Marked red are the amino acid that are proven essential for the function of the corresponding catalytic domain. Mutations indicate the specific mutated amino acids for mutSAM and mutHAT Elp3 constructs used in B. **B.** APM northern blot of wild type Ax2 strain and different elp3$^-$ mutant strains expressing different pDM317 Elp3 constructs. mutHAT GFG $\rightarrow$ FAF. mutSAM CVYC $\rightarrow$ SVYS. From left to right: probe against tQ^{UUG}, probe against tE^{UUC}, probe against tK^{UUU}, probe against tG^{CCG}.

for tK^{UUU} (Table 16 A and B). The functional pathways that give rise to the stress phenotypes, however, have an average codon usage of around 70% lys-AAA [112].

D. discoideum features a very AT rich genome with a strong codon bias towards A ending codons [70]. The codon usage for lys-AAA and glu-GAA are shown in Figure 27. Strongly expressed genes shows a codon usage of 70 – 80% AAA to 20 – 30% AAG. The codon usage thus seems to have a similar ratio as the ratio of tRNA genes decoding these codons (Table 16 C). The genome of *D. discoideum* also features a greater copy number of tRNA genes in general (Figure 26, Table 16 and Appendix Figure 58.) An analysis of codon bias of different functional pathways in *D. discoideum* did not reveal significant differences in codon usage for lysine or glutamate (Figure 28). Also, there is no evidence for a varying codon bias in specific pathways. Rather, there seems to be a clear correlation in *D. discoideum* between tRNA copy number and codon frequency in all investigated functional gene groups.

Table 16: Codon usage and tRNA gene copy number of *S. pombe*, *S. cerevisiae* and *D. discoideum*

A.

S. pombe[a]

AMINO ACID	CODON	CDN USE*	REL. CDN USE	tRNA**
Glutamate	GAA	44.4	67.9%	5
(E)	GAG	21.0	32.1%	6
Glutamine	CAA	27.5	71.5%	4
(Q)	CAG	10.9	28.5%	2
Lysine	AAA	39.8	61.9%	4
(E)	AAG	24.5	38.1%	9

B.

S. cerevisiae[a]

AMINO ACID	CODON	CDN USE*	REL. CDN USE	tRNA**
Glutamate	GAA	45.6	69.7%	15
(E)	GAG	19.2	30.3%	2
Glutamine	CAA	27.3	69.3%	9
(Q)	CAG	12.1	30.7%	1
Lysine	AAA	41.9	57.6%	8
(E)	AAG	30.8	42.4%	14

C.

D. discoideum[b]

AMINO ACID	CODON	CDN USE*	REL. CDN USE	tRNA**
Glutamate	GAA	49.1	84.8%	19
(E)	GAG	8.8	15.2%	3
Glutamine	CAA	48.6	96.2%	13
(Q)	CAG	1.9	3.8%	1
Lysine	AAA	65.1	85.0%	22
(E)	AAG	11.5	15.0%	10

* CDN USE = codon usage in 1000 codons

** tRNA = tRNA gene copy number

[a] data collected from www.kazusa.or.jp/codon/ and http://gtrnadb.ucsc.edu/

[b] data collected from www.dictybase.org

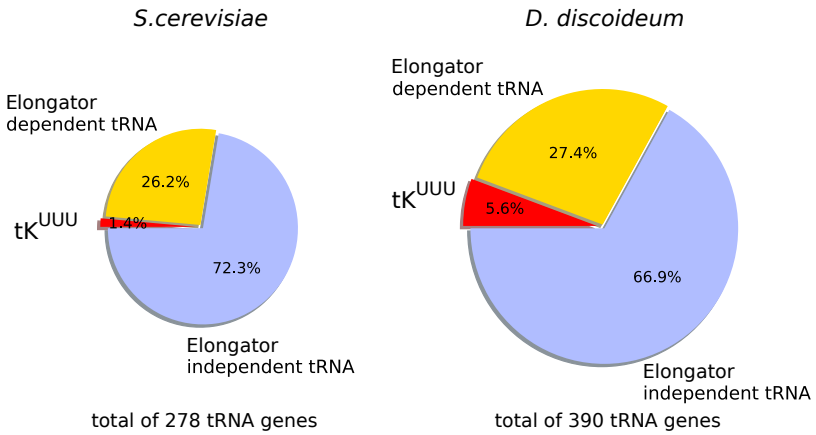

Figure 26: Pie chart comparison of Elongator dependent modified tRNA copy number to the global tRNA gene copy number in *S. cerevisae* and *D. discoideum*.

Indicated in yellow are the relative copy numbers of all Elongator dependent modified tRNA genes combined (-tK^{UUU}). The relative tK^{UUU} gene copy number is shown in red. All other tRNA are indicated. The sizes of the pie charts reflect the total tRNA gene number in the *S. cerevisae* and *D. discoideum*.

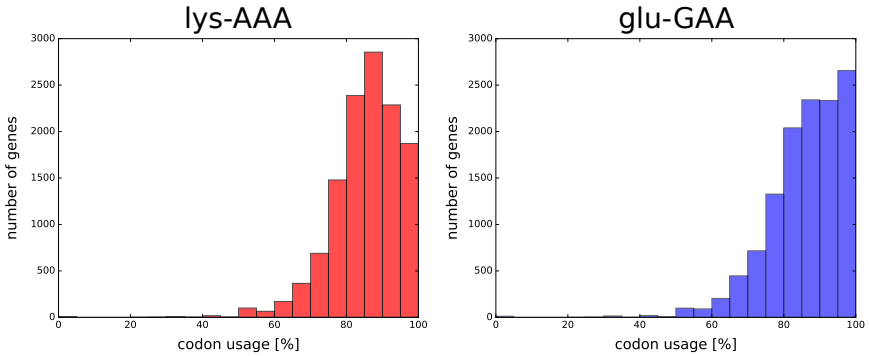

Figure 27: Histograms of the distribution of the relative codon usage for lysine AAA/AAG (left) and glutamate GAA/GAG (right) of all *D. discoideum* genes.

3.2.5 *The generation of an unconditional tQ^{CUG} null mutant and tRNA overexpressors in D. discoideum*

In contrary to yeast, the abundance of tK^{UUU} and tE^{UUC} genes in *D. discoideum* should - in theory - prevent any mutant strains lacking the U_{34} modification to display severe growth phenotypes, if the same situation is to be found as in *S. pombe* [112]. The extreme codon usage for glutamine in *D. discoideum* (Table 16 C) raises the question if the single tQ^{CUG} tRNA gene might be dispensable. The prokaryotic tQ^{UUG} is able to read the CAG codon, while the eukaryotic counterpart may not be able to do so [113]. Attempts to remove the single copy of tQ^{CUG} gene in *S. cerevisiae* was only successful, when that tRNA was simultaneously ectopically expressed [107].

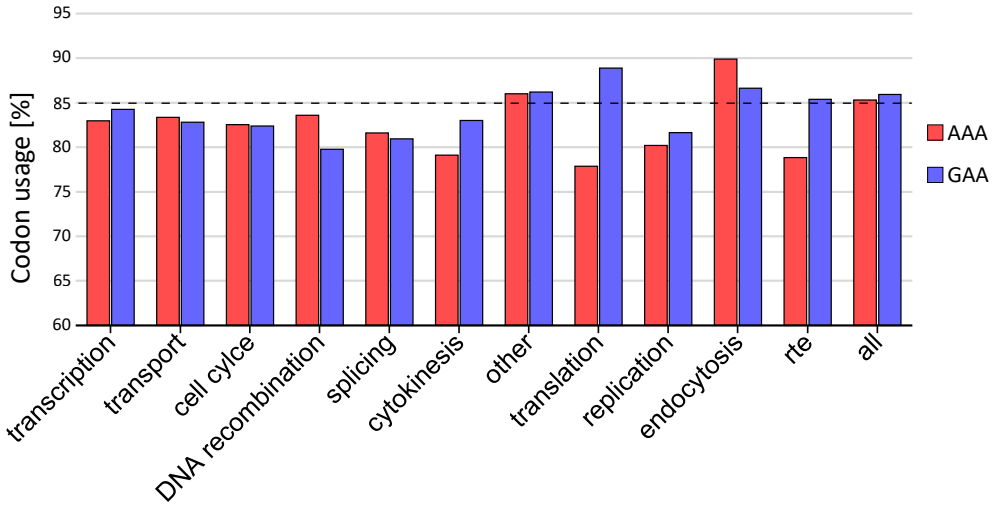

Figure 28: Bar chart of the relative codon usage in *D. discoideum* for lysine AAA/AAG (red) and glutamate GAA/GAG (blue) in different functional pathways (defined by GO-terms).
The dashed black line indicates the average codon usage of lys-AAA and glu-GAA (both around 85%). rte = retrotransposable elements. Data generated by Kim Philipp Jablonski.

To address if the single tQ^{CUG} gene is also essential in *D. discoideum*, a knockout construct targeting the genomic surrounding of the tQ^{CUG} gene was constructed and used for transformation of the Ax2 wild type and *elp3*$^-$ strains. Figure 29 A shows the design of the construct. Figure 29 B shows an ethidium bromide stained agarose gel image of the PCR products retrieved from the Ax2 wild type and a potential tQ^{CUG} deficient strain. The size of the 2 individual PCR amplicon met the expectations (Ax2 approx. 650 bp; tQ^{CUG} 1850 bp). This indicates a successful deletion of the targeted genomic area in the Ax2 background. A Northern blot against tQ^{CUG} confirmed the successful deletion of the tQ^{CUG} gene in the Ax2 background (Figure 30). Contrary to this, knockout attempts in the *elp3*$^-$ background failed, as PCR analysis revealed signals for both, the wild type and knockout (Figure 29 D). No further attempts were carried out to delete the tQ^{CUG} gene in the *elp3* deficient strain (discussed in Section 4.2.1). Since a viable tQ^{CUG} deficient strain was obtained in the Ax2 wild type background, it seems possible that tQ^{UUG} might be able to read the CAG codon to some extent.

The question if functional tRNA genes can be overexpressed in *D. discoideum* was addressed next. Therefore the genomic surrounding approximately +/− 250 bp from tRNA genes were amplified and cloned into a pDM-Vector backbone. The pDM plasmids for *D. discoideum* have with 40 to 60 copies per cell a high copy number [80]. Northern blot analysis of the tQ^{CUG-} deficient and the overexpressor strains showed clear expression differences compared to the Ax2 wild

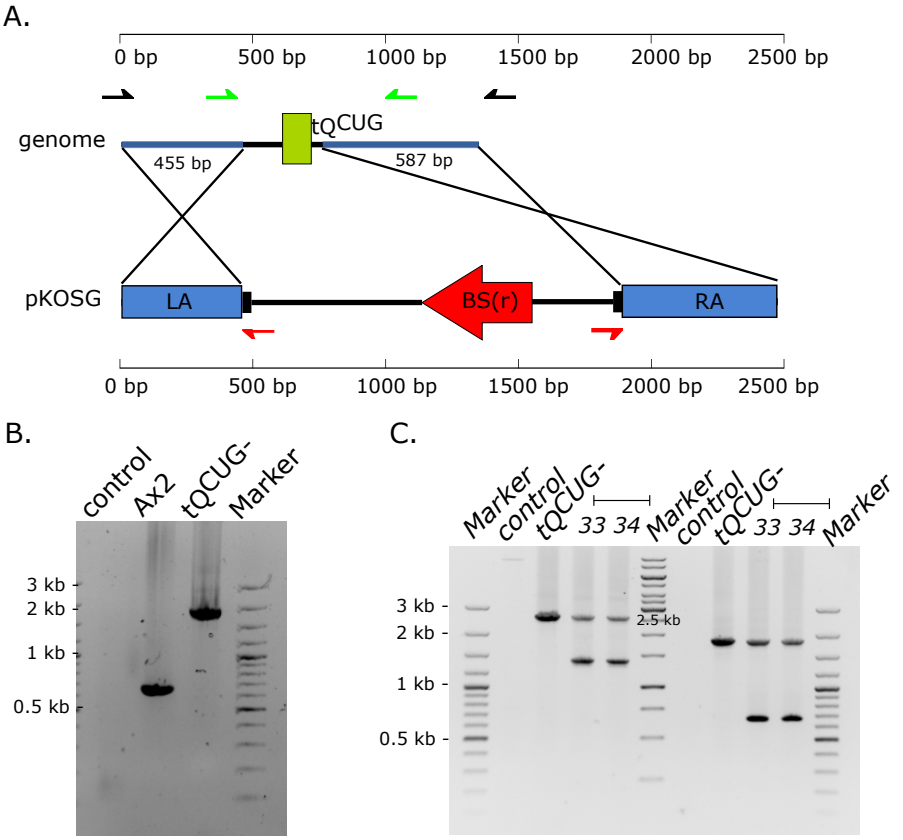

Figure 29: Deletion of the single copy tRNA tQ^{CUG}.
A. Sketch of the tQ^{CUG} gene (green box) and genomic surrounding. Indicated in blue are LA and RA where the homologous recombination takes place. The genomic sequence in between the sequence will be replaced by the BS(r) cassette. The green and black arrow indicate the primer site for the screening PCRs. **B.** Agarose gel (1%) picture of the PCR amplicons received from Ax2 and the potential tQ^{CUG} deletion strain. The primer used for this PCR are indicated in A. green. **C.** Agarose gel (1%) picture of the PCR amplicons received the tQ^{CUG} deletion strain shown in B. and two potential tQ^{CUG} knockouts in an *elp3*$^{-}$ strain (clone 33 and 34). The two clones in the *elp3*$^{-}$ background display a wild type and a knockout signal. Marker = GeneRuler 100bp DNA Ladder Plus

type. The tQ^{CUG} lacking strain showed only a weak signal (crossbinding of the tQ^{CUG}-probe to tQ^{UUG}), while the overexpressors displayed a several fold increase of the signal (Figure 30). The experiment thus proved that the tRNA gene is transcribed from the pDM plasmid, and the transcript is processed in a product of the size of the mature tQ^{UUG}.

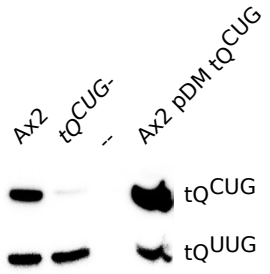

Figure 30: Northern blot confirmation of tQ^{CUG} null mutant and tQ^{UUG} overexpressor strains.

Northern blot image probed for tQ^{CUG} and tQ^{UUG} RNA. From left to right: Ax2 wild type; tQ^{CUG} deletion strain; Ax2 expressing the multicopy plasmid pDM tQ^{CUG} that carries tQ^{CUG} with genomic surrounding (+/- 250 bp). 5 µg total RNA.

3.2.6 *The effect of the loss of anticodon U_{34} modification on glutamine codon translation*

The abundance of tRNA genes in *D. discoideum* might make it hard to predict potential gene products that could be affected by the loss of U_{34} modification. However, *D. discoideum* possesses the prion-richest proteome known to date [71]. A significant portion of proteins feature long poly glutamine stretches within their amino acid sequences. *D. discoideum* genes use almost exclusively one glutamine codon, which leads to an overall glutamine codon usage of 96% CAA to 4% CAG (Figure 31).

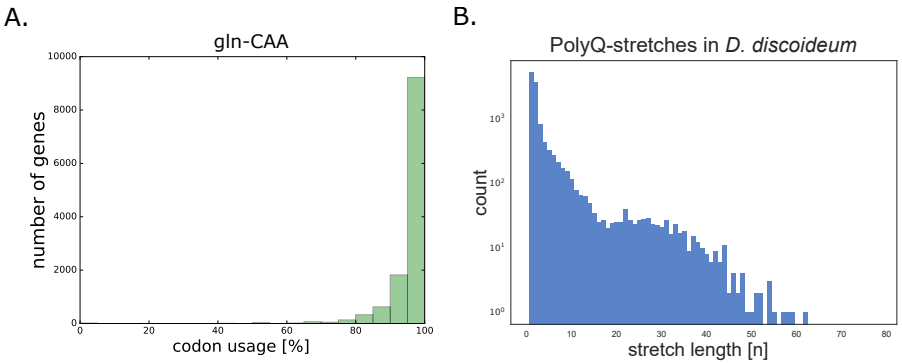

Figure 31: relative CAA/CAG codon usage and PolyQ-stretches in *D. discoideum*.

A. Histogram of the relative glutamine codon usage for CAA per gene. Over 9000 genes use > 95% CAA resulting in the overall CAA codon usage at 96%. **B.** Histogram of length of PolyQ-stretches and their number of appearances in genes. Data and Figure generated by Kim Philipp Jablonski.

In an attempt to quantify expression differences between the generated mutant strains and the Ax2 wild type, leader constructs with

different CAA to CAG ratios coupled to GFP were generated (Figure 32 A). The extended human huntingtin exon 1 (103Q) features a 1:1 ratio of CAA: CAG, erkA (52Q) features only the CAA codon and a synthetic polyQ (Q15) only features the CAG codon. The pDM353 Q103 was provided by Liliana Malinovska [71], all other leader constructs were cloned into the pDM323[3] and are under the control of an actin 15 promotor (Figure 32 A and B). tRNA overexpression in leader construct strains was achieved by cloning the tRNA into the same plasmids (Figure 32 C). Expression was meassured via flow cytometry and Western blotting with an antibody against GFP was performed as a quality control. Glutamine-leader-GFP expression of Ax2 wild was set to 100%. No normalization towards global gene expression differences was implemented (see discussion Section 4.2.4).

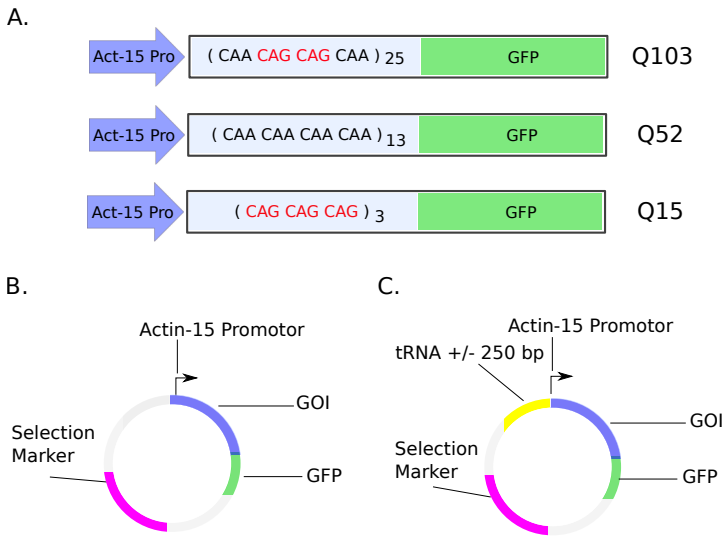

Figure 32: Sketch of different polyglutamine leader construct fused to GFP, used to determine the translation efficiency of the different mutant strains.

A. The 3 different polyglutamine leader used: Q103 is the extended human Huntington exon 1 and features a stretch of 103 glutamine codons 50% of which read CAA or CAG, respectively. Q52 is part of the endogenous *D. discoideum* gene *erkA*. It features a 52 long stretch of the glutamine codon CAA. Q15 is a synthetic leader construct consisting of 15 CAG codons. **B.** All leaders were expressed from pDM323/pDM353 plasmids. **C.** For control expression experiments featuring overexpression of tRNA, tRNA +/- 250 bp were placed on the same plasmid, that the leaders were expressed from to ensure similar expression conditions between different strains and cell lines.

Figure 33 shows the fluorescence intensity of the Q103-GFP expression in different mutant strains compared to the Ax2 wild type (red curve). Q103-GFP expression was significantly reduced in the

3 pDM323 and pDM353 are nearly identical. Both feature the GFP gene 3′ of the GOI. The only difference lies in the applied cloning strategy

elp3$^-$ background (Figure 33 A). A minor reduction can be seen in the *trm9*$^-$ mutant background (Figure 33 B) and no reduction of the Q103-GFP fluorescence is observed in the *ctu1* mutant (Figure 33 C). The Q103-GFP fluorescence profile in the *elp3*$^-$*ctu1*$^-$ strain displays a narrower fluorescence peak width compared to all other mutants with a reduction of the fluorescence signal similar to that of the *elp3*$^-$ background (Figure 33 D). The tQ^{CUG-} knockout, finally, shows the strongest reduction of Q103-GFP expression compared to the wild type. The fluorescence signal is, however, still several fold above the signal of the negative control, suggesting that tQ^{UUG} can *wobble* over the CAG codon (Figure 33 E).

Overexpression of tQ^{CUG}, shown as the green curves in the center panels, did not influence expression level in the Elongator mutant nor *trm9*$^-$ and *ctu1*$^-$ strains, but it increased the expression of Q103-GFP in the knockout tQ^{CUG-} to approximately 70% of the wild type level. Expression of tRNA tQ^{UUG} had a positive effect on Q103-GFP expression in the *elp3*$^-$ and *elp3*$^-$*ctu1*$^-$ strains, as can be seen from the increased expression to almost the wild type expression level. The average (geometric mean) fluorescence intensities of the different constructs, in the single mutants, are summarized and compared in the bar chart on the very right of Figure 33. 3 to 6 individual measurements, with around 30000 cells were taken in independent experiments. All fluorescence measurements of the individual constructs in the single mutants, however, were compared to the Ax2 wild type expression of the same day. Error bars are derived of the minimum and maximum value of all repetition experiments (at least 3 times 30000 counts), thus indicating the maximum observed deviation. It is worth to note, that in all experiments Q103-GFP expression level in the Ax2 wild type background dropped when tRNA gene was introduced on plasmid while this was not observed in the mutant strains (Figure 59). Figure 33 F shows a Western blot image displaying Q103-GFP expression in the different strains.

Taken together, the data shown in Figure 33 provide a good indication that the mcm^5s^2U modification has a positive effect on the translation of glutamine codons. In the mutant background of *elp3*$^-$ and *elp3*$^-$*ctu1*$^-$, overexpression of the unmodified tQ^{UUG} increased the expression level of Q103-GFP.

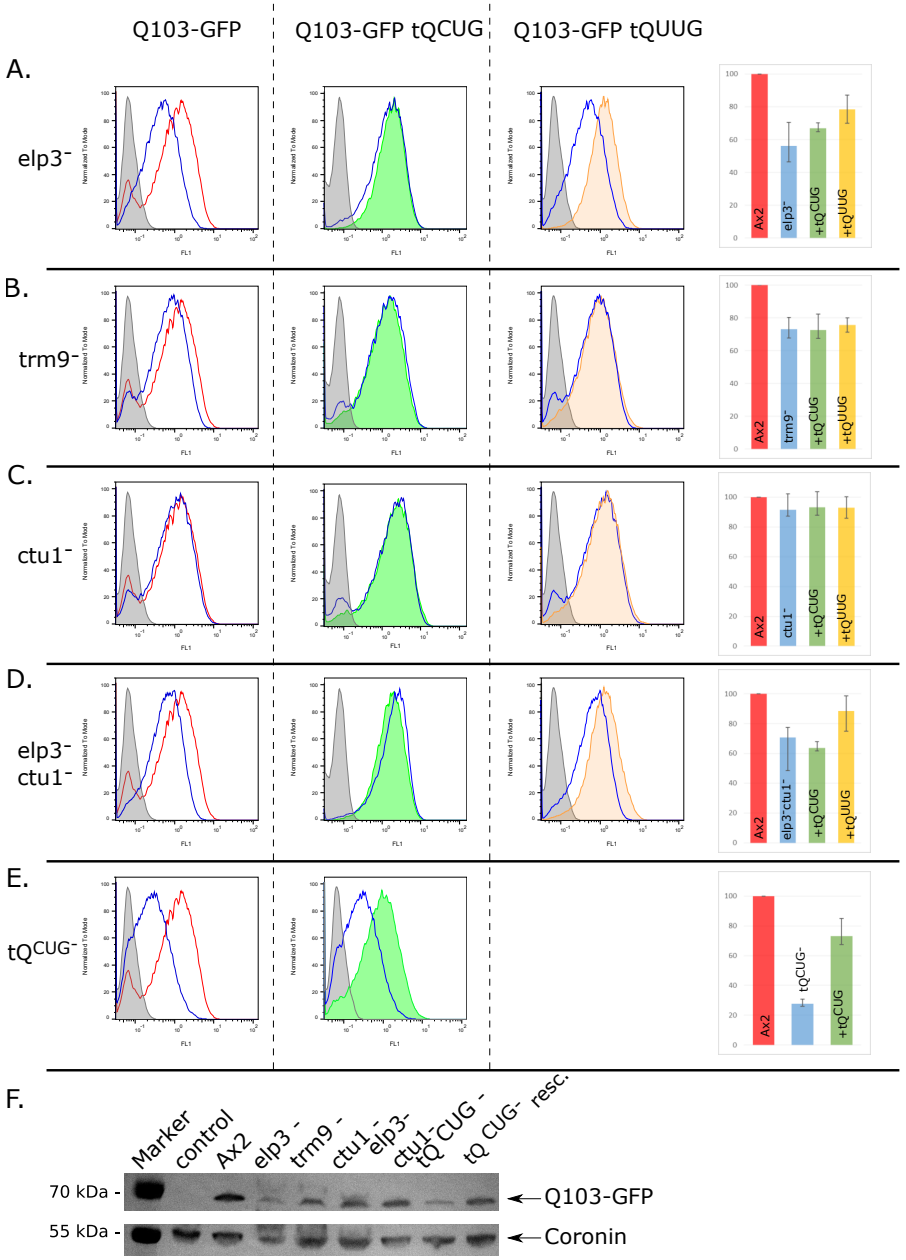

Figure 33: Q103-GFP expression in mutant strains compared to Ax2.

Flow cytometry detected fluorescence profile of Q103-GFP in Ax2 (red) (**left panel**) compared to different mutant strains. **Middle panel**: expression profile of the mutant strains expressing Q103-GFP (blue curve) compared to the mutant strains expressing Q103-GFP + tQ ^{CUG} overexpression (green). **Right panel**: expression profile of Q103-GFP (blue) compared to Q103-GFP + tQ ^{UUG} overexpression (orange) in the mutant strains. The **bar chart** on the very right compares the geometric mean of the peak areas of the different experiments in mutant background against expression in the Ax2 wild type (set to 100% expression). Error bars are derived of the minimum and maximum value of all repetition experiments (at least 3 times 30000 counts), thus indicating the maximum observed deviation. **A.** *elp3⁻*, **B.** *trm9⁻*, **C.** *ctu1⁻*, **D.** *elp3⁻ctu1⁻*, **E.** *tQ^{CUG-}*, **F.** Western blot anti-GFP and anti-Coronin of the strains used in the flow cytometer analysis. Marker = PageRuler Plus Prestained Protein Ladder.

The fluorescence signal of the Q52-GFP expression is shown for the different mutant strains compared to Ax2 wild type in Figure 34. The expression levels are significantly reduced in the *elp3*$^-$ (Figure 34 A) and *elp3*$^-$*ctu1*$^-$ (Figure 34 D). A lesser reduction of the expression level of Q52-GFP can also be detected in the *trm9*$^-$ and *ctu1*$^-$ strains. Even the tQ^{CUG} mutant shows a slight reduction of expression. This observation might be due to a global reduction of protein expression in the tRNA mutant. No direct comparison between Q52-GFP and Q52-GFP + tQ^{UUG} control can be made, since the flow cytometric Q52-GFP measurements with simultaneous overexpression of tQ^{UUG} were not performed at the same time as the measurements without the tRNA control. A comparison of 52-GFP with tQ^{UUG} control can, however, be done to the Ax2 wild type. The expression differences between Ax2 and the mutants vanish in the tRNA overexpressor controls, indicating a positive effect of tQ^{UUG} overexpression on protein level of Q52-GFP in the individual mutant backgrounds (Figure 34 A to D right compared to left image).

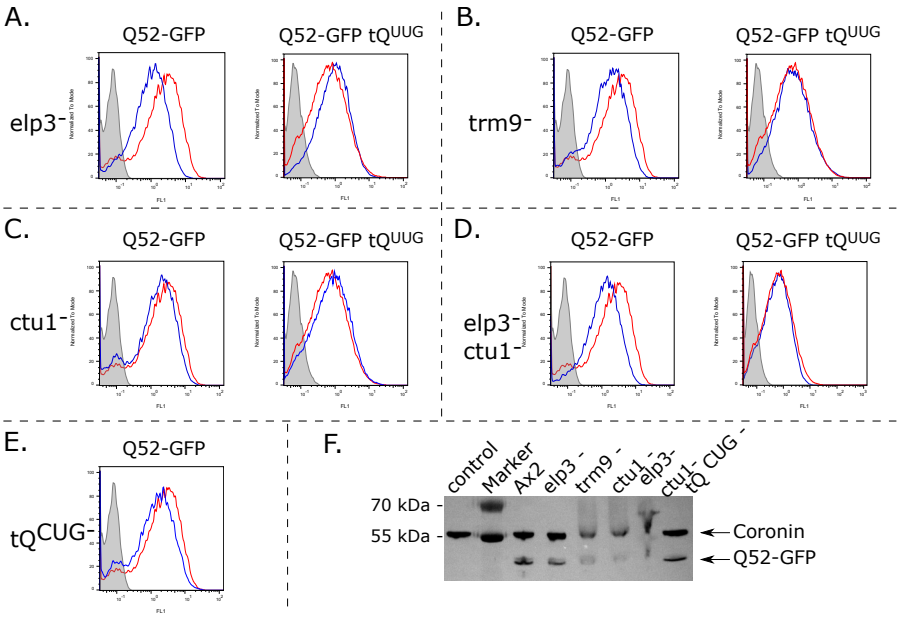

Figure 34: Q52-GFP expression in mutant strains compared to Ax2.
Flow cytometry detected expression profile of Q52-GFP (left) and Q52-GFP + tQ^{UUG} (right) in Ax2 (red) compared to **A.** *elp3*$^-$, **B.** *trm9*$^-$, **C.** *ctu1*$^-$, **D.** *elp3*$^-$*ctu1*$^-$, **E.** *tQ^{CUG-}*, **F.** Western blot anti GFP and anti-Coronin of the strains used in the flow cytometer analysis. Marker = PageRuler Plus Prestained Protein Ladder.

Q15-GFP features 15 CAG codons followed by the GFP gene. It serves as a control to determine the translation limits of the *tQ^{CUG-}* strain towards the CAG codon, as well as global translation differences that may occur in the different modification deficient strains. Figure 35 shows that Q15-GFP expression is slightly reduced in *elp3*$^-$

strain (A) but nearly at wild type level in *trm9*⁻ (B) and *ctu1*⁻(C). The difference between *elp3*⁻ and Ax2 wild type are most likely due to a general reduction of protein translation in the mutant. The expression in the tQ^{CUG} deficient strain is greatly reduced with almost no Q15-GFP signal above the negative control (Figure 35 D). This is confirmed independently by Western blotting (Figure 35 E). This result gives another indication that $mcm^5s^2tQ^{UUG}$ can read over the CAG codon, yet with a much lower efficiency than tQ^{CUG}.

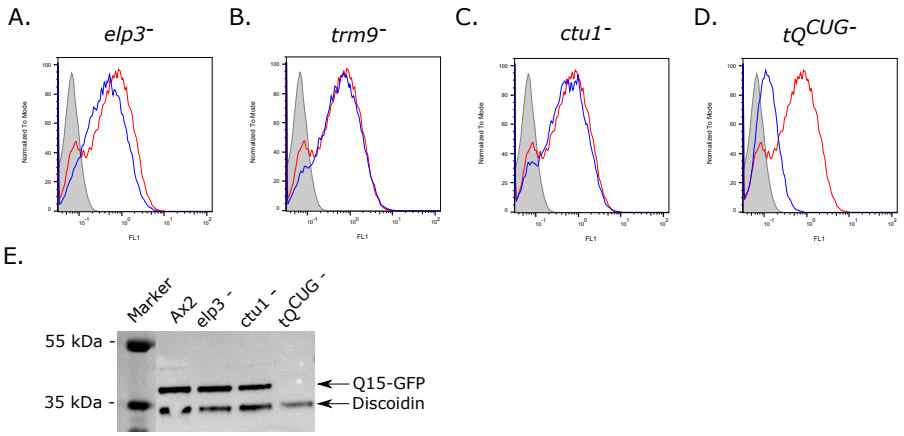

Figure 35: Q15-GFP expression in mutant strains compared to Ax2.

Flow cytometry detected expression profile of Q15-GFP in Ax2 (red) compared to **A.** *elp3*⁻, **B.** *trm9*⁻ **C.** *ctu1*⁻, **D.** tQ^{CUG-}, **E.** Western blot image anti-GFP and anti-Discoidin of the different strains used in the flow cytometric analysis. (Please note that Q15-GFP is detectable via Western blot in tQ^{CUG-} background, but only after a longer incubation time. Marker = PageRuler Plus Prestained Protein Ladder.)

3.3 γ-TOXIN, A TOOL TO INVESTIGATE DEFECTS IN ELONGATOR DEPENDENT TRNA MODIFICATION

The observation that led to the discovery of the target and function of γ-toxin, the γ-subunit of killer toxin zymocin, led also to the discovery of the Elongator function. Zymocin is a toxin produced and secreted by *K. lactis* to inhibit the growth of other yeast. The γ-subunit cleaves the modified anticodon of the glutamate tRNA tE^{UUC} at position 34. tE^{UUC} depletion impairs translation which leads to growth arrest and eventually cell death. Only in presence of a completely modified $mcm^5s^2U_{34}$ tE^{UUC} can γ-toxin cleave efficiently, making Elongator deficient cells resistant against zymocin. This characteristic makes γ-toxin a fast and inexpensive tool to investigate loss of U_{34} modification. It was known that γ-toxin can cleave the tRNA of different species *in vitro* [20]. The toxin and a point mutated form (E8G mutant) of the toxin were cloned into pET24a-HM3C vectors, expressed in and purified from *E. coli* and tested whether it can also cleave *D.*

discoideum tRNA. After induction of γ-toxin expression in BL21 strain, the culture growth was significantly reduced. Within three days, the $OD_{600\,nm}$ doubled once indicative of only one cell division in that time period (Figure 36 C). This was in contrast to the observations made on the growth of the uninduced strain, and also of BL21 strains expressing any other protein (Elp3, 4, 5, 6 and RNaseIII domain of DrnA and DrnB. data not shown). The question arose if γ-toxin can cleave prokaryotic tRNA *in vivo* but not *in vitro*, since no tRNA cleavage could be observed *in vitro* ([114] and Figure 36 B). Northern blot analysis of RNA samples taken from different time point of the toxin expression in BL21 cells revealed that γ-toxin mediated tE^{UUC} cleavage occurs indeed *in vivo*, and that the cleavage extent corresponds to the expression level of γ-toxin in the *E.coli* cells (Figure 36 A and B). The mutant-toxin showed a reduced cleavage activity with tRNA halves only appearing 360 minutes after induction. It can be concluded that γ-toxin can act on the anticodon of the prokaryotic tE^{UUC}, but most likely with a reduced catalytic activity. The prokaryotic tRNA may be protected by an additional modification (pseudouridine) present at position U_{35} in tE^{UUC} [114].

In order to test *D. discoideum* tRNA cleavage *in vitro*, 10 µg total RNA from Ax2 wild type were incubated with different concentrations of γ-toxin (1 nM to 1000 nM) for 30 minutes at 22°C. Total RNA from *S. cerevisiae* was treated identical to the sample of *D. discoideum* RNA served as a positive control in the cleavage experiment. Figure 37 shows the results of the experiment. Anticodon cleavage of tE^{UUC} occurred in the RNA sample of *S. cerevisiae* and *D. discoideum* at a toxin concentration of 100 nM and above. The cleavage reaction appears tE^{UUC} specific since no tRNA halves could be detected in a Northern blot probing for tK^{UUU}, which features the same U34 modification. The point mutated γ-toxin displayed no cleavage activity in this experimental setup.

Since γ-toxin cleavage of *D. discoideum* tE^{UUC} could be confirmed, the system was used to test cleavage activity on tRNA of the different mutant strains. Figure 37 C shows a Northern blot against tE^{UUC} of the different mutant strains compared to Ax2. Specific tRNA halves only appeared in RNA of the Ax2 wild type and to a significantly lower extent in the *ctu1*$^-$ strain. No cleavage could be observed in tRNA of *trm9*$^-$ and *elp3*$^-$ strains. This indicates that only fully modified *D. discoideum* tE^{UUC} can be efficiently cleaved by γ-toxin *in vitro*.

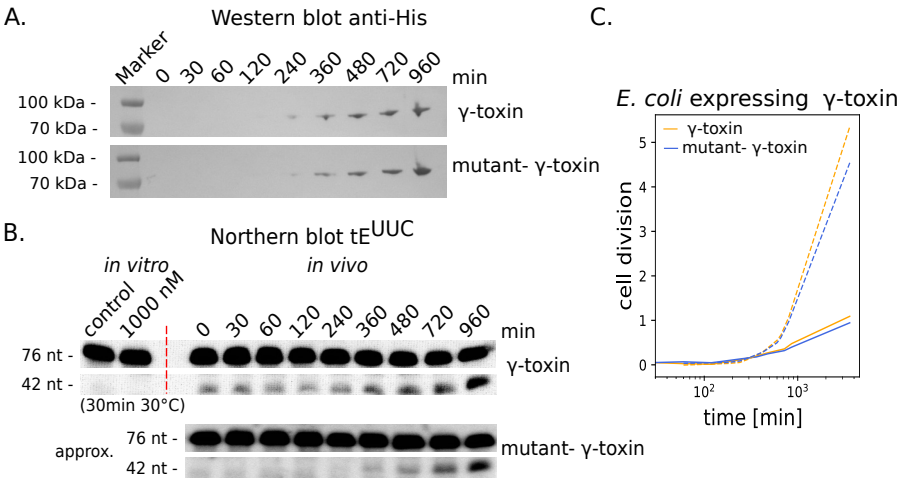

Figure 36: γ-toxin expression and *in vivo* effect on *E. coli* tRNA level.

A. Western blot image anti-His on *E. coli* strain BL21 Codon$^+$ expressing either γ-toxin or mutant-γ-toxin. Marker = PageRuler Plus Prestained Protein Ladder. **B.** Northern blot image against tE^{UUC} on RNA extracted from *E. coli* strain BL21 Codon$^+$ expressing either γ-toxin or mutant-γ-toxin (E8G mutant). *in vitro*: 5 µg total RNA extracted from *E. coli* strain Dh5α were incubated with 1000nM γ-toxin for 30 min 30°C. *in vivo*: total RNA was extracted from *E. coli* strain BL21 Codon$^+$ expressing either γ-toxin or mutant-γ-toxin at given timepoints. Marker = GeneRuler Ultra Low Range DNA Ladder. **C.** Time course of OD_{600nm} measurements during γ-toxin expression. The y-axis is represented as fold change OD since the different cultures could not be induced at the same OD value. Dashed lines = uninduced growth.

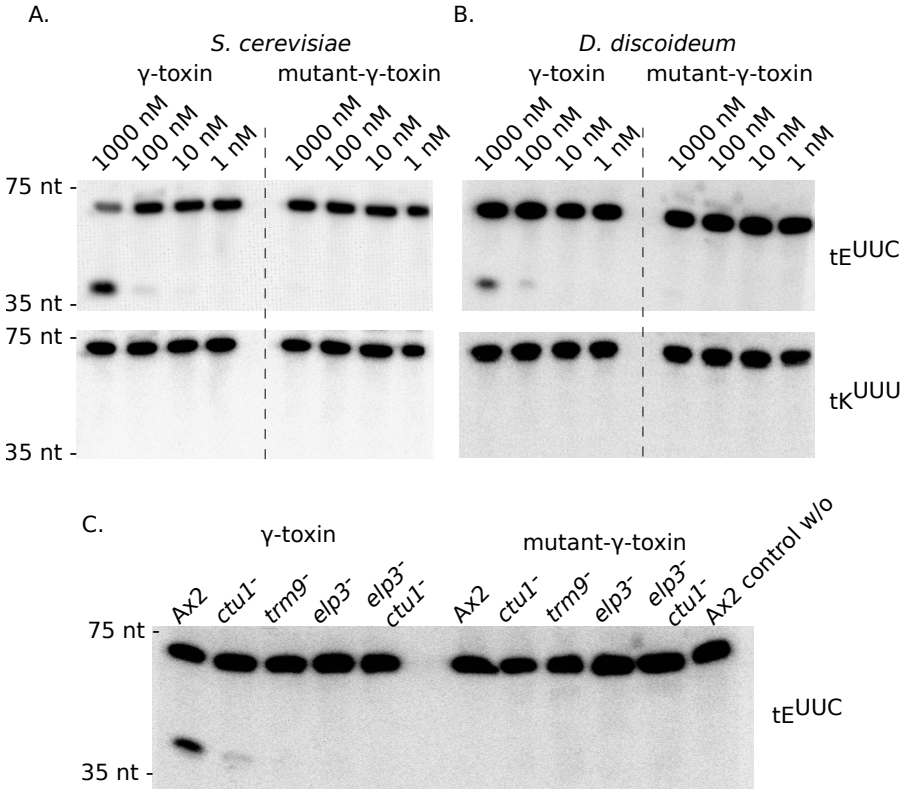

Figure 37: Northern blot image of cleavage assays γ-toxin.

All assays were performed with 10 µg total RNA for 30 min at 22°C in a buffer containing 50 mM NaCl 20 mM Tris pH7.5 and 2 mM DTT. **A.** Northern blot images of cleavage assays γ-toxin with total RNA from *S. cerevisiae* strain incubated with different concentration of γ-toxin. left: wt γ-toxin. right: mutant γ-toxin. top: tE^{UUC}. bottom: tK^{UUU} control. **B.** Northern blot images of cleavage assays γ-toxin with total RNA from *D. discoideum* Ax2. left: wt γ-toxin. right: mutant γ-toxin. top: tE^{UUC}. bottom: tK^{UUU} control. **C.** Northern blot image of cleavage assays γ-toxin with total RNA of different *D. discoideum* strains. Protein concentration was 1000 nM. Marker = GeneRuler Ultra Low Range DNA Ladder

4 DISCUSSION

4.1 THE IDENTITY OF THE ELONGATOR COMPLEX

4.1.1 *Complex formation in D. discoideum*

In the process of this thesis, it was not possible to identify all 6 Elongator proteins together in one pulldown approach. Rather, the subcomplexes Elp123 and Elp456 were found separately, indicating that the two subcomplexes largely exist independently. This is in line with observations in other organisms, like *S. cerevisieae*, where the subcomplexes can also be found apart from each other [41]. The mouse and human Elongator subcomplexes have a weaker affinity towards each other than their yeast counterparts (personal communication with Sebastian Glatt).

It cannot be excluded that the findings in *D. discoideum* are to some extent of artificial nature. Overexpression of proteins can lead to increased expression level of its interaction partners [115]. The overexpression of one Elongator protein in *D. discoideum* could therefore lead to an expression increase of its subcomplex interaction partners. In consequence, there would be a disproportion of the subcomplexes in the overexpressor strains that could explain the findings presented in Section 3.1.2. The fact that no Elp456 subcomplex was found in Elp3 pulldowns might be due to this artificial, or naturally occurring, disproportion in expression levels of the subcomplexes. In consequence, not enough Elp456 was present for detection in the SDS-PAGE. One other - less likely - possibility that could explain the absence of the Elp456 subcomplex in the Elp3 pulldown might be that the protein tags used for the pulldowns decreased the stability of the holocomplex in such a way, that the interaction of the two subcomplexes becomes almost transient. It also cannot be excluded that these findings are due the purification procedures. Blue native PAGE analysis of the Elp123 subcomplex showed a signal below 480 kDa, suggesting a monomeric Elp123 complex (Figure 12), although it is known from the literature that the Elp123 complex forms a dimer in yeast [41].

Overall, (*in vivo*) Elongator protein interaction studies with *D. discoideum* overexpressor strains proved to be suboptimal. In the pulldown approaches with Elongator proteins other than Elp3, the majority of the overexpressed protein was considerably stronger expressed than its interaction partners. Unfortunately, there are no expression

systems for *D. discoideum* available that would allow for overexpression of several POI on different plasmids in an equal ratio. Expression of 2 pDM Plasmids with different selection markers rather leads to a heterogeneous expression of the 2 POI with a low percentage of the cell population expressing both POI in equal amounts inside a single cell [80].

In an attempt to overexpress several Elongator proteins in one strain, fusion plasmid of the pDM series were generated, consisting of 2 or more GOI expression cassettes on one pDM plasmid (as described in [80]). The expression cassettes featured similar actin 15 promotors. Appendix Figure 42 shows experimental analysis of an Ax2 strain of such a fusion plasmid with mRFP-Elp5 and GFP-Elp6. Both proteins are expressed in an equal ratio within the individual cells (2D scatter plot Figure 42 C). This could also be confirmed by laser scanning microscopy of the strain shown in Figure 8. A GFP-trap pull-down experiment shown in Figure 42 D finds similar band intensities for mRFP-Elp5 and GFP-Elp6 in a colloidal Coomassie stained SDS-PAGE. This observation suggests that Elp5 and Elp6 bind to each other upon overexpression. The finding is in line with the observations on the Elongator proteins from *S. cerevisiae* where Elp5 and Elp6 dimerize upon simultaneous expression in *E. coli* [53].

In an attempt to create a strain overexpressing all subunits of the Elp456 subcomplex, fusion plasmids with mRFP-Elp5, GFP-Elp6 and FLAG-Strep-Elp4 were constructed, but not yet transformed into *D. discoideum* strains. A fusion plasmid consisting of mRFP-Elp4 and GFP-Elp3 did not lead to a detectable GFP-Elp3 signal by Western blotting or flow cytometry in the Ax2 background and an *elp3*$^{-}$ background (data not shown).

4.1.2 *Cross complementation*

It is shown in several papers that Elongator proteins from different species are able to interact and to form a functional complex [116, 117]. One particular case is Elp3. Cross species complementation with the Elp3 protein only succeeded when Elp1 of the same species was introduced as well [118]. In order to investigate cross complementation in *D. discoideum*, a fusion plasmid with mRFP-yElp1 and GFP-yElp3 was introduced into the Ax2 strain and the *elp1*$^{-}$ strain. The strains failed to show any expression of the proteins (data not shown). Expression of the yeast Elongator proteins from pDM317 was significantly weaker that any other tested protein expression (Figure 48). It can be concluded that expression of yeast proteins in *D. discoideum* is so low that complementation of the wild type phenotype seems improbable. Likely, the yeast genes would need codon adaptation to increase their expression level in *D. discoideum* to a sufficient level.

4.1.3 *Recombinant Elp456 in E. coli*

The expression of the *D. discoideum* proteins Elp4, Elp5 and Elp6 from a polycistronic expression vector in *E. coli* led to Elp456 complex formation ([85] and Section 3.1.3). The mass of the complex was estimated to be 612 kDa (+MBP affinity tag) and 435 kDa when MBP is cleaved off. This result differs from the expected mass of the complex (approx. 348 kDa with MBP and approx. 266 kDa without MBP). One explanation could be that the *D. discoideum* Elp456 subcomplex forms a heterocyclic trimer instead of a dimer shown in *S. cerevisiae*. It can, however, not be excluded that the detected mass differences of the Elp456 complex to its theoretical mass is due to experimental shortcomings in the purification procedure. The complex is known to interact with nucleic acids and the purification procedure was lacking any DNase and RNase treatment before gel filtration was applied. Alina Stein discussed this possibility in her thesis as one reason the complex appeared to have a greater mass than predicted [85]. She thus, applied DNase and RNase to the sample, before comparing the running behavior to an untreated purification sample on a blue native PAGE. No differences in the running behavior between the two samples could be detected.

Many proteins are associated to chaperones that ensure proper folding. If stably associating, these chaperones can influence the gel filtration size analysis, since they would increase the mass of the complex. As the matter of fact, MALDI mass spectrometric analysis on the recombinant Elp456 complex identified the DnaK, a member of the prokaryotic Hsp70 chaperone family, and GroEL, a member of the prokaryotic Hsp60 chaperonin family in the elution fraction (Figure 15 B and Table 18). These chaperones should release the bound proteins upon ATP-hydrolysis; as does the Elp456 complex release tRNA upon ATP hydrolysis. To investigate if the release of bound chaperones and nucleic acids the elution volume of Elp456 subcomplex, a concentrated elution fraction of a recombinant MBP-Elp456 purification sample was incubated with 10 mM ATP for 30 minutes before injection into the FPLC. The available ATP may lead to the release of the chaperones and the actively bound nucleic acids from the complex, influencing the retention volume in the gel filtration. The $UV_{280\,nm}$ curve received from this sample did not differ in the complex size from a sample without prior ATP incubation (Figure 16) but a strong signal emerged around 2 mL (corresponding to approx. 25 kDa) which is thought to be nucleic acids that are released from the complex.

Thus, neither RNase and DNase treatment nor ATP addition influenced the mass of the complex significantly. Yet it cannot be excluded that it is the combination of DNA, RNA and chaperones bound to the complex that resulted in the increased mass. To exclude this possibil-

ity, a good control would be to apply DNase and RNase treatment with ATP incubation prior to gel filtration.

Additional methods to investigate the stoichiometry of Elp456 could include cryo electron microscopy (cryo EM) and crystallography. Cryo EM would give a visual indication if the recombinant *D. discoideum* complex forms a ring structure and would allow to estimate the size thereof. The crystal structure of the *D. discoideum* subcomplex would, of course, give an in depth view on the complex and may reveal the potential particularities of the *D. discoideum* homologues compared to other Elp456. Such experiments have been initiated in a cooperation with the group of Sebastian Glatt. Further experiments could also include studies tRNA binding of the subcomplex. This could be done with Electrophoretic Mobility Shift Assays (EMSA) studies and Isothermal Titration Calorimetry (ITC).

4.1.4 *The stability of Elp3*

Elp3 seems to be the only Elongator subunit that cannot be expressed above the level of its interaction partners. In every Co-IP and affinity chromatographic purification of a tagged Elp3, it appeared in the same intensity as Elp1 and Elp2. On the protein level, the data on the 2A-peptide sequence experiment in Figure 18 give a direct indication that the Elp3 protein is less stable than mRFP. Additionally to the protein instability of Elp3, the data in Figure 51 indicated that the *elp3* gene cannot be translated with the same efficiency as other tested genes. The protein expression level of its gene fusion partner (= the gene seperated from *elp3* by the 2A sequence) was significantly decreased when the *elp3* gene was placed 5´ of the 2A sequence compared to 3´ of the 2A sequence. If Elp3 is stabilized by the interaction with Elp1 and Elp2, could not be shown in this experiment, but several observations point towards this possibility. First, no GFP-Elp3 expression (from pDM317) could be detected in an *elp1*$^{-}$ strain (data not shown). Similar observations were made in yeast where it was possible to detect Elp3 on a Western blot in an *elp1*$^{-}$ strains, but it could not be found in pulldowns (personal communication with Raffael Schaffrath). Second, until now no eukaryotic Elp3 was found soluble when expressed in *E. coli*. Only some bacterial and archeal Elp3 seem to be stable alone. These organisms, however, do not feature any Elp1-Elp6 counterparts.

4.2 ELONGATOR DEPENDENT ANTICODON U_{34} MODIFICATIONS IN D. DISCOIDEUM

4.2.1 *Gene deletion strain generation*

In this thesis, the Elongator dependent modification pathway of *D. discoideum* could be described and disrupted at all major steps. Gene deletions of *elp3* and *elp4* abolished the initial Elongator cm^5 modification. A disruption of *elp6*, however, failed repeatedly (data not shown). There is, however, no indication for the gene being essential in *D. discoideum*. It is rather likely that the failed mutant generation is due to a poorly designed pKOSG knockout construct.

Trm9 gene deletion prevented the generation of the mcm^5 modification. Yet, *trm112* knockout generation, which should disrupt the modification pathway at the same step, failed. Since there were clear indications that part of the transformed pKOSG construct integrating into the right genomic locus, it seems likely that not enough clones where screened for knockout identification (data not shown).

Ctu1 deletion led to the absence of the s^2U modification, while generation of an *urm1* mutant strain failed. It was even possible to generate a double mutant of *elp3*$^-$*ctu1*$^-$ in *D. discoideum*, as the third investigated protist, after *S. pombe* [33] and *S. cerevisiae* [107], where this is possible.

Deletion of the single copy of the tQ^{CUG} gene was successful in the Ax2 wild type background. This makes *D. discoideum* the only eukaryotic model organism to date where the very tRNA is not strictly required for viability. This is likely due to the highly unusual codon usage for glutamine in *D. discoideum*. Attempts to knockout the tQ^{CUG} gene in *elp3*$^-$ background, however, failed. When performing the PCR screening of the potential tQ^{CUG} deletion in the *elp3*$^-$ background, two clones were found which featured a clear knockout signal, but also a wild type signal. These clones seem to have incorporated the resistance cassette at the right genomic location with removal of the tRNA gene, but also feature a copy of the genomic location, in which the integration of the resistance cassette did not take place. No further investigations on the genomic surrounding were performed. This unusual situation for a haploid genome is occasionally observed in *Dictyostelium*, and it might be indicative for the essentialness of the gene to be deleted. As the same construct could be used for tRNA gene deletion in the Ax2 wild type, but not in the *elp3*$^-$ background, it stands to surmise that the mcm^5s^2U modification, which is missing in the *elp3*$^-$ background, might be essential for tQ^{UUG} to read over the CAG codon. In other words, the tQ^{CUG} gene can be considered essential for viability upon loss of the mcm^5s^2U modification. An experiment, which could prove this hypothesis, would be the conditional ectopic expression of tQ^{CUG} and subsequent removal of the genomic

copy of the tQ^{CUG} gene in an Elongator deficient background. In this, cells are expected to die when tQ^{CUG} expression is stopped. Unfortunately, there are no suitable tools available to perform such experiments in *D. discoideum*. The tRNA sequences themselves are their own promotors, which makes them not tuneable in expression and there are no plasmids available that are stable without integration and allow for transient expression.

If a tQ^{CUG} deletion in a *ctu1* deficient strain would be viable could not be answered, as attempts to remove the BS(r) cassette from the *ctu1*$^-$ strain and *tQ*$^{CUG-}$ strain failed repeatedly. As a consequence, no knockout attempts of the corresponding other gene could be performed in these strains.

4.2.2 *Elongator dependent modifications*

While there is little doubt about catalytic activity of the complex and the chemical reaction taking place to modify the U_{34} nucleotide of the anticodon, the Elongator dependent modification itself could not be experimentally verified in eukaryotes. Only one study on Elp3 of the *archaeon Methanocaldococcus infernus* could reproduce the modification reaction *in vitro* [24]. Reproduction of this experiment with Elp3 from *Dehalococcoides mccartyi* by Glatt and colleagues failed [51].

Which protein is responsible for the modification of cm^5U to ncm^5U is still unknown [21]. An analysis of the ncm^5U modification in the *trm9*$^-$ background in *D. discoideum* by Stefanie Kellner shows no increase of ncm^5U formation compared to the Ax2 wild type. This result is unexpected, if assuming that mcm^5U is generated from ncm^5U. Since there is the possibility that mcm^5 might be synthesized from a cm^5U precursor molecule, one would expect to find an increased level of the cm^5U intermediates in the *trm9*$^-$ backgrounds. The data, however, also showed no increase of cm^5U in this mutant. Yet, ncm^5s^2U is found in the analysis of *trm9*$^-$ strain, indicating that ncm^5s^2U is formed when mcm^5U formation is disrupted.

Disruption of the thiouridylation pathway resulted in an increase of the mcm^5 modification in the expected ratio. The increased level of mcm^5U found in the *ctu1*$^-$ background was directly corresponding to the levels of the mcm^5 and mcm^5s^2U modifications found in the Ax2 wild type. All together, it can be said that the U_{34} thiouridylation modification pathway exists in *D. discoideum* and the disruption leads to an expected accumulation of modification intermediates. The thiolation of U_{34} seems to be conditionally dependent on the Elongator modification. Only a small amount of s^2 thiolated uridine (approx. 20 fold decrease to wild type) was found in the Elongator deficient strains. There is a clear increase of the thiolation level in the *trm9*$^-$ strain where ncm^5U is present compared to the thiolation level in the Elongator mutant. One explanation for this finding is that U_{34} might

be more accessible for the thiolation reaction when the initial Elongator modification is present. If ncm^5U is sufficient for a thiolation efficiency increase to the level of mcm^5U cannot be determined, since the ncm^5s^2U level in *trm9*$^-$ is distinct from that of mcm^5s^2U in Ax2.

4.2.3 *Codon usage and tRNA genes*

Within the coding sequences of the genome, individual genes may feature different codon usage. These differences are modulating the translational speed, thereby influencing the folding dynamics of the emerging amino acid chain [119]. Too fast or too slow translation processes can lead to misfolding and aggregation of the protein – or worse, aggregation of the protein with ribosomes [120]. Nonetheless, the codon usage within the genome of lower eukaryotes tends to be, to some extend, homogenous. Highly expressed genes tend to have a rather "ideal" codon composition corresponding to their tRNA gene repertoire [121]. The major differences thus exist between lowly and highly expressed genes.

Codon bias and tRNA gene copy numbers can vary a lot from organism to organism [122], even though the GC content and codon usage tends to correlate within habitats [123]. Codon adaptation of genes obtained from other organisms, as a result of lateral or horizontal gene transfer, is a fast process [124, 125]. Selection pressure towards a species-specific codon usage is essential for proper gene expression and may also help to distinguish between foreign and own genes, e.g. as viral defence. The tRNA gene copy numbers of lower eukaryotes correlate to some extend to the codon usage of the organism or vice versa [119]. In higher eukaryotes, codon composition of single genes can vary a lot more, depending on which chromosome and in which chromosomal location the gene is found. Within their genomes, tRNA gene copy number and codon usage seem to be to some extend uncoupled [126]. A good example is the zebrafish which features thousands of tRNA genes. In which evolutionary context this uncoupled tRNA copy number stands is unclear. Certain tRNA may have additional functions within the cell [127].

D. discoideum features a rather extreme codon usage compared to other eukaryotes. The coding sequences have a codon bias towards A-ending codons, and long extensions of single A rich codons (AAT and CAA) lead to an exceptionally low GC content of 27% in coding sequences (23% GC overall) [70]. The tRNA gene copy number and codon usage seem to correlate. The copy number of one particular tRNA gene, tK^{CUU}, seems to be overrepresented compared to their corresponding codon usage (Figure 58). Presuming that all these gene copies are transcribed, the relatively large tK^{CUU} copy number is certainly beneficial for the translation efficiency of the lysine codon AAG. tK^{CUU} and tK^{UUU} form the energetically weakest codon-anticodon in-

teraction [128]. The large tK^{CUU} copy number might also reduce the amount of tK^{UUU} *wobble* recognition of the AAG codon. This would result in reduced +1 and +2 translational frameshifts and less translational stress (discussed in Section 4.2.6).

Some tRNA genes, featured with a single genomic copy and a low corresponding codon usage, may not be required for viability in *D. discoideum*. Bloom-Ackermann and colleagues investigated the viability and growth phenotypes of their comprehensive tRNA deletion strain library in *S. cerevisiae*. They found four (tS^{CGA}, tR^{CCG}, tQ^{CUG} and tT^{CGU}) of the six single copy tRNA genes to be essential, while tR^{CCU}, tL^{GAG} were not [113]. The *D. discoideum* genome features 8 single copy tRNA genes: tS^{CGA}, tR^{UCG}, tR^{UCC} tQ^{CUG}, tL^{CAG}, tP^{AGG}, tV^{CAC} and tT^{CGU}. In this thesis, it was shown that the tRNA gene tQ^{CUG} is non-essential for viability in *D. discoideum*. Comparing the tRNA gene copy number and codon usage (Figure 58), and taking near cognate recognition of the individual tRNA into account (Figure 2), further non-essential tRNA genes can be postulated.

Deletion of the tS^{CGA} and tT^{CGU} genes might be compensated by the Elongator dependent modified tRNAs tS^{UGA} and tT^{UGU}, since the codons TCG and ACG are rarely used. Also, deletion of tV^{CAC} may be compensated by tV^{UAC} since this tRNA is capable to decode GTG. A deletion attempt of tP^{AGG} in Ax2 and an Elongator mutant would be of particular interest, since ncm^5tP^{UGA} is capable to decode all four proline codons. So far, there are no *in vivo* studies in eukaryotes available, that investigate the decoding capability of unmodified tP^{UGA} towards all four codons. Also the contribution of ncm^5U to translation in eukaryotes is not yet clearly determined experimentally.

The remaining 2 single copy tRNA, tR^{UCG} and tL^{CAG}, have no counterparts in *S. cerevisiae*. Their existence appears to be quite interesting, since their corresponding codons are rarely used (once every 2000 codons). This is, respectively, 10 and 3 times lower than in *S. cerevisiae*. The low codon usage and the fact that there are no *S. cerevisiae* counterparts make these tRNAs also interesting targets for gene deletion studies in *D. discoideum*.

As shown in 3.2.6, tQ^{UUG} is only to some extent capable to decode the CAG codon. This may lead to translational and consequently cellular stress. The same would likely be true for the hypothetical tRNA deletion strains mentioned above. Some of the tRNA genes may even prove to be essential.

4.2.4 *The effect of loss of modification on glutamine codon translation*

The loss of mcm^5s^2 modification reduces A-site binding of tK^{UUU}. The effect of the reduced AAA translation efficiency on gene expression is shown in the study by Bauer et al. [112]. The reduced expression of the individual proteins, shown on the Cdr2 kinase can be rescued by

changing the lysine codon AAA to the synonymous codon AAG, or the overexpression of the unmodified tK^{UUU} [112]. In *S. cerevisiae*, elevated levels of unmodified tK^{UUU} and tQ^{UUG} also rescued the stress specific growth defects in Elongator mutants [32].

D. discoideum possesses almost twice the copy number of Elongator dependent modified tRNA genes in general and specifically, an almost 3 times higher gene copy of tK^{UUU} compared to *S. cerevisiae* (Table 16). Since in lower eukaryotes tRNA copy numbers correspond to tRNA expression level, *D. discoideum* is considered to have a greater amount of mature tK^{UUU}, which will consequently reduce the effects of the loss of the mcm^5s^2 modification greatly. Tests on the expression level of different overexpressed gene products (DrnA, BirA) did not show any significant change in expression level between wild type and mutant stains (data not shown). A detectable difference in expression level between Ax2 wild type and Elongator deficient strains could only be found when large stretches of glutamine codons leaders were used. This is likely due to the accumulative effects of reduced codon translation efficiency in these long stretches, as quantitative differences in fluorescence intensity (correlating to protein expression) can be detected. It could not be determined, beyond doubt, if the expression differences observed between the individual strains are only due to differences in translation efficiencies of the particular codons. But the fact that the overexpression of tQ^{UUG} increased the GFP expression level in the mutant background points towards this possibility. A weakness of the glutamine leader experiment in Section 3.2.6 is that a normalization to global gene expression in the different strains is missing. The expression of GFP alone varied significantly between different Elongator deficient strains (Figure 59 A). These expression differences vanished when the glutamine leaders were fused before the GFP (Figure 59 C). Due to these observations, an internal fluorescence control in the flow cytometer experiments was not pursued further. One experiment, by which global expression differences of the individual strains could be determined is discussed in Section 4.2.5 below.

4.2.5 *Global translation in modification deficient mutants*

Nedialkova and Leidel showed in their study on Elongator mutants in *S. cerevisiae* and *C. elegans* that some proteins aggregate during translation with the ribosomal machinery, when the mcm^5s^2U modification is absent [31]. Generally, *Dictyostelium* has the unusual capacity to resist aggregation of proteins with long polyglutamine tracts [71, 129]. It was shown that *Dictyostelium* is able to suppress aggregation of the polyglutamine-expanded Huntingtin construct (Q103-GFP) that aggregates in other model organisms like yeast [71, 129, 130]. Formations of polyglutamine aggregates are selectively targeted for degra-

dation but have no influence on the level of soluble polyglutamine [129, 131]. In *S. cerevisiae*, it was shown that the mRNA translation and synthesis of the Gln-rich prion Rnq1 are severely impaired in the absence of Ψ38/39 and mcm^5U_{34} or s^2U_{34} modifications but elevated level of tQ^{UUG} rescued the expression in the mutant background [130]. If such protein aggregates also form in *D. discoideum* Elongator mutants, or how strong translation is affected in general in these mutants remains unknown. Nedialkova and Leidel investigated protein aggregates in yeast via differential centrifugation and mass spectrometry. *D. discoideum* cells have large amounts of cytoskeleton proteins [132]. In the process of the pulldown presented in this thesis, the cytoskeleton proteins actin and myosin would polymerize and block any purification if not properly handled. An adaptation of the approach of Nedialkova and Leidel to *D. discoideum* - if possible - thus would have to include specific toxins, like colchicine and cytochalasins, that prevent the cytoskeleton from polymerizing.

A simple approach to investigate whether translation is globally affected in the Elongator mutants, could be realized using click chemistry. In recent years, a variety of synthetic amino acid derivatives with alkyne groups of almost all essential amino acids became commercially available. In several studies it was shown that these amino acids are loaded onto tRNAs and are subsequently incorporated into amino acid chains in many organisms. Addition of these amino acids to the media for a fixed period of time, followed by fixation of cells and coupling of fluorophores to these alkyne groups, allows for relative quantitative detection of translation rates. Global translation differences between different strains thus could be determined by measuring and comparing the relative fluorescence intensity. An example of a similar experimental setup can be found in a study on the translational effects of hypomodified m^1A_{58} tRNAs [133].

4.2.6 *Elongator mutants and +1 translational frameshifting*

Recently, two studies have shown that +1 frameshifting inside the ribosome is increased in yeast Elongator mutants, concluding that U_{34} modification may be important for reading frame maintenance [134, 135].

D. discoideum features an unusual high amount of "slippery sequences", where long stretches of single ribonucleotides - in many instances, up to 9 consecutive adenosines or uridines can be found. These sequences are known to have an increased probability towards +1 frameshifts [136]. It would be of particular interest to study how *D. discoideum* maintains the correct reading frame - not only in an Elongator context. The artificial constructs used in the above mentioned studies might be easily adopted to *D. discoideum* for the use in similar experiments.

4.2.7 *Elongator mutants growth phenotypes*

As mentioned in the introduction, yeast Elongator mutants display severe stress specific growth defects. These growth defects can be rescued by elevated level of tK^{UUU} [32, 112]. In *D. discoideum*, it was shown by Balachandar Ammapatti [87] (and in this thesis in the Appendix Section A.2.5) that *D. discoideum* Elongator mutants display a slightly prolonged cell cycle (12h) compared to the Ax2 wild type (10h). The mutants did not display an increased stress sensitivity towards caffeine and heat stress. The cell division rate of $trm9^{-}$, $ctu1^{-}$ and tQ^{CUG-} are even closer to Ax2 with only 1h prolongation [137]. Section 3.2.4 and Section 4.2.3 discuss the genomic differences of yeast and *D. discoideum*. These differences make predictions of specific stress phenotypes difficult. If the *D. discoideum* Elongator mutants display any specific stress phenotypes is currently under investigation.

4.2.8 *Translational regulation by tRNA modification*

Over the last 50 years, it became evident that gene expression is regulated by an extraordinary complex fashion. In fact, every part of gene expression itself is regulated. Regulation occurs on the genomic, gene, transcriptional, posttranscriptional, translational and posttranslational level. Because of the great variety in regulatory mechanisms, it took till recent years to discover a translational regulation mechanism by tRNA modification. One good example for such a regulatory tRNA modification is the reversible m^1A_{58} modification in the TΨC loop of mammalian tRNA. The modification is found in 10 different mature tRNAs and is dependent on glucose availability. Upon starvation, the modification is absent, which leads to a reduced number of free initiator tRNA tM^{CAT} as well as tM^{CAT} in the eEF1α bound tRNA pool. Thereby both, translational initiation and translational elongation was influenced, resulting in a decreased translation in general [133].

The Elongator complex and its catalytic activity are regulated via a complex phosphorylation pattern at the C-terminal domain of Elp1 [44]. Loss of the modification has severe pleiotropic effects in many organisms. Yeast features an Elongator dependent lysine codon bias of certain gene groups [112] and a relatively low copy number of the tK^{UUU} gene in their genomes (Table 16). Bauer and Hermand postulate in their paper a translational control of cell division by the Elongator complex [112]. They base their argument on the differences in codon usage of different gene groups and in particular on the Cdr2 kinase, one of the major mitotic regulator proteins. They show that the Cdr2 kinase expression level is highly reduced in Elongator mutants and that the expression level can be rescued by changing all lysine codons within the gene from AAA to AAG. But there are two

problems with their postulate. Firstly, the lysine amino acid is underrepresented in the Cdr2 kinase compared to a normalized protein of *S. pombe*. The coding sequence of *cdr2* features the same amount of AAA codons as a normalized coding sequence with 70% AAG. It could be possible that the reduced lysine translation rate and a shortage of available chaperones leads to misfolding of the Cdr2 protein and proteolytic decay. But - secondly - it seems rather improbable that the global impairment of translation, and the translational and proteolytic stress that is caused by it, is there to regulate the transition of the cell from the G2/M-phase to mitosis. Especially considering the fact that Cdr2 activity is regulated by Pom1 and that the cell cycle and mitosis are regulated by a complex and elegant network of cellular processes [138–140].

4.3 γ-TOXIN

As described in the introduction, the γ-subunit of the trimeric *K. lactis* killer-toxin zymocin (γ-toxin) cleaves fully modified $mcm^5s^2tE^{UUC}$. Γ-toxin assays provide a fast and inexpensive molecular diagnostic tool to assign function to different proteins and protein motifs that are involved in the the U_{34} modification. These characteristics were the inspiration to establish similar assays for the Elongator dependent U_{34} modification studies in *D. discoideum*. Unfortunately, the intracellular expression of γ-toxin on pDM-Vectors in *D. discoideum* was not successful [141]. But, γ-toxin was successfully used to cleave $mcm^5s^2tE^{UUC}$ of *D. discoideum in vitro*. Γ-toxin displayed a reduced cleavage activity towards tE^{UUC} of mutant strains missing parts of or the complete *wobble* uridine modification. These findings are in line with the literature [64].

Looking at the results in Figure 37 C in more detail, it seems that the cleavage activity of γ-toxin is higher for tE^{UUC} from the *ctu1*$^-$ strain than from the *trm9*$^-$ (and lowest for the Elongator mutants). This might suggest that mcm^5tE^{UUC} is cleaved with a higher efficiency than $ncm^5s^2tE^{UUC}$. The results shown in Figure 23 indicate that the ncm^5s^2U modification in the *trm9*$^-$ strain is 3 times less abundant than the mcm^5s^2U in the Ax2 wild type. Additionally, there is no increase of the ncm^5U in the *trm9*$^-$ strain detectable, while there is a great increase of mcm^5U in the *ctu1*$^-$ strain, where s^2 formation is disrupted. Consequently, there should be 3 times more unmodified tE^{UUC} in the *trm9*$^-$ strain, compared to the *ctu1*$^-$ strain. This makes it difficult to make a definite conclusion, that the ncm^5s^2U and mcm^5U modifications have to the cleavage activity of γ-toxin.

The E8G point mutated γ-toxin was accidentally generated by Balachandar Ammapatti in his approach to clone and express γ-toxin in *D. discoideum* [87]. When recloned to the pET24a-HM3c vector for recombinant expression and purification in *E. coli*, it was found

that the expression of the E8G mutant had an inhibitory effect on the growth *E. coli* expressing the toxin, while it failed to cleave eukaryotic $mcm^5s^2tE^{UUC}$. This led to an initial false assumption that this point mutation changes the specificity of the toxin from the eukaryotic $mcm^5s^2tE^{UUC}$ to the prokaryotic $mnm^5s^2tE^{UUC}$. The experiment was repeated with the wild type γ-toxin protein, allowing for a comparision of the two proteins. The E8G point mutated γ-toxin has a strongly reduced cleavage activity to both, $mcm^5s^2tE^{UUC}$ and $mnm^5s^2tE^{UUC}$, compared to the wild type γ-toxin. But for both γ-toxin versions, *in vivo* γ-toxin cleavage activity towards the prokaryotic $mnm^5s^2tE^{UUC}$ seems to be higher than *in vitro*, where no cleavage can be observed. This might be due to the greater intracellular concentration of γ-toxin or the more complex *in vivo* surrounding that better suits the cleavage requirements compared to the minimal surrounding provided by the *in vitro* experiment.

BIBLIOGRAPHY

[1] M. A. Machnicka et al. "MODOMICS: a database of RNA modification pathways–2013 update." eng. In: *Nucleic acids research* 41 (Database issue 2013), pp. D262–7.

[2] Y. Motorin and M. Helm. "RNA nucleotide methylation." eng. In: *Wiley interdisciplinary reviews. RNA* 2 (5 2011), pp. 611–31.

[3] H. H. "Methylated nucleosides in tRNA and tRNA methyltransferases." In: *Front. Genet. 5* 5:144 (May 2014).

[4] P. C. Dedon and T. J. Begley. "A system of RNA modifications and biased codon use controls cellular stress response at the level of translation." eng. In: *Chemical research in toxicology* 27 (3 2014), pp. 330–7.

[5] A. K. Hopper. "Transfer RNA Post-Transcriptional Processing, Turnover, and Subcellular Dynamics in the Yeast Saccharomyces cerevisiae." In: *Genetics* 194.1 (Jan. 2013), pp. 43–67. ISSN: 1943-2631.

[6] A. K. Hopper and E. M. Phizicky. "tRNA transfers to the limelight." eng. In: *Genes & development* 17 (2 2003), pp. 162–80.

[7] M. B. Basma El Yacoubi and V. de Crécy-Lagard. "Biosynthesis and Function of Posttranscriptional Modifications of Transfer RNAs." In: *Annual Review of Genetics* (2012).

[8] J. E. Jackman and J. D. Alfonzo. "Transfer RNA modifications: Nature's combinatorial chemistry playground." In: *Wiley interdisciplinary reviews. RNA* 4.1 (Nov. 2012), pp. 35–48. ISSN: 1757-7012.

[9] G. Kawai, Y. Yamamoto, T. Kamimura, T. Masegi, M. Sekine, T. Hata, T. Iimori, T. Watanabe, T. Miyazawa, and S. Yokoyama. "Conformational rigidity of specific pyrimidine residues in tRNA arises from posttranscriptional modifications that enhance steric interaction between the base and the 2'-hydroxyl group." eng. In: *Biochemistry* 31 (4 1992), pp. 1040–6.

[10] M. Helm and J. D. Alfonzo. "Posttranscriptional RNA Modifications: playing metabolic games in a cell's chemical Legoland." eng. In: *Chemistry & biology* 21 (2 2014), pp. 174–85.

[11] V. A. N. Rezgui, K. Tyagi, N. Ranjan, A. L. Konevega, J. Mittelstaet, M. V. Rodnina, M. Peter, and P. G. A. Pedrioli. "tRNA tKUUU, tQUUG, and tEUUC wobble position modifications fine-tune protein translation by promoting ribosome A-site binding." In: *Proceedings of the National Academy of Sciences* 110.30 (2013), pp. 12289–12294.

[12] F. H. Crick. "Codon–anticodon pairing: the wobble hypothesis." eng. In: *Journal of molecular biology* 19 (2 1966), pp. 548–55.

[13] R. W. Holley, G. A. Everett, J. T. Madison, and A. Zamir. "Nucleotide sequences in the yeast alanine transfer ribonocleic acid." eng. In: *The Journal of biological chemistry* 240 (1965), pp. 2122–8.

[14] P. F. Agris. "Decoding the genome: a modified view." eng. In: *Nucleic acids research* 32 (1 2004), pp. 223–38.

[15] P. F. Agris, F. A. P. Vendeix, and W. D. Graham. "tRNA's wobble decoding of the genome: 40 years of modification." eng. In: *Journal of molecular biology* 366 (1 2007), pp. 1–13.

[16] F. Tuorto and F. Lyko. "Genome recoding by tRNA modifications." In: *Open Biology* 6.12 (Nov. 2016), p. 160287. ISSN: 2046-2441.

[17] M. J. O. Johansson, A. Esberg, B. Huang, G. R. Björk, and A. S. Byström. "Eukaryotic Wobble Uridine Modifications Promote a Functionally Redundant Decoding System." In: *Molecular and Cellular Biology* 28.10 (Feb. 2008), pp. 3301–3312. ISSN: 1098-5549.

[18] H. Sierzputowska-Gracz, E. Sochacka, A. Malkiewicz, K. Kuo, C. W. Gehrke, and P. F. Agris. "Chemistry and structure of modified uridines in the anticodon, wobble position of transfer RNA are determined by thiolation." In: *J. Am. Chem. Soc.* 109.23 (Nov. 1987), pp. 7171–7177. ISSN: 0002-7863.

[19] L. Pintard, F. Lecointe, J. M. Bujnicki, C. Bonnerot, H. Grosjean, and B. Lapeyre. "Trm7p catalyses the formation of two 2-O-methylriboses in yeast tRNA anticodon loop." In: *The EMBO Journal* 21.7 (Feb. 2002), pp. 1811–1820. ISSN: 1460-2075.

[20] B. O. Huang, M. J. O. Johansson, and A. S. Byström. "An early step in wobble uridine tRNA modification requires the Elongator complex." In: *RNA* 11.4 (Jan. 2005), pp. 424–436. ISSN: 1469-9001.

[21] C. Chen, B. Huang, J. T. Anderson, and A. S. Byström. "Unexpected Accumulation of ncm5U and ncm5s2U in a trm9 Mutant Suggests an Additional Step in the Synthesis of mcm5U and mcm5s2U." In: *PLOS ONE* 6.6 (June 2011), e20783.

[22] S. Glatt et al. "Structure of the Kti11/Kti13 Heterodimer and Its Double Role in Modifications of tRNA and Eukaryotic Elongation Factor 2." In: *Structure* 23.1 (Dec. 2014), pp. 149–160. ISSN: 0969-2126.

[23] S. Glatt and C. W. Müller. "Structural insights into Elongator function." In: *Theory and simulation / Macromolecular assemblies* 23.2 (Apr. 2013), pp. 235–242. ISSN: 0959-440X.

[24] K. Selvadurai, P. Wang, J. Seimetz, and R. H. Huang. "Archaeal Elp3 catalyzes tRNA wobble uridine modification at C5 via a radical mechanism." In: *Nature chemical biology* 10.10 (Aug. 2014), pp. 810–812. ISSN: 1552-4469.

[25] M. P. Guy, B. M. Podyma, M. A. Preston, H. H. Shaheen, K. L. Krivos, P. A. Limbach, A. K. Hopper, and E. M. Phizicky. "Yeast Trm7 interacts with distinct proteins for critical modifications of the tRNAPhe anticodon loop." eng. In: *RNA (New York, N.Y.)* 18 (10 2012), pp. 1921–33.

[26] M. Dewez, F. Bauer, M. Dieu, M. Raes, J. Vandenhaute, and D. Hermand. "The conserved Wobble uridine tRNA thiolase Ctu1-Ctu2 is required to maintain genome integrity." In: *Proceedings of the National Academy of Sciences of the United States of America* 105.14 (Oct. 2007), pp. 5459–5464. ISSN: 1091-6490.

[27] Y. Nakai, M. Nakai, and H. Hayashi. "Thio-modification of yeast cytosolic tRNA requires a ubiquitin-related system that resembles bacterial sulfur transfer systems." eng. In: *The Journal of biological chemistry* 283 (41 2008), pp. 27469–76.

[28] A. Noma, Y. Sakaguchi, and T. Suzuki. "Mechanistic characterization of the sulfur-relay system for eukaryotic 2-thiouridine biogenesis at tRNA wobble positions." eng. In: *Nucleic acids research* 37 (4 2009), pp. 1335–52.

[29] S. S. Ashraf, E. Sochacka, R. Cain, R. Guenther, A. Malkiewicz, and P. F. Agris. "Single atom modification (O–>S) of tRNA confers ribosome binding." eng. In: *RNA (New York, N.Y.)* 5 (2 1999), pp. 188–94.

[30] R. Schaffrath and S. A. Leidel. "Wobble uridine modifications - a reason to live, a reason to die?!" In: *RNA Biology* (Feb. 2017), pp. 0–0. ISSN: 1547-6286.

[31] D. Nedialkova and S. Leidel. "Optimization of Codon Translation Rates via tRNA Modifications Maintains Proteome Integrity." In: *Cell* 161.7 (2015), pp. 1606–1618. ISSN: 0092-8674.

[32] A. Esberg, B. Huang, M. J. Johansson, and A. S. Byström. "Elevated Levels of Two tRNA Species Bypass the Requirement for Elongator Complex in Transcription and Exocytosis." In: *Molecular Cell* 24.1 (2006), pp. 139 –148. ISSN: 1097-2765.

[33] F. Bauer and D. Hermand. "A coordinated codon-dependent regulation of translation by Elongator." In: *Cell Cycle* 11.24 (Dec. 2012), pp. 4524–4529. ISSN: 1551-4005.

[34] R. J. Jackson, C. U. T. Hellen, and T. V. Pestova. "The mechanism of eukaryotic translation initiation and principles of its regulation." In: *Nat Rev Mol Cell Biol* 11.2 (Feb. 2010), pp. 113–127. ISSN: 1471-0072.

[35] R. J. Jackson, C. U. T. Hellen, and T. V. Pestova. "Termination and post-termination events in eukaryotic translation." eng. In: *Advances in protein chemistry and structural biology* 86 (2012), pp. 45–93.

[36] N. Demeshkina, L. Jenner, E. Westhof, M. Yusupov, and G. Yusupova. "A new understanding of the decoding principle on the ribosome." In: *Nature* 484.7393 (Apr. 2012), pp. 256–259. ISSN: 0028-0836.

[37] R. M. Voorhees and V. Ramakrishnan. "Structural basis of the translational elongation cycle." eng. In: *Annual review of biochemistry* 82 (2013), pp. 203–36.

[38] G. Otero, J. Fellows, Y. Li, T. de Bizemont, A. M. G. Dirac, C. M. Gustafsson, H. Erdjument-Bromage, P. Tempst, and J. Q. Svejstrup. "Elongator, a Multisubunit Component of a Novel RNA Polymerase II Holoenzyme for Transcriptional Elongation." In: *Molecular Cell* 3.1 (), pp. 109–118. ISSN: 1097-2765.

[39] N. J. Krogan and J. F. Greenblatt. "Characterization of a Six-Subunit Holo-Elongator Complex Required for the Regulated Expression of a Group of Genes in Saccharomyces cerevisiae." In: *Molecular and Cellular Biology* 21.23 (Aug. 2001), pp. 8203–8212. ISSN: 1098-5549.

[40] H. Xu, Z. Lin, F. Li, W. Diao, C. Dong, H. Zhou, X. Xie, Z. Wang, Y. Shen, and J. Long. "Dimerization of elongator protein 1 is essential for Elongator complex assembly." In: *Proceedings of the National Academy of Sciences* 112.34 (Aug. 2015), pp. 10697–10702.

[41] M. I. Dauden et al. "Architecture of the yeast Elongator complex." In: *EMBO reports* (2016). ISSN: 1469-221X.

[42] D. T. Setiaputra, D. T. Cheng, S. Lu, J. M. Hansen, U. Dalwadi, C. H. Lam, J. L. To, M.-Q. Dong, and C. K. Yip. "Molecular architecture of the yeast Elongator complex reveals an unexpected asymmetric subunit arrangement." eng. In: *EMBO reports* 18 (2 2017), pp. 280–291.

[43] L. Fichtner, D. Jablonowski, A. Schierhorn, H. K. Kitamoto, M. J. R. Stark, and R. Schaffrath. "Elongator's toxin-target (TOT) function is nuclear localization sequence dependent and suppressed by post-translational modification." eng. In: *Molecular microbiology* 49 (5 2003), pp. 1297–307.

[44] W. Abdel-Fattah, D. Jablonowski, R. Di Santo, K. L. Thüring, V. Scheidt, A. Hammermeister, S. ten Have, M. Helm, R. Schaffrath, and M. J. R. Stark. "Phosphorylation of Elp1 by Hrr25 Is Required for Elongator-Dependent tRNA Modification in Yeast." In: *PLoS Genetics* 11.1 (Dec. 2014), e1004931. ISSN: 1553-7404.

[45] R. Di Santo, S. Bandau, and M. J. R. Stark. "A conserved and essential basic region mediates tRNA binding to the Elp1 subunit of the Saccharomyces cerevisiae Elongator complex." In: *Molecular Microbiology* 92.6 (Apr. 2014), pp. 1227–1242. ISSN: 1365-2958.

[46] C. Dong, Z. Lin, W. Diao, D. Li, X. Chu, Z. Wang, H. Zhou, Z. Xie, Y. Shen, and J. Long. "The Elp2 Subunit Is Essential for Elongator Complex Assembly and Functional Regulation." In: *Structure* 23.6 (), pp. 1078–1086. ISSN: 0969-2126.

[47] B. Huang, J. Lu, and A. S. Bystrom. "A genome-wide screen identifies genes required for formation of the wobble nucleoside 5-methoxycarbonylmethyl-2-thiouridine in Saccharomyces cerevisiae." eng. In: *RNA (New York, N.Y.)* 14 (10 2008), pp. 2183–94.

[48] T. G. Petrakis, B. O. Wittschieben, and J. Q. Svejstrup. "Molecular architecture, structure-function relationship, and importance of the Elp3 subunit for the RNA binding of holo-elongator." eng. In: *The Journal of biological chemistry* 279 (31 2004), pp. 32087–92.

[49] F. Li, J. Ma, Y. Ma, Y. Hu, S. Tian, R. E. White, and G. Han. "hElp3 Directly Modulates the Expression of HSP70 Gene in HeLa Cells via HAT Activity." In: *PLOS ONE* 6.12 (Dec. 2011), pp. 1–8.

[50] G. S. Winkler, A. Kristjuhan, H. Erdjument-Bromage, P. Tempst, and J. Q. Svejstrup. "Elongator is a histone H3 and H4 acetyltransferase important for normal histone acetylation levels in vivo." In: *Proceedings of the National Academy of Sciences of the United States of America* 99.6 (Jan. 2002), pp. 3517–3522. ISSN: 1091-6490.

[51] S. Glatt et al. "Structural basis for tRNA modification by Elp3 from Dehalococcoides mccartyi." In: *Nature structural & molecular biology* 23.9 (July 2016), pp. 794–802. ISSN: 1545-9985.

[52] Z. Lin, W. Zhao, W. Diao, X. Xie, Z. Wang, J. Zhang, Y. Shen, and J. Long. "Crystal structure of elongator subcomplex Elp4-6." eng. In: *The Journal of biological chemistry* 287 (25 2012), pp. 21501–8.

[53] S. Glatt, J. Létoquart, C. Faux, N. M. I. Taylor, B. Séraphin, and C. W. Müller. "The Elongator subcomplex Elp456 is a hexameric RecA-like ATPase." In: *Nat Struct Mol Biol* 19.3 (Mar. 2012), pp. 314–320. ISSN: 1545-9993.

[54] Y. Okada, K. Yamagata, K. Hong, T. Wakayama, and Y. Zhang. "A role for elongator in zygotic paternal genome demethylation." In: *Nature* 463.7280 (Jan. 2010), pp. 554–558. ISSN: 1476-4687.

[55] C. Creppe et al. “Elongator Controls the Migration and Differentiation of Cortical Neurons through Acetylation of &x3b1;-Tubulin.” In: *Cell* 136.3 (2009), pp. 551–564. ISSN: 0092-8674.

[56] P. B. Rahl, C. Z. Chen, and R. N. Collins. “Elp1p, the Yeast Homolog of the FD Disease Syndrome Protein, Negatively Regulates Exocytosis Independently of Transcriptional Elongation.” In: *Molecular Cell* 17.6 (), pp. 841–853. ISSN: 1097-2765.

[57] F. Bauer, A. Matsuyama, J. Candiracci, M. Dieu, J. Scheliga, D. Wolf, M. Yoshida, and D. Hermand. “Translational Control of Cell Division by Elongator.” In: *Cell Reports* 1.5 (2012), pp. 424–433. ISSN: 2211-1247.

[58] N. Gunge, A. Tamaru, F. Ozawa, and K. Sakaguchi. “Isolation and characterization of linear deoxyribonucleic acid plasmids from Kluyveromyces lactis and the plasmid-associated killer character.” In: *Journal of Bacteriology* 145.1 (Jan. 1981), pp. 382–390. ISSN: 1098-5530.

[59] M. J. Stark, A. Boyd, A. J. Mileham, and M. A. Romanos. “The plasmid-encoded killer system of Kluyveromyces lactis: a review.” eng. In: *Yeast (Chichester, England)* 6 (1 1990), pp. 1–29.

[60] R. Schaffrath and F. Meinhardt. “Kluyveromyces lactis zymocin and other plasmid-encoded yeast killer toxins.” In: *Microbial Protein Toxins*. Berlin, Heidelberg: Springer Berlin Heidelberg, 2005, pp. 133–155.

[61] F. Frohloff, L. Fichtner, D. Jablonowski, K. D. Breunig, and R. Schaffrath. “Saccharomyces cerevisiae Elongator mutations confer resistance to the Kluyveromyces lactis zymocin.” eng. In: *The EMBO journal* 20 (8 2001), pp. 1993–2003.

[62] D. Jablonowski, F. Frohloff, L. Fichtner, M. J. Stark, and R. Schaffrath. “Kluyveromyces lactis zymocin mode of action is linked to RNA polymerase II function via Elongator.” eng. In: *Molecular microbiology* 42 (4 2001), pp. 1095–105.

[63] L. Fichtner, F. Frohloff, K. Burkner, M. Larsen, K. D. Breunig, and R. Schaffrath. “Molecular analysis of KTI12/TOT4, a Saccharomyces cerevisiae gene required for Kluyveromyces lactis zymocin action.” eng. In: *Molecular microbiology* 43 (3 2002), pp. 783–91.

[64] J. Lu, B. Huang, A. Esberg, M. J. O. Johansson, and A. S. Bystrom. “The Kluyveromyces lactis gamma-toxin targets tRNA anticodons.” eng. In: *RNA (New York, N.Y.)* 11 (11 2005), pp. 1648–54.

[65] D. Jablonowski, S. Zink, C. Mehlgarten, G. Daum, and R. Schaffrath. “tRNAGlu wobble uridine methylation by Trm9 identifies Elongator’s key role for zymocin-induced cell death in yeast.” eng. In: *Molecular microbiology* 59 (2 2006), pp. 677–88.

[66] D. Jablonowski, A. R. Butler, L. Fichtner, D. Gardiner, R. Schaffrath, and M. J. R. Stark. "Sit4p protein phosphatase is required for sensitivity of Saccharomyces cerevisiae to Kluyveromyces lactis zymocin." In: *Genetics* 159.4 (Dec. 2001), p. 1479.

[67] L. Fichtner and R. Schaffrath. "KTI11 and KTI13, Saccharomyces cerevisiae genes controlling sensitivity to G1 arrest induced by Kluyveromyces lactis zymocin." eng. In: *Molecular microbiology* 44 (3 2002), pp. 865–75.

[68] P. Studte, S. Zink, D. Jablonowski, C. Bar, T. von der Haar, M. F. Tuite, and R. Schaffrath. "tRNA and protein methylase complexes mediate zymocin toxicity in yeast." eng. In: *Molecular microbiology* 69 (5 2008), pp. 1266–77.

[69] C. Mehlgarten et al. "Use of a Yeast tRNase Killer Toxin to Diagnose Kti12 Motifs Required for tRNA Modification by Elongator." eng. In: *Toxins* 9 (9 2017).

[70] L. Eichinger et al. "The genome of the social amoeba Dictyostelium discoideum." In: *Nature* 435.7038 (May 2005), pp. 43–57. ISSN: 0028-0836.

[71] L. Malinovska, S. Palm, K. Gibson, J.-M. Verbavatz, and S. Alberti. "Dictyostelium discoideum has a highly Q/N-rich proteome and shows an unusual resilience to protein aggregation." eng. In: *Proceedings of the National Academy of Sciences of the United States of America* 112 (20 2015), E2620–9.

[72] P. Gaudet, J. G. Williams, P. Fey, and R. L. Chisholm. "An anatomy ontology to represent biological knowledge in Dictyostelium discoideum." In: *BMC Genomics* 9 (Mar. 2008), pp. 130–130. ISSN: 1471-2164.

[73] Y. Maeda and J. Chida. "Control of cell differentiation by mitochondria, typically evidenced in dictyostelium development." eng. In: *Biomolecules* 3 (4 2013), pp. 943–66.

[74] Q.-s. Du, J. Cui, C.-j. Zhang, and K. He. "Visualization analysis of CRISPR/Cas9 gene editing technology studies." In: *Journal of Zhejiang University. Science. B* 17.10 (Aug. 2016), pp. 798–806. ISSN: 1862-1783.

[75] R. Jansen, J. D.A. v. Embden, W. Gaastra, and L. M. Schouls. "Identification of genes that are associated with DNA repeats in prokaryotes." eng. In: *Molecular microbiology* 43 (6 2002), pp. 1565–75.

[76] S. Horowitz and M. A. Gorovsky. "An unusual genetic code in nuclear genes of Tetrahymena." In: *Proceedings of the National Academy of Sciences of the United States of America* 82.8 (Apr. 1985), pp. 2452–2455. ISSN: 1091-6490.

[77] N. Hanyu, Y. Kuchino, S. Nishimura, and H. Beier. "Dramatic events in ciliate evolution: alteration of UAA and UAG termination codons to glutamine codons due to anticodon mutations in two Tetrahymena tRNAs(Gln)." In: *The EMBO Journal* 5.6 (June 1986), pp. 1307–1311. ISSN: 1460-2075.

[78] C. Schüll and H. Beier. "Three Tetrahymena tRNA(Gln) isoacceptors as tools for studying unorthodox codon recognition and codon context effects during protein synthesis in vitro." In: *Nucleic Acids Research* 22.11 (June 1994), pp. 1974–1980. ISSN: 1362-4962.

[79] J. Faix, L. Kreppel, G. Shaulsky, M. Schleicher, and A. R. Kimmel. "A rapid and efficient method to generate multiple gene disruptions in Dictyostelium discoideum using a single selectable marker and the Cre-loxP system." In: *Nucleic Acids Research* 32.19 (Sept. 2004), e143–e143. ISSN: 1362-4962.

[80] D. M. Veltman, G. Akar, L. Bosgraaf, and P. J. M. Van Haastert. "A new set of small, extrachromosomal expression vectors for Dictyostelium discoideum." eng. In: *Plasmid* 61 (2 2009), pp. 110–8.

[81] M. Malicki. "The Retrotransposon Silencing Complex (RSC) is a key repressor of retrotransposons in Dictyostelium discoideum." In: *PhD thesis Jacobs University Bremen* (2016).

[82] J. M. Kruse. "Dicer-like proteins in Dictyostelium discoideum." In: *PhD Thesis, Jacobs University* (2014).

[83] D. M. Veltman, I. Keizer-Gunnink, and P. J.M. V. Haastert. "An extrachromosomal, inducible expression system for Dictyostelium discoideum." eng. In: *Plasmid* 61 (2 2009), pp. 119–25.

[84] M. Dubin and W. Nellen. "A versatile set of tagged expression vectors to monitor protein localisation and function in Dictyostelium." eng. In: *Gene* 465 (1-2 2010), pp. 1–8.

[85] A. Stein. "Expression, purication and characterization of the Elongator subcomplex Elp456 (HAP complex) of Dictyostelium discoideum." In: *Bachelor Thesis Jacobs University Bremen* (2016).

[86] S. Gronemann. "Diplomarbeit Elp1." In: *Diplomarbeit TU Darmstadt* (2011).

[87] A. V. Balachandar. "Studies on A Dicer homolog (DrnA) & The Elongator Complex of Dictyostelium discoideum ." In: *PhD Thesis, Jacobs University* (2014).

[88] J. M. Ashworth and D. J. Watts. "Metabolism of the cellular slime mould Dictyostelium discoideum grown in axenic culture." eng. In: *The Biochemical journal* 119 (2 1970), pp. 175–82.

[89] D. Hanahan. "Studies on transformation of Escherichia coli with plasmids." eng. In: *Journal of molecular biology* 166 (4 1983), pp. 557–80.

[90] D. Knecht and K. M. Pang. "Electroporation of Dictyostelium discoideum." eng. In: *Methods in molecular biology (Clifton, N.J.)* 47 (1995), pp. 321–30.

[91] P. Gaudet, K. E. Pilcher, P. Fey, and R. L. Chisholm. "Transformation of Dictyostelium discoideum with plasmid DNA." eng. In: *Nature protocols* 2 (6 2007), pp. 1317–24.

[92] R. S. Haun and J. Moss. "Ligation-independent cloning of glutathione S-transferase fusion genes for expression in Escherichia coli." In: 112.1 (Mar. 1992), pp. 37–43. ISSN: 0378-1119.

[93] S. Wiegand, J. Kruse, S. Gronemann, and C. Hammann. "Efficient generation of gene knockout plasmids for Dictyostelium discoideum using one-step cloning." In: *Genomics* 97.5 (May 2011), pp. 321–325. ISSN: 0888-7543.

[94] K. Mullis, F. Faloona, S. Scharf, R. Saiki, G. Horn, and H. Erlich. "Specific enzymatic amplification of DNA in vitro: the polymerase chain reaction." eng. In: *Cold Spring Harbor symposia on quantitative biology* 51 Pt 1 (1986), pp. 263–73.

[95] R. K. Saiki, D. H. Gelfand, S. Stoffel, S. J. Scharf, R. Higuchi, G. T. Horn, K. B. Mullis, and H. A. Erlich. "Primer-directed enzymatic amplification of DNA with a thermostable DNA polymerase." eng. In: *Science (New York, N.Y.)* 239 (4839 1988), pp. 487–91.

[96] S. J. Charette and P. Cosson. "Preparation of genomic DNA from Dictyostelium discoideum for PCR analysis." eng. In: *BioTechniques* 36 (4 2004), pp. 574–5.

[97] P. Chomczynski and N. Sacchi. "Single-step method of RNA isolation by acid guanidinium thiocyanate-phenol-chloroform extraction." eng. In: *Analytical biochemistry* 162 (1 1987), pp. 156–9.

[98] G. L. Igloi. "Interaction of tRNAs and of phosphorothioate-substituted nucleic acids with an organomercurial. Probing the chemical environment of thiolated residues by affinity electrophoresis." In: *Biochemistry* 27.10 (May 1988), pp. 3842–3849. ISSN: 0006-2960.

[99] U. Rothbauer, K. Zolghadr, S. Muyldermans, A. Schepers, M. C. Cardoso, and H. Leonhardt. "A versatile nanotrap for biochemical and functional studies with fluorescent fusion proteins." eng. In: *Molecular & cellular proteomics : MCP* 7 (2 2008), pp. 282–9.

[100] U. K. Laemmli. "Cleavage of structural proteins during the assembly of the head of bacteriophage T4." eng. In: *Nature* 227 (5259 1970), pp. 680–5.

[101] A. Shevchenko, H. Tomas, J. Havlis, J. V. Olsen, and M. Mann. "In-gel digestion for mass spectrometric characterization of proteins and proteomes." eng. In: *Nature protocols* 1 (6 2006), pp. 2856–60.

[102] H. Xu, J. Bygdell, G. Wingsle, and A. S. Byström. "Yeast Elongator protein Elp1p does not undergo proteolytic processing in exponentially growing cells." In: *MicrobiologyOpen* 4.6 (July 2015), pp. 867–878. ISSN: 2045-8827.

[103] M. D. Ryan, A. M. King, and G. P. Thomas. "Cleavage of foot-and-mouth disease virus polyprotein is mediated by residues located within a 19 amino acid sequence." eng. In: *The Journal of general virology* 72 (Pt 11) (1991), pp. 2727–32.

[104] M. L. Donnelly, G. Luke, A. Mehrotra, X. Li, L. E. Hughes, D. Gani, and M. D. Ryan. "Analysis of the aphthovirus 2A/2B polyprotein 'cleavage' mechanism indicates not a proteolytic reaction, but a novel translational effect: a putative ribosomal 'skip'." eng. In: *The Journal of general virology* 82 (Pt 5 2001), pp. 1013–25.

[105] P. A. Radcliffe and K. A. Mitrophanous. "Multiple gene products from a single vector: /'self-cleaving/' 2A peptides." In: *Gene Ther* 11.23 (0), pp. 1673–1674. ISSN: 0969-7128.

[106] A. L. Szymczak, C. J. Workman, Y. Wang, K. M. Vignali, S. Dilioglou, E. F. Vanin, and D. A. A. Vignali. *Correction of multigene deficiency in vivo using a single 'self-cleaving' 2A peptide-based retroviral vector.* eng. United States, 2004.

[107] R. Klassen, P. Grunewald, K. L. Thuring, C. Eichler, M. Helm, and R. Schaffrath. "Loss of anticodon wobble uridine modifications affects tRNA(Lys) function and protein levels in Saccharomyces cerevisiae." eng. In: *PloS one* 10 (3 2015), e0119261.

[108] L. Copoiu. "Function and Localization of Elp5 and Elp6 subunits of the Elongator Complex in Dictyostelium discoideum." In: *Bachelor thesis Jacobs University Bremen* (2015).

[109] A. De Lozanne and J. A. Spudich. "Disruption of the Dictyostelium myosin heavy chain gene by homologous recombination." In: *Science* 236.4805 (May 1987), p. 1086.

[110] H. Kuwayama. "Enhancement of Homologous Recombination Efficiency by Homologous Oligonucleotides." In: *Cell Interaction*. Ed. by S. Gowder. Rijeka: InTech, 2012, Ch. 09.

[111] V. Lemau de Talancé, F. Bauer, D. Hermand, and S. P. Vincent. "A simple synthesis of APM ([p-(N-acrylamino)-phenyl]mercuric chloride), a useful tool for the analysis of thiolated biomolecules." In: 21.24 (Dec. 2011), pp. 7265–7267. ISSN: 0960-894X.

[112] F. Bauer, A. Matsuyama, J. Candiracci, M. Dieu, J. Scheliga, D. Wolf, M. Yoshida, and D. Hermand. "Translational Control of Cell Division by Elongator." In: *Cell Reports* 1.5 (2012), pp. 424–433. ISSN: 2211-1247.

[113] Z. Bloom-Ackermann, S. Navon, H. Gingold, R. Towers, Y. Pilpel, and O. Dahan. "A Comprehensive tRNA Deletion Library Unravels the Genetic Architecture of the tRNA Pool." In: *PLoS Genetics* 10.1 (Nov. 2013), e1004084. ISSN: 1553-7404.

[114] J. Lu, A. Esberg, B. Huang, and A. S. Byström. "Kluyveromyces lactis -toxin, a ribonuclease that recognizes the anticodon stem loop of tRNA." In: *Nucleic Acids Research* 36.4 (Dec. 2007), pp. 1072–1080. ISSN: 1362-4962.

[115] A. Grigoriev. "A relationship between gene expression and protein interactions on the proteome scale: analysis of the bacteriophage T7 and the yeast Saccharomyces cerevisiae." In: *Nucleic Acids Research* 29.17 (July 2001), pp. 3513–3519. ISSN: 1362-4962.

[116] Z. Chen, H. Zhang, D. Jablonowski, X. Zhou, X. Ren, X. Hong, R. Schaffrath, J.-K. Zhu, and Z. Gong. "Mutations in ABO1/ELO2, a subunit of holo-Elongator, increase abscisic acid sensitivity and drought tolerance in Arabidopsis thaliana." eng. In: *Molecular and cellular biology* 26 (18 2006), pp. 6902–12.

[117] Y.-T. Chen, M. M. Hims, R. S. Shetty, J. Mull, L. Liu, M. Leyne, and S. A. Slaugenhaupt. "Loss of mouse Ikbkap, a subunit of elongator, leads to transcriptional deficits and embryonic lethality that can be rescued by human IKBKAP." eng. In: *Molecular and cellular biology* 29 (3 2009), pp. 736–44.

[118] C. Mehlgarten, D. Jablonowski, U. Wrackmeyer, S. Tschitschmann, D. Sondermann, G. Jäger, Z. Gong, A. S. Byström, R. Schaffrath, and K. D. Breunig. "Elongator function in tRNA wobble uridine modification is conserved between yeast and plants." In: *Molecular Microbiology* 76.5 (Apr. 2010), pp. 1082–1094. ISSN: 1365-2958.

[119] E. M. Novoa and L. Ribas de Pouplana. "Speeding with control: codon usage, tRNAs, and ribosomes." In: *Trends in Genetics* 28.11 (), pp. 574–581. ISSN: 0168-9525.

[120] P. S. Spencer and J. M. Barral. "Genetic code redundancy and its influence on the encoded polypeptides." In: 1.1 (Apr. 2012), e201204006. ISSN: 2001-0370.

[121] R. Hershberg and D. A. Petrov. "Selection on Codon Bias." In: *Annu. Rev. Genet.* 42.1 (Dec. 2008), pp. 287–299. ISSN: 0066-4197.

[122] J. B. Plotkin and G. Kudla. "Synonymous but not the same: the causes and consequences of codon bias." In: *Nature reviews. Genetics* 12.1 (Nov. 2010), pp. 32–42. ISSN: 1471-0064.

[123] M. Botzman and H. Margalit. "Variation in global codon usage bias among prokaryotic organisms is associated with their lifestyles." In: *Genome Biology* 12.10 (Oct. 2011), R109–R109. ISSN: 1465-6914.

[124] L. B. Koski, R. A. Morton, and G. B. Golding. "Codon Bias and Base Composition Are Poor Indicators of Horizontally Transferred Genes." In: *Molecular Biology and Evolution* 18.3 (Mar. 2001), pp. 404–412. ISSN: 0737-4038.

[125] T. Tuller. "Codon bias, tRNA pools and horizontal gene transfer." In: *Mobile Genetic Elements* 1.1 (Mar. 2011), pp. 75–77. ISSN: 2159-256X.

[126] S. Kanaya, Y. Yamada, M. Kinouchi, Y. Kudo, and T. Ikemura. "Codon Usage and tRNA Genes in Eukaryotes: Correlation of Codon Usage Diversity with Translation Efficiency and with CG-Dinucleotide Usage as Assessed by Multivariate Analysis." In: *Journal of Molecular Evolution* 53.4 (2001), pp. 290–298. ISSN: 1432-1432.

[127] S. Kirchner and Z. Ignatova. "Emerging roles of tRNA in adaptive translation, signalling dynamics and disease." In: *Nat Rev Genet* 16.2 (Feb. 2015), pp. 98–112. ISSN: 1471-0056.

[128] H. Grosjean and E. Westhof. "An integrated, structure- and energy-based view of the genetic code." eng. In: *Nucleic acids research* 44 (17 2016), pp. 8020–40.

[129] S. Santarriaga, A. Petersen, K. Ndukwe, A. Brandt, N. Gerges, J. Bruns Scaglione, and K. M. Scaglione. "The Social Amoeba Dictyostelium discoideum Is Highly Resistant to Polyglutamine Aggregation." eng. In: *The Journal of biological chemistry* 290 (42 2015), pp. 25571–8.

[130] R. Klassen, A. Ciftci, J. Funk, A. Bruch, F. Butter, and R. Schaffrath. "tRNA anticodon loop modifications ensure protein homeostasis and cell morphogenesis in yeast." In: *Nucleic Acids Research* 44.22 (2016), p. 10946.

[131] A. F.H.H.M. S. Stephanie Santarriaga Adam Kanack. "Identification of a new chaperone that suppresses polyglutamine aggregation in Dictyostelium." In: *Dicty 2017 Meeting Booklet* (2017), Poster 127.

[132] A. A. Noegel and M. Schleicher. "The actin cytoskeleton of Dictyostelium: a story told by mutants." eng. In: *Journal of cell science* 113 (Pt 5) (2000), pp. 759–66.

[133] F. Liu et al. "ALKBH1-Mediated tRNA Demethylation Regulates Translation." eng. In: *Cell* 167 (3 2016), 816–828.e16.

[134] H. Tukenmez, H. Xu, A. Esberg, and A. S. Bystrom. "The role of wobble uridine modifications in +1 translational frameshifting in eukaryotes." eng. In: *Nucleic acids research* 43 (19 2015), pp. 9489–99.

[135] R. Klassen, A. Bruch, and R. Schaffrath. "Independent suppression of ribosomal +1 frameshifts by different tRNA anticodon loop modifications." eng. In: *RNA biology* (2016), pp. 1–8.

[136] P. J. Farabaugh and G. R. Bjork. "How translational accuracy influences reading frame maintenance." eng. In: *The EMBO journal* 18 (6 1999), pp. 1427–34.

[137] B. Kanunnikov. "The role of Uridine-34 modifications in stress response: Dictyostelium discoideum mutants lacking 5-methoxycarbonylmethyl-2-thiouridine show impaired growth under iron stress." In: *Bachelor Thesis Jacobs University Bremen* (2017).

[138] S. A. Rincon et al. "Pom1 regulates the assembly of Cdr2-Mid1 cortical nodes for robust spatial control of cytokinesis." In: *J Cell Biol* 206.1 (July 2014), p. 61.

[139] K. J. Barnum and M. J. O'Connell. "Cell Cycle Regulation by Checkpoints." In: *Methods in molecular biology (Clifton, N.J.)* 1170 (2014), pp. 29–40. ISSN: 1940-6029.

[140] G. R. Stark and W. R. Taylor. "Analyzing the G2/M checkpoint." eng. In: *Methods in molecular biology (Clifton, N.J.)* 280 (2004), pp. 51–82.

[141] D. Choezom. "-toxin activity on tRNA of Dictyostelium discoidium." In: *Bachelor thesis Jacobs University Bremen* (2016).

[142] R. Longtin. "A Forgotten Debate: Is Selenocysteine the 21st Amino Acid?" In: *JNCI: Journal of the National Cancer Institute* 96.7 (Apr. 2004), pp. 504–505. ISSN: 0027-8874.

[143] A. Bo¨ck, K. Forchhammer, J. Heider, and C. Baron. "Selenoprotein synthesis: an expansion of the genetic code." In: 16 (Jan. 1991), pp. 463–467. ISSN: 0968-0004.

[144] M. J. Berry, L. Banu, J. W. Harney, and P. R. Larsen. "Functional characterization of the eukaryotic SECIS elements which direct selenocysteine insertion at UGA codons." In: *The EMBO Journal* 12.8 (Aug. 1993), pp. 3315–3322. ISSN: 1460-2075.

[145] D. Fagegaltier, N. Hubert, K. Yamada, T. Mizutani, P. Carbon, and A. Krol. "Characterization of mSelB, a novel mammalian elongation factor for selenoprotein translation." In: *EMBO J* 19.17 (Sept. 2000), p. 4796.

[146] T. Winckler, C. Trautwein, C. Tschepke, C. Neuhauser, I. Zundorf, P. Beck, G. Vogel, and T. Dingermann. "Gene function analysis by amber stop codon suppression: CMBF is a nuclear protein that supports growth and development of Dictyostelium amoebae." eng. In: *Journal of molecular biology* 305 (4 2001), pp. 703–14.

A

APPENDIX

A.1 ADDITIONAL EXPERIMENTS ON ELONGATOR LOCALIZATION AND COMPLEX IDENTITY

A.1.1 *Fluorescence microscopy*

Figure 38 A shows a Western blot and fluorescence images of N- and C-terminal GFP tagged Elp3 and Elp4 proteins. All fluorescence images show cytoplasmic GFP signals (Figure 38). The fluorescence images of pointmutanted GFP-Elp3 overexpressor strains do not show any difference in the localization of the GFP signals (Figure 39 B) but the signals appears to be weaker compared to the GFP-Elp3 in an *elp3*$^{-}$. This was confirmed by flow cytometric analysis of these strains (data not shown).

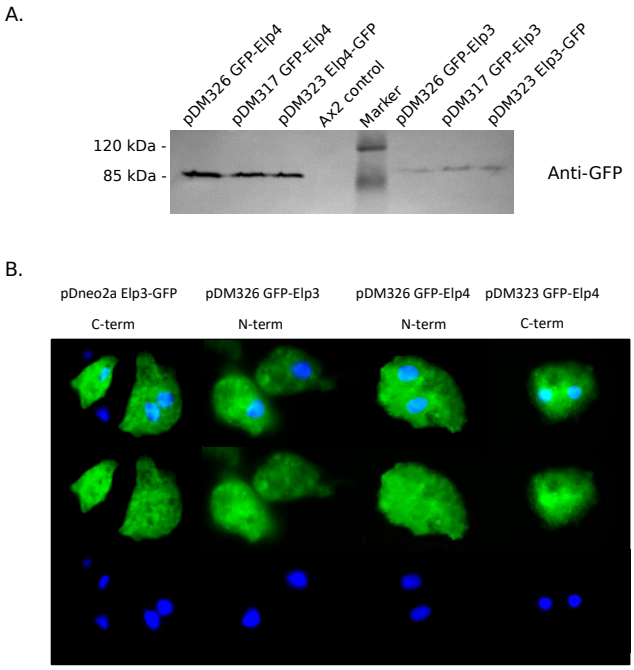

Figure 38: Expression of ectopically expressed, GFP-tagged Elp3 and Elp4 proteins. **A.** Western blot image anti-GFP of different strains with N- and C-terminally tagged Elp3 and Elp4 proteins used for fluorescence imaging in B. Marker = Molecular Weight Marker. **B.** Fluorescence image show that the GFP signal is found throughout the cells. (blue = DAPI staining of the nuclear DNA). No scale is provided in the images.

LSM fluorescence images of GFP-Elp5 and GFP-Elp6 indicate that these proteins appear mainly in the cytoplasm (Figure 40).

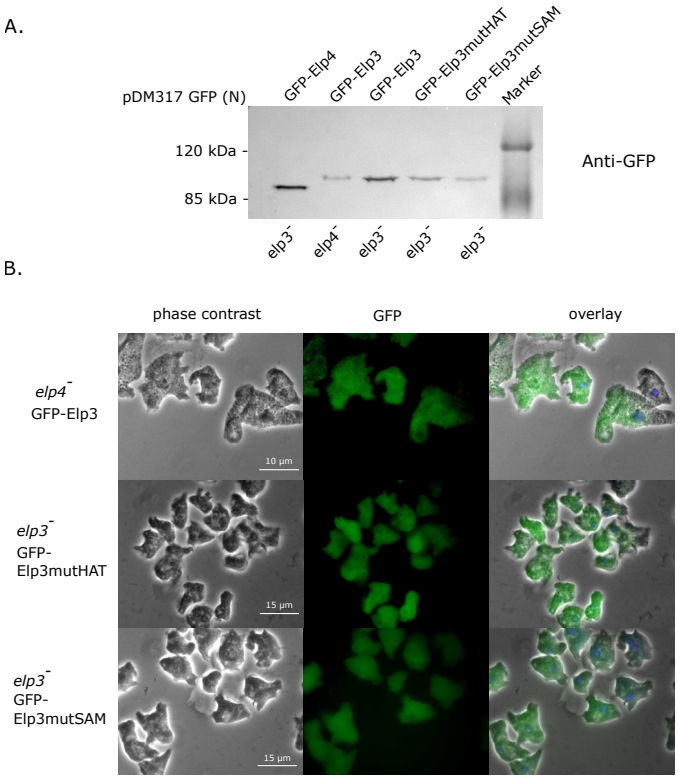

Figure 39: Expression of ectopically expressed, GFP-tagged Elp3 protein variants in different strains. **A.** Western blot anti-GFP of point mutated Elp3 proteins and the Elp3 protein expressed from the pDM317 plasmid in the *elp3*⁻ strain and *elp4*⁻. Marker = Molecular Weight Marker. **B.** Fluorescence microscopy image of different strains. The GFP signal can be found throughout the cells. (blue = DAPI staining of the nuclear DNA). **B.** Fluorescence images show that the point mutation of the Elp3 proteins does not influence its location within the cell. The localization of Elp3 is also not influenced when expressed in an *elp4*⁻ strain. Scales are 10 µm in picture one and 15 µm in the other images.

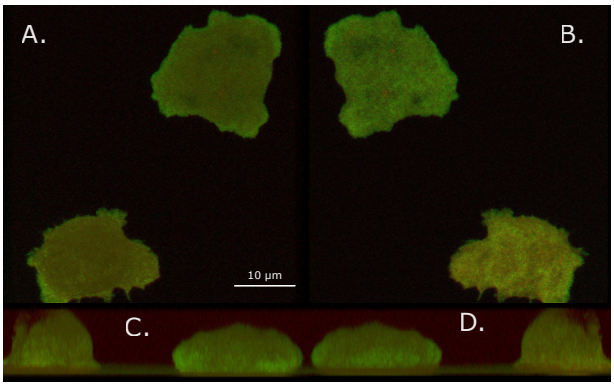

Figure 40: LSM 3D images of cells expressing mRFPElp5 GFP-Elp6. Images were taken with confocal LSM **A.** top view of the z-stack overlay of GFP and RFP channel . **B.** bottom view of the z-stack overlay of GFP and RFP channel. **C.** view from the left. **D.** view from the right. Scale = 10 µm.

A.1.2 *Additonal data on Elongator proteins*

Additional Western blot for expression verification of different ectopically expressed Elongator proteins

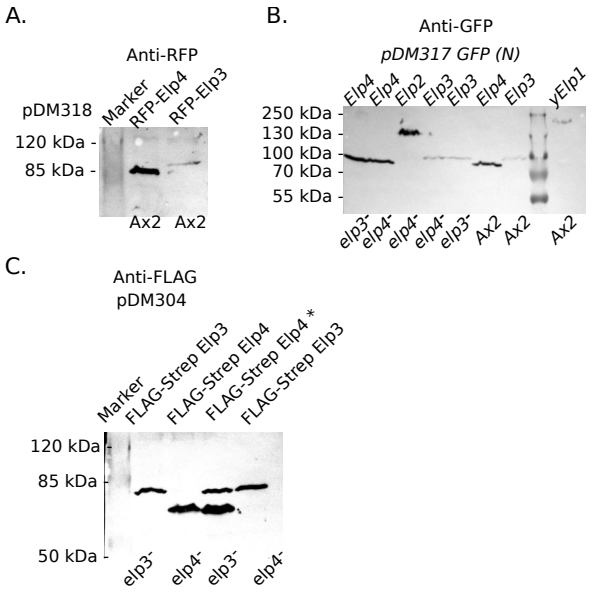

Figure 41: Additional Western blots on strains expressing Elongator proteins. **A.** anti-RFP. Marker = Prestained Molecular Weight Marker **B.** anti-GFP. Marker = PageRuler Plus Prestained Protein Ladder. **C.** anti-FLAG. Lane *elp3*$^{-}$ FLAG-Strep-Elp4* shows 2 signal bands. This strain was terminated. Marker = Prestained Molecular Weight Marker.

A.1.2.1 *pDM-fusion mRFP-Elp5 GFP-Elp6*

A pDM fusion construct of mRFP-Elp5 and GFP-Elp6 was generated, both with their own expression cassette (Figure 42). Both expression cassettes feature the identical actin 15 promotor. The 2D scatter plot in Figure 42 C indicates that both fusion gene products are expressed in a similar ratio. A GFP trap pulldown of this strain, shown in Figure 42 D, revealed that Elp5 and Elp6 come done together in equimolar ratio. This is in line with the literature where Elp5 and Elp6 are also found to form a dimer [53].

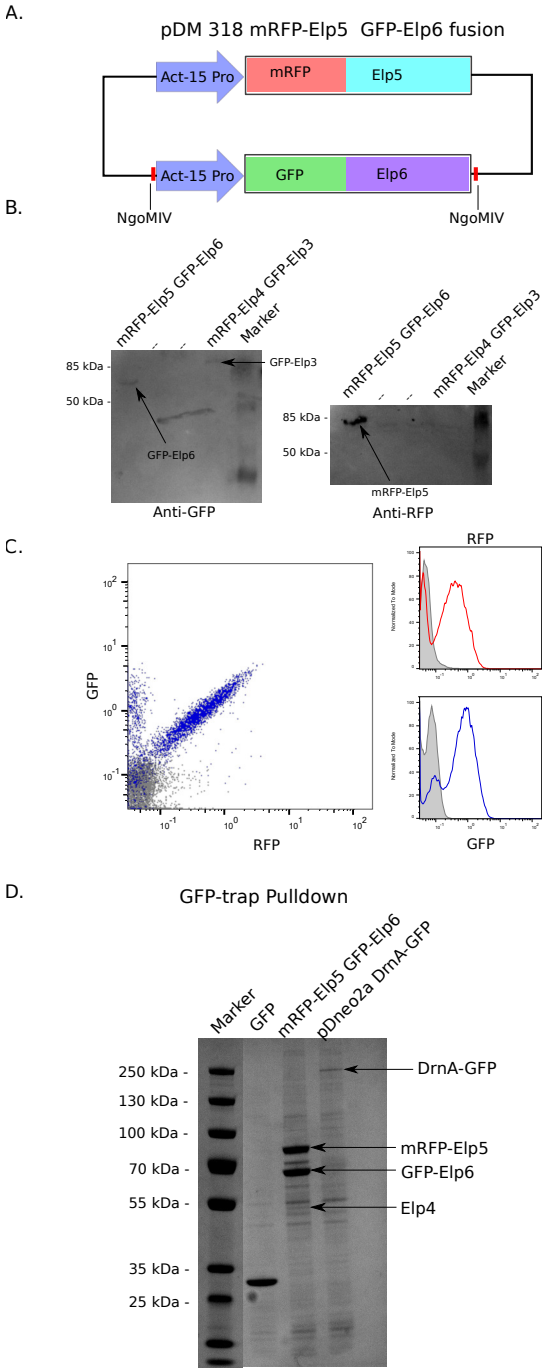

Figure 42: Expression of mRFP-Elp5 and GFP-Elp6 from a single pDM Vector. **A.** Sketch of the vector fusion. The Expression cassette of of pDM317 GFP-Elp6 was PCR amplified and flanked with to *Ngo*MIV restriction sites and cloned into the pDM318 Elp5 via the very restriction site. **B.** Western blot images anti-GFP (left) and anti-RFP (right) revealed that both proteins pf the pDM-fusion mRFP-Elp5 GFP-Elp6 are expressed. The other sample in the image is from the pDM-fusion mRFP-Elp4 GFP-Elp3. Marker = Prestained Molecular Weight Marker. **C.** 2D scatter blot from flow cytometric analysis indicated a similar expression of mRFP-Elp5 (red) and GFP-Elp6 (blue) within single cells. Non-fluorescent cell control = 17518 counts; sample = 24116 counts. **D.** gradient (4-12%) SDS-PAGE image of a GFP-trap pulldown performed from the strain used in C. GFP-Elp6 brings down mRFP-Elp5 in an equimolar ratio. This indicates that the two proteins bind to each other. Marker = PageRuler Plus Prestained Protein Ladder.

A.1.2.2 *MALDI mass spectrometric results*

Please note that the MASCOT verification for Elp1, Elp4 and Elp5 was significantly more difficult than for the other analyzed proteins. These proteins were mainly analysed with mMass without MASCOT BLAST searches (indicated by n.a. = not applicable).

Figure 43 shows a Coomassie stained GFP trap pulldown of strains expressing either GFP, Elp1-GFP or Elp3-GFP (the pulldown experiment was performed together with Balachandar Ammapatti). No protease inhibitor was used in this experiment. Elp1-GFP, as well as endogenous Elp1 in the lane of the Elp3-GFP pulldown, are found in 2 distinged bands. The same observation was done when ever protease inhibition failed. This is in line with the literature [102].

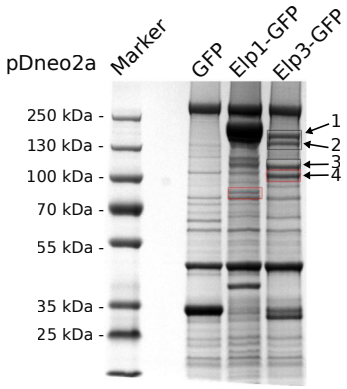

Figure 43: GFP trap pulldown without protease inhibitor.
Gradient SDS-PAGE image GFP-trap pulldown of GFP, Elp1-GFP and Elp3-GFP expressed in Ax2 wild type background. In this approach no protease inhibitor was used. Elp1 appears in 2 bands in the Elongator pulldowns due to a specific protease cleavage. The protein band inside the red box in the elp1 lane was identified as Elp3 [87]. Marker = PageRuler Plus Prestained Protein Ladder.

Table 17: MALDI mass spectrometric analysis of GFP-trap pulldowns from Elp3 without protease inhibitor

Band	Protein	Mass	Score	Sequ coverage
1	Elp1	160 kDa	138	41.8%
2	Elp1	160 kDa	101	31.4%
3	Elp2	100 kDa	110	46.8%
4	Elp3-GFP	90 kDa	122	40.2%

MALDI mass spec analysis of recElp456 from the SEC elution fraction 1.4 mL (Refering to Figure 15 B).

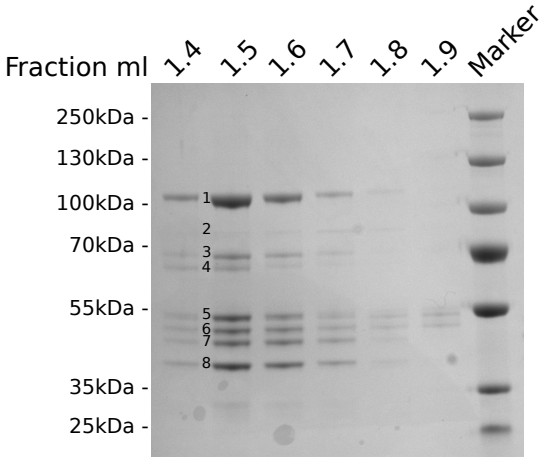

Figure 44: Different Elution fractions of recElp456 after SEC. Image already shown and described in Figure 15 B. The individual protein bands indicated with numbers next to them were subjected to MALDI mass spectrometry analysis. The results are shown in the table below. Marker = PageRuler Plus Prestained Protein Ladder.

Table 18: MALDI mass spectrometric analysis of recElp456 purified from *E. coli*

Band	Protein	Mass	Score	Expect	coverage	matched
1	MBP-Elp4	90 kDa	n.a.	n.a.	23%	15
2	n.d.	-	-	-	-	-
3	MBP-Elp4	90 kDa	n.a.	n.a.	18%	11
4	DnaK	69 kDa	114	9.2e-08	30%	15
5	FLAG-Elp5	47 kDa	n.a.	n.a.	22%	6
5 (2)	GroEL	57 kDa	95	6.6e-06	37%	13
6	MBP*	45 kDa	92	1.6e-05	47%	14
7	MBP	43 kDa	84	8.4e-05	46%	15
8	Elp6	38 kDa	90	3.9e-06	29%	10

[*]His-MBP tag
Coverage = protein sequence coverage; Matched = matched peptides.

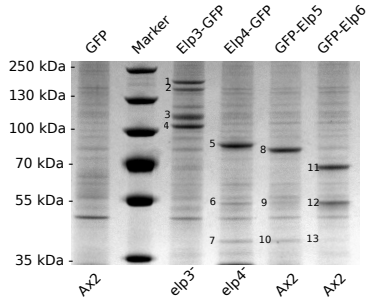

Figure 45: Gel picture of the GFP-trap pulldown of Elp3-Elp6 already shown and described in Figure 9. The individual protein bands indicated with numbers next to them were subjected to MALDI mass spectrometry analysis. The results are shown in the table below. Marker = PageRuler Plus Prestained Protein Ladder.

Table 19: MALDI mass spectrometric analysis of GFP-trap pulldowns from Elp3-Elp6

Band	Protein	Mass	Score	Expect	coverage	matched
1	Elp1	160 kDa	n.a.	n.a.	11%	19
2	Elp1	160 kDa	n.a.	n.a.	8%	10
3	Elp2	100 kDa	n.a.	n.a.	3%	3
4	Elp3*-GFP	90 kDa	69	0.00051	26%	14
5	Elp4-GFP	75 kDa	n.a.	n.a.	23%	15
6	Elp5	45 kDa	n.a.	n.a.	20%	23
7	Elp6	38 kDa	104	1.6e-07	26%	11
8	GFP-Elp5	72 kDa	n.a.	n.a.	48%	14
9 (1)	Elp4	48 kDa	n.a.	n.a.	10%	4
9 (2)	Elp5	45 kDa	n.a.	n.a.	30%	10
10	Elp6	38 kDa	70	0.0015	24%	9
11	GFP-Elp6	61 kDa	n.a.	n.a.	22%	12
12 (1)	Elp4	48 kDa	n.a.	n.a.	16%	7
12 (2)	Elp5	45 kDa	n.a.	n.a.	11%	5
13	Elp6	38 kDa	n.d.	n.d.	n.d.	n.d.

*only Elp3 was considered

Coverage = protein sequence coverage; Matched = matched peptides.

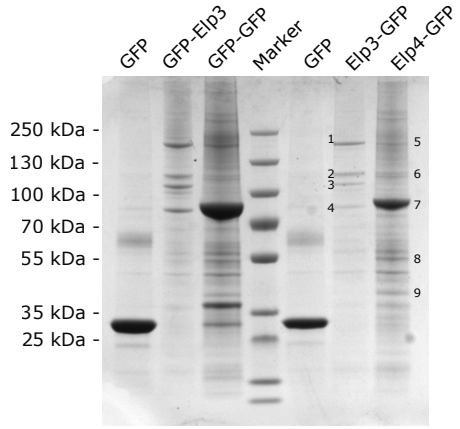

Figure 46: Gel picture of crosslinked GFP-trap pulldown of Elp3 and Elp4 (N- and C-terminal), the right side is already shown and described in Figure 10. Both pulldown of Elp4 show similar protein band patterns, suggesting that also GFP-Elp4 is capable to bind Elp1 and Elp2. The individual protein bands indicated with numbers next to them were subjected to MALDI mass spectrometry analysis. The results are shown in the table below. Marker = PageRuler Plus Prestained Protein Ladder.

Table 20: MALDI mass spectrometric analysis crosslinked GFP-trap

Band	Protein	Mass	Score	Expect	coverage	matched
1	Elp1	160 kDa	n.a.	n.a.	11%	15
2	Elp2	100 kDa	108	6.6e-08	20%	18
3	Elp3-GFP	90 kDa	n.d.	n.d.	n.d.	n.d.
3 (1)	Elp3	63 kDa	118	6.6e-09	35%	22
3 (2)	GFP	27 kDa	n.a.	n.a.	29%	8
4	Hsp70	70 kDa	86	1.1e-05	30%	16
5	Elp1	160 kDa	n.a.	n.a.	8%	11
6	Elp2	100 kDa	n.a.	n.a.	5%	4
7	Elp4-GFP	75 kDa	n.d.	n.d.	n.d.	n.d.
7 (1)	Elp4	48 kDa	64	0.0016	12%	6
7 (2)	GFP	27 kDa	n.a.	n.a.	50%	13
8	Elp5	45 kDa	n.a.	n.a.	20%	7
9	Elp6	38 kDa	72	0.00025	24%	10

Coverage = protein sequence coverage; Matched = matched peptides.

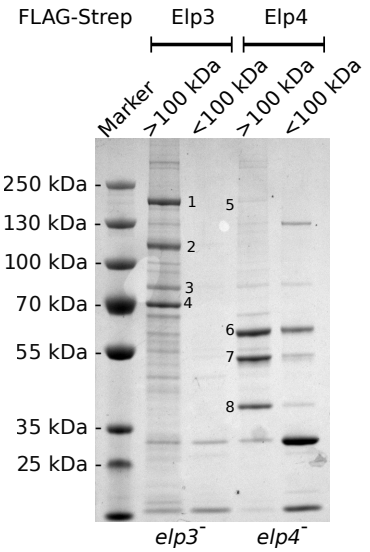

Figure 47: Gel picture of the Elp3 and Elp4 Strep pulldown, already shown and described in Figure 11. The individual protein bands indicated with numbers next to them were subjected to MALDI mass spectrometry analysis. The results are shown in the table below. Marker = PageRuler Plus Prestained Protein Ladder.

Table 21: MALDI mass spectrometric analysis strep pulldwown

Band	Protein	Mass	Score	Expect	coverage	matched
1	Elp1	160 kDa	n.d.	n.a.	19%	27
2	Elp2	100 kDa	102	2.6e-07	26%	21
3	Hsp70	70 kDa	141	3.3e-11	43%	17
4	Strep-Elp3	68 kDa	142	2.6e-11	43%	25
5	Elp1	160 kDa	n.a.	n.a.	11%	15
6	Strep-Elp4	52 kDa	n.a.	n.a.	6%	4
7	Elp5	45 kDa	n.d.	n.d.	n.d.	n.d.
8	Elp6	38 kDa	109	5.2e-08	20%	13

Coverage = protein sequence coverage; Matched = matched peptides.

A.1.3 *Cross complementation with yeast Elongator proteins in* D. discoideum

It was shown that hybrids of Elongator subunits of different species form a functional complex. One particular case is Elp3 were Elp1 of the same organism is needed to rescue the wild type phenotype [118]. *S. cereviseae* Elp1 and Elp3 were cloned into pDM expression plasmids and transformed in Ax2 wild type and different Elongator mutant backgrounds. The expression level were measured with the flow cytometer and Western blot. Expression of the yeast Elongator proteins was significantly weaker that any other tested protein expression. It is concluded that expression of yeast proteins in *D. discoideum* is too low for complementation of the wild type phenotype and that the yeast genes would need a codon adaptation to increase their expression level in *D. discoideum*.

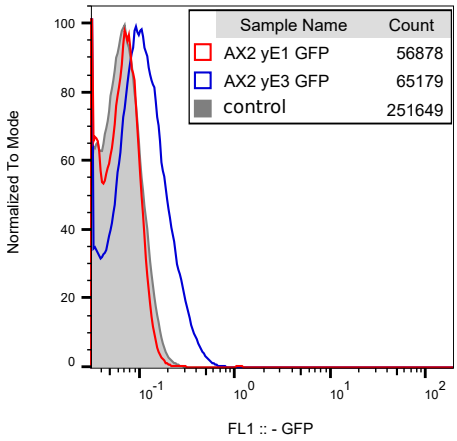

Figure 48: Flow cytometric detected expression profile of GFP-yElp1 (red) and GFP-yElp3 (blue) in *D. discoideum* (gray = nonfluorescent control cells). The counts are given in the picture. The expression of the yeast proteins is significant lower than their endogenous *Dictyostelium* counterparts.

A.1.4 *Recombinant Elps in E. coli*

Elp3 was the first Elongator gene that was cloned into the pET24a HM3C vector and expressed in *E. coli*. Expression of Elp3 at different temperatures (28° to 4°C) always led to formation of insoluble inclusion bodies (Figure 49).

The individual genes of the Elp456 subcomplex were cloned into pET24a HM3C vector and expressed in *E. coli*. The majority of all 3 proteins appeared to be soluble when expressed below 20°C (Figure 50). Attempts (*in vitro*) of complex formation and detection via native PAGE followed by Western blot failed (data not shown).

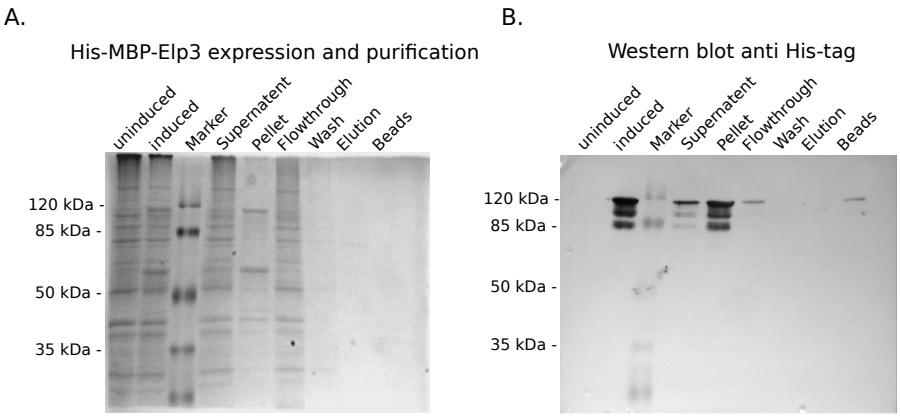

Figure 49: MBP-Elp3 expression and purification from *E. coli*. **A.** 12.5% SDS-PAGE analysis of different fractions collected in a MBP-Elp3 purification. **B.** Western blot image anti-His-MBP of the same fractions. Most of the MBP-Elp3 is found insoluble. Marker = Prestained Molecular Weight Marker.

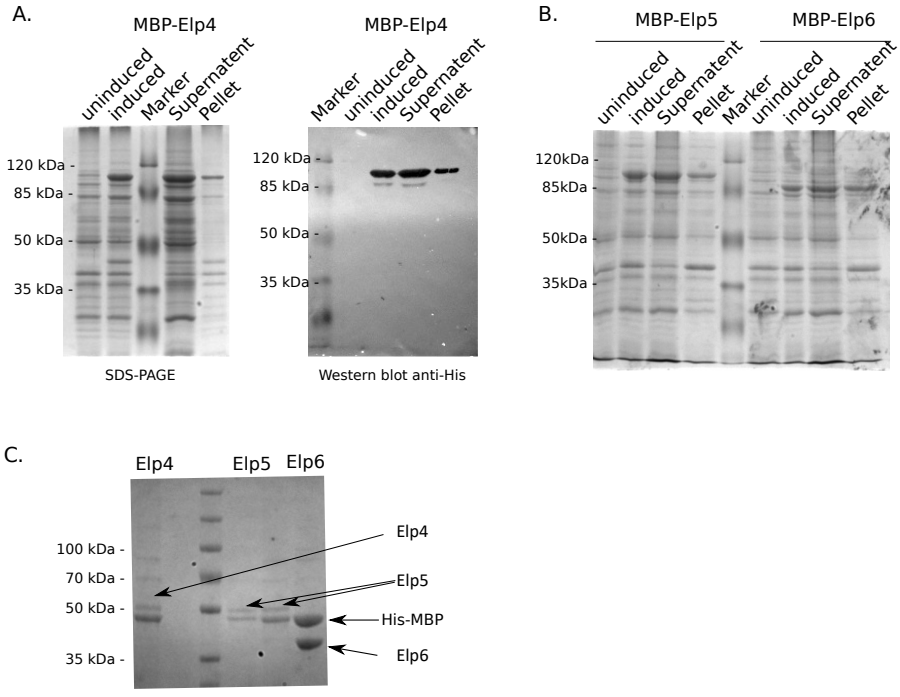

Figure 50: MBP-Elp4, MBP-Elp5 and MBP-Elp6 expression and purification from *E. coli*.
A. MBP-Elp4 purification (12.5% SDS-PAGE (left), Western blot anti-His (right). **B.** MBP-Elp5 and MBP-Elp6 expression and protein samples of the single purification steps shown on a image of a colloidal Coomassie stained 12.5% SDS PAGE. **C.** Running behavior of Elp4, Elp5, Elp6 and the cleaved off MBP-tag in a 12.5% SDS-PAGE. Marker = Prestained Molecular Weight Marker.

A.1.5 *Elp gene fusions with the 2A sequence*

In an approach to determine the stability of Elp3 and other Elongator proteins, the following construct were created: mRFP-Elp6-2A-Elp3/4-GFP and mRFP-Elp3/4-2A-Elp3/4-GFP. Expression level of genes 3´ of the 2A sequence was significantly reduce compared to the gene located 5´ of the 2A sequence. If Elp3 was located 5´ of the 2A sequence Elp4-GFP expression level would be similar to mRFP-Elp3 (Figure 51). It was concluded from those experiments that translation of large 2A constructs has its limitation. As an explanation one can postulate that the ribosomes - frequently - "falls off" the fusion mRNA after the 2A sequence and cannot complete the translation of the second amino acid chain.

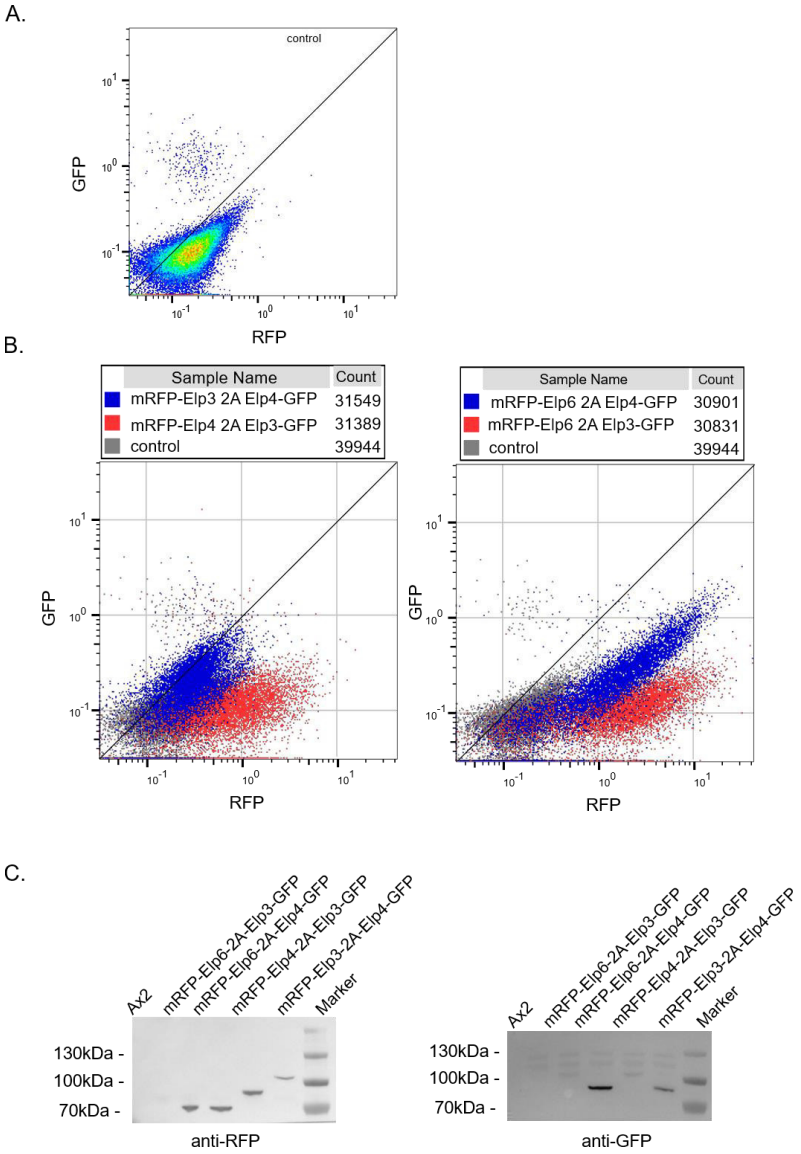

Figure 51: Elongator 2A fusion construct expression

A. 2D scatter blot of the fluorescence signal received from the fluorescence negative control strain (channel corresponding to GFP (y-axis) and RFP (x-axis)). The control strain shows a disproportion indicating that the channels were not normalizes properly to each other. Consequently the cells appear more red than green. **B.** left: 2D scatter blot of strains expressing mRFP-Elp3-2A-Elp4-GFP (blue) and mRFP-Elp4-2A-Elp3-GFP (red). right: 2D scatter blot of strains expressing mRFP-Elp6-2A-Elp4-GFP (blue) and mRFP-Elp6-2A-Elp3-GFP (red). **C.** Western blot images against RFP (left) and GFP (right) from the strains used in A and B. Marker = PageRuler Plus Prestained Protein Ladder.

A.2 ADDITIONAL DATA AND EXPERIMENTAL DATA ON ELONGATOR DEPENDENT TRNA MODIFICATION

A.2.1 *tRNA modification analysis by Stefanie Kellner*

Total RNA extracts from different *D. discoideum* strains were send to the research group of Stefanie Kellner at the LMU Munich. There, the total tRNA fraction was seperated from the total RNA via SEC. The total tRNA fraction was digested to the nucleosides with Benzonase and alkaline phosphatase in the presence of antioxidants and deaminase inhibitors. 15N-dA was added as internal standard and 100 ng of digested tRNAs were subjected to separation on a Phenomenex Fusion Rp column. The effluent was analyzed on an Agilent 6490 Triple Quadrupol mass spec.

The following Figures were generated as shown by Stefanie Kellner . Figures 52 and 53 show the first analysis and Figures 54 and 55 show the second analysis done by her on the RNA modifications.

In the Figures 52 to 55, the following abbreviation are used:
WT = Ax2 wt,
dE1 = *elp1*$^{-}$,
dE2 = *elp2*$^{-}$,
dE31 = *elp3*$^{-}$ clone 1,
dE3 E3 = *elp3*$^{-}$ clone 1 pDM317 GFP-Elp3,
dE3 SAM = *elp3*$^{-}$ clone 1 pDM317 GFP-Elp3mutSAM,
dE3 HAT = *elp3*$^{-}$ clone 1 pDM317 GFP-Elp3mutHAT,
dE3 15 = *elp3*$^{-}$ clone 15,
dE3 dCTU = *elp3*$^{-}$*ctu1*$^{-}$,
dCTU = *ctu1*$^{-}$,
dE4 = *elp4*$^{-}$,
dE4 E4 = *elp4*$^{-}$ pDM317 GFP-Elp4,
dTrm9 = *trm9*$^{-}$,
dTQ CUG = tQ^{CUG-},
dE5 = *elp5*$^{-}$

Absolute quantification of wobble uridines
Wobble uridine modifications were quantified by normalizing to the amount of injected tRNA. The graph shows how many tRNAs are modified in %. The numbers are given in the table. In yellow, mcm5s2U and mcm5U are highlighted, since they were above the LOQ in the wildtype samples. These numbers are highly trustworthy. Since cm5U was just around the LOQ, it is highlighted in grey. Cm5s2U, ncm5s2U and s2U were below the LOQ in wildtype.

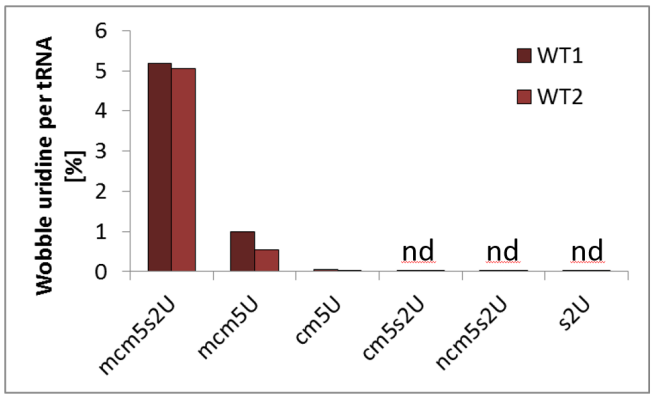

	WT1	WT2
mcm5s2U	5,184789	5,050578
mcm5U	1,000912	0,551153
cm5U	0,056854	0,0078
cm5s2U	0,005083	0,000659
ncm5s2U	0,000355	4,6E-05
s2U	0,000152	1,97E-05

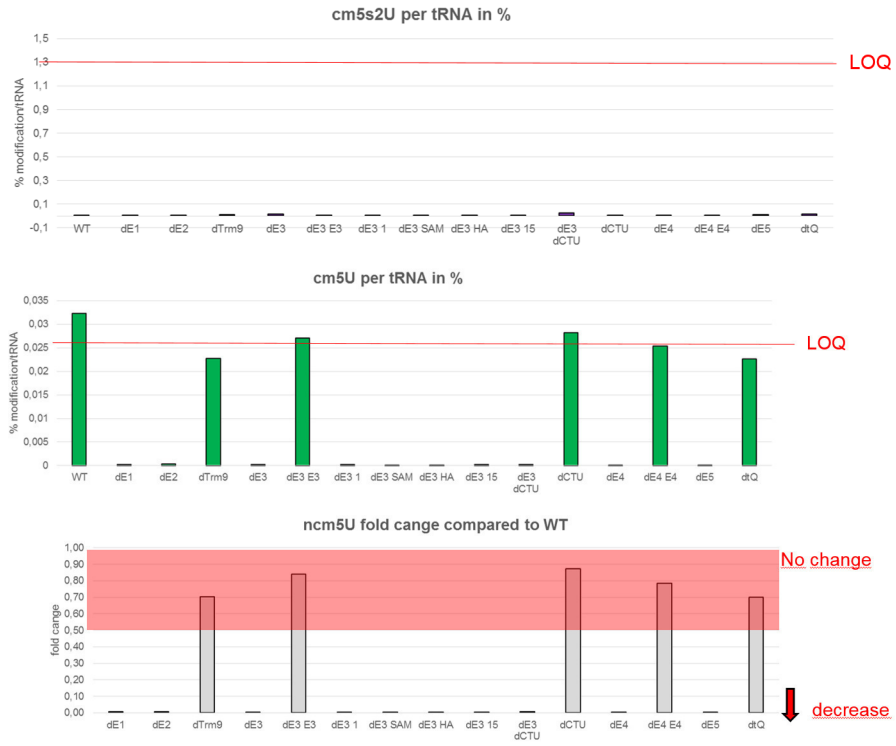

Figure 52: tRNA modifications 1.1
Data and Figure generated by Stefanie Kellner, LMU Munich. For abbreviations see page 125.

* verification needed – samples might have been switched

Figure 53: tRNA modifications 1.2

Data and Figure generated by Stefanie Kellner, LMU Munich. For abbreviations see page 125.

Sensitivity
The limit of quantification (LOQ) for injection of 100 ng tRNA is:

	modification per tRNA [%]	LOQ in fmol	LOD in fmol
cm5s2U	1,318	100	10
cm5U	0,26	2	1
mcm5s2U	0,26	10	1
mcm5U	0,26	10	1
ncm5s2U	0,26	10	10
s2U	0,052	2	10

LOQ is not indicated in the following graphs, as all samples are well above the LOQ

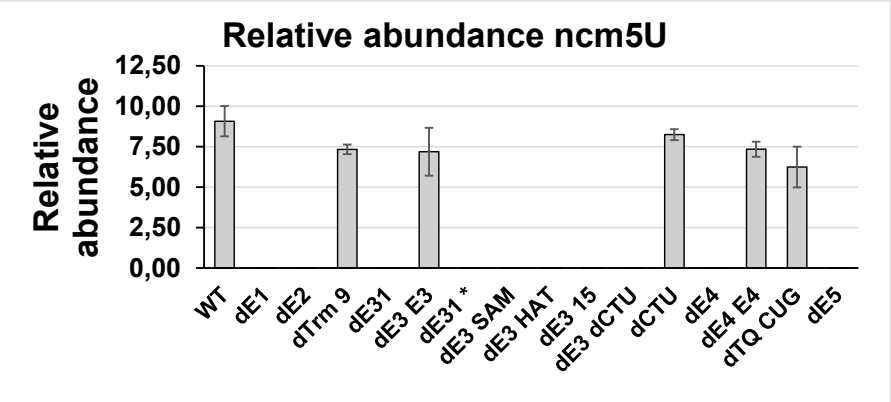

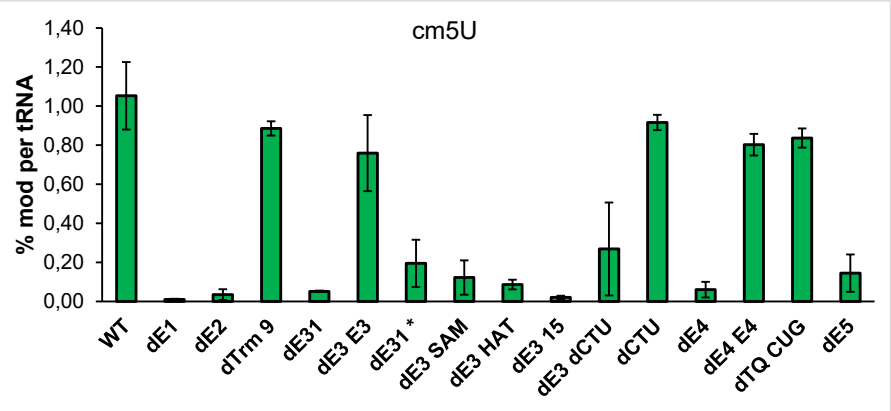

Figure 54: tRNA modifications 2.1
Data and Figure generated by Stefanie Kellner, LMU Munich. For abbreviations see page 125.

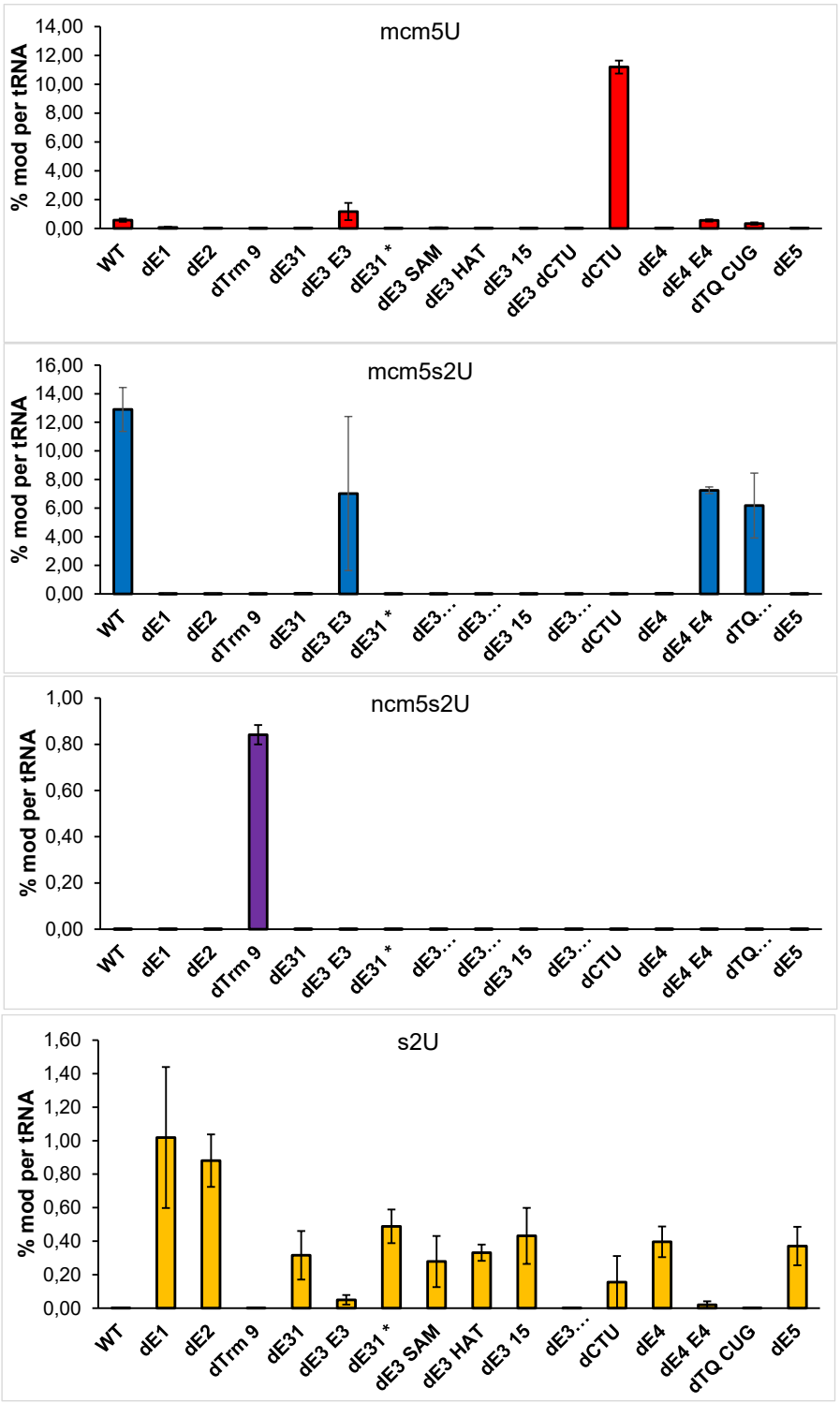

Figure 55: tRNA modifications 2.2

Data and Figure generated by Stefanie Kellner, LMU Munich. For abbreviations see page 125.

A.2.2 *APM Northern blots to determine if ectopically overexpressed Elongator proteins can rescue the s^2U modification*

Figure 56 and Figure 57 show APM Northern blots that were performed to (indirectly) determine if the ectopically expressed Elongator proteins are functional and are able to rescue the wild type thiolation in the individual mutant backgrounds. Strep-Elp1 as well as GFP-Elp2 and GFP-Elp4 seem to rescue the wild type s^2 thiolation phenotype (to some extent). tRNAs from *elp4*⁻ Elp4-GFP show the same thiolation level as from the *elp4*⁻.[1]

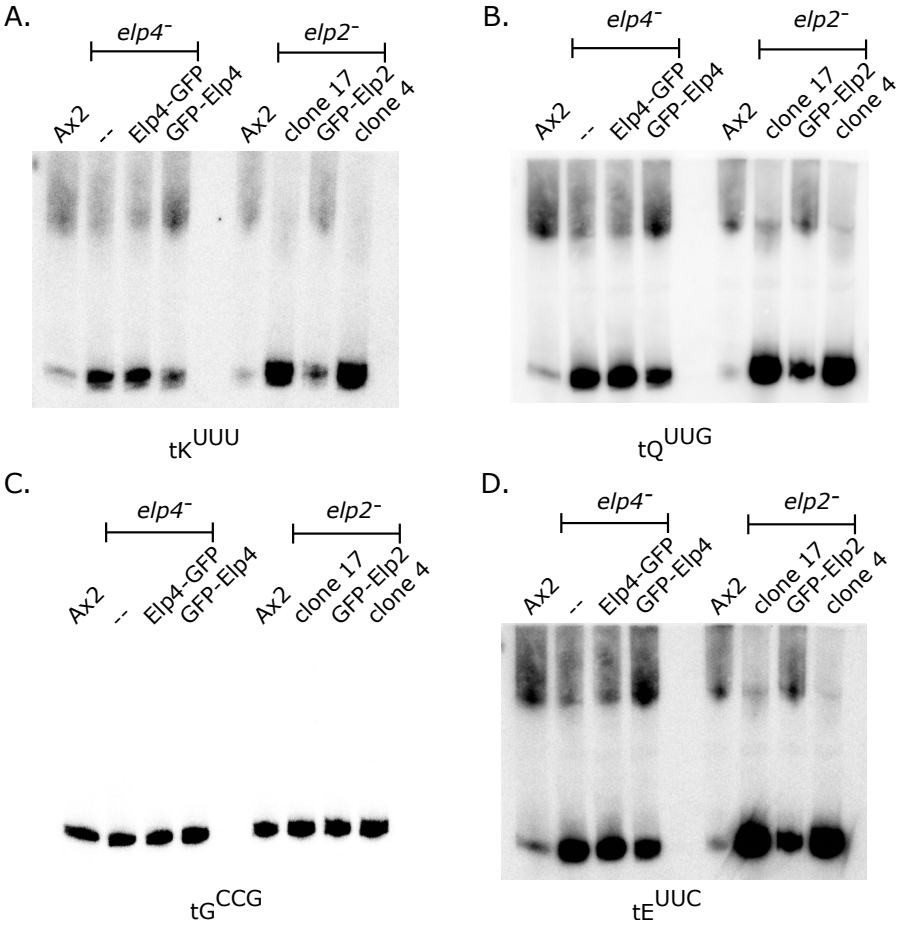

Figure 56: APM Northern blot against tRNAs from Ax2 *elp4*⁻ and *elp2*⁻ strain with and without rescue constructs. Northern blot probed for tK^{UUU} (top left), tQ^{UUG} (top right), tG^{CCG} (bottom left) and tE^{UUC} (bottom right).

1 The growth profile of *elp4*⁻ pDM323 Elp4-GFP and *elp4*⁻ are also similar (Figure 61). Both observations imply that the C-terminal GFP fusion protein cannot rescue the Elongator function. Interestingly, GFP trap pulldowns show that Elp4-GFP interacts with Elp5 and Elp6 as well as Elp1 and Elp2.

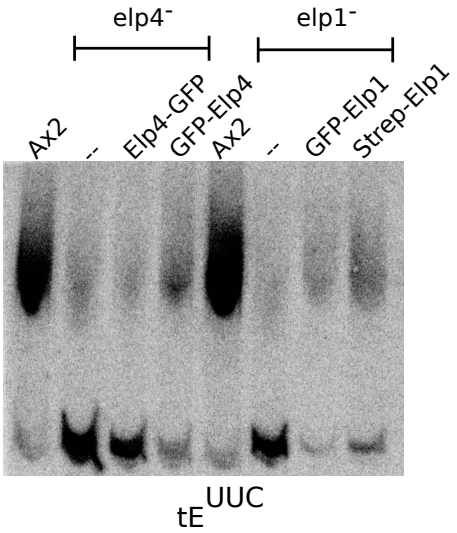

Figure 57: APM Northern blot against tE^{UUC} from Ax2, *elp4*⁻ and *elp1*⁻ strains with and without rescue constructs.

A.2.3 *Codon usage and tRNA gene*

		S. cerevisiae		*D. discoideum*				*S. cerevisiae*		*D. discoideum*	
Amino acid	Codon	Codon usage	tRNA genes	Codon usage	tRNA gene	**Amino acid**	**Codon**	Codon usage	tRNA genes	Codon usage	tRNA genes
Val (V)	GUU	22.1	14	23.7	22	Ala (A)	GCU	21.2	11	9.9	15
	GUC	11.8	0	3.2	0		GCC	12.6	0	3.2	0
	GUA	11.8	2	13.3	6		GCA	16.2	5	16.4	0
	GUG	10.8	2	2.3	1		GCG	6.2	0	0.6	0
Leu (L)	CUU	12.3	0	9.5	11	Pro (P)	CCU	13.5	2	5.9	1
	CUC	5.4	1	3.3	0		CCC	6.8	0	1.2	0
	CUA	13.4	3	5.2	3		CCA	18.3	10	31.9	15
	CUG	10.5	0	0.4	1		CCG	5.3	0	0.5	0
Leu (L)	UUA	26.2	7	56.8	18	Ser (S)	UCU	23.5	11	15.4	9
	UUG	27.2	10	10.6	4		UCC	14.2	0	3.9	0
Phe (F)	UUU	26.1	0	33.9	0		UCA	18.7	3	50.2	15
	UUC	18.4	10	13.6	3		UCG	8.6	1	2.3	1
Ile (I)	AUU	30.1	13	51.9	17	Thr (T)	ACU	20.3	11	20.7	16
	AUC	17.2	0	11	0		ACC	12.7	0	7.7	0
	AUA	17.8	2	21.8	4		ACA	17.8	4	30.3	6
Met(M)	AUG	20.9	4+5	15.6	14		ACG	8	1	1	1
Asp (D)	GAU	37.6	0	47.6	0	Gly (G)	GGU	23.9	0	32.3	0
	GAC	20.2	15	4.5	22		GGC	9.8	16	2.1	18
Glu (E)	GAA	45.6	14	49.1	19		GGA	10.9	3	9	5
	GAG	19.2	2	8.8	3		GGG	6	2	1	0
Tyr (Y)	UAU	18.8	0	30.4	0	Cys (C)	UGU	8.1	0	12.8	0
	UAC	14.8	8	5.2	12		UGC	4.8	4	1.5	8
Stopp	UAA		0		0	Stopp	UGA		0		0
Stopp	UAG		0		0	Trp (W)	UGG	10.4	6	7.3	7
Asn (N)	AAU	35.7	0	101.9	0	Ser (S)	AGU	14.2	0	22.4	0
	AAC	24.8	10	11.8	18		AGC	9.8	4	2.5	12
Lys (K)	AAA	41.9	7	65.1	22	Arg (R)	AGA	21.3	11	19.9	10
	AAG	30.8	14	11.5	10		AGG	9.2	1	1.4	1
His (H)	CAU	13.6	0	15	0	Arg (R)	CGU	6.4	6	5.7	6
	CAC	7.8	7	2.7	9		CGC	2.6	0	0.1	0
Gln (Q)	CAA	27.3	9	48.6	13		CGA	3	0	0.5	1
	CAG	12.1	1	1.9	1		CGG	1.7	1	0.1	0

Figure 58: Codon usage and tRNA genes of *S. cerevisiae* and *D. discoideum*

The particular codon usages are given in number of appearances per 1000 codons. Yellow and red boxes indicate codons with corresponding Elongator dependent modified tRNA genes (yellow = ncm^5U and mcm^5U; red =mcm^5s^2U). Blue boxes indicate single copy tRNA genes in *D. discoideum*.

A.2.4 *PolyQ-GFP expression in mutant strains*

Figure 59 A and C show the flow cytometric detected expression profile of GFP and Q103-GFP in Elongator deficient strains *elp1*$^{-}$, *elp3*$^{-}$ and *elp4*$^{-}$ (and Q103-GFP in *elp5*$^{-}$). GFP expression varies between the different Elongator mutants (A). It is likely that these large differences are artifacts of the high expression level of GFP. When the Q103 leader was fused to GFP the overall expression was reduced and the expression differences between the Elongator mutants was reduced (C). The *elp1*$^{-}$ strain showed the lowest expression of any Elongator mutant, independent of the expressed protein. Figure 59 B shows the flow cytometric detected expression profile of Q103-GFP+tQ^{CUG} overexpression compared to the Q103-GFP in the Ax2 background. Q103-GFP expression in Ax2 with simultaneous tQ^{CUG} overexpression is lower than in the strain without tRNA overexpression.

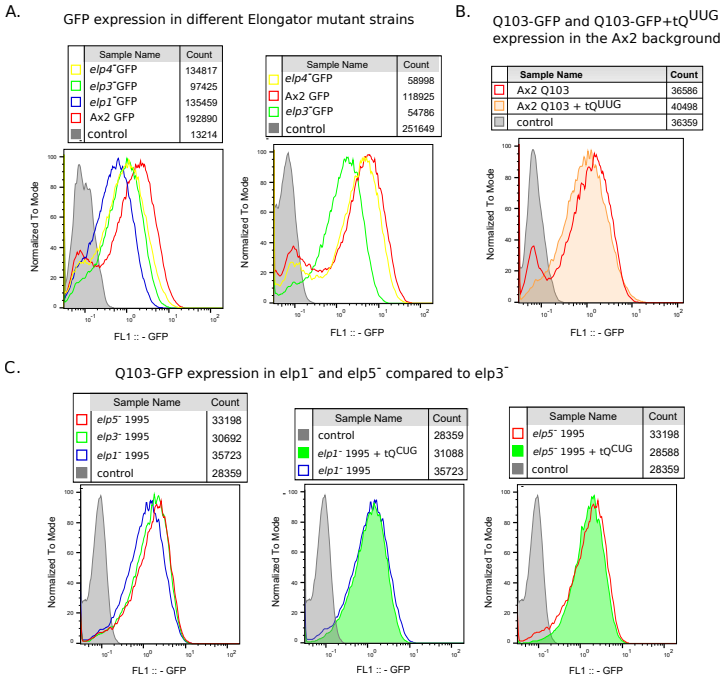

Figure 59: Flow cytometric detected expression profile of GFP and Q103-GFP in different strains. **A.** GFP expression level in different Elongator mutant backgrounds differs. High variations of expression level are detectable between individual experiments (comparison left to right). **B.** Comparison of Q103-GFP and Q103-GFP+tQ^{CUG} overexpression in the Ax2 background. Q103-GFP expression in the strain with simultaneous tQ^{CUG} overexpression is lower than in the strain without tRNA overexpression. **C.** Q103-GFP expression in different Elongator mutant is much more homogenous than GFP alone. As with all the other tested modification deficient strains tQ^{CUG} overexpression has no influence on the expression of Q103. All samples >=28000 counts (except for control in A left).

A.2.4.1 *The umber stop codon experiment*

Eukaryotic organisms feature 3 stop codons (TAA, TGA and TAG) for which no tRNA is decoding. Yet, several eukaryotic, bacterial and archeal organisms feature the selenocysteine proteome [142]. Selenocysteine is decoded by a posttranscriptionally modified tRNA with the anticodon UCA that can decode the stop codon TGA [143]. In order to achieve seleno cysteine insertion, a special sequence in front of the TGA codon is needed [144]. The selenocysteine insertion sequence (SECIS) is about 60 nt long and forms a hairpin. This hairpin is recognized by special Elongation factors (SelB), that is also binding to the selenocysteine tRNA [145]. In the process translation occurs over the TGA codon and goes on till another stop codon (TAA, TAG) is reached.

The stop codons TAA and TGA both feature a A at *wobble* position of the codon. The theoretical corresponding tRNAs that decode for these codons, would most likely carry an Elongator dependent anticodon modification of ncm^5U for UCA and mcm^5s^2U for UUA. 90% of the stop codons in *D. discoideum* read TAA, 5% TGA and 5% TAG [70]. The generation of a suppressor tRNA decoding the TAA stop codon was ruled out, since the majority of genes rely on TAA as a stop codon[2]. A synthetic suppressor tRNA was designed by altering the tryptophane tRNA tW^{CAA} sequence in the first position of the anticodon changing the cytosine to uracil (Figure 60 A). The suppressor tRNA should be able to read over the TGA stop codon and inserting a tryptophane tRNA at the stop codon. A plasmid carrying a fusion expression construct consisting of mRFP-TGA-GFP was expressed together with the suppressor tRNA to measure the capability of the decoding of the TGA stop codon (Figure 60 B). Fluorescence measurements were performed with a flow cytometer. Figure 60 C shows the result of these experiments. Neither in the control without suppressor tRNA nor in the strain with suppressor tRNA a GFP signal could be detected. Strains expression the suppressor tRNA grew significantly slower (data not shown). This led to the subjective impression that the suppressor tRNA is in general working. It is very likely that the non-functionality of the fusion construct is due to an inadequate experimental design, since no SECIS sequence was placed between the mRFP and the TGA stop. Figure 60 D shows the flow cytometric fluorescence profile of an RFP-GFP fusion as a control that the fusion construct itself is functional.

2 successful use of an amber stop codon suppression experiment in *D. discoideum* [146]

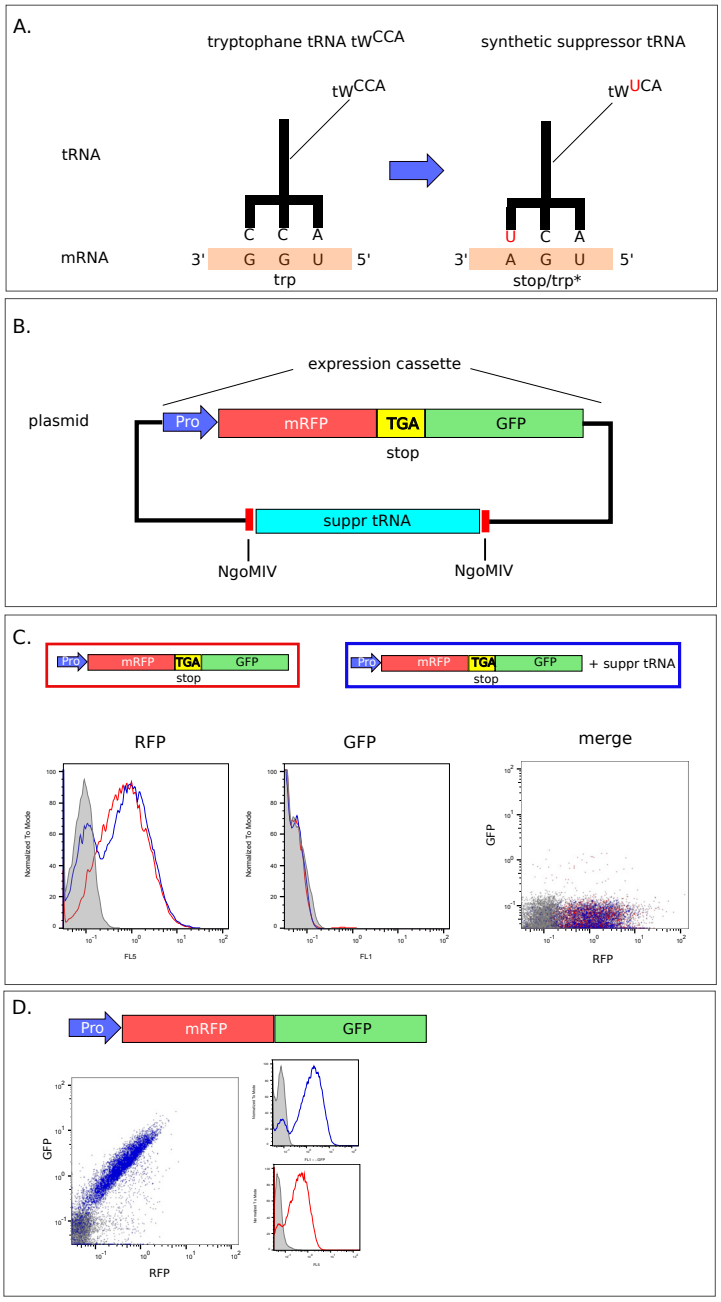

Figure 60: The Umber stop codon experiment. **A.** Sketch of the tryptophane tRNA tW^{CCA} and its designated codon GGU. The tRNA gene was synthesized (without intron) and altered in the anticodon position 34 to feature a Uracil. The synthetic tRNA should be able to decode for the stop codon TGA. **B.** Sketch of a vector construct used to determine the decoding capability of the synthetic tRNA for the TGA stop codon. The TGA stop codon was placed in between the mRFP gene and the GFP gene. The suppressor tRNA was placed on the same vector to ensure equal expression in all cells. **C.** Flow cytometric analysis of vector construct with (blue = 36120 counts) and without suppressor tRNA (red = 21087 counts) in the Ax2 background was performed. No GFP expression could be detected. Gray = nonfluorescent control cells (7579 counts) **D.** Flow cytometric analysis of the vector construct without TGA stop codon (38147 counts)(Gray = nonfluorescent control cells (17518 counts). This experiment served as a control for the experiment shown in C.

A.2.5 *Growth and Development*

Elongator deficient strains display a slightly reduced cell division rate (Figure 61 A [87] [137]). Caffeine an heatshock[3] seem to have minor effects on the *elp4*$^{-}$ strain and the cell division rate increases in the same proportion as the cell divion rate of Ax2. The *elp3*$^{-}$ (clone Pri I) strain showed an increased stress sensitivity. A second, independently generated *elp3*$^{-}$ strain (clone 15) displays a cell division rate similar to *elp4*$^{-}$ [137].

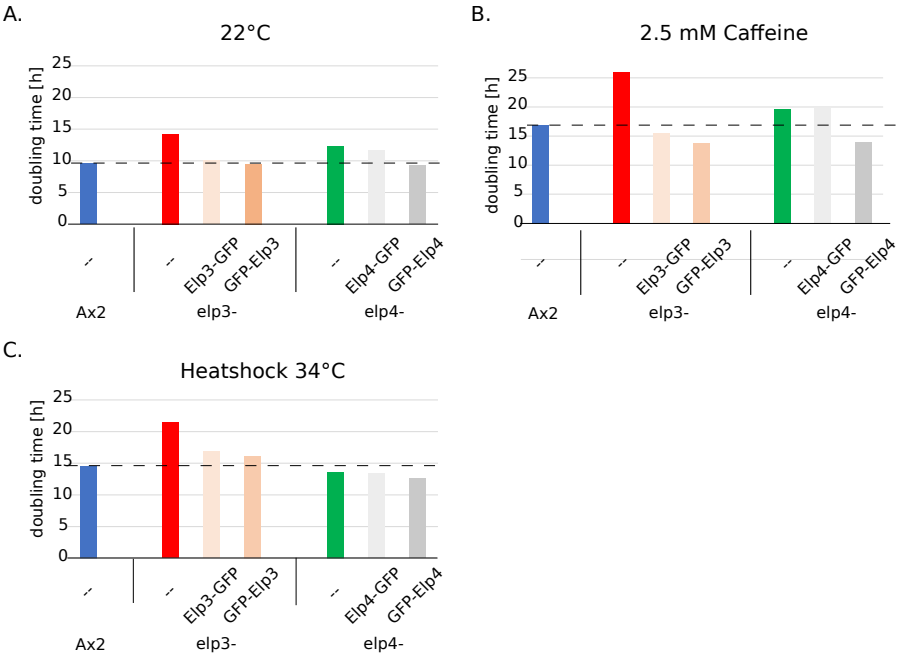

Figure 61: Doubling time of Elongator mutants compared to Ax2
These doubling times represent only estimates of the growth rate. All cells division rates were achieved by cell concentration measurements for a period of 3 days. **A.** Doubling time of the different strains under normal growth conditions. **B.** Doubling time of the different strains under caffeine stress. **C.** Doubling time of the different strains after a heatshock of 34°C for one 1h was applied.

3 heatshock was performed at 34°C for 1h. The cells were afterwards grown at 22°C.

Comparison of the Elongator mutant strains *elp1*$^{-}$, *elp3*$^{-}$ and *elp4*$^{-}$ to Ax2 revealed a delayed early development. This might be explained by the reduced cell division rate since the cells may undergo 1 cell devisions before entering the stages of early development. No differences in late development are detectable. There were no differences in the spore head formation to Ax2 observed (Figure 62).

Links to the timelaps videos of *elp1*$^{-}$, *elp3*$^{-}$ and *elp4*$^{-}$ development compared the Ax2 wild type:

https://goo.gl/SgeJRL

(videos have to be saved to play)

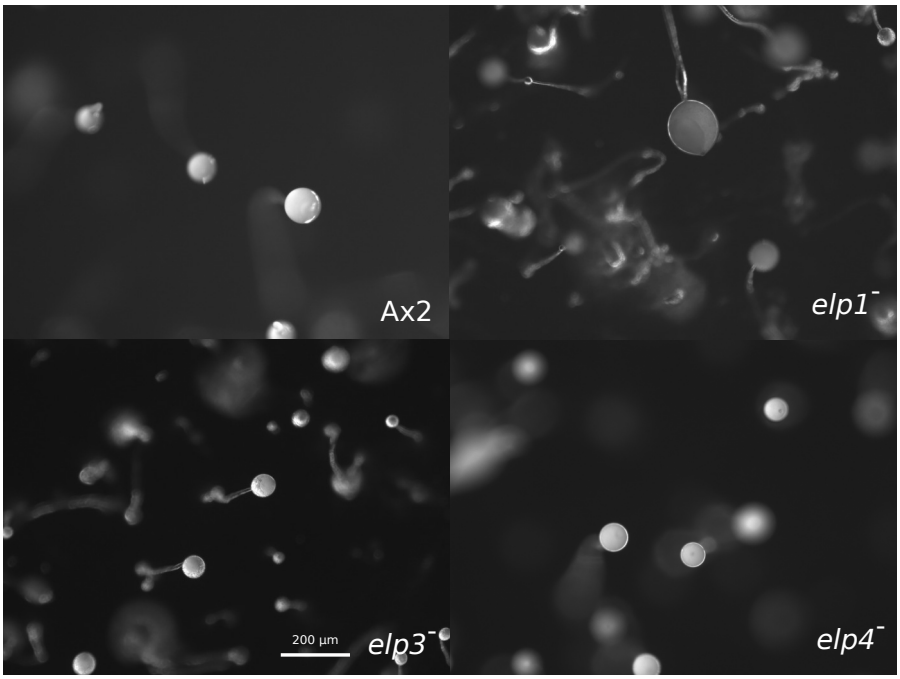

Figure 62: Images of spore heads from Ax2, *elp1*$^{-}$, *elp3*$^{-}$ and *elp4*$^{-}$ after 48h of development.
The Elongator mutants display normal spore heads formation.

A.3 γ-TOXIN

Figure 63 shows individual steps of the recombinant γ-toxin expression and purification from *E. coli*.

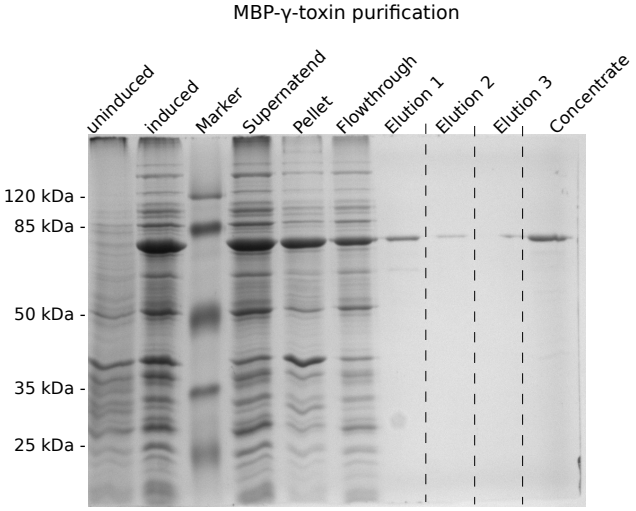

Figure 63: Purification of recombinant γ-toxin produced in *E. coli*.
Image of a colloidal Coomassie stained 12% SDS-PAGE with protein samples of the single purification steps. Purficiation of the recombinant γ-toxin via its affinity tag (MBP) was performed over amylose beads and eluted with Maltose. The 3 elution fractions (1 mL each) were combined and concentrated via differential centrifugation with Amicons 30 kDa MWCO. Marker = Prestained Molecular Weight Marker.

A.4 SUPPLEMENTARY MATERIALS

A.4.1 *Plasmids*

The following figures give an overview of the expression plasmids generated and/or used within this thesis. Additional plasmids that were used can be found in the Diplom Thesis of Sina Gronemann (pDneo2a Elp1 Strep; [86]) and the PhD thesis of Balachandar Ammappatti (pDM317 Elp2; [87]) and Janis Kruse (pDneo2A DrnA-GFP and pDM304FS-DrnA; [82]).

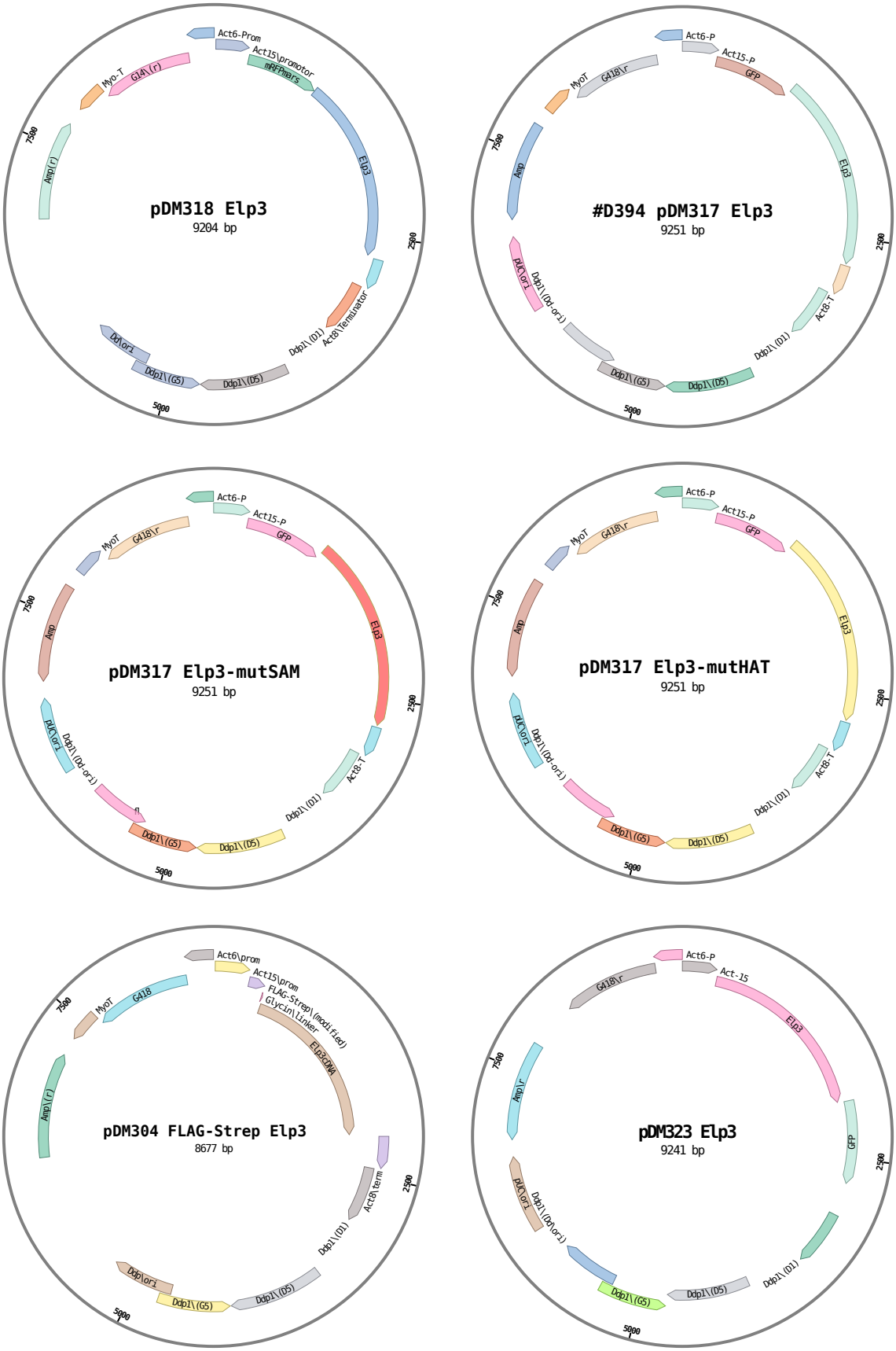

Figure 64: Elp3 expression plasmids for *D. discoideum*. The cDNA of *elp3* was cloned into the individual pDM plasmids via the *Bgl*II and *Spe*I restriction sites.

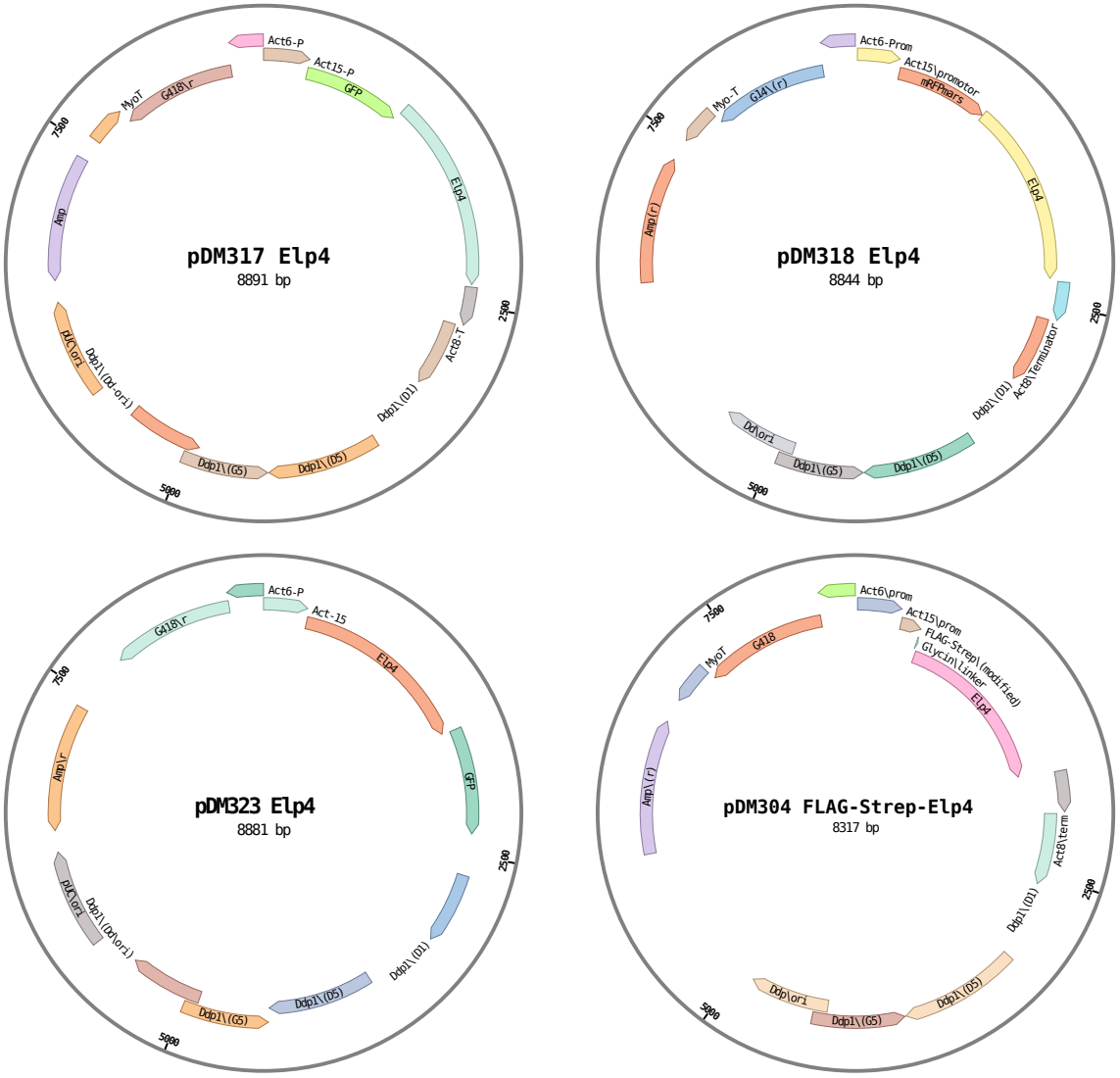

Figure 65: Elp4 expression plasmids for *D. discoideum*. The coding sequence of *elp4* was cloned into the individual pDM plasmids via the *Bgl*II and *Spe*I restriction sites.

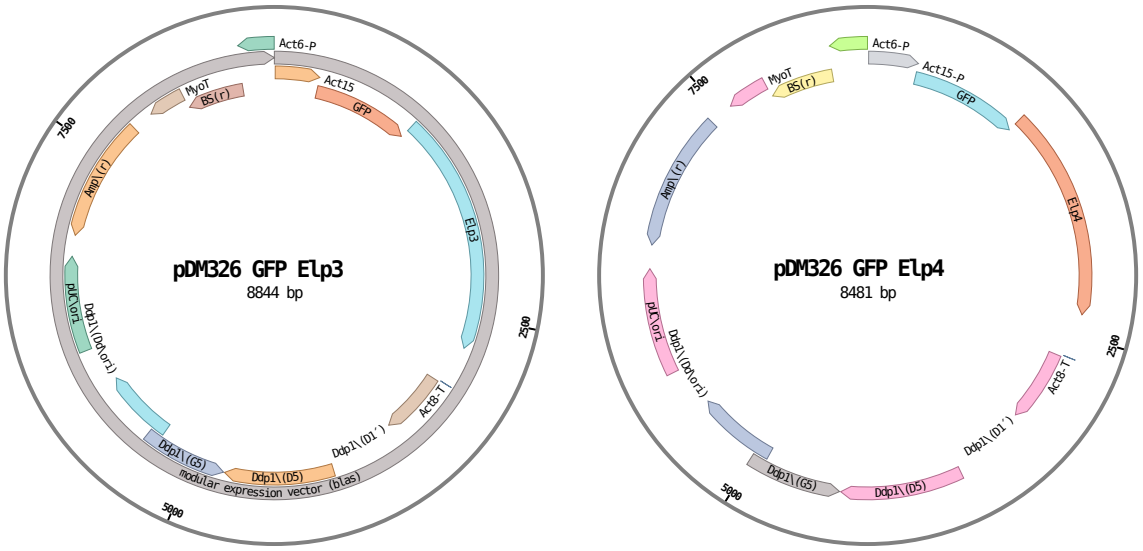

Figure 66: Expression plasmids with BS(r) for *D. discoideum*. The coding sequence of*elp3* and *elp4*, respectively, was cloned into the individual pDM326 via the *Bgl*II and *Spe*I restriction sites.

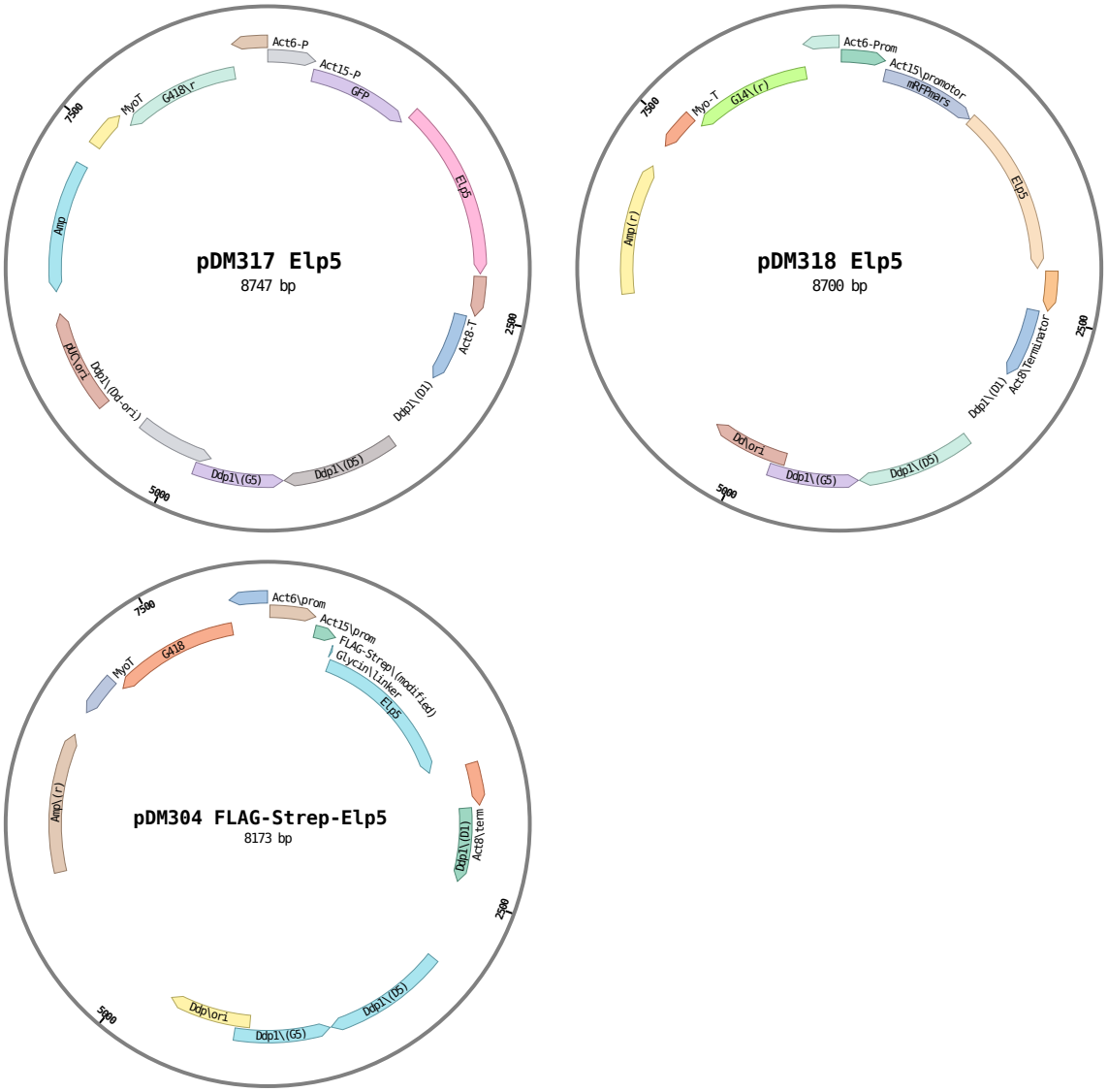

Figure 67: Elp5 expression plasmids for *D. discoideum*. The cDNA of *elp5* was cloned into the individual pDM plasmids via the *Bgl*II and *Spe*I restriction sites.

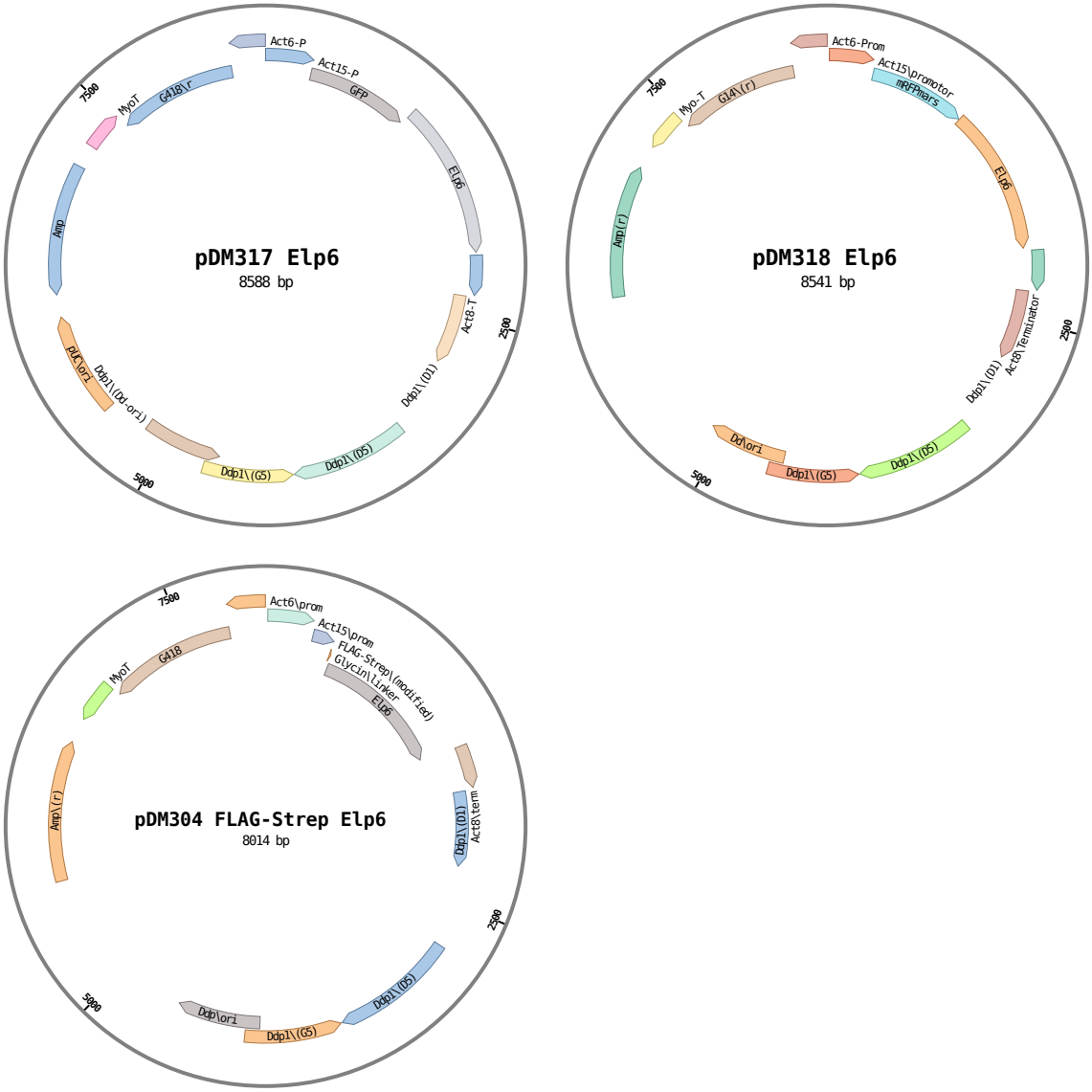

Figure 68: Elp6 expression plasmids for *D. discoideum*. The cDNA of *elp6* was cloned into the individual pDM plasmids via the *Bgl*II and *Spe*I restriction sites.

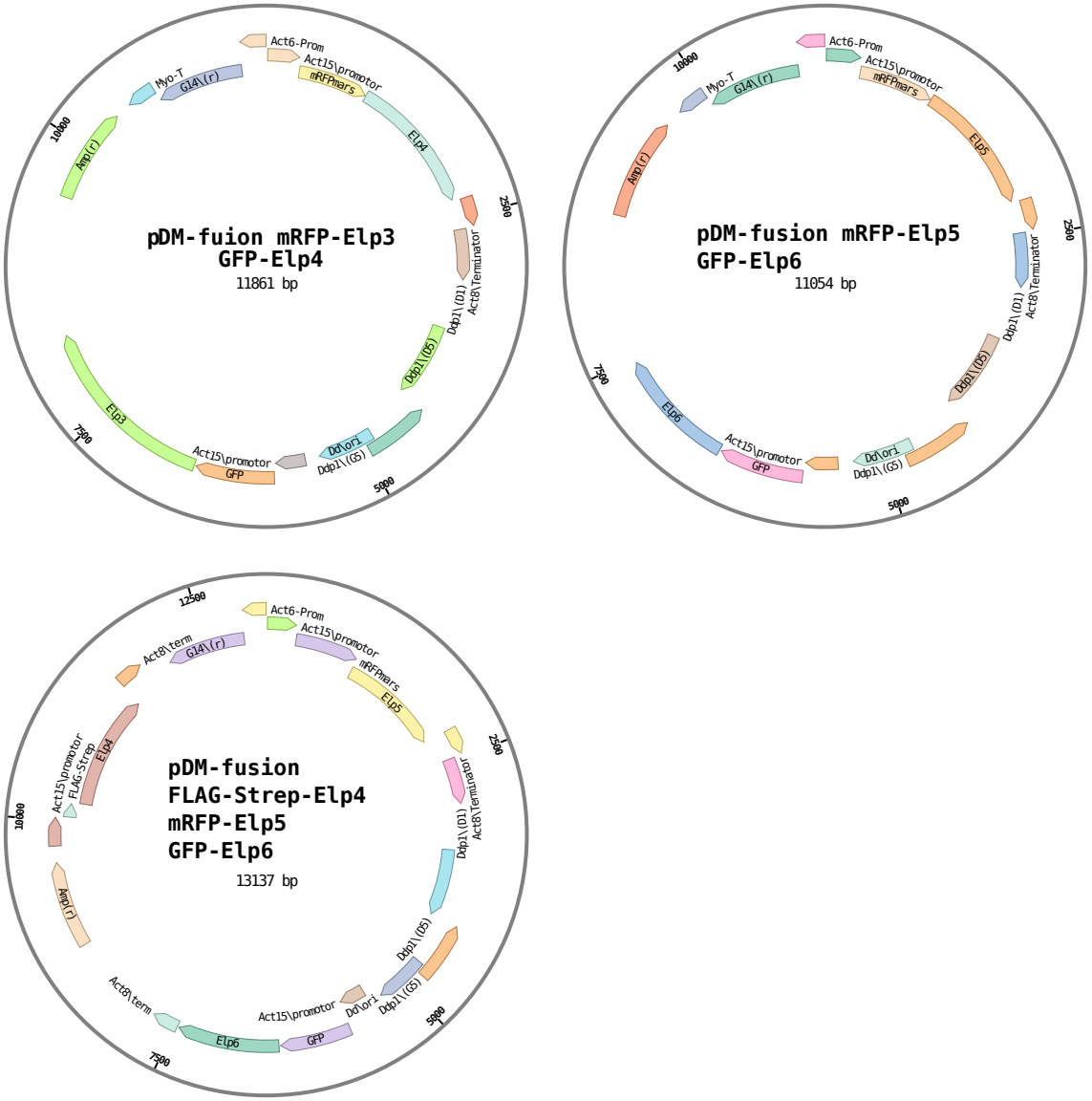

Figure 69: pDM-fusion plasmids for expression of several proteins in *D. discoideum*. Therefore the expression cassette of the pDM317 constructs with a given GOI was amplified with specific primers that included a *Ngo*MIV restriction site and cloned via this site into a pDM318 Plasmid containing another Elongator gene. (Both expression cassettes feature an actin 15 promotor.)

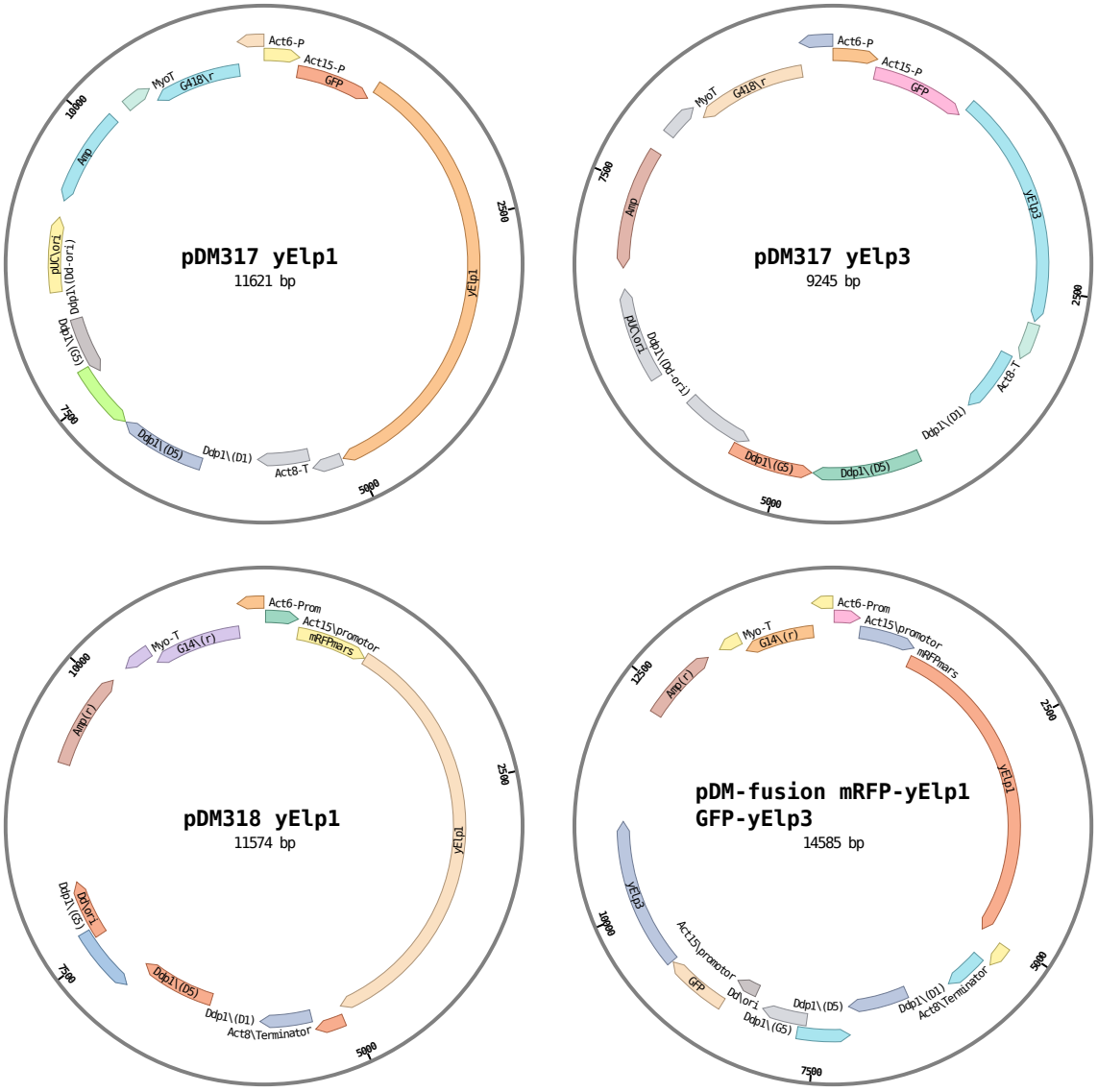

Figure 70: Yeast Elongator proteins on expression plasmids for *D. discoideum*. The *S. cerevisiae* Elp1 and Elp3 genes were provided by the reserch group of Raphael Schaffrath. The genes were amplified from yeast expression vectors with specific primers that included *Bgl*II site (fwd primer) and a *Spe*I site (reverse primer). The genes were then cloned via those restriction sites into the individual pDM plasmids. The fusion pDM plasmid was accomplished by amplification of the pDM317 yElp3 expression cassette and directed cloning into the *Ngo*MIV restriction site into the pDM318 yElp1 plasmid.

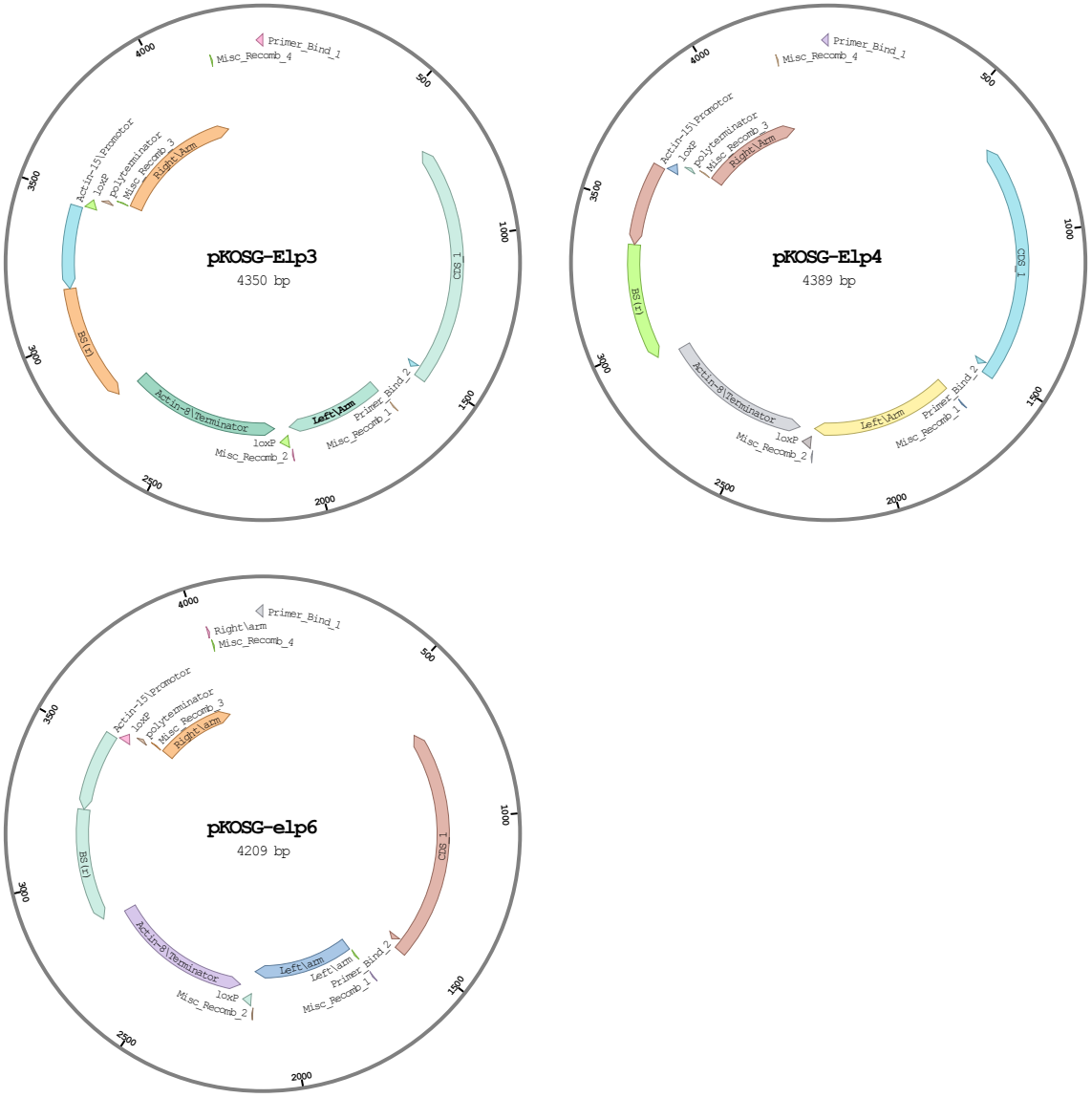

Figure 71: pKOSG vectors for knockout generation in *D. discoideum* 1. Primer designs with specific overhangs and cloning procedure were done according to [93]. All constructs were designed with additional *Spe*I restriction sites. These restriction sites was used to remove the vector backbone befor transfection into *D. discoideum* cell lines.

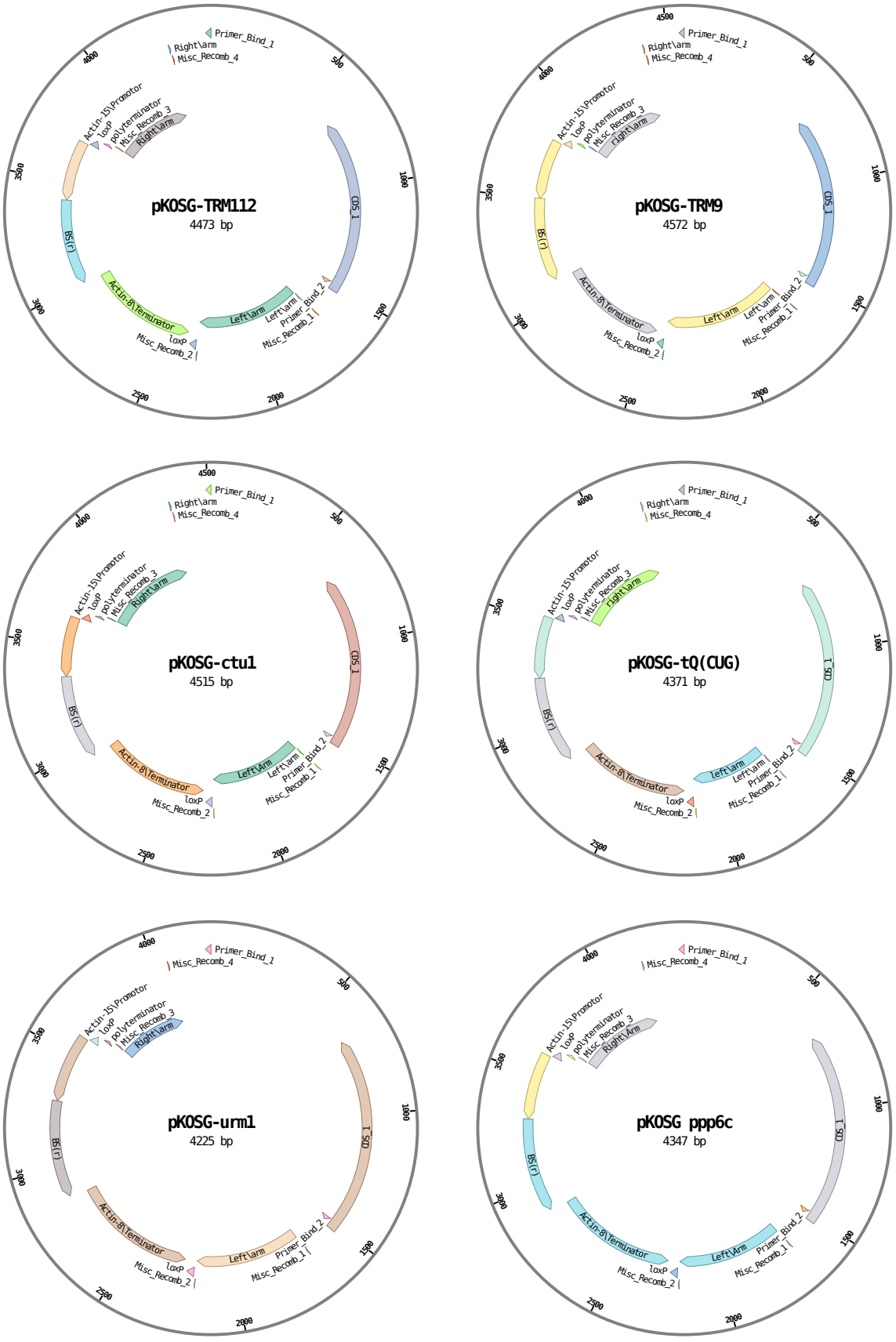

Figure 72: pKOSG vectors for knockout generation in *D. discoideum* 2. Primer designs with specific overhangs and cloning procedure were done according to [93]. All constructs were designed with additional *Spe*I restriction sites. These restriction sites was used to remove the vector backbone befor transfection into *D. discoideum* cell lines.

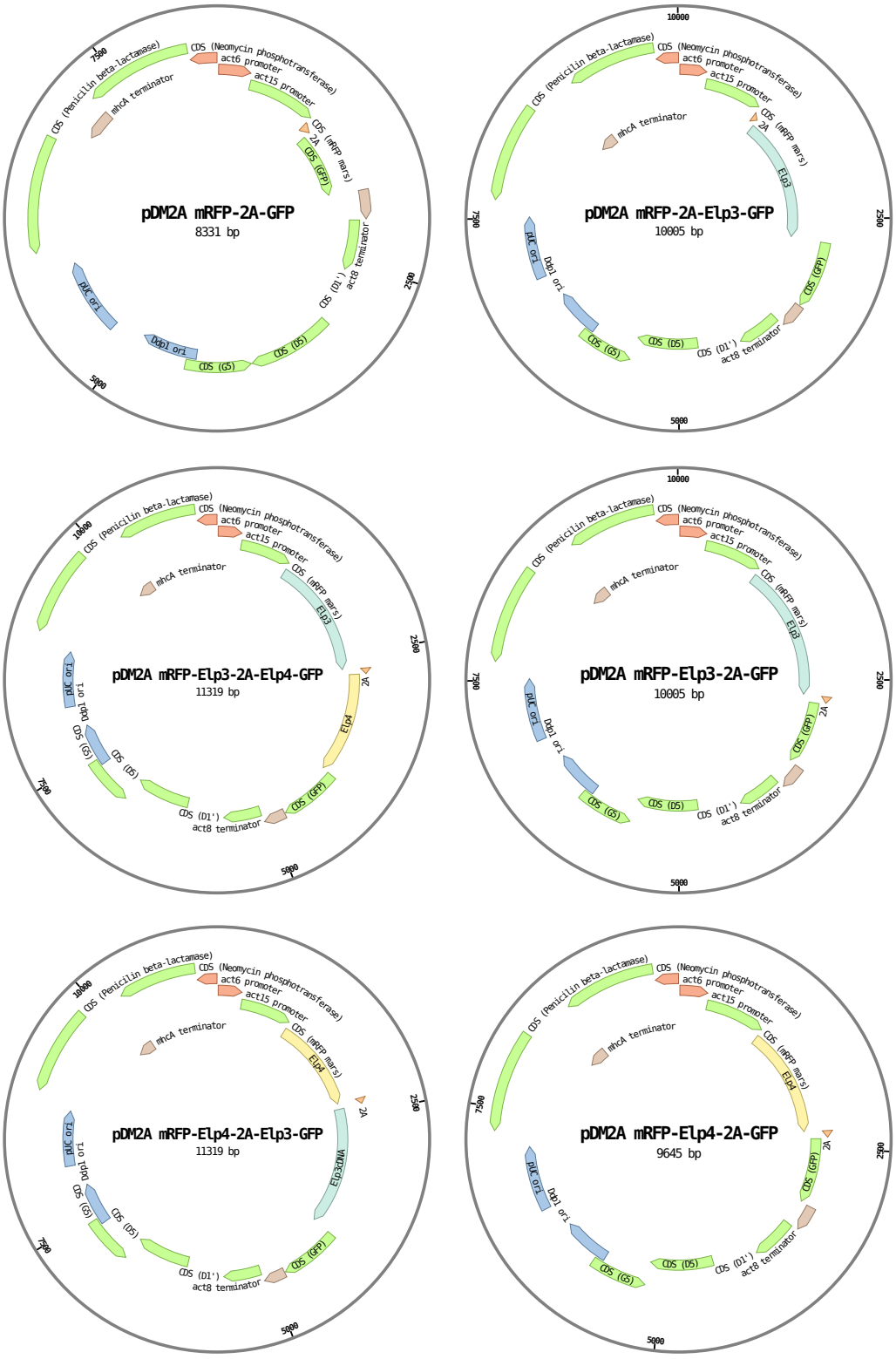

Figure 73: pDM2A plasmids for *D. discoideum* 1. The terminator sequence of the expression cassette of the pDM318 was replaced by the GFP gene and terminator sequence of pDM323 (via *Spe*I and *Hind*III directed cloning). The 2A sequence was produced synthetically (oligo hybridization) and cloned into the plasmid via the *Bgl*II and *Spe*I restriction site. 5´ of the 2A sequence an additional *Age*I restriction site was introduced. 3´ of the 2A sequence an additional *Bsp*EI restriction site was included. Gene fusions with mRFP were accomplished via directed cloning with *Bgl*II and *Age*I. Gene fusions with GFP were accomplished via directed cloning with *Bsp*EI and *Spe*I. Vector design and generation of the cloning intermediates were done by Felix Uecker.

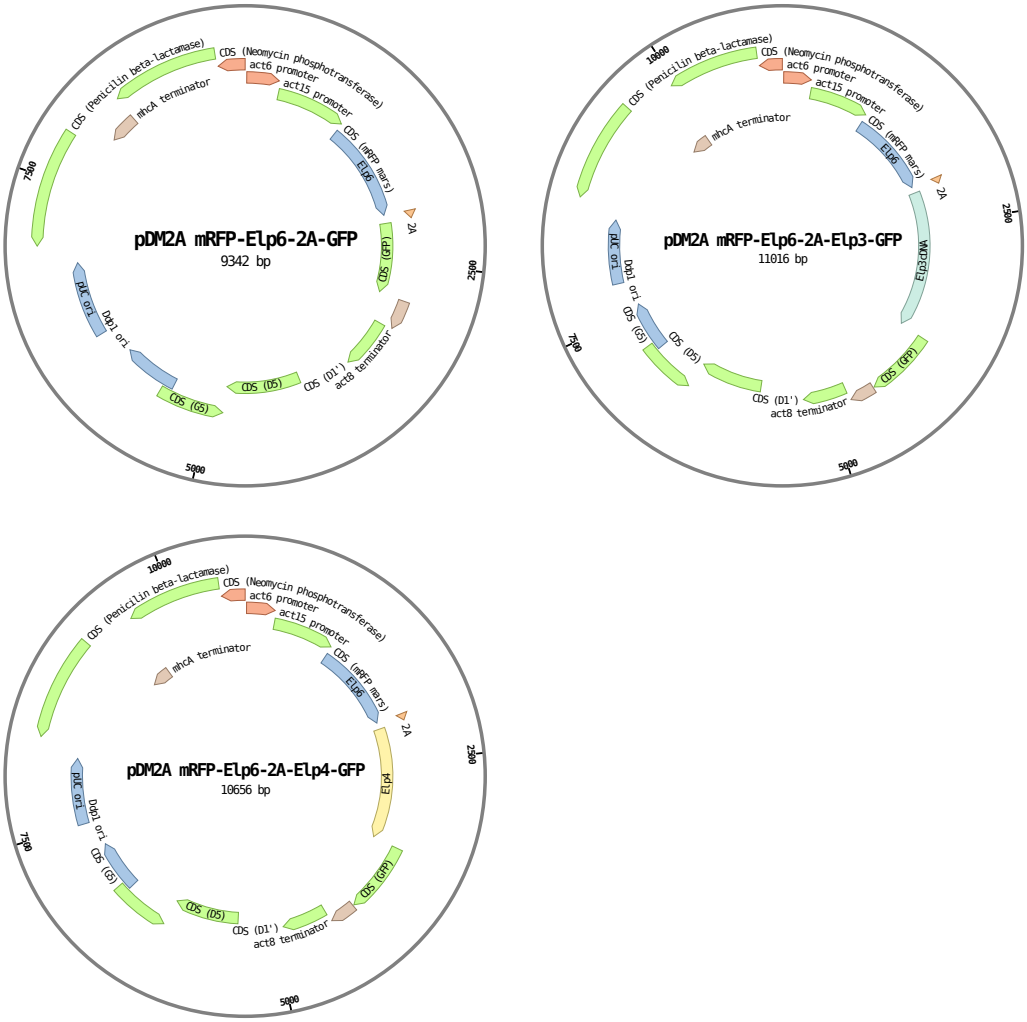

Figure 74: pDM2A plasmids for *D. discoideum* 2. The terminator sequence of the expression cassette of the pDM318 was replaced by the GFP gene and terminator sequence of pDM323 (via *Spe*I and *Hind*III directed cloning). The 2A sequence was produced synthetically (oligo hybridization) and cloned into the plasmid via the *Bgl*II and *Spe*I restriction site. 5 prime of the 2A sequence an additional *Age*I restriction site was introduced. 3´ of the 2A sequence an additional *Bsp*EI restriction site was included. Gene fusions with mRFP were accomplished via directed cloning with *Bgl*II and *Age*I. Gene fusions with GFP were accomplished via directed cloning with *Bsp*EI and *Spe*I. Vector design and generation of the cloning intermediates were done by Felix Uecker.

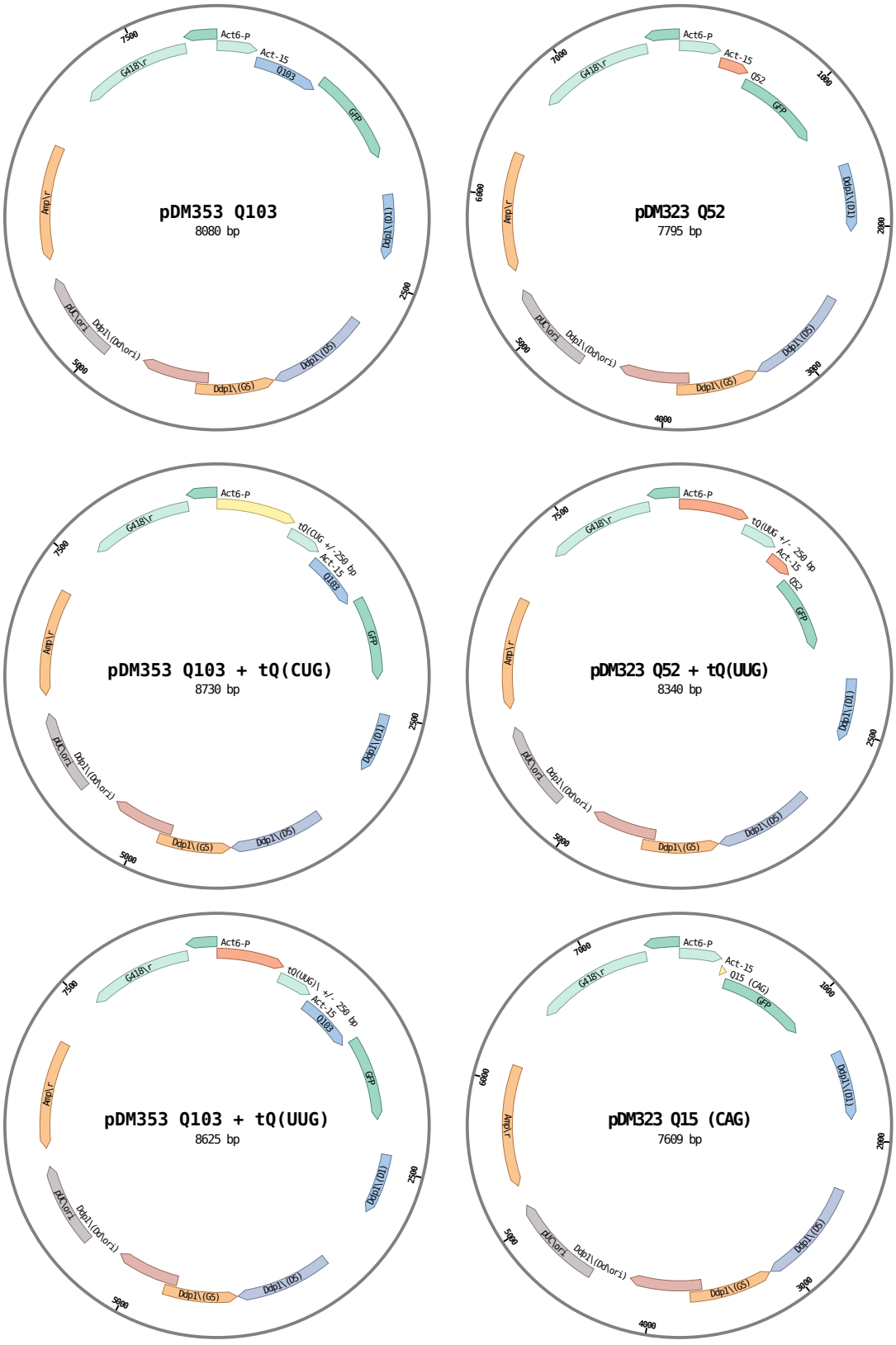

Figure 75: Glutamine leader expression plasmids for *D. discoideum*. The pDM353 Q103 was provided by Liliana Malinovska [71]. pDM323 Q52 was amplified from genomic DNA of D. discoideum, pDM323 Q15 was generated by cloning of the synthetic oligos between the *Bgl*II and *Spe*I restriction sites. tRNA genes +/− 250 bp were introduced via the *Xho*I restriction site.

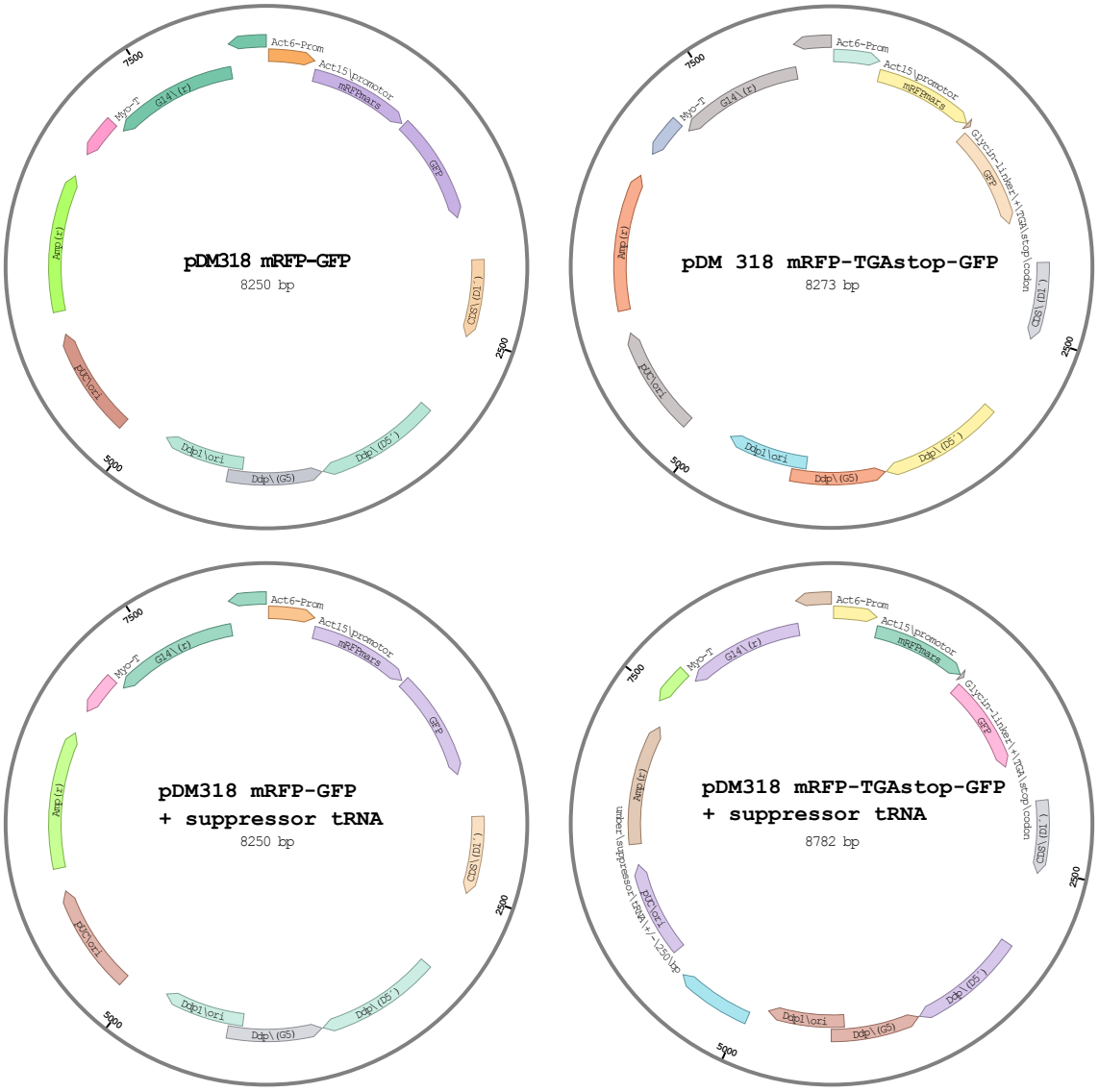

Figure 76: Umber stop codon experiment expression plasmids for *D. discoideum*. The pDM318 mRFP-GFP plasmid was constructed by cloning the GFP-tag and terminator of the pDM323 into the pDM318 via *Spe*I and *Hind*III. The TGA stop codon with glycine-linker was cloned between the mRFP and GFP genes of the pDM318 mRFP-GFP construct via the *Spe*I and *Bgl*II restriction sites. The suppressor tRNA was cloned into the vectors via the *Ngo*MIV restriction site.

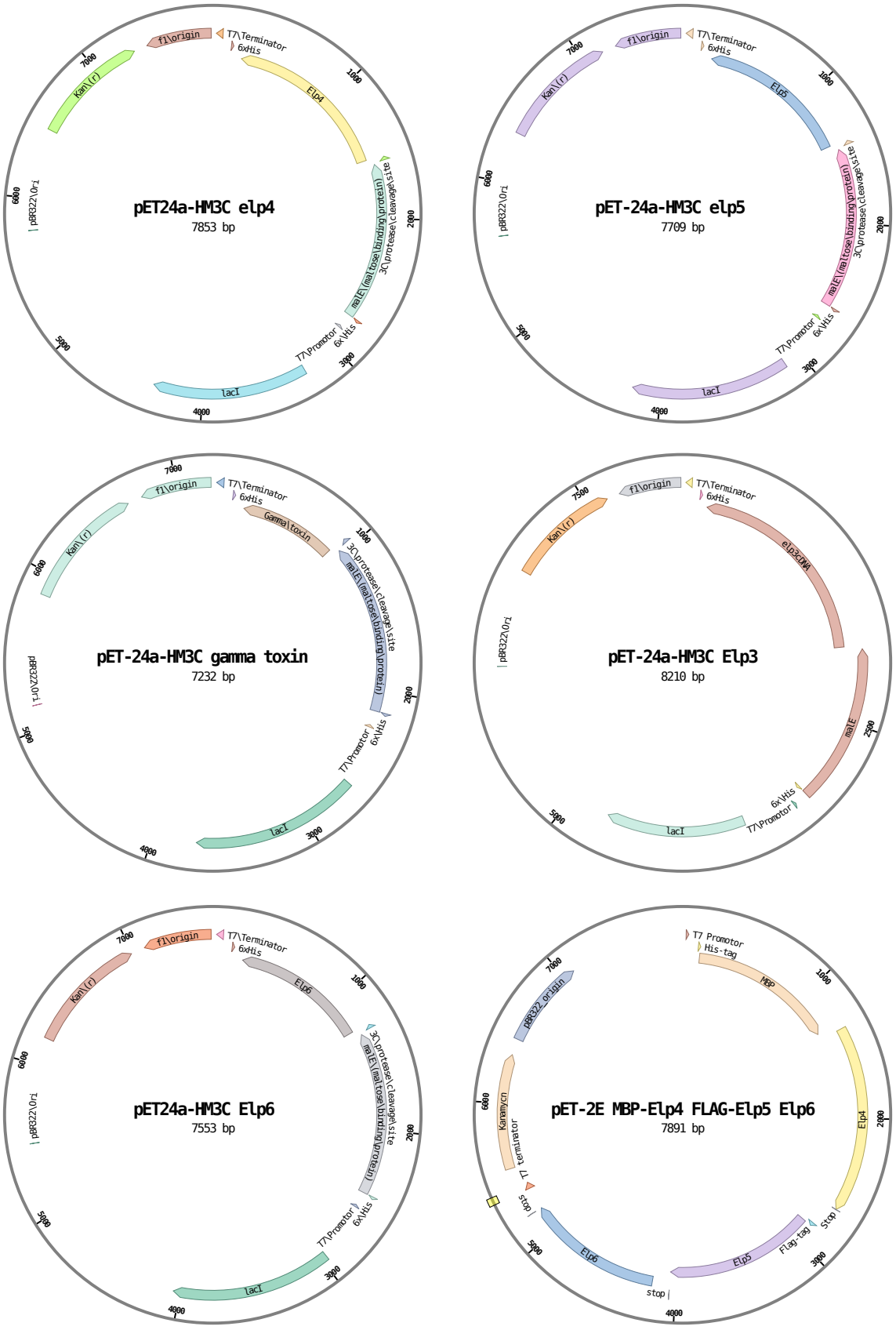

Figure 77: Expression plasmids for *E. coli*. Cloning procedures are described in 2.2.3.3 and the bachelor thesis of Alina Stein [85]. (pET2E Elp456 Vector design and generation of the single pET-LIC intermediates by Manfred Schäck.)

A.4.2 *Oligo nucleotides*

Additional primers and oligos associated (but not used by the author) with the projects of this thesis can be found in the lab book of Felix Uecker (labbook 2), Dolma Choezom (labbook 2), Alina Stein and Liviu Copoiu.

Table 22: Primer and Oligo DNA list 1: pKOSG and screening primers

NUMBER	NAME	SEQUENCE
# 324	loxP for	GTTATCCATGGTTAATTAATTAACCC
# 325	loxP rev	CTCGGATCTGATATCATAACTTC
#163	pKOSG Fusion Primer rev	GAGCGTCGATTTTTGTGATGC
#164	pKOSG Fusion Primer for	GGGAATAAGGGCGACACGG
#2046	pKOSG elp3 right arm rev	AGCGCGTCTCCTCCCACTAGTAAGGAAACCTCAAATCATATCTTACTTGG
#2045	pKOSG elp3 right arm fwd	AGCGCGTCTCCCTTCGGTTTACTTCGTCTTAGAAAATGTTCAG
#2044	pKOSG elp3 left arm rev	AGCGCGTCTCCGTTGTTGCTAAATGTGGGCAACGATGTGG
#2043	pKOSG elp3 left arm fw	AGCGCGTCTCCAATGACTAGTGCAGGCGCTAAACCAGTTTGTAAG
#2047	elp3 outer wt fw	TGAATGACCCAAGACCTGTTTC
#2050	elp3 outer wt rev	GCCTTCAACAAGCCATGCTCC
#2048	elp3 inner wt primer fw	GCACGTGATACAAATCGTGGTCAT
#2049	elp3 inner wt primer rev	ACCTGGACAATATACACAAATATTACC
#2041	elp4 inner wt rev	GAAACATATTGTTGATATCTCCATGCA
#2040	elp4 inner wt fwd	GATGTGTATCGAAACAATTCATTTACC
#2038	pKOSG elp4 right arm rev	AGCGCGTCTCCTCCCACTAGTCCAAGGCCACCAGTTTCCCC
#2037	pKOSG elp4 right arm for	AGCGCGTCTCCCTTCGTGGTGGAGGTGGTGGTGGT
#2036	pKOSG elp4 left arm rev	AGCGCGTCTCCGTTGACTACCAATTGGTATACCACCACC
#2035	pKOSG elp4 left arm for	AGCGCGTCTCCAATGACTAGTCAATCTGAAATATTGGCCGATGCAATTTCA
#2039	elp4 outer wt fwd	CGTTACAATCCATACACTCAATCAATTGAAA
#2040	elp4 outer wt rev	ACCTACCTCTCCAATACCAACTATGT
#2379	pKOSG elp5 LA fwd	AGCGCGTCTCCAATGACTAGTTAAGTGATAACATAAAAGACCCAAATCTCATTTAT
#2380	pKOSG elp5 LA rev	AGCGCGTCTCCGTTGATTATTCCAACCAAATGAATCTGAATAATAATC
#2381	pKOSG elp5 RA fwd	AGCGCGTCTCCCTTCAGAGAAACAAGAAAAGGAACAAAAAGAACAA
#2382	pKOSG elp5 RA rev	AGCGCGTCTCCTCCCACTAGTGTTTGTTCATTATTATTACCTTGATGTCTATAT
#2383	elp5 outer wt fwd	GATTTGCTTTAATTTTCCGTTGATTTAATGTTA
#2384	elp5 inner wt rev	CATTGGAATTTGTTGTAAATTCTCTGTTATATT
#2385	elp5 inner wt fwd	AGAGTGGATTATCAGATACATGTAATTTAATTA
#2386	elp5 outer wt rev	TCTAAATCATCATCAGGATCTTCATCAT
#2387	pKOSG elp6 LA fwd	AGCGCGTCTCCAATGACTAGTAGTGGCGATTTTATGAATGAAGATGG
#2388	pKOSG elp6 LA rev	AGCGCGTCTCCGTTGGAGGAGGAAGTGATATTCTTATTATCAA
#2389	pKOSG elp6 RA fwd	AGCGCGTCTCCCTTCCCAAGTGGTTCAAATATGGATATTTTAAAC
#2390	pKOSG elp6 RA rev	AGCGCGTCTCCTCCCACTAGTGAATCTAATTGAATTATCTAATGCTTGATAATG
#2391	elp6 outer wt fwd	ATGGATTTATTTAGTCATTTAAATTGGTAT
#2393	elp6 inner wt rev	CTCCTCCTCTTCTTATTCAAACTCTAGAGTTTGAATAAGAAGAGGAGGAG
#2394	elp6 inner wt fwd	TGATGGTTTAAATTTATTAGAGAGTCATTA
#2392	elp6 outer wt rev	CTTCTCAATGGGTTCAAGAATTCAATTGAATTCTTGAACCCATTGAGAAG
#2512	pKOSG ppp6c LA fwd (LA2)	AGCGCGTCTCCAATGACTAGTGTAGCTTTGTGAAGTCATTCTTTGCT
#2334	pKOSG ctu1 LA fwd	AGCGCGTCTCCAATGACTAGTGACAGGGGGGCGTCATTAACAA
#2335	pKOSG ctu1 LA rev	AGC GCGTCTCCGTTGTTTGTTGCTGTATTTTCCATTTTATTTATTTATTTGTTTG
#2336	pKOSG ctu1 RA fwd	AGCGCGTCTCCCTTCAGTACTTCAGCAGCAACAACAACAAC
#2337	pKOSG ctu1 RA rev	AGCGCGTCTCCTCCCACTAGTTCAGATTTACTTGTTTTTGGATCAACTTTAATAATC
#2339	ctu1 outer wt rev	TATCCTTACTTTTCTTTCCAACCTAAGTAA
#2338	ctu1 outer wt fwd	GATGAATTTTAAACAAATATTCAAAGGGGGAG
#2341	ctu1 inner wt rev	CTTGATACATTACAAACTTCACATAATTTTGATTTC
#2340	ctu1 inner wt fwd	AGAGGAAAAGATAATAATAATAGTAATAATAATGAT

Table 23: Primer and Oligo DNA list 1: pKOSG and screening primers 2

NUMBER	NAME	SEQUENCE
#2583	pKOSG tQCUG LA fwd	AGCGCGTCTCCAATGACTAGTCTCCTTCATATGCTAATTCTCCACTAC
#2584	pKOSG tQCUG LA rev	AGCGCGTCTCCGTTGCCTCACATTATCATTTGGACAGATTCCA
#2585	pKOSG tQCUG RA fwd	AGCGCGTCTCCCTTCCAACGAAAAATGCGCAATTTGGATACGT
#2586	pKOSG tQCUG RA rev	AGCGCGTCTCCTCCCACTAGTCCTGAAAGTTTTTCAATAACAATTTCACTAATTTCC
#2537	pKOSG TRM 9 LA fwd	AGCGCGTCTCCAATGACTAGTCATGACCATTGATTATCATAGATCTTTTGA
#2538	pKOSG TRM 9 LA rev	AGCGCGTCTCCGTTGTCATCACTAATCTCTGGTACTCCT
#2538	pKOSG TRM9 RA fwd	AGCGCGTCTCCCTTCAGAATGTGAAATGGTTGAAAATAATTTAGATCA
#2539	pKOSG TRM9 RA rev	AGCGCGTCTCCTCCCACTAGTTCTAGTGAAGTTTGGATTGGTACTTC
#2540	TRM9 outer wt rev	CCAGAAGGTACAGTAGATACAAC
#2541	TRM9 outer wt fwd	CAAGATGATACTAATGGTGATGGC
#2542	TRM9 inner wt fwd	GAAGAAGATAAAATTATTGAAAAATCAGGTTC
#2543	TRM9 inner wt rev	GGTATTTACCATTACCACAACCAAC
#2554	pKOSG TRM112 LA fwd	AGCGCGTCTCCAATGACTAGTGTAACTTCATATAATCTATCATTCAATTCCA
#2555	pKOSG TRM112 LA rev	AGCGCGTCTCCGTTGAGTGCAAGCCATCATATTGTGTG
#2556	pKOSG TRM112 RA fwd	AGCGCGTCTCCCTTCTAAGAGAAGATGAAATTTATCAAGAAATTAAAG
#2557	pKOSG TRM112 RA rev	AGCGCGTCTCCTCCCACTAGTTTTTGTGGAGGTATTTTCGGTGC
#2540	TRM112 outer wt rev	TCACATATATTAGCACGTGGACG
#2541	TRM112 outer wt fwd	GACAAACTCTTTTATTTTCATTATCTTCTGT
#2542	TRM112 inner wt rev	GGAAACCTTTACCCATACATTGCT
#2543	TRM112 inner wt fwd	ACAGGTAGTTTAACATGTCCAAATTGT
#2550	pKOSG urm1 LA fwd	AGCGCGTCTCCAATGACTAGTGTTGTTGCACAACTGTTATTGATATAG
#2551	pKOSG urm1 LA rev	AGCGCGTCTCCGTTGAGATATATACCTTAATTCAATTTTAACTTTCAT
#2552	pKOSG urm1 RA fwd	AGCGCGTCTCCCTTC GTAGTTGATGATACAGTGTAAGTATATATA
#2553	pKOSG urm1 RA rev	AGCGCGTCTCCTCCCACTAGTGATATTGTTTTATCATTTCCAATTTTAAATTATTG
#2322	pKOSG ppp6c LA fwd	AGCGCGTCTCCAATGACTAGTGTAGCTTTGTGAAGTCATTCTTTGCT
#2323	pKOSG ppp6c LA rev	AGCGCGTCTCCGTTGCCATTCATCAAGTGGAAGTGCGT
#2324	pKOSG ppp6c RA fwd	AGCGCGTCTCCCTTCCGCTTCCATCCTTTCACTCAATG
#2325	pKOSG ppp6c RA rev	AGCGCGTCTCCTCCCACTAGTGTTTCAGTATCCATAATGAGATCAAAAC
#2326	ppp6c outer wt rev	GATGGTGTGATTGCTAAATTAATTGCAT
#2327	ppp6c outer wt fwd	GACGTGGTTGTATCCTAAAATATTTGA
#2328	ppp6c inner wt rev	CTGCACGTCAATGCAAATATTTACCA
#2329	ppp6c inner wt fwd	GGTCTGCTCCAAACTATTGTTATAGA

Table 24: Primer and Oligo DNA list 3: pDM cloning primers and others

NUMBER	NAME	SEQUENCE
-	mutagenisis p1_elp3 HAT	AGCGGCTCTTCAATGATGTCATTAATGAATGACCCAAG
-	mutagenisis p2_elp3 HAT	AGCGGCTCTTCGATAAAATTGATGTTGAAATTTAGTTGGATC
-	mutagenisis p3_elp3 HAT	AGCGGCTCTTCGTATTTTACTTTATTAATGGAAGAAGCTG
-	mutagenisis p4_elp3 HAT	AGCGGCTCTTCTCCCACCAAGATATTTTGAAACGTAAAC
#2205	Elp3 mut sam outer fwd	AGCGGCTCTTCAATGATGTCATTAATGAATGACCCAAG
#2205	Elp3 mut sam rev 1	AGCGGCTCTTCGTATACTGAAATATTACCAGTCATTGCTAAAT
#2205	Elp3 mut sam fwd 2	AGCGGCTCTTCGATATTCACCAGGTGGACCAGATTCAG
#2206	Elp3 mut sam outer rev	AGCGGCTCTTCTCCCACCAAGATATTTTGAAACGTAAAC
#2059	elp3 n-term fwd	AGAAGATCTATGTCATTAATGAATGACCCAAGACC
#2106	elp3 n-term rev	AGAACTAGTTTAACCAAGATATTTTGAAACGTAAACACC
#2061	elp3 c-term fwd	AGAAGATCTTCATTAATGAATGACCCAAGACCTGTT
#2062	elp3 c-term rev	AGAACTAGTTTAACCAAGATATTTTGAAACGTAAACACC
#2063	elp4 n-term fwd	AGAAGATCTATGACAACACCAAGAGTACCAACAAC
#2108	elp4 n-term rev	AGAACTAGTAAAATCTAAAGGATTGTTATTACTAGAACCAC
#2064	elp4 c-term fwd	AGAAGATCTACAACACCAAGAGTACCAACAACATTT
#2066	elp4 c-term rev	TCTACTAGTTTAAAAATCTAAAGGATTGTTATTACTAGAACCAC
#2052	elp5 n-term fwd	AGAAGATCTATGTCATCAACGATTGTATCATCAATTGG
#2053	elp5 n-term rev	AGAACTAGTTTAAATATCTAAATCATCATCAGGATCTTCATCAT
#2050	elp6 N-term fwd	AGAAGATCTATGGATTTATTTAGTCATTTAAATTGG
#2051	elp6 N-term rev	AGAACTAGTTTGAATTCTTGAACCCAT
#2039	yeast elp3 n-term fwd	AGAAGATCTATGGCTCGTCATGGAAAAGGC
#2040	yeast elp3 n-term rev	AGAACTAGTTTAAATTCTTTTCGACATGTATGGACC
#2041	yeast elp1 n-term fwd	AGAAGATCTATGGTTGAACATGACAAGAGTGG
#2042	yeast elp1 n-term rev	AGAACTAGTTCAAAAATCAACAATATGACTCTTAGGG
#2526	tQCUG gen fwd hindIII	AGAAAGCTTGGAATCTGTCCAAATGATAATGTGAG
#2527	tQCUG gen rev hindIII	TCTAAGCTTGATTAACATTCTTATTTTAATTTGTGGAGATTAG
#2554	urm1 fwd nterm	AGAAGATCTATGAAAGTTAAAATTGAATTAAGTGGTGGA
#2555	urm1 rev nterm	AGAACTAGTTTAACCTCCATGTAAAGTTGAAATGAAAAT
#2549	γ-toxin n-term fwd	AGAAGATCTATGGCAGCTACTACTGCGAGA
#2550	γ-toxin n-term rev	AGAACTAGTTTATTATACACATTTTCCATTCTGTAGATTATTC
# 281	pJET1 forward	GCCTGAACACCATATCCATCC
# 282	pJET1 reverse	GCAGCTGAGAATATTGTAGGAGATC
#1860	mRFP seq fwd	GGGTTGGGAAGCATCAACAG
#1861	mRFP seq rev	CTGTTGATGCTTCCCAACCC
#	γ-toxin pDM n-term fwd	AGAAGATCTATGGCAGCTACTACTGCGAGA
#	γ-toxin pDM n-term rev	AGAACTAGTTTATTATACACATTTTCCATTCTGTAGATTATTCA
#2530	tQ(UUG) 13 genomic xhoI fwd	AGACTCGAGCAAATCTAGGTATTGGGCAAAAATAG
#2529	tQ(UUG) 13 genomic xhoI rev	TCTCTCGAGGTTTTGTTTTATTTTGTTTTTATTTTGGTTTTGTG
#2530	tE(UUC) genomic fwd	CGAGAAATCGATCCCATTTTTTTCTAA
#2031	tE(UUC) genomic rev	AATTTTTCCTATTTTTGAGTAATATCTAATAGC
#2532	fusion pDM xhoI promotor amplif	AGAGCCGGCCTCGAGACTAGAGCTAGATA
#2533	fusion pDM hindIII terminator amplif	TCTGCCGGCGAAATCGATAAGCTTTATCTTTTTG

Table 25: Primer and Oligo DNA list 4: Primers for bacterial cloning primers and other primers

NUMBER	NAME	SEQUENCE
#188	GFP L AvaI	CATTCTTGGACACAAATTGGAA
#1677	pet24a sequencing rev	CCACGATGCGTCCGGCGTAG
#1678	malE rev	CCAGCGGTCGTCAGACTGTCG
#2142	LIC elp6 fwd	CAAGGAACCGAGCAGCCCCTCCATGGATTTATTTAGTCATTTAAATTGGTATAGTGGCA
#2143	LIC elp6 rev	ACCACGGGGAACCAACCCTTATTATTGAATTCTTGAACCCATTGAGAAGAATCTAATTG
#2431	LIC elp4 fwd	TTTAAGAAGGAGATATAGATCATGACAACACCAAGAGTACCAAC
#2432	LIC elp4 rev	ATTATTCTAGGGTTGAGGTATTTTAAAAATCTAAAGGATTGTTATTACTAG
#2518	LIC MBP (polycistr) n-term fwd	TTTAAGAAGGAGATATAGATCATGGGTTCTTCTCACCATCACCAT
#2520	LIC elp5 c-term rev	TTATGGAGTTGGGATCTTATTATTAAATATCTAAATCATCATCAGGATCTTCATCAT
#2521	LIC elp5 n-term flag fwd	TTTAAGAAGGAGATATAGATCATGGATTATAAAGATGATGATGATAAATCATCAAC-GATTGTATCATCAATTGG
# 2237	γ-toxin pET24a fwd	CAAGGACCGAGCAGCCCCTCCATGGCAGCTACTACTGCGAGA
# 2238	γ-toxin pET24a rev	ACCACGGGGAACCAACCCTTATTATACACATTTTCCATTCTGTAGATTATTC
-	tE^{UUC} 5´ probe	TTACCGACTACACCAATGAGGA
-	tE^{UUC} 3´ probe	CTCCCCATTCGGGAATCGAA
-	tK^{UUU} 5´ probe	TGCGCTCTACCGACTGAGCT
-	tK^{UUU} 3´ probe	CGCCCAAAGGGGGGCTCGAA
-	tQ^{UUG} 5´ probe	GGTGCTAACCAATTACACTATAAAA
-	tQ^{UUG} 3´ probe	TGGTTCTACTGAGACTCGAACT
-	tG^{GCC} probe	GGCAGGGATGCATCATACCA
-	*E. coli* tK^{UUU} 3´ probe	TGGGTCGTGCAGGATTCGAACCT
-	*S. cerevisiae* tK^{UUU} 3´ probe	CTCCTCATAGGGGGCTCGAACCC
-	*S. cerevisiae* tE^{UUC} 3´ probe	CTCCGCTACGGGGAGTCGAAC

A.4.3 *Strains generated in this thesis*

A.4.3.1 *Overview of bacterial strains generated in this thesis*

Table 26: Overview of bacterial strains generated in this thesis

STRAIN	STARTING STRAIN	VECTOR	RESISTANCE
Codon+ pET24a HM3C-Elp3	*E. coli* BL21 (Codon plus (R)) RIL	pET24a HM3C-Elp3	Kan/CAM
Codon+ pET24a HM3C-Elp4	*E. coli* BL21 (Codon plus (R)) RIL	pET24a HM3C-Elp4	Kan/CAM
Codon+ pET24a HM3C-Elp5	*E. coli* BL21 (Codon plus (R)) RIL	pET24a HM3C-Elp5	Kan/CAM
Codon+ pET24a HM3C-Elp6	*E. coli* BL21 (Codon plus (R)) RIL	pET24a HM3C-Elp6	Kan/CAM
Codon+ pET24a HM3C-γ-toxin	*E. coli* BL21 (Codon plus (R)) RIL	pET24a HM3C-γ-toxin	Kan/CAM
Codon+ pET24a HM3C-mut-γ-toxin	*E. coli* BL21 (Codon plus (R)) RIL	pET24a HM3C-γ-toxin	Kan/CAM
Codon+ pABY1633 GST-γ-toxin	*E. coli* BL21 (Codon plus (R)) RIL	pABY1633 GST-γ-toxin	Kan/CAM
Codon+ pABY1650 GST	*E. coli* BL21 (Codon plus (R)) RIL	pABY1650 GST	Kan/CAM

A.4.3.2 *Overview of D. discoideum Strains*

Table 27: Overview of *D. discoideum* strains created in this thesis 1: Ax2

STRAIN	ST.STRAIN	VECTOR	RESISTANCE
AX2 pDM317 GFP	AX2	pDM317 GFP	G418
AX2 pDM326 GFP	AX2	pDM326 GFP	Blasticidin
AX2 pDM317 GFP Elp3	AX2	pDM317 GFP Elp3	G418
AX2 pDM317 GFP mutHAT-Elp3	AX2	pDM317 GFP mutHAT-Elp3	G418
AX2 pDM317 GFP mutSAM-Elp3	AX2	pDM317 GFP mutSAM-Elp3	G418
AX2 pDM323 Elp3 GFP	AX2	pDM323 Elp3 GFP	G418
AX2 pDM326 Elp3 GFP	AX2	pDM326 Elp3 GFP	Blasticidin
AX2 pDM317 GFP Elp4	AX2	pDM317 GFP Elp4	G418
AX2 pDM323 Elp4 GFP	AX2	pDM323 Elp4 GFP	G418
AX2 pDM326 Elp4 GFP	AX2	pDM326 Elp4 GFP	Blasticidin
AX2 pDM318 RFP Elp3	AX2	pDM318 RFP Elp3	G418
AX2 pDM318 RFP Elp4	AX2	pDM318 RFP Elp4	G418
AX2 pDM318 RFP Elp5	AX2	pDM318 RFP Elp5	G418
AX2 pDM318 RFP Elp6	AX2	pDM318 RFP Elp6	G418
AX2 pDM304 TwinStrep-Flag Elp3	AX2	pDM304 TwinStrep-Flag Elp3	G418
AX2 pDM304 TwinStrep-Flag Elp4	AX2	pDM304 TwinStrep-Flag Elp4	G418
AX2 pDM304 TwinStrep-Flag Elp5	AX2	pDM304 TwinStrep-Flag Elp5	G418
AX2 pDM304 TwinStrep-Flag Elp6	AX2	pDM304 TwinStrep-Flag Elp6	G418
AX2 pDM359 TwinStrep-Flag Elp6	AX2	pDM359 Flag Elp6	Hygr/Dox
AX2 pDM317 GFP yElp3	AX2	pDM317 GFP Elp3	G418
AX2 pDM317 GFP yElp1	AX2	pDM317 GFP Elp3	G418

Table 28: Overview of *D. discoideum* strains created in this thesis 2: Ax2, *elp1*$^-$ and *elp5*$^-$

STRAIN	ST.STRAIN	VECTOR	RESISTANCE
AX2 fusion-pDM318 RFP Elp5 GFP Elp6	AX2	fusion-pDM318 RFP Elp5 GFP Elp6	G418
AX2 fusion-pDM318 RFP Elp3 GFP Elp4	AX2	fusion-pDM318 RFP Elp3 GFP Elp4	G418
AX2 fusion-pDM318 RFP yElp1 GFP yElp3	AX2	fusion-pDM318 RFP yElp1 GFP yElp3	G418
AX2 pDM353 Q103 GFP	AX2	pDM353 Q103 GFP	G418
AX2 pDM353 Q103 GFP tQ(UUG)	AX2	pDM353 Q103 GFP tQ(UUG)	G418
AX2 pDM353 Q103 GFP tQ(CUG)	AX2	pDM353 Q103 GFP tQ(CUG)	G418
AX2 pDM323 Q52 GFP	AX2	pDM323 Q52 GFP	G418
AX2 pDM323 Q52 GFP tQ(UUG)	AX2	pDM323 Q52 GFP tQ(UUG)	G418
AX2 pDM323 Q15 GFP	AX2	pDM323 Q12 GFP	G418
AX2 pDM359 TwinStrep-Flag γ-toxin	AX2	pDM359 TwinStrep-Flag γ-toxin	Hygr/Dox
AX2 pDM359 TwinStrep-Flag mutE4G-γ-toxin	AX2	pDM359 TwinStrep-Flag mutE4G-γ-toxin	Hygr/Dox
elp1$^-$ pDM317 GFP	elp1$^-$ cl 69 rox	pDM317 GFP	G418
elp1$^-$ pDM317 GFP Elp3	elp1$^-$ cl 69 rox	pDM317 GFP Elp3	G418
elp1$^-$ pDM353 Q103 GFP	elp1$^-$ cl 69 rox	pDM353 Q103 GFP	G418
elp5$^-$ pDM353 Q103 GFP	elp5$^-$ flox	pDM353 Q103 GFP	G418
elp5$^-$ pDM353 Q103 GFP tQ(UUG)	elp5$^-$ flox	pDM353 Q103 GFP tQ(UUG)	G418
elp5$^-$ pDM353 Q103 GFP tQ(CUG)	elp5$^-$ flox	pDM353 Q103 GFP tQ(CUG)	G418

Table 29: Overview of *D. discoideum* strains created in this thesis 3: *elp3*$^-$

STRAIN	ST.STRAIN	VECTOR	RESISTANCE
elp3$^-$ clon 5 flox	AX2	pKOSG Elp3	Blasticidin
elp3$^-$ clon PrI flox	AX2	pKOSG Elp3	Blasticidin
elp3$^-$ clon 5 rox	elp3$^-$ clon 5 flox	pDEX RH NLS-Cre	-
elp3$^-$ clon PrI rox	elp3$^-$ clon PrI flox	pDEX RH NLS-Cre	-
elp3$^-$ pDM317 GFP Elp3	elp3$^-$ clon PrI flox	pDM317 GFP Elp3	G418/Blasticidin
elp3$^-$ pDM326 Elp3 GFP	elp3$^-$ clon PrI flox	pDM326 Elp3 GFP	G418/Blasticidin
elp3$^-$ pDM317 GFP Elp3	elp3$^-$ clon PrI rox	pDM317 GFP Elp3	G418
elp3$^-$ pDM317 GFP mutHAT-Elp3	elp3$^-$ clon PrI rox	pDM317 GFP mutHAT-Elp3	G418
elp3$^-$ pDM317 GFP mutSAM-Elp3	elp3$^-$ clon PrI rox	pDM317 mutSAM-Elp3	G418
elp3$^-$ pDM323 Elp3 GFP	elp3$^-$ clon PrI rox	pDM323 Elp3 GFP	G418
elp3$^-$ pDM317 GFP	elp3$^-$ clon PrI rox	pDM317 GFP	G418
elp3$^-$ pDM353 Q103 GFP	elp3$^-$ clon PrI rox	pDM353 Q103 GFP	G418
elp3$^-$ pDM353 Q103 GFP tQ(UUG)	elp3$^-$ clon PrI rox	pDM353 Q103 GFP tQ(UUG)	G418
elp3$^-$ pDM353 Q103 GFP tQ(CUG)	elp3$^-$ clon PrI rox	pDM353 Q103 GFP tQ(CUG)	G418
elp3$^-$ pDM323 Q52 GFP	elp3$^-$ clon PrI rox	pDM323 Q52 GFP	G418
elp3$^-$ pDM323 Q52 GFP tQ(UUG)	elp3$^-$ clon PrI rox	pDM323 Q52 GFP tQ(UUG)	G418
elp3$^-$ pDM323 Q15 GFP	elp3$^-$ clon PrI rox	pDM323 Q15 GFP	G418
elp3$^-$ pDM304 TwinStrep-Flag Elp3	elp3$^-$ clon PrI rox	pDM304 TwinStrep/Flag Elp3	G418
elp3$^-$ pDM304 Elp3 TwinStrep-Flag	elp3$^-$ clon PrI rox	pDM304 Elp3 TwinStrep/Flag	G418
elp3$^-$ pDM317 GFP Elp2	elp3$^-$ clon PrI rox	pDM317 GFP Elp2	G418
elp3$^-$ pDM317 GFP Elp4	elp3$^-$ clon PrI rox	pDM317 GFP Elp4	G418
elp3$^-$ pDM304 TwinStrep-Flag Elp4	elp3$^-$ clon PrI rox	pDM304 TwinStrep/Flag Elp4	G418

Table 30: Overview of *D. discoideum* strains created in this thesis 4: *elp3*$^{-}$

STRAIN	ST.STRAIN	VECTOR	RESISTANCE
elp3^{-} cl5 pDM317 GFP Elp3	elp3^{-} elp3^{-} clon 5 rox	G418	
elp3^{-} cl5 pDM323 GFP mutHAT-Elp3	elp3^{-} clon 5 rox	GFP mutHAT-Elp3	G418
elp3^{-} cl5 pDM317 GFP mutSAM-Elp3	elp3^{-} clon 5 rox	pDM317 mutSAM-Elp3	G418
elp3^{-} cl5 pDM323 Elp3 GFP	elp3^{-} clon 5 rox	pDM323 Elp3 GFP	G418
elp3^{-} cl5 pDM317 GFP	elp3^{-} clon 5 rox	pDM317 GFP	G418
elp3^{-} cl5 pDM353 Q103 GFP	elp3^{-} clon 5 rox	pDM353 Q103 GFP	G418
elp3^{-} cl5 pDM353 Q103 tQ(UUG) GFP	elp3^{-} clon 5 rox	pDM353 Q103 GFP tQ(UUG)	G418
elp3^{-} cl5 pDM353 Q103 GFP tQ(CUG)	elp3^{-} clon 5 rox	pDM353 Q103 GFP tQ(CUG)	G418
elp3^{-} cl5 pDM353 erkA GFP	elp3^{-} clon 5 rox	pDM353 Q103 GFP	G418
elp3^{-} cl5 pDM353 erkA GFP tQ(UUG)	elp3^{-} clon 5 rox	pDM353 Q103 GFP tQ(UUG)	G418
elp3^{-}/ctu1^{-} flox	elp3^{-} clon PrI rox	pKOSG ctu1	BS10
elp3^{-}/ctu1^{-} rox	elp3^{-}/ctu1^{-} flox	pDEX RH NLS-Cre	-
elp3^{-}/ctu1^{-} pDM353 Q103 GFP	elp3^{-}/ctu1^{-} rox	pDM353 Q103 GFP	G418
elp3^{-}/ctu1^{-} pDM353 Q103 GFP tQ(UUG)	elp3^{-}/ctu1^{-} rox	pDM353 Q103 GFP tQ(UUG)	G418
elp3^{-}/ctu1^{-} pDM353 Q103 GFP tQ(CUG)	elp3^{-}/ctu1^{-} rox	pDM353 Q103 GFP tQ(CUG)	G418
elp3^{-}/ctu1^{-} pDM353 erkA GFP	elp3^{-}/ctu1^{-} rox	pDM353 Q103 GFP	G418
elp3^{-}/ctu1^{-} pDM353 erkA GFP tQ(UUG)	elp3^{-}/ctu1^{-} rox	pDM353 Q103 GFP tQ(UUG)	G418

Table 31: Overview of *D. discoideum* strains created in this thesis 5: *elp4*$^-$

STRAIN	ST.STRAIN	VECTOR	RESISTANCE
elp4$^-$ cl 13 flox	AX2	pKOSG Elp4	Blasticidin
elp4$^-$ rox	elp4$^-$ flox	pDEX RH NLS-Cre	-
elp4$^-$ pDM317 GFP Elp4	elp4$^-$ rox	pDM317 GFP Elp4	G418
elp4$^-$ pDM323 Elp4 GFP	elp4$^-$ rox	pDM323 Elp4 GFP	G418
elp4$^-$ pDM326 Elp4 GFP	elp4$^-$ rox	pDM326 Elp4 GFP	Blasticidin
elp4$^-$ pDM318 RFP Elp4	elp4$^-$ rox	pDM318 RFP Elp4	G418
elp4$^-$ pDM304 TwinStrep-Flag Elp4	elp4$^-$ rox	pDM304 TwinStrep-Flag Elp4	G418
elp4$^-$ pDM304 Elp4 TwinStrep-Flag	elp4$^-$ rox	pDM304 Elp4 TwinStrep-Flag	G418
elp4$^-$ pDM304 TwinStrep-Flag Elp4	elp4$^-$ rox	pDM304 TwinStrep-Flag Elp4	G418
elp4$^-$ pDM317 GFP Elp3	elp4$^-$ rox	pDM317 GFP Elp3	G418
elp4$^-$ pDM353 Q103 GFP	elp4$^-$ rox	pDM353 Q103 GFP	G418
elp4$^-$ pDM353 Q103 GFP tQ(UUG)	eelp4$^-$ rox	pDM353 Q103 GFP tQ(UUG)	G418
elp4$^-$ pDM353 Q103 GFP tQ(CUG)	elp4$^-$ rox	pDM353 Q103 GFP tQ(CUG)	G418
elp4$^-$ pDM323 Q52 GFP	elp4$^-$ rox	pDM323 Q52 GFP	G418
elp4$^-$ pDM323 Q52 GFP tQ(UUG)	elp4$^-$ rox	pDM323 Q52 GFP tQ(UUG)	G418
elp4$^-$ pDM323 Q15 GFP	elp4$^-$ rox	pDM323 Q15 GFP	G418
elp4$^-$ pDM359 TwinStrep-Flag γ-toxin	elp4$^-$ rox	pDM359 TwinStrep-Flag γ-toxin	Hygr/Dox
elp4$^-$ pDM359 TwinStrep-Flag mutE4G-γ-toxin	elp4$^-$ rox	pDM359 TwinStrep-Flag mutE4G-γ-toxin	Hygr/Dox

Table 32: Overview of *D. discoideum* strains created in this thesis 6: other mutant strains

STRAIN	ST.STRAIN	VECTOR	RESISTANCE
ctu1⁻ flox	AX2	pKOSG ctu1	Blasticidin
ctu1⁻ pDM353 Q103 GFP	tu1⁻ flox	pDM353 Q103 GFP	Blasticidin/G418
ctu1⁻ pDM353 Q103 GFP tQ(UUG)	ctu1⁻ flox	pDM353 Q103 GFP tQ(UUG)	Blasticidin/G418
ctu1⁻ pDM353 Q103 GFP tQ(CUG)	ctu1⁻ flox	pDM353 Q103 GFP tQ(CUG)	Blasticidin/G418
ctu1⁻ pDM323 Q52 GFP	ctu1⁻ flox	pDM323 Q52 GFP	Blasticidin/G418
ctu1⁻ pDM323 Q52 GFP tQ(UUG)	ctu1⁻ flox	pDM323 Q52 GFP tQ(UUG)	Blasticidin/G418
ctu1⁻ pDM323 Q15 GFP	ctu1⁻ flox	pDM323 Q15 GFP	Blasticidin/G418
trm9⁻ flox	AX2	pKOSG trm9	Blasticidin
trm9⁻ pDM353 Q103 GFP	trm9⁻ flox	pDM353 Q103 GFP	Blasticidin/G418
trm9⁻ pDM353 Q103 GFP tQ(UUG)	trm9⁻ flox	pDM353 Q103 GFP tQ(UUG)	Blasticidin/G418
trm9⁻ pDM353 Q103 GFP tQ(CUG)	trm9⁻ flox	pDM353 Q103 GFP tQ(CUG)	Blasticidin/G418
trm9⁻ pDM323 Q52 GFP	trm9⁻ flox	pDM323 Q52 GFP	Blasticidin/G418
trm9⁻ pDM323 Q52 GFP tQ(UUG)	trm9⁻ flox	pDM323 Q52 GFP tQ(UUG)	Blasticidin/G418
trm9⁻ pDM323 Q15 GFP	trm9⁻ flox	pDM323 Q15 GFP	Blasticidin/G418
tQ(CUG)⁻ flox	AX2	pKOSG tQ(CUG)	Blasticidin
tQ(CUG)⁻ pDM353 Q103 GFP	tQ(CUG)⁻ flox	pDM353 Q103 GFP	G418
tQ(CUG)⁻ pDM353 Q103 GFP tQ(UUG)	tQ(CUG)⁻ flox	pDM353 Q103 GFP tQ(UUG)	Blasticidin/G418
tQ(CUG)⁻ pDM353 Q103 GFP tQ(CUG)	tQ(CUG)⁻ flox	pDM353 Q103 GFP tQ(CUG)	Blasticidin/G418
tQ(CUG)⁻ pDM353 Q52 GFP	tQ(CUG)⁻ flox	pDM353 Q103 GFP	Blasticidin/G418
tQ(CUG)⁻ pDM353 Q52 GFP tQ(CUG)	tQ(CUG)⁻ flox	pDM353 Q52 GFP tQ(CUG)	Blasticidin/G418
tQ(CUG)⁻ pDM353 Q15 GFP	tQ(CUG)⁻ flox	pDM323 Q15 GFP	Blasticidin/G418

ACKNOWLEDGMENTS

I would like to thank my academic supervisor Prof. Dr. Christian Hammann to have given me the opportunity to perform research in his group. I also thank him for all the support he gave me over the years.

I thank Prof. Dr. Matthias Ullrich who kindly agreed to be in my PhD exam committee.

Many thanks go to my external committee member Prof. Dr. Raffael Schaffrath, who contributed a big part of the knowledge about the Elongator dependent U_{34} modification pathway and its proteins.

Thanks to all my Bachelor students over the years: Dolma Choezom, Serban Ilca, Liviu Copoiu, Boris Kanunnikov and ...

... a special thanks goes to Alina Stein, Felix Uecker and Kim Philipp Jablonski for their help and intellectual contribution to the work presented in this thesis.

Many thanks to all the former Ribogenetics Lab members. They were great support for my labwork and kept me company over last the years:
Particularly Marek Malicki, Anne Kalweit, Janis Kruse, Balachandar Ammapatti, Sandra Becker, Utz Ermel, Geno Villafano, Maro Iliopoulou, Julie Trolle, Bianca Mocanu, Tobias Schraink and many more that made labwork so much fun.

Thanks to Stefanie Kellner (LMU Munich) for her tRNA modification analysis on our Dicty strains.

Many thanks to the all other members of Lab2 and particular to Mircea, the Springer work group with Zeynep, Venkat, Raghavendra, Linda and Ursula Wellbrock, and many many more that helped me during my time here.

I thank my friends and family for their support and the distraction they provided whenever needed.

...And of course I thank You, the reader, for looking into my thesis.